Doctorat de l'Observatoire de Paris –
Dynamique des Systèmes Gravitationnels

Universidad de Granada - Spain

Environmental quantification and Hα characterisation of the most isolated galaxies in the local Universe

THÈSE DE DOCTORAT

Simon Verley

20 décembre 2005

JURY

President:	Gary A. Mamon
Thesis referee:	Alessandro Boselli
Thesis referee:	Santiago García-Burillo
Examinator:	Chantal Balkowski
Examinator:	José M. Vílchez Medina
Supervisor:	**Françoise Combes**
Supervisor:	**Lourdes Verdes-Montenegro**

LERMA - Observatoire de Paris - France

Instituto de Astrofísica de Andalucía - Spain

Contents

List of Figures

List of Tables

It is a pleasure to thank the many persons involved in the thesis,
I am indebted to them for their help, guidance and support.

Abstract

The role of the environment on galaxy evolution is still not fully understood. In order to quantify and set limits on the role of nurture one must identify and study a sample of isolated galaxies. The AMIGA project "**A**nalysis of the Interstellar **M**edium of **I**solated **GA**laxies" is doing a multi-wavelength study of a large sample of isolated galaxies in order to examine their interstellar medium and star formation activity.

We processed 950 galaxies from the Catalogue of Isolated Galaxies (Karachentseva 1973) and evaluated their isolation using an automated star-galaxy classification procedure (down to $M_B \approx 17.5$) on large digitised POSS-I fields surrounding each isolated galaxy. We defined, compared and discussed various criteria to quantify the degree of isolation for these galaxies: e.g. Karachentseva's revised criterion, local surface density computations, estimation of the external tidal force affecting each isolated galaxy. We find galaxies violating Karachentseva's original criterion, and we define various subsamples of galaxies according to their degree of isolation. Additionally, we sought for the redshifts of the primary and companion galaxies to access the radial dimension and have an accurate three dimensional picture of the surroundings. Finally, we applied our pipeline to triplets, compact groups and clusters and interpret the isolated galaxy population in light of these control samples.

The star formation is known to be affected by the local environment of the galaxies, but the star formation rate also highly depends on the intrinsic interstellar medium features. Disentangling these two effects is still a challenging subject. To address this issue, we observed and gathered photometric data (Hα narrow- & r Gunn broad-band filters) for 200 spiral galaxies from the Catalogue of Isolated Galaxies which are, by definition, in low-density regions. We subsequently studied the Hα morphological aspect of the 45 biggest and less inclined galaxies. Using Fast Fourier Transform techniques, we focus on the modes of the spiral arms, quantify the strength of the bars, and we give the torques between the newly formed stars and the bulk of the optical matter. We interpret the various bar and Hα morphologies observed in terms of the secular evolution experienced by galaxies in isolation. The observed frequency of particular patterns bring constraints

on the lifetime of bars, and their fading time-scales. Through numerical simulations, trying to fit the Hα distributions yields constraints on the star formation law, which is likely to differ from a simple Schmidt law.

Resumen

El papel del entorno en la evolución galáctica aún no se comprende totalmente. Para cuantificar y poner límites al papel del proceso de evolución se debe identificar y estudiar una muestra de galaxias aisladas. El proyecto AMIGA "**A**nálisis del **M**edio **I**nterestelar de **G**alaxias **A**isladas" está llevando a cabo un estudio multifrecuencia de una gran muestra de galaxias aisladas con el fin de estudiar su medio interestelar y la actividad de formación estelar.

Hemos procesado los datos de 950 galaxias del Catálogo de Galaxias Aisladas (Karachentseva 1973) y evaluado su criterio de aislamiento usando un procedimiento automático de clasificación entre estrellas y galaxias (hasta $M_B \approx 17.5$) en campos digitalizados del POSS-I alrededor de cada galaxia aislada. Definimos, comparamos y discutimos varios criterios para cuantificar el grado de aislamiento de estas galaxias: criterio revisado de Karachentseva, cálculo de la densidad superficial local y estimación de la fuerza de marea externa que afecta a cada galaxia. Encontramos galaxias que violan el criterio original de Karachentseva y definimos varias submuestras según su grado de aislamiento. Adicionalmente buscamos el corrimiento al rojo de la galaxia primaria y sus vecinas para acceder a la dimensión radial y obtener una visión tridimensional de los alrededores. Finalmente aplicamos nuestro procedimiento automático a tripletes, grupos compactos y cúmulos de galaxias e interpretamos la población de galaxias aisladas a la luz de estas muestras de control.

Es conocido que la formación estelar se ve afectada por el entorno de las galaxias pero la tasa de formación estelar también depende de las propiedades intrínsecas del medio interestelar. Separar estos dos efectos aún es una tarea dificultosa. Para llevarla a cabo obtuvimos datos fotométricos (filtro Hα estrecho y r Gunn ancho) de 200 galaxias del Catálogo de Galaxias Aisladas que, por definición, se encuentran en regiones de baja densidad de galaxias. Estudiamos la morfología en Hα de las 45 galaxias mayores y menos inclinadas. Usando técnicas de Transformada Rápida de Fourier nos centramos en los modos de los brazos espirales, cuantificando la fuerza de éstos. Obtuvimos los momentos angulares entre las estrellas recién formadas y el

grueso de la materia visible en óptico. Interpretamos las diferentes barras y morfologías Hα observadas en términos de evolución secular experimentada por las galaxias aisladas. La frecuencia observada de patrones particulares impone condiciones sobre los tiempos de vida de las barras, y las escalas de tiempo asociada a su destrución. Usando simulaciones numéricas, cuando intentamos ajustar las distribuciones de morfología Hα obtenemos restricciones en la ley de formación estelar, la cual probablemente difiere de una simple ley de Schmidt.

Résumé

Le rôle de l'environnement sur l'évolution des galaxies n'est pas encore entièrement connu. Pour quantifier et mettre des limites aux rôles joués par les processus externes, on doit identifier un échantillon de galaxies isolées. Le projet AMIGA "Analyse du Milieu interstellaire des galaxies isolées" fait une étude multi-longueur d'ondes d'un grand échantillon de galaxies isolées pour examiner leur milieu interstellaire et l'activité de formation d'étoiles.

Nous avons étudié 950 galaxies en provenance du Catalogue de Galaxies isolées (Karachentseva 1973) et évalué leur isolation au moyen d'une procédure de classification automatique de séparation étoile/galaxie (jusqu'à $M_B = 17.5$) sur de larges champs digitalisés POSS-I autour de chaque galaxie isolée. Nous avons défini, comparé et discuté différents critères pour quantifier le degré d'isolation de ces galaxies, comme la révision du critère de Karachentseva, la densité de surface locale, l'estimation des forces de marées externes affectant chaque galaxie isolée. Nous trouvons des galaxies n'obéissant pas au critère de base de Karachentseva et nous définissons différents sous-échantillons de galaxies selon leurs degrés d'isolation. De plus nous avons cherché les redshifts des galaxies centrales ainsi que ceux de leurs compagnons pour avoir accès à la dimension radiale et ainsi une image en trois dimensions de l'environnement. Enfin, nous avons appliqué nos procédures aux triplets, groupes compacts et amas de galaxies et interprété la population de galaxies isolées à la lumière de ces échantillons de contrôle.

La formation d'étoiles est connue pour être affectée par l'environnement local des galaxies mais le taux de formation d'étoiles dépend aussi grandement des caractéristiques intrinsèques du milieu interstellaire. Séparer ces deux effets reste un problème difficile. Pour solutionner, nous avons observé et compilé des données photométriques pour 200 galaxies spirales issues du Catalogue des Galaxies Isolées qui sont par définition dans des régions de faible densité. Ensuite, nous avons étudié l'aspect de la morphologie en Hα des 45 galaxies les plus grandes et les moins inclinées. En utilisant les techniques de Transformation de Fourier Rapide, nous nous focalisons sur les modes des bras spiraux. Nous quantifions la force des barres et nous donnons les couples entre les étoiles nouvellement formées et la matière op-

tique. Nous interprétons les diverses barres et morphologies Hα observées en termes d'évolution séculaire subie par les galaxies isolées. La fréquence observée des modèles morphologiques particuliers apporte des contraintes sur la durée de vie des barres, et les temps de destruction associés. En utilisant des simulations numériques, l'essai d'adapter les distributions Hα apporte des contraintes sur la loi de formation d'étoiles, qui est susceptible de différer d'une simple loi de Schmidt.

Introduction

The role of the environment on galaxy evolution is still not fully understood. In order to quantify and set limits on the role of nurture one must identify and study an isolated sample of galaxies. The AMIGA project "**A**nalysis of the Interstellar **M**edium of **I**solated **GA**laxies" is doing a multi-wavelength study of a large sample of isolated galaxies in order to examine their interstellar medium and star formation activity.

The thesis presented here is focused on two aspects of this project: in the first part we have quantified the degree of isolation of our sample, and then we have concentrated on an Hα study of a selected subsample of 45 spiral galaxies.

We processed 950 galaxies from the Catalogue of Isolated Galaxies (Karachentseva 1973) and evaluate their isolation using an automated star-galaxy classification procedure (down to $M_B \approx 17.5$) on large digitised POSS-I fields surrounding each isolated galaxy. We define, compare and discuss various criteria to quantify the degree of isolation for these galaxies: e.g. Karachentseva's revised criterion, local surface density computations, estimation of the external tidal force affecting each isolated galaxy. Additionally, we seek for the redshifts of the primary and companion galaxies to access the radial dimension and have a three dimensional picture of the surroundings. Finally, we apply our pipeline to triplets, compact groups and clusters which serve as control samples.

The star formation is known to be affected by the local environment of the galaxies, but the star formation rate also highly depends on the intrinsic interstellar medium features. Disentangling these two effects is still a challenging subject. To address this issue, we observe and gather photometric data (Hα narrow- & r Gunn broad-band filters) for more than 200 spiral galaxies from the Catalogue of Isolated Galaxies which are, by definition, in low-density regions. So we can subsequently study the Hα morphological aspect of the biggest and less inclined galaxies (the fourth part of the Hα sample). Using Fast Fourier Transform techniques, we focussed on the modes of the spiral arms and also on the strength of the bars, looking at the

torques between the newly formed stars and the bulk of the optical matter.

More specifically, the dissertation is articulated as follow:

The first chapter [1] presents an overview on the galaxy topic: an historical introduction on the discovery followed by the main features of galaxies, then the distribution of matter in the Universe is summarised and how this latter distribution could possibly affect the formation and evolution of galaxies.

The second chapter [2] introduces the AMIGA project, framework of the present thesis. First, the refinements done on the original catalogue of isolated galaxies are presented. Second, the ISM multi-wavelength study is evoked.

An exhaustive study [3] of the isolation presents the method used to identify the galaxies around the primary CIG ones, the revision of the Karachentseva's criterion and the new statistical isolation criteria applied to the CIGs: local density and tidal force estimation.

Comparison samples, including triplets, compact groups and clusters of galaxies are used to see how the CIG sample is situated respecting to these higher density samples [4].

Finally, the next chapter [5] uses the redshift information available in the literature, to discuss the validity of our statistical study.

The sixth chapter [6] opens the Hα analysis. It presents the issue of the SFR dependency on environment and our sample of isolated spiral galaxies, which aimed to be taken as a reference to interpret SFR in denser environments.

We observed and gathered Hα data [7] for more than 200 CIG galaxies. A typical reduction procedure is shown for one galaxy.

The last Hα chapter [8] focuses on the 45 biggest and less inclined galaxies observed for which we developed a study to estimate the torques between the newly formed stars and the bulk of the optical matter.

The appendices gather various tables [A], reduction scripts [B] and numerical simulations [C].

Chapter 1

Overview

Contents

1.1 Historical background

At the end of the XIXth century, the extension of the Universe was generally assimilated to the one of our galaxy, the *Milky Way*, for which the astronomers could calculate the shape and the dimensions. At the same time, some of them were wondering about the nature of the nebulae visible in the sky. Already, in 1781, some 100 of these nebulae had been gathered in a catalogue by Messier. In particular, some observations had suggested that these nebulae could be other gathering of stars, similar to our galaxy, "*island-universes*" as imagined by the philosopher Emmanuel Kant at the same epoch.

The debate began accentuated about the nature and distance of these objects. From 1898, Keeler photographied some of the already catalogued nebulae and discovered many thousands of new ones. He also made the surprising discovery that more than half of all the nebulae were spiral in form. Since 1911, at the Lowell observatory, the astronomer Slipher conducted spectrographic investigations of spiral nebulae and showed that they were animated by high velocities (Slipher 1911a,b, 1917); these observations strengthened the theory that spiral nebulae were stellar systems (like the Milky Way itself) seen at great distances. Edwin Hubble confirmed this view in the twenties, showing that the brightest of these spiral nebulae, *Andromeda*, was very outside our own galaxy. Hubble (1929) also found a linear relation between distance and apparent radial velocity among Extra-Galactic Nebulae (see Fig. 1.1). Hence, astronomers understood that the Universe was vaster than the Milky Way, and was inhabited by unnumbered other galaxies.

Actually, a galaxy is a gravitationally-bound collection of stars, with dust and gas. A typical spiral galaxy such as the Milky Way has a mass of about 10^{11} solar masses. All the stars in our galaxy are not identical. Some are old, not very massive and not very bright. Mainly cold and red, they are distributed in our galaxy in a halo more or less spherical. On the other hand, young and blue stars are distributed within a thin disk where they draw spiral arms. The diameter of the disk is 30 kpc with a width of the order of 1 kpc.

The interstellar gas only represents a weak fraction of the total mass of the galaxies, the amount is about 10% in spiral galaxies. Nevertheless, it plays a major role in the formation and evolution of galaxies: the stars form from this gas. This gas is essentially constituted by Hydrogen, in the atomic, molecular or ionised state, mixed with Helium (25% in mass) and traces of other elements.

In the galaxies, the loci of stars and gas draw characteristic features: the galaxies were classified for the first time in various types following criteria

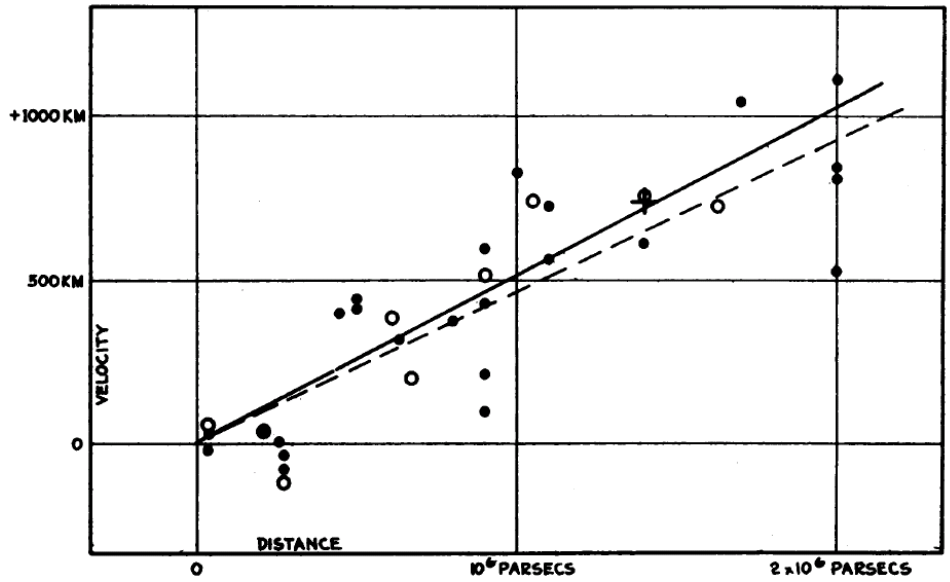

Figure 1.1: Hubble's velocity-distance relation.

essentially based on morphology.

1.2 The morphologies of galaxies

Hubble (1936), in the *Realm of the Nebulae*, classifies galaxies following their optical morphology (see Fig. 1.2). There are 3 fundamental categories: *spirals* amount $\sim 70\%$ of galaxies, *ellipticals* about 10% and *lenticulars* represent $\sim 20\%$, although these proportions can widely be sensitive to the environment.

Spiral galaxies are essentially made up by two major components: a flat, large disk gathering billions of bright stars, where one can sometimes see spiral arms (and often other structures as bars or rings) and in the centre, an ellipsoidal bulge. The disk also contains a lot of gas from which new stars are forming, while the bulge concentrates an older stellar population without interstellar matter. Spirals are rotating around their disk axis: stars within the disk are orbiting the galactic centre in nearly circular orbits.

Elliptical galaxies are named after their appearance in projection on the sky, but have a three-dimensional structure (i.e. an ellipsoid, with three axes of symmetry). They contain very little dust and gas and, as a consequence, only old stars dispatching up into the ellipsoid. Their dynamics also differ from the spirals: they do not rotate as a whole, the stars have velocities randomly distributed. Intermediate types are classified by the degrees of ellipticity observed in the galaxy.

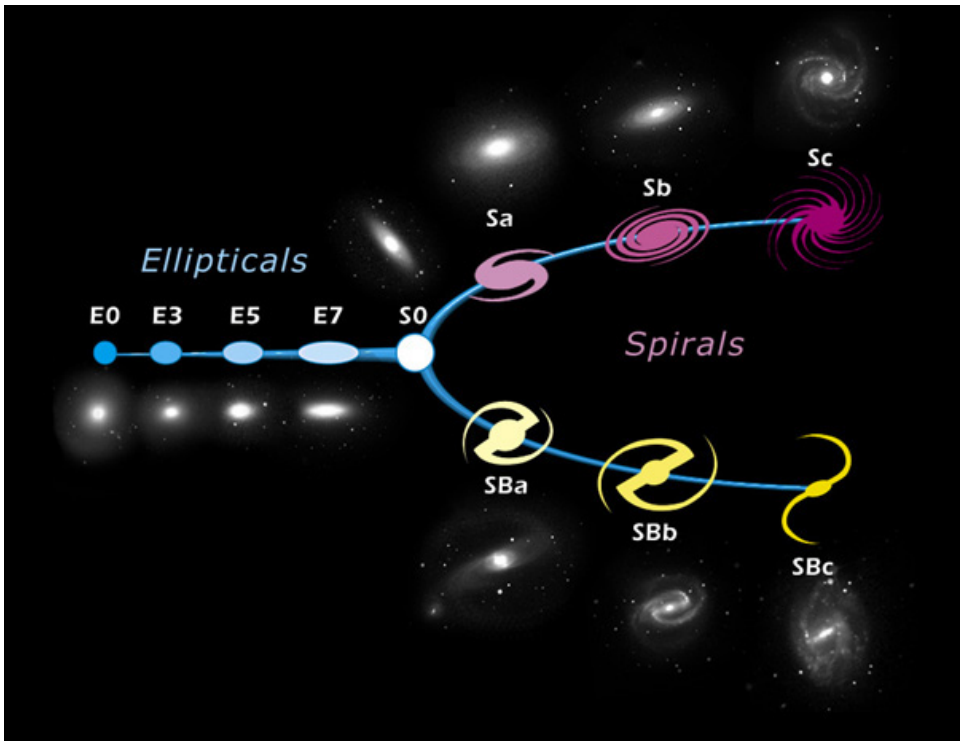

Figure 1.2: Hubble's morphological classification (kindly from the University of Manitoba).

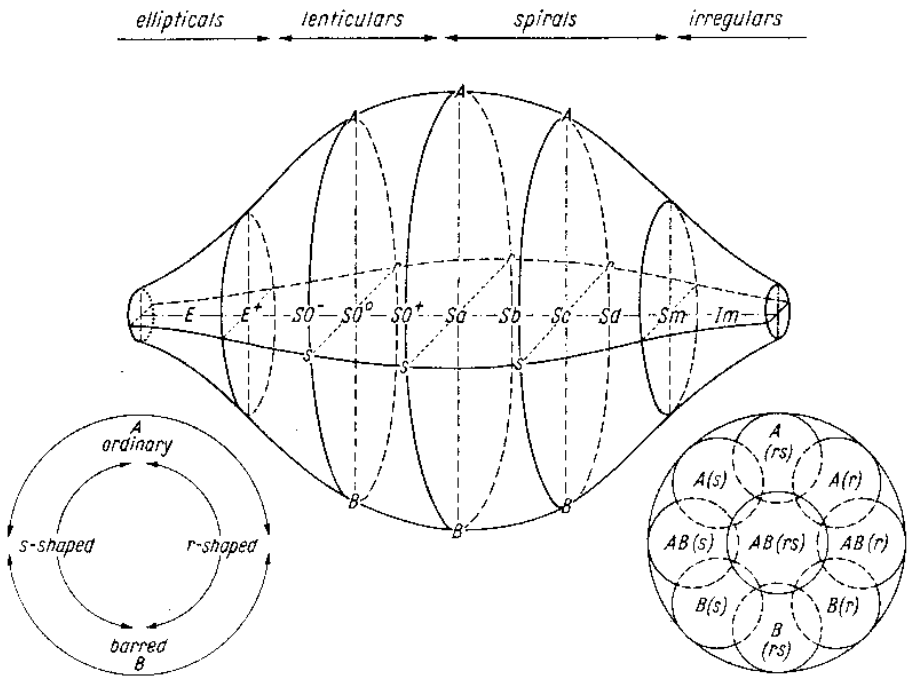

Figure 1.3: De Vaucouleurs' morphological classification.

Lenticulars (also called S0) have intermediate properties between spirals and ellipticals. Lenticular galaxies are composed by a spherical central bulge and by a flattened outer disk, allowing the presence of a bar but without spiral arms. Their interstellar medium is quite poor.

De Vaucouleurs (1959) refined the pioneering Hubble classification (see Fig. 1.3) to include mixed types and features such as inner rings, intermediate bar strength, compactness, ... On the Hubble scheme, de Vaucouleurs also added irregular galaxies, the dwarves and the giants, and active galaxies, which nuclei emit huge quantities of energy in other ways than in the form of stars.

Along the Hubble sequence, the link between these categories is still unclear but there are general trends within the Hubble sequence, from Sd to E: increasing bulge-to-disk luminosity ratio, increasing stellar age, decreasing fractional gas content, decreasing ongoing star formation. For a review describing the dependency of the fundamental properties of the galaxies along the Hubble sequence, please see Roberts & Haynes (1994). Did the E have a SF in an early phase of their evolution? Are spirals and ellipticals generated in different conditions? Or do the latter result from the evolution of the former? At least in some cases, the merging of two spirals lead to the

formation of a giant elliptical. Is it a general feature?

1.3 The distribution of matter in the Universe

The Andromeda galaxy was the first neighbour of the Milky Way discovered. Our neighbourhood gathers, under the name of *Local Group*, a small group of galaxies: our galaxy (the Milky Way), Andromeda and about 15 smaller galaxies.

Nowadays, large surveys reveal that galaxies are not randomly distributed but gathered in groups and clusters. The Local Group is the nearest example. Beyond, the Virgo cluster, located at about 10 Mpc, is richer, although quite poor compared to the average of the clusters. Lots of clusters exist beyond. The nearest ones have been catalogued by Abell (1958).

Matter, in the nearest tens of megaparsecs, draws a larger structure, the *Local Supercluster*. Also known as the Virgo supercluster, it contains eleven clusters along with groups and isolated galaxies. Its shape is flat, about 1 Mpc thick. The distribution of galaxies or clusters is not regular: at large scales, superclusters are the rule. More or less lengthened and flattened, as ours, with a typical scale of about 20 megaparsecs, they seemed linked by immense bridges of matter.

If clusters and superclusters appear as condensations of matter at very large scales, reciprocally, huge zones deprived of matter also exist. An immense void has been detected in the Boötes constellation, at about 150 Mpc from us, with a size of about 30 Mpc (Kirshner et al. 1981). Such voids seem common, at these or smaller scales. Hoyle & Vogeley (2004) presented an analysis of voids in the 2dF Galaxy Redshift Survey: they detected 289 voids with radii larger than 10 h^{-1} Mpc[1]. These voids filled 40% of the total volume of the survey and contain 5% of all galaxies in the sample (see Fig. 1.4); these results are consistent with similar studies done on voids in the SDSS (Rojas et al. 2004, 2005).

1.4 Influence of the environment

Decades ago, a debate about the influence of the environment on the formation and evolution of galaxies began:

Oemler (1974), in a pioneering work, studied the properties of clusters of galaxies, identifying three main classes. The first class is spiral-rich, the second one consists of spiral-poor clusters dominated by S0 galaxies, and clusters prevailed by central supergiant galaxies (cD) with a complete absence of spirals in their cores constitute the third class. The -rich, spiral-poor sequence could be interpreted as a progression in dynamical evolution,

[1] Hubble's constant can be parametrised as $H_0 = 100\,h$ km s^{-1} Mpc^{-1}.

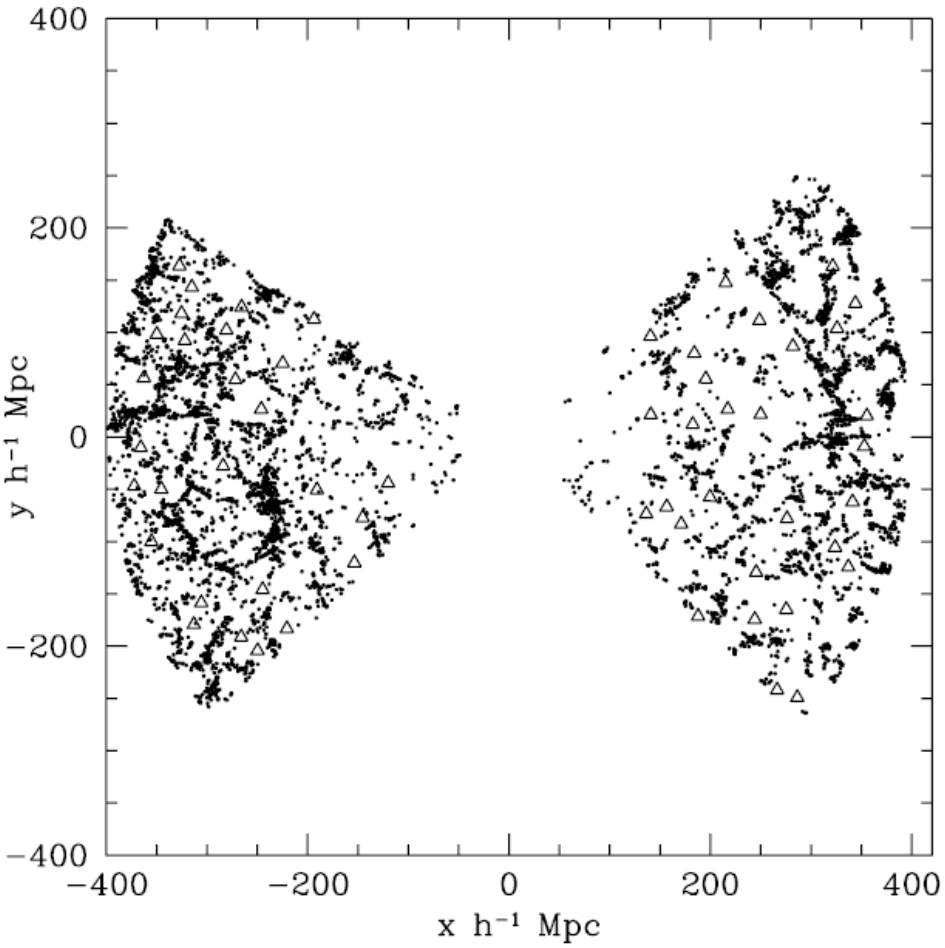

Figure 1.4: Distribution of wall galaxies (*circles*) and the centres of voids (*triangles*) in thin (1°) slices of the North and South Galactic Poles (from Hoyle & Vogeley 2004).

but the cD clusters may represent an intrinsically different archetype of clusters.

A few years later, Dressler (1980) found a strong relationship between the density and the morphological type of $\sim$ 6000 galaxies distributed among 55 rich clusters in the Local Universe (z$\leq$0.06). Figure 1.5 shows the fraction of elliptical, S0 and spiral+irregular galaxies as a function of the log of the projected density, in galaxies Mpc^{-2}. On the very left-hand, the location of the field galaxies (combination of isolated galaxies and loose groups) is shown. Dressler (1980) also find a trend of increasing luminosity of the spheroidal component with increasing local density.

Dressler et al. (1997) confirmed the validity of the morphology-density relation at intermediate redshifts (z$\sim$0.5), though with a lower fraction of lenticular galaxies, suggesting that a fraction of spiral galaxies could have been converted into S0 at a recent epoch.

Postman & Geller (1984) extended the morphology-density relation to groups.

Rojas et al. (2004) identified void galaxies in the SDSS and found that they are bluer than wall galaxies of the same intrinsic brightness: they demonstrated that the difference in colour could not be explained by the morphology-density relation.

Hence, the situation is still not fully understood, especially for the galaxies in low density environments. In this thesis, we will identify a well defined sample of strongly isolated galaxies (based on the Catalogue of isolated galaxies). In a second part, we will characterise the Hα properties of some of the most isolated galaxies, focussing on the different cycles experienced by the bars of these galaxies.

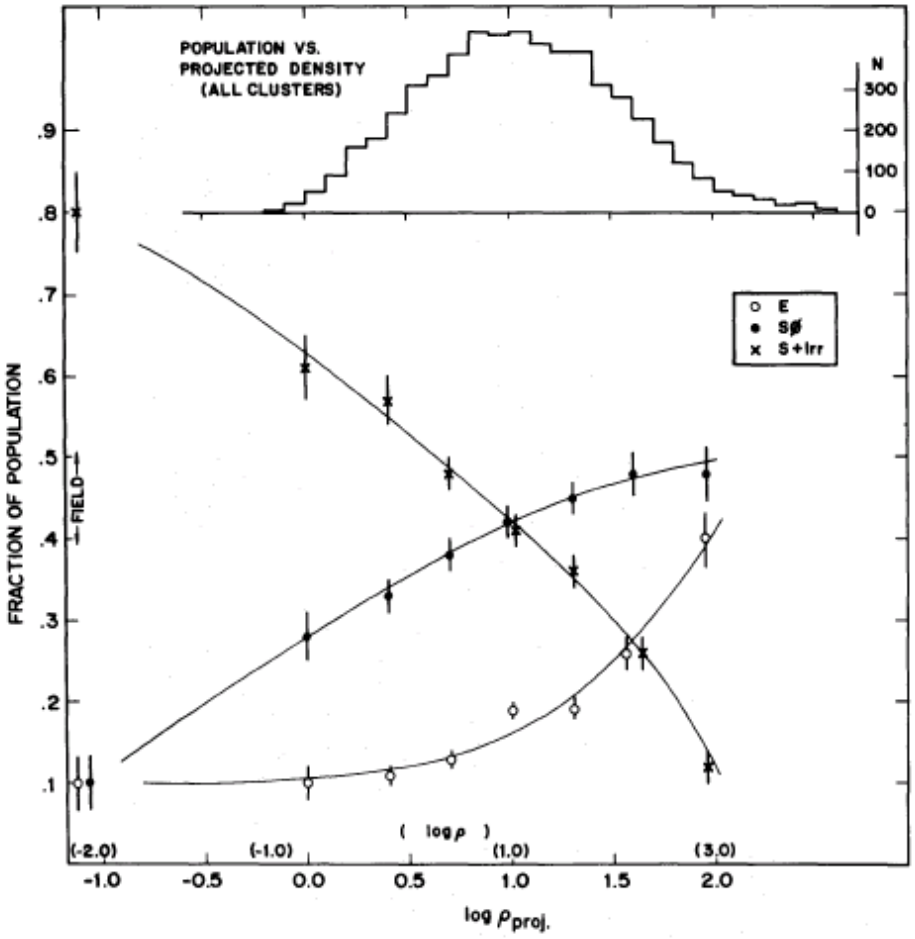

Figure 1.5: Morphology - density relation.

Chapter 2

Introduction to the AMIGA Project

Contents

2.1 Introduction

The evolutionary history of galaxies is thought to be strongly conditioned by the environment. Evidence has emerged for interaction-induced emission enhancements (e.g. Sulentic 1976; Larson & Tinsley 1978; Joseph & Wright 1985; Bushouse 1987; Xu & Sulentic 1991) and interaction-driven secular evolutionary effects (e.g. Moore et al. 1996; Verdes-Montenegro et al. 2001b). This includes properties like stellar and gaseous content, kinematics, mass distribution or star formation activity. The observational evidence is sometimes weak or unclear.

For instance, there is a large incertitude concerning the efficacy of interactions in the triggering of star formation and, still, no law is really well established, which could link the local density of gas, or its velocity dispersion, to the star formation rate (SFR). Globally in a given galaxy, one of the best relation seems to be the Schmidt law (Kennicutt 1998), linking the available quantity of gas (essentially the HI reserve) to the rate of stars newly formed, but lots of exceptions are observed to this relation, showing that others parameters have to be taken into account.

Part of the difficulty lies in the confusion between the roles of one-on-one interactions vs. more general correlations with average galaxy environmental density. Many of the uncertainties, both of the amplitude of enhancements and the connection between environment and parameters, reflect a lack of suitable control samples to which interacting sample properties can be compared. Ideally this would involve samples of isolated galaxies.

The most common reference or control samples found in the literature can be described as either "field" or "normal". The former can refer to the most isolated galaxies while the latter refer to galaxies which show none of the generally accepted signs of interaction-induced activity. A field sample (e.g. Kennicutt & Kent 1983) might include any galaxy not belonging to a cluster, so galaxies in pairs, triplets and loose/compact groups would not necessarily be excluded. Normal galaxy samples would be defined in terms of specific parameters such as HI content (Boselli et al. 2001) or a specified level of nuclear activity. Study of a selected quantity as a function of the environment is then one way to quantify the level of environmentally induced activity.

The alternative approach involves sample selection using an isolation criterion. Studies of isolated galaxies usually involve from 10s to 100-200 objects (e.g. Huchra & Thuan 1977; Vettolani et al. 1986; Márquez & Moles 1999; Márquez et al. 2000; Colbert et al. 2001; Pisano et al. 2002; Varela et al. 2004). The largest samples of isolated galaxies in the literature involve, in most cases, monochromatic observations of subsamples from the Catalogue of Isolated Galaxies CIG: (Karachentseva 1973) (Adams et al. 1980; Haynes & Giovanelli 1980; Sulentic 1989; Young et al. 1986; Xu & Sulentic

1991; Perea et al. 1997; Toledo et al. 1999; Sauty et al. 2003).

Previous work suggests that small samples of isolated galaxies have limited statistical value. Ideally we seek a sample large enough to isolate a significant population of the most isolated galaxies.

This motivated us to use the CIG as the basis for a large, well-defined and statistically significant multiwavelength database that can serve as a comparison template for the study of galaxies in denser environments. CIG galaxies were selected to be free of equal mass perturbers but hierarchical pairs and groups could not be removed without reducing the sample to negligible size. A large sample like CIG can be refined and quantified in terms of degrees of isolation. It can then be correlated with multiwavelength interstellar medium (ISM) properties. The result can be a sample large enough to characterize the low density tail of the two-point correlation function.

This constitutes the AMIGA **A**nalysis of the Interstellar **M**edium of **I**solated **GA**laxies -**AMIGA**- (Verdes-Montenegro et al. 2001a, 2002, 2004, 2005). In particular, we are building a multi-wavelength database to compare and discuss the properties of different phases of the ISM (cf. section 2.4). Our catalogue of galaxies is based on the Catalogue of Isolated Galaxies (Karachentseva 1973) and the refinements we have done so far are presented in section 2.2.

2.2 The Catalogue of Isolated Galaxies

Karachentseva (1973) compiled the Catalogue of Isolated Galaxies (CIG, hereafter) which includes 1051 objects. All of the CIG objects are found in the Catalogue of Galaxies and Clusters of Galaxies (Zwicky et al. 1968) with $m_{\rm pg} < 15.7$ and $\delta > -3°$, $\sim$3% of the CGCG).

The catalogue, built in 1973, could now be improved due to the better material available, including the digitized sky surveys (POSS-I and POSS-II). The sample is large with 1050 galaxies (one object, CIG 0781, was a globular cluster). This means that after refinement we will still be left with a statistically useful sample of several hundred galaxies. We refine the pioneering CIG on several aspects, the better accuracy on the positions is presented in the subsection 2.2.1, the collection of recession velocities in subsection 2.2.2 and the morphological identification in subsection 2.2.3. The revision of the isolation will be detailed in Chapters 3, 4 & 5, since it constitutes one of the goals of this thesis.

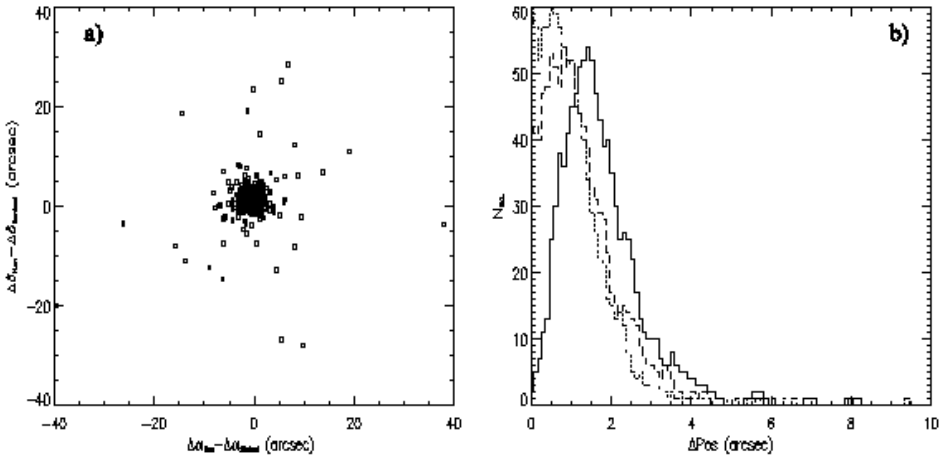

Figure 2.1: **a)** Differences between the measured positions and those retrieved from SIMBAD for the CIG galaxies. **b)** Histogram of the difference between the new positions and the SIMBAD positions for the α (*dotted line*), δ (*dashed line*) coordinates and the total distance (*solid line*) in arcsec. The plotted range is restricted to 10" for clarity of the plot.

2.2.1 Positions

This part is mainly carried out by
Stephane Leon & Lourdes Verdes-Montenegro
on behalf of the AMIGA project.

Leon & Verdes-Montenegro (2003) revised the positions for all the CIG galaxies comparing CIG positions in the SIMBAD database and the Updated Zwicky Catalogue (UZC, Falco et al. 1999). They found differences of up to several tens of arcsec for some galaxies, large enough to make accurate telescope pointings or cross correlations with on-line databases difficult. This motivated them to systematically revise all of the CIG positions using SExtractor on the images of the digitized sky surveys. The differences found between old and new positions reached 38", with a mean difference of about 2.5" (see Fig. 2.1). They provided new positions with uncertainty of the order of 1" using SExtractor (Bertin & Arnouts 1996) on DSS images, checking visually the results (see Fig. 2.2).

2.2.2 Redshifts and distances

This part is mainly carried out by
Lourdes Verdes-Montenegro & Jose Sabater Montes
on behalf of the AMIGA project.

Publications to date report distances for 476 galaxies (Xu & Sulentic

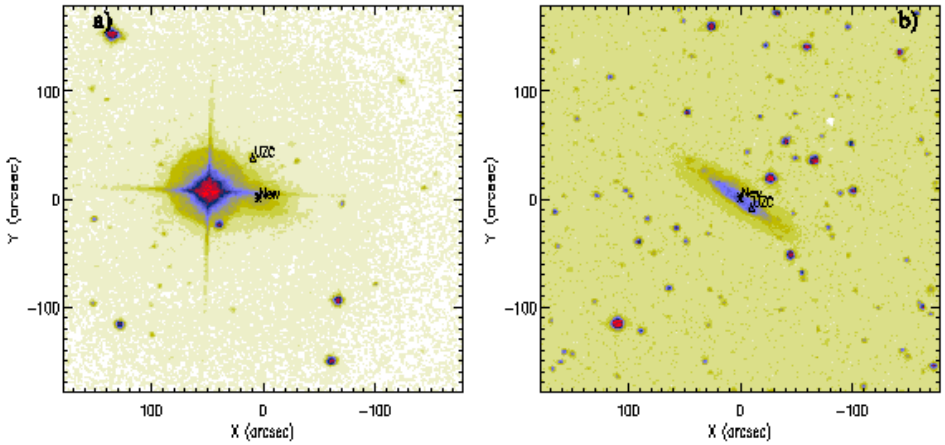

Figure 2.2: DSS images of the **a)** CIG 0402 field, where a bright star is superposed on the galaxy, and **b)** CIG 0828 field. The *stars* indicate the newly calculated positions, whereas the *triangles* correspond to the UZC positions.

1991). We retrieved distances for 574 additional galaxies, after compilation from 41 references, as well as from our own observations (Verdes-Montenegro et al. 2005). Figure 2.3 shows the distribution of the recession velocities of 988 CIG galaxies (there are still missing the redshifts for 62 CIGs). The mean recession velocity is 6624 km s^{-1} (z∼0.022): the catalogue samples the Local Universe.

The CIG redshift distribution re-enforces the evidence for a bimodal structure seen earlier in smaller samples. The peaks at redshift near 1500 and 6000 km s^{-1} correspond respectively to galaxies in the local supercluster and those in more distant large-scale components (particularly Perseus-Pisces). The two peaks in the redshift distribution are superimposed on 50% or more of the sample that is distributed in a much more homogeneous way. The CIG probably represents the most homogeneous local field example that has ever been compiled.

Redshift distances were derived for all galaxies with V $>$ 1000 km s^{-1} and are expressed as $D = V_{3K}/H_0$ where V_{3K} is the velocity after the 3K correction and assuming $H_0 = 75$ km s^{-1} Mpc^{-1}. 3K corrected velocities are computed in the reference frame defined by the 3K cosmological background radiation. They are corrected for local velocity inhomogeneities due to the Local Group and Virgo Cluster. The velocity conversion is made with the standard correction as defined in (Courteau & van den Bergh 1999). The velocity and apex directions of the Sun relative to the comoving frame have been derived from an analysis of the FIRAS data (Fixsen et al. 1996) with V_{apex} = 371 km s^{-1} and (l_{apex}, b_{apex}) = (264.14, 48.26). Redshift-

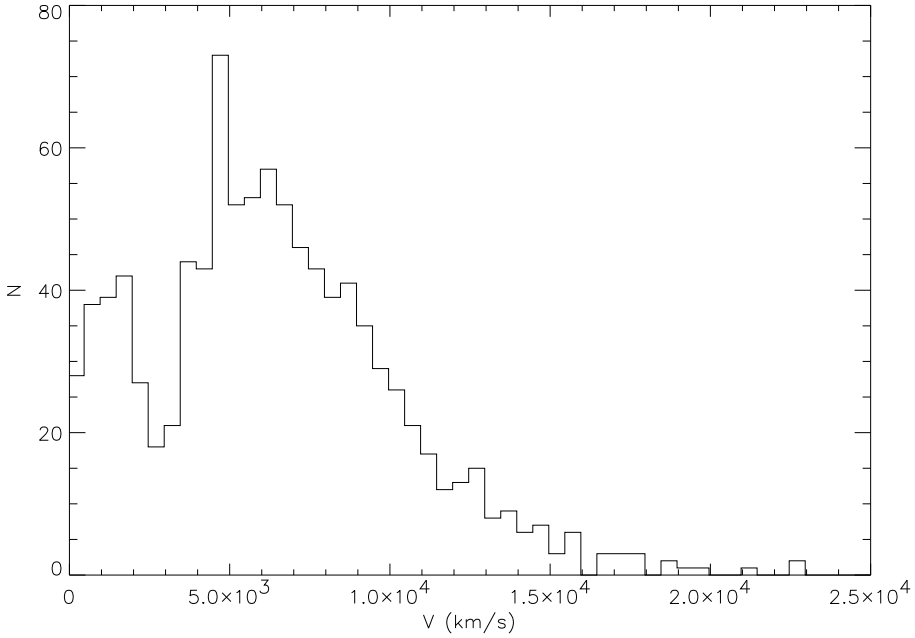

Figure 2.3: Histogram of the CIG recession velocities.

independent distance estimates and references are provided for galaxies with $V < 1000$ km s^{-1}.

2.2.3 Morphologies

This part is mainly carried out by
Jack Sulentic & Gilles Bergond
on behalf of the AMIGA project.

Morphological classification available for AMIGA galaxies from the literature are not uniform, and even contradictory for the most part. So we downloaded POSS-II images for 80% of the sample for which spatial resolution was sufficient to achieve a new classification. We obtained CCD images for the remaining 20% with the 1.5m telescope at the Sierra Nevada Observatory. An analysis shows that many of the galaxies classified as early-type display a spiral structure with a predominance of Sc galaxies (Sulentic et al. 2005). This most isolated sample of galaxies in the local Universe is dominated by two populations: 1) 82% spirals (Sa–Sd) with the bulk being luminous systems with small bulges (63% between types Sb–Sc) and 2) a significant population of early-type E–S0 galaxies (14%). The derived types will be used in order to optically characterise the CIG sample (see sect. 2.3).

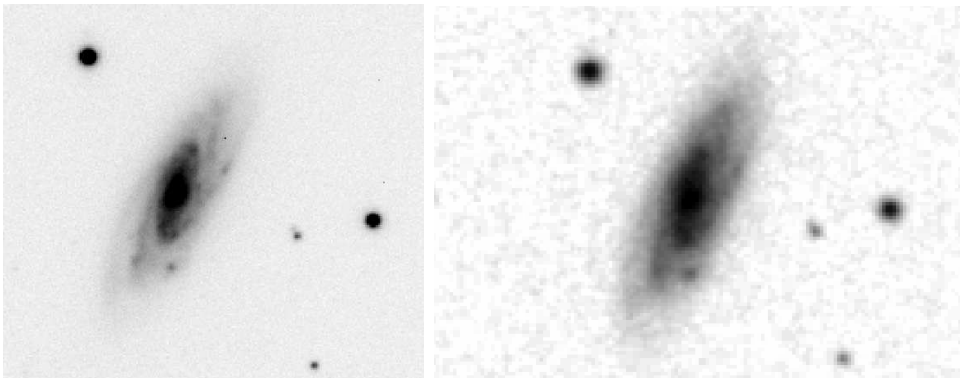

Figure 2.4: **Left:** OSN rGunn 12 min., **Right:** POSS II red.

2.2.4 Isolation

The revision of the isolation for 950 CIGs is presented in chapters 3, 4 & 5.

2.3 Optical characterisation of the sample

This part is mainly carried out by
Lourdes Verdes-Montenegro
on behalf of the AMIGA project.

The optical emission (L_B, in the blue band) traces the stellar content of a galaxy, hence we first performed an optical characterization of our sample. Verdes-Montenegro et al. (2005) inferred L_B for each galaxy with known recession velocity, compiling optical magnitudes while applying required corrections. This magnitude was supposed to be used only as a parameter in the multi-wavelength correlations, but we found of interest to derive the optical luminosity function of the sample. Using the V/V_m Schmidt test, Verdes-Montenegro et al. (2005) find the CIG to be 80-95% complete down to $m_{zw} = 15.0$ (see also Xu & Sulentic 1991). Its 2D distribution is reasonably homogeneous; in the redshift distribution, we again find evidence that 50% or more of the sample shows a quasi-homogeneous redshift distribution.

The CIG samples a large enough volume of space to allow us to sample the majority of the optical luminosity function (OLF). Galaxies with a recession velocity less than 1,000 km s^{-1} include the most isolated nearby dwarfs. Significant sampling at and beyond 10,000 km s^{-1} allows us to also sample the extreme bright end of the OLF. We have calculated the OLF which we compare with other recent estimates of the OLF for a variety of environments. Our derivation of the CIG OLF is consistent with other studies of the OLF for lower density environments, re-enforcing the idea that CIG OLF is representative of the lower density parts of the galaxy environment. This comparison via the Schechter parameter formalization

shows that: 1) M* increases with galaxy surface density on the sky and 2) α shows a weaker tendency to do the same. Care must be taken with the local supercluster contribution to the CIG because it samples the OLF to much lower luminosities than the rest of the sample. In the Schechter formalism, M* represents the absolute magnitude of the galaxies which suppose a turn-off in the distribution and α is the slope of the faint-end distribution.

2.4 ISM multi-wavelength study

There are numerous works that study the effect of interactions on the ISM. Most of them have not used strictly isolated galaxies as reference samples, and when it happened they were concentrated on few (usually no more than 2) components of the ISM. In the following sub-sections we sum up their main results.

2.4.1 Hα

A study of the Hα emission of a subsample of CIG galaxies is presented in Chapters 6, 7 & 8.

2.4.2 Far infrared

This part is mainly carried out by
Ute Lisenfeld & Lourdes Verdes-Montenegro
on behalf of the AMIGA project.

L_{FIR} is the thermal emission re-radiated by dust grains, previously warmed up by UV radiation from young stars. Most of the studies about FIR emission of interacting galaxies are skewed towards bright galaxies, although it is unanimously recognised that they present an higher infrared emission (Young & Scoville 1991; Braine & Combes 1993; Young et al. 1996; Solomon et al. 1997).

Xu & Sulentic (1991) studied 528 pairs from the Catalogue of isolated pairs of galaxies (Karachentsev 1972, 1980) covering a large luminosity range, and 295 galaxies from the CIG as a reference sample, and find out that late type galaxies in pairs show a higher infrared emission compared with the isolated galaxies and that the pairs made with two spirals have a higher L_{FIR}/L_B ratio. Nevertheless, this study carries the problem, as shown by the authors, that the pairs sample is deeper than the isolated one, which clearly shows that the excess could be due to the brightest galaxies. Lisenfeld et al. (2005) found a non-linear relation between L_{FIR} and L_B (see

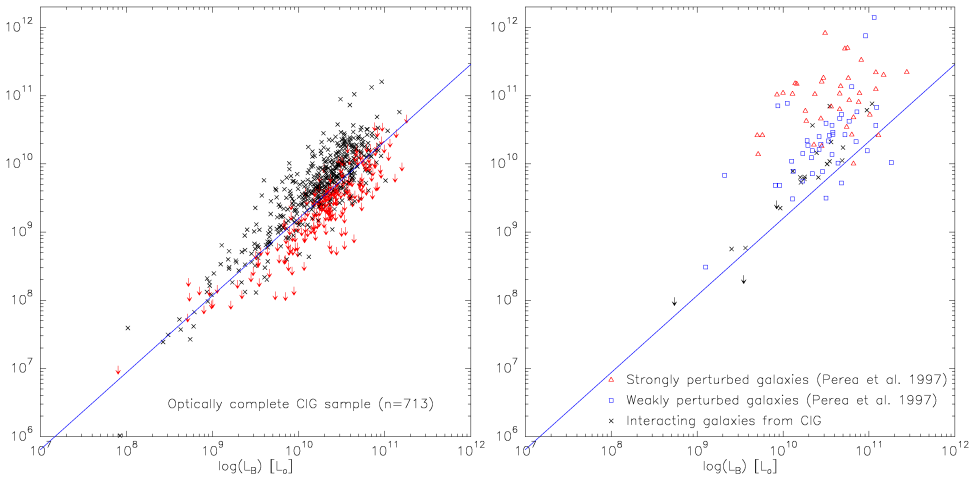

Figure 2.5: The relation between the FIR and blue luminosity for an optically complete subsample of the CIG, excluding 23 interacting CIG galaxies **(left)** and for different samples of interacting galaxies **(right)**. The line is in both panels the regression found for the CIG (eq. 2.1) (from Lisenfeld et al. 2005).

Figure 2.5):

$$\log(L_{FIR}) = (1.13 \pm 0.03)\log(L_B) - (2.1 \pm 0.03) \tag{2.1}$$

2.4.3 Radio-continuum

This part is mainly carried out by
Stephane Leon & Jose Sabater Montes
on behalf of the AMIGA project.

Believed to be principally synchrotron radiation produced by relativistically accelerated electrons by supernovae explosions (Lequeux 1971), the radio-continuum emission is directly proportional to the supernovae formation rate (Xu et al. 1994). This idea is reinforced by the narrow correlation between radio luminosity and FIR for spiral galaxies, indicating that both are produced by the same stars (Lisenfeld et al. 1996a). This relation is quite robust and also valid for galaxies spanning a wide range in luminosity, including starburst galaxies (Lisenfeld et al. 1996b).

The effect of the environment on the radio-FIR correlation is still not fully understood. Some studies indicate that there exist a small excess of radio emission for galaxies in clusters (Menon 1991; Niklas et al. 1995) although other works suggest that there is no clue that the interaction influence the correlation (Niklas 1997). However, the correlation between nuclear activity and environment is not fully clarified. Dultzin-Hacyan et al. (1999)

found that the interactions with a companion would produce the central activity, but the environment is likely to play a more complex role for the production of the central activity (Schmitt 2001). Thus, the study of radio galaxies with the IRAM-30m (Leon et al. 2001) would suggest that minor mergers are more important to feed the central black hole.

2.4.4 Atomic gas

This part is mainly carried out by
Daniel Espada
on behalf of the AMIGA project.

The atomic gas is a light component of the ISM dominating the gas in late type galaxies, and extending to the double of the optical disk (Cayatte et al. 1994). It makes the HI a very sensible tracer for the interaction. Haynes & Giovanelli (1984) characterise the HI content of a sample of 324 CIG galaxies as a function of the morphological type and the luminosity or the optical diameter, sample which will serve as a reference for further studies of the HI content in different environments. Spiral galaxies in clusters present a deficiency in HI, especially the ones very near the centre of the cluster, where the hot intra-cluster medium emitting X rays dominates (van Gorkom 1996). As well, compact groups show a level of deficiency as high as 90%, although lots of them are within the error bars of the relations found by (Haynes & Giovanelli 1984) reaching 0.5 mag (Verdes-Montenegro et al. 2001b). On the other hand, Zasov & Sulentic (1994) studied 50 E+S pairs and the comparison with the CIG sample does not show any deviation from the normality in the spiral of the pairs, though an increase of the star formation.

The shape of the HI profiles is a powerful tool to characterise the HI distribution in a given galaxy, and the level of perturbation (Espada et al. 2005). It was used by Sulentic & Arp (1983) as a diagnostic in a sample of pair galaxies, groups, also CIG, or by Richter & Sancisi (1994) connecting the predominance of a spiral arm (lopsidedness) with asymmetries in the profile of the 21cm line.

2.4.5 Molecular gas

This part is mainly carried out by
Ute Lisenfeld & Daniel Espada
on behalf of the AMIGA project.

The lines emitted by simple molecules, excited by collisions and going back to their fundamental state correspond to weak energy transitions. The CO molecule was first observed in 1970. It is quite abundant and its presence is linked to that of H_2: collisions between H_2 and CO molecules excite the latter to an excited state which corresponds to 2.6 mm. The H_2 molecule

is more abundant but hard to observe in radio spectroscopy: the spectrum of symmetric molecules is far poorer than the one of asymmetric molecules.

It was claimed that interactions could enhance the molecular content of the galaxies, but this is skewed towards the brightest galaxies in FIR (Braine & Combes 1993; Combes et al. 1994), and on the ratio $M(H_2)/L_B$ which augment with L_B so gets higher values for the brightest galaxies. When this effect is removed (Perea et al. 1997; Verdes-Montenegro et al. 1998; Leon et al. 1998), the molecular gas content of the samples seems indistinguishable from the isolated one.

2.5 Database

This part is mainly carried out by
EMILIO GARCIA
on behalf of the AMIGA project.

All the refinements done by the AMIGA project on the CIG are available at this web site: www.amiga.iaa.es/AMIGA.html/. As well, the ISM multi-wavelength data will become public by means of the web database (based on MySQL) via a simple and efficient interface.

To access the AMIGA catalogue, two approaches are possible: using a web browser or directly from a terminal using scripts. Queries could be made entering the number of the CIG or any other identifiant (CGCG, NGC, UGC, ...) or entering parameters. The parameters could be applied separately (coordinates, velocities, morphologies, ...) or tangled one with another. The tool "Conesearch" allows to choose an ascension, a declination and a search radius. The user has also the possibility to specify the output options. Finally, XML files containing compatible VO tables will also be produced.

Part I

Isolation

Chapter 3

The isolation study

Contents

3.1 Introduction

It is now generally recognised that the environment experienced by the galaxies during their whole lifetime plays a role perhaps as important as the initial conditions of their formation: the evolutionary history of galaxies is thought to be strongly conditioned by the environment. But the role and the influence of the environment on galaxy evolution are still not fully understood. In order to quantify and set limits on the role of nurture one must identify and study a sample of isolated galaxies. Systematic work on isolated galaxies is needed to separate the influence of the environment and of the initial conditions at formation. The purpose of the coming Chapters is to provide a sample of isolated galaxies, with a well characterised isolation definition.

A debate on the nature of the spatial distribution of galaxies took place in the 1970s: using the covariance function of the distribution of galaxies, Peebles (1974a,b) found no evidence of an initially homogeneous component of the galaxy population and, on the contrary, indorsed the view of hierarchical series of densities. However, studying galaxies brighter than 14^{th} magnitude, Turner & Gott (1975) found two distinct populations, one strongly clustered and a population of "single" galaxies (32%) distributed homogeneously on scales $\leq$ 20 Mpc. But Soneira & Peebles (1977) showed that the previous sample did not constitute a true field population because of artifacts and if such a population exists, it amounted to substantially less than 18% in a catalogue selected by apparent magnitude. Huchra & Thuan (1977) revised the Turner & Gott sample down to a fainter magnitude (15.7 mag.) and found that isolated galaxies could only represent 3.6% of all the galaxies. As well, Vettolani et al. (1986) emphasised that isolated galaxies did not exist in an absolute sense because clustering on large scale dominates in all regions of space (for small z at least).

Studies comparing redshifts of isolated galaxies with redshifts of groups confirmed that isolated galaxies generally belong to groups, but at such large distances from their centres ($\sim$ 4 Mpc) that they have certainly not undergone any physical influence from these groups (Balkowski & Chamaraux 1981). Haynes & Giovanelli (1983) likewise showed that most of the isolated galaxies are outer components of groups or clusters.

Hence, it seems difficult to find a truly isolated population of galaxies, but instead one can have access to regions of very low galaxy density, where the galaxies found reflect properties characterising their formation. For 30 years, a variety of widely different criteria has been used (magnitude limited samples, redshift information used or not, distance to the nearest galaxies different from one definition to the other, etc.), as shown

by the abundant literature: Turner & Gott (1975); Balkowski & Chamaraux (1981); Vettolani et al. (1986); Zaritsky et al. (1993); Aars et al. (2001); Colbert et al. (2001); Pisano et al. (2002); Prada et al. (2003); Márquez & Moles (1996, 1999); Márquez et al. (2002, 2003); Varela et al. (2004). Most of these studies only sample ten to few hundreds of galaxies, which is not sufficient for further statistical significance.

We are constructing a control sample of the most isolated galaxies of the northern sky which will serve as a template in the study of star formation and galaxy evolution in denser environments (Verdes-Montenegro et al. 2001a, 2002, 2004, 2005; Leon & Verdes-Montenegro 2003). The Catalogue of Isolated Galaxies compiled by Karachentseva (1973) has a well defined criterion of isolation and compiles a reasonably large, homogeneous sample ($\sim 10^3$ galaxies) to allow us statistical significance (even for the properties of morphological subtypes).

In this chapter, we study and quantify the environment of the most isolated galaxies of the northern hemisphere, in the local Universe. In section 3.2, we will present the principal features of the CIG and also several revisions and improvements done so far. In section 3.3, we describe in detail our automated pipeline which allows us to infer various parameters (section 3.4) to quantify the surroundings of the isolated galaxies.

3.2 The Catalogue of Isolated Galaxies

3.2.1 Definition

The catalogue is a compilation of information on 1051 objects with apparent magnitude brighter than 15.7 and north declination $> -3°$. Karachentseva visually inspected the Palomar Sky Survey prints, trying to identify those galaxies in the Catalogue of Galaxies and Clusters of Galaxies (CGCG, Zwicky et al. 1968) which have no near neighbours. Primary galaxies with angular major-axis diameter D_p are considered *isolated* if any neighbours with diameters D_i, $D_p/4 \leq D_i \leq 4D_p$ have an apparent angular separation R_{ip}, from the primary galaxy under consideration, greater than $20D_i$:

$$R_{ip} \geq 20 \times D_i$$

$$\frac{1}{4} D_p \leq D_i \leq 4 \times D_p$$

Karachentseva (1980) discussed her isolation criterion and found that 24 galaxies (with known radial velocities) passed the isolation criterion and belong to pairs, groups, or clusters. Other authors (Stocke 1978; Haynes & Giovanelli

1984; Xu & Sulentic 1991) reported that some CIG galaxies are, in fact, members of interacting systems: CIGs 0006, 0007, 0080, 0197, 0247, 0278, 0324, 0347, 0349, 0444, 0469, 0559, 0663, 0781, 0802, 0809, 0819, 0850, 0851, 0853, 0938, 0940, 0946, 1027, 1028.

Adams et al. (1980) and Karachentseva (1986[1]), refined the original isolation criterion by assigning codes:

- Code 0: Isolated according to Karachentseva (902 galaxies);
- Code 1: Marginally isolated (85 galaxies);
- Code 2: Member of a group or cluster (64 galaxies).

Nevertheless, the CIG remains a good starting point to analyse a large sample of isolated galaxies. For instance, for a CIG galaxy with $D_p = 3'$, no neighbour with $D_i = 12'$ may lie within 240' and no companion with $D_i = 0.75'$ may lie within 15'. If one assumes an average $D_p = 25$ kpc for a CIG galaxy and a typical "field" velocity V = 150 km s^{-1} then an approximately equal mass perturber would require $3{\times}10^9$ years to traverse a distance of $20D_i$. All possible effects of a past interaction, on the morphological or dynamical properties or those concerning the enhancement of star formation processes, have been erased at the present time (Márquez & Moles 1996). Because this is a lower limit on the time since the last galaxy-galaxy interaction for a typical-size galaxy in the CIG, these galaxies have apparently been isolated for much, if not all, of their existence (Stocke 1978). This is a quite conservative criterion but it is clear that dwarf companions are not excluded.

Galaxies isolated in space do not necessarily appear isolated in the sky: the CIG is not complete due to the projection effects, but ensures that all the galaxies that have passed through are really isolated. Nevertheless, the sample is still reasonably complete, according to the Schmidt (1968) luminosity volume test which gives $<V/V_m> = 0.42$ (Huchra & Thuan 1977; Xu & Sulentic 1991; Toledo et al. 1999; Verdes-Montenegro et al. 2005).

3.2.2 Is the Milky Way isolated?

The Milky Way is a common spiral galaxy (its mass is about 10^{11} M$_\odot$), with a disk of about 30 kpc in diameter. Hence, all the galaxies which would possibly violate the Karachentseva criterion would have diameters comprised between $\sim$ 7.5 kpc for the smallest and 120 kpc will be the upper

[1]Unpublished documentation supplied with the catalogue by the Centre de Données Astronomiques, Strasbourg.

limit. As the companion galaxies can lie 20 times their diameter away, we would have to check for all the members within 2.4 Mpc. Among the nearby groups of galaxies, only the Sculptor group (1.8 Mpc away) lie inside this limit, the others are all father than 3 Mpc, hence not concerned (M81: 3.1 Mpc; Centaurus: 3.5 Mpc; M101: 7.7 Mpc; M66 + M96: 9.4 Mpc; NGC 1023: 9.5 Mpc; ...). The Sculptor group (1.8 Mpc away) is constituted by six members, NGC 0253 (diameter of 14.4 kpc), the brightest galaxy of the group would not violate the isolation criterion.

Hence, the question of isolation of the Milky Way would involve galaxies of the Local Group (see Fig. 3.1). The table 3.1, data taken from Galactic Astronomy (Binney & Merrifield 1998), shows the Local Group members. Our galaxy's brightest satellite systems are the Magellanic Clouds: the LMC is 49 kpc away and have a diameter of $\sim$ 9.3 kpc: this companion violates the Karachentseva's criterion! The Small Magellanic Cloud has a diameter of about 5.4 kpc and would not be taken into account by the Karachentseva criterion: we see here a limitation of the criterion, already evoked in the previous section.

Also belonging to the local Group but farther away, the Andromeda Galaxy (M31) has an apparent angular major diameter of 190 arcmin., corresponding to about 40 kpc. Its influence would affect the galaxies as far as 800 kpc from it. Hence, since the distance separating the Milky Way from the Andromeda galaxy is about 725 kpc, this latter would also violate the Karachentseva criterion (see Fig. 3.2). On the other hand, the Triangulum galaxy (M33) is about 795 kpc away, and due to its relatively small diameter ($\sim$ 16.2 kpc) would not exert any influence on the Milky Way. This would be true if the system Milky Way-M33 would have been seen in the best case (the line of sight perpendicular to the plane constituted by the two galaxies). If the system is seen from other points of view, the apparent distance separating the two galaxies will become smaller and reach a point where the Milky Way would not any longer appear isolated respectively to M33. This implies that all the galaxies in the CIG catalogue really are isolated but that the catalogue is not 100% complete due to this very strong definition of isolation, depending on apparent 2-dimensions distances.

3.3 The AMIGA revision

Despite the various revisions done by the authors above-cited, we choose to improve the Karachentseva sample in several ways: (1) check in an automated, homogeneous way the isolation of the galaxies (this section), (2) give continuous parameters describing the degree of isolation for the isolated galaxy candidates (next section).

Table 3.1: Local Group members.

Name	Type	Distance(kpc)$_\odot$
M31	Sb	725
Milky Way	Sbc	8
M33	Sc	795
LMC	Irr	49
IC 10	Irr	1250
NGC 6822	Irr	540
M32	dE2	725
NGC 205	dE5	725
SMC	Irr	58
NGC 3109	Irr	1260
NGC 185	dE3	620
IC 1613	Irr	765
NGC 147	dE4	589
Sextans A	Irr	1450
Sextans B	Irr	1300
WLM	Irr	940
Sagittarius	dSph/E7	24
Fornax	dSph/E3	270
Pegasus	Irr	759
Leo I	dSph/E3	270
Leo A	Irr	692
And II	dSph/E3	587
And I	dSph/E0	790
SagDIG	Irr	1150
Antlia	dSph/E3	1150
Sculptor	dSph/E3	78
And III	dSph/E6	790
Leo II	dSph/E0	230
Sextans	dSph/E4	90
Phoenix	Irr	390
LGS 3	Irr	760
Tucana	dSph/E5	900
Carina	dSph/E4	87
Ursa Minor	dSph/E5	69
Draco	dSph/E3	76

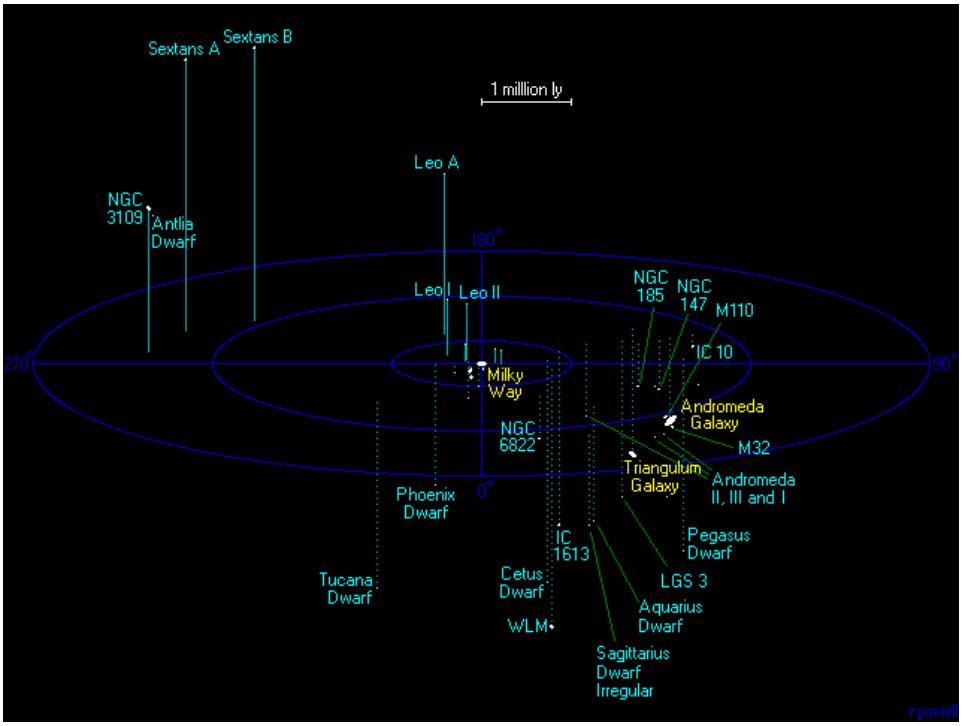

Figure 3.1: Local group *[drawing from this web site]*.

3.3.1 The sample used and revised fields

The radial velocities of the nearest galaxies in the CIG cannot be totally interpreted by the Hubble flow, because of the importance of the local dispersion velocity where galaxies can overcome the expansion on small scales. Also, as pointed out by Stocke (1978) and Haynes & Giovanelli (1984), the area searched for potential companions of the nearby CIG galaxies is spread over a large surface on the sky, which makes the search overwhelmed. To avoid these cases, we removed all the galaxies with radial velocities less than 1500 km s^{-1}, which result of being 101 objects, thus our final sample contains 950 galaxies.

We chose to evaluate the isolation degree in a minimum physical radius of 0.5 Mpc (see Figure 3.3), centred on each CIG galaxy. If we assume a typical "field" velocity of 150 km s^{-1}, it will require about 3×10^9 years for a companion to cross this distance.

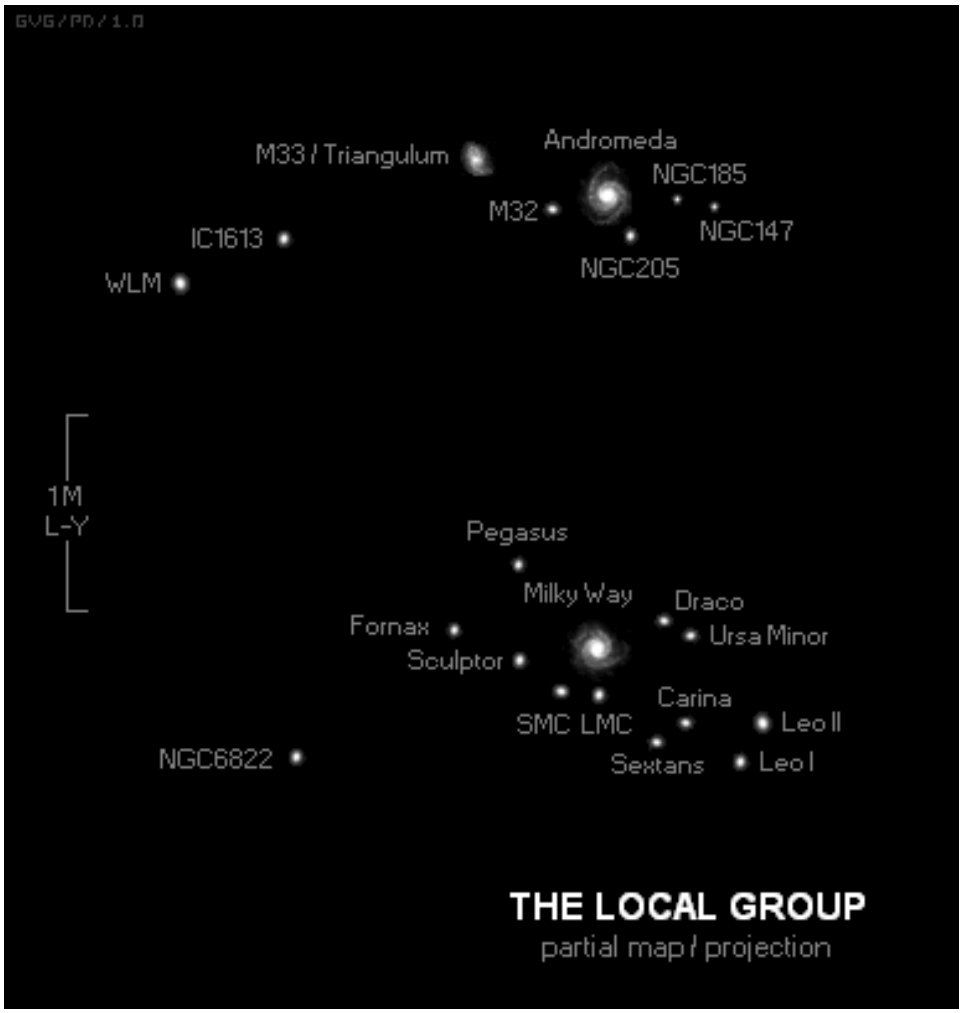

Figure 3.2: Local group *[kindly from Wikipedia]*.

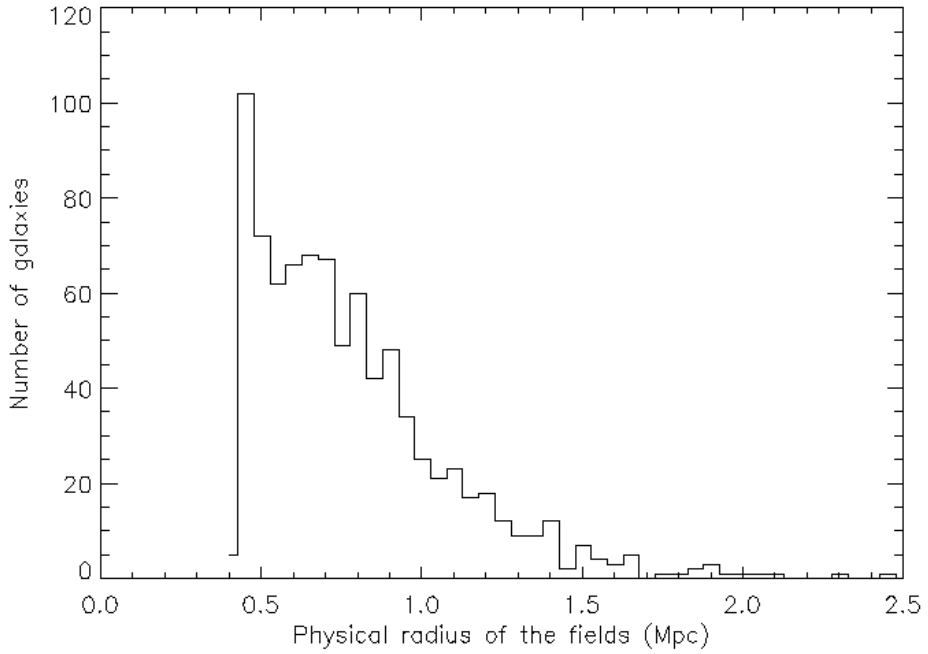

Figure 3.3: Physical radius of the fields inspected for our CIG sample (available velocity for 888 CIGs).

3.3.2 Data analysis

We developed an original method to check the isolation of the CIG galaxies. This work was motivated by the fact that images brighter than $B \approx 17$ are miss-classified at a high rate in present on-line reductions of the all-sky Schmidt surveys. In the following, we describe a method used to reliably identify bright (i.e. $B < 17.5$) galaxies around our CIG fields of interest.

Size of the fields

We performed star/galaxy separation in 55×55 square arcminutes fields centred on each galaxy in the CIG. In order to recover the bright galaxies at high success rate, we reduced bright image classification in our CIG fields using Palomar Observatory Sky Survey (POSS-I E, central wavelength = 6510 Å) images obtained with DSS. We have assembled a software pipeline for producing star-galaxy catalogues in the area around each CIG field. The digital images have a pixel size of 25 microns (1.7 arcsec. per pixel).

We searched the companion galaxies within a minimum physical radius of 0.5 Mpc, centred on each CIG. Due to pipeline capacity and server limits, we could not handle fields larger than $55' \times 55'$. To reach the physical

Table 3.2: 62 unknown CIG redshifts.

CIG	CIG	CIG	CIG	CIG	CIG	CIG
0003	0272	0479	0629	0717	0814	0899
0017	0297	0535	0632	0729	0821	0908
0026	0311	0558	0664	0730	0822	0964
0035	0320	0583	0673	0737	0842	0968
0046	0360	0587	0681	0765	0846	0977
0048	0369	0594	0687	0774	0869	0995
0070	0394	0597	0704	0787	0878	0996
0254	0414	0607	0707	0790	0885	1049
0263	0459	0628	0713	0804	0887	

radius of 0.5 Mpc, the fields larger than $55' \times 55'$ are composed by various $55' \times 55'$ fields, with small strip overlapping between two adjacent fields. We developed a tool to keep only one source when an object was detected more than once on various fields. Below, we gathered CIG galaxies by the number of fields employed:

- **767** galaxies with $55' \times 55'$;
- **134** galaxies with multi-fields 2×2;
- **49** galaxies with multi-fields 3×3.

The 55×55 square minutes fields concerned galaxies with an observed recession velocity greater than 4,687 km s^{-1} (including the 62 galaxies with no velocity data, see Table 3.2); the 2×2 multi-fields correspond to galaxies between 2,343 and 4,687 km s^{-1}; the 3×3 multi-fields to recession velocities lower than 2,343 km s^{-1}.

At high latitude (declination $\gtrsim$ 37 degrees), an issue arises: the coordinate system drastically converges in RA towards the pole. The composition of contiguous fields became very problematic: two fields with the centres shifted by $\sim$ 55 arcmin. were not overlapping properly anymore. We tried to get images directly from the DSS DVDs but the compression level used highly deteriorate the quality of the images and any further star/galaxy separation. As we found no way to get around this matter, we decided to manually pull down the fields, adapting the offsets to obtain the proper overlaps.

The DSS scans come from 6.5 square degrees plates. When our fields reached the edges of the scans, we downloaded bands from the adjacent DSS scans to complete our 55×55 fields.

Detection of the sources

We used SExtractor (Bertin & Arnouts 1996) to detect the sources in the images, with the following parameters: a threshold 3 times higher than the root mean square (RMS) of the background estimation. Before the detection of pixels above the threshold, there was the option of applying a filter. This filter essentially smooths the image, we used a Gaussian convolution with a FWHM of 2 pixels and a typical size of 5 × 5 pixels. Then, all the objects larger than 4 pixels had been detected.

Star/galaxy separation

The images are reduced using AIMTOOL in LMORPHO (Odewahn 1995; Odewahn et al. 1996, 2002), and GUI-driven star/galaxy separation procedure was used to classify detected sources as: STAR, GALAXY or UNKNOWN (for the faint, small extended sources). We performed a star/galaxy separation by using the method of log(star/galaxy area) vs. star/galaxy magnitude – which is shown to work well down to the 17.5 magnitude, as displayed in Fig. 3.4. The galaxies have a lower surface brightness than the stars and in the log(area) vs. magnitude plane, the two classes of objects follow different loci. The stellar locus in logAREA vs. MAG_ISO space was manually located using an interactive GUI approach because the shape and location of this locus changes significantly on different POSS-I Schmidt plates. A typical star/galaxy separation parameter space from a POSS-I E image (CIG 0714). All the points that lie above the curve defined by the BLUE points were classified as GALAXY. The points below this curve (which is described with a cubic spline) were classed as STAR. Points that lie outside the spline range (brighter or fainter in MAG_ISO than the extent of the red points) were classified as UNKNOWN. As a final step, we archived our catalogues in the form of simple ASCII files; a CIG database manager (CIGWORK) has been developed under LMORPHO to manage and evaluate these catalogues.

First visual check

As a visual check, the GUI allowed the user to view the image catalogue in the form of coloured-ellipse markers over-plotted on the DSS in a ds9 window (see Fig. 3.5). The blue ellipses indicate the GALAXIES detected, the red ones over-plot the STARS and the green circles mark the sources that were not classified. One of us (S. V.) systematically verified all the objects (GALAXY, STAR and UNKNOWN) and changed the types if needed. This task was very (very!) time consuming as the mean number of objects detected amounted to 4,000 per single 55 × 55 square minutes field (up to

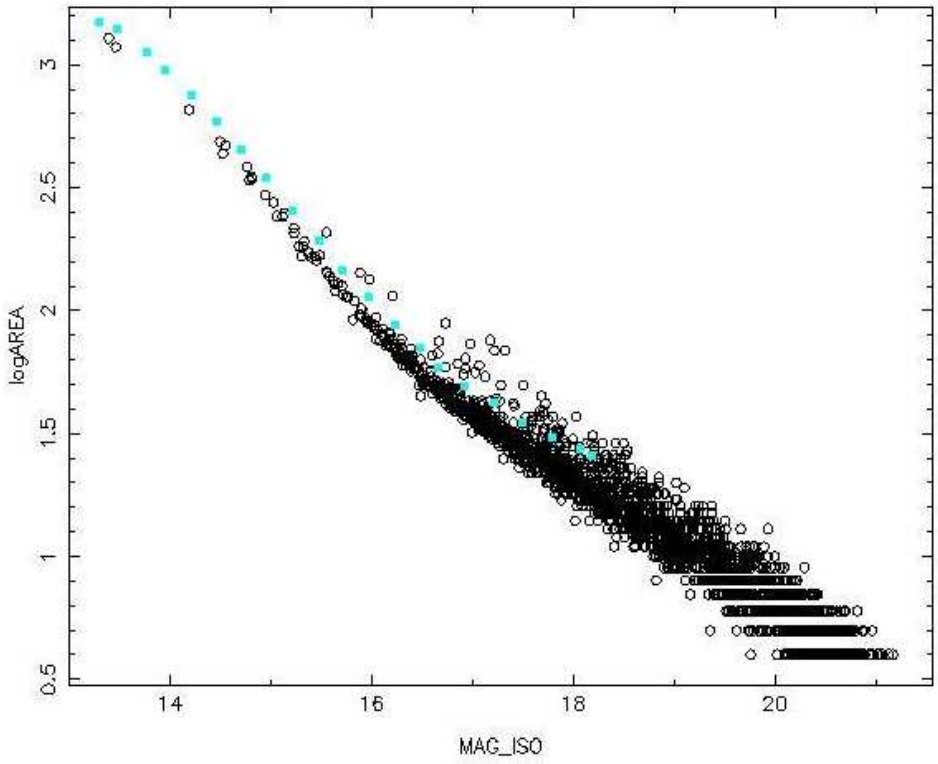

Figure 3.4: Star/galaxy separation parameter space.

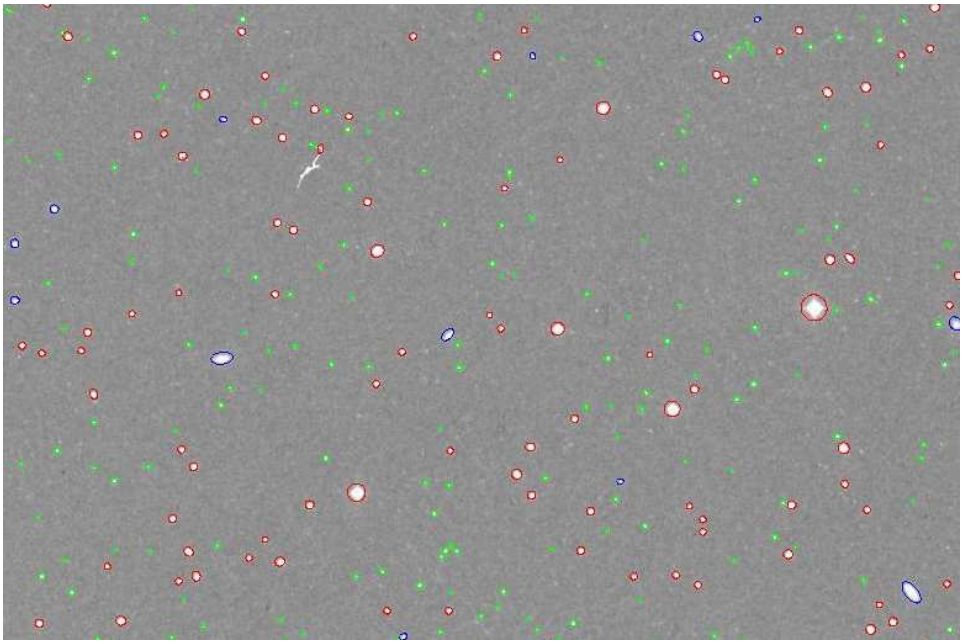

Figure 3.5: The distribution of galaxies around CIG 0714 (the bottom-right galaxy).

14,000 at low galactic latitude!).

Second visual check

Finally, we also used POSS-II red plates of all our GALAXY objects to perform a final check of our final catalogues of GALAXY companions (55,154 stamps, visually checked by L. V.-M.). The choice of POSS-II instead of POSS-I for this second check removed the detected plate defects in the POSS-I survey that could have passed through our first revision and provided a better spatial resolution to distinguish compact galaxies from stars. We sum up the results of this second visual inspection of the GALAXY objects: 98% really were GALAXY ($\sim$ 54,000 objects), almost 2% were plate defects (1,119 sources), 0.04% were STAR (23 objects).

Catalogues of galaxies

The parameters that we keep for each GALAXY were stored in the form of ASCII catalogues; the first lines of the catalogues associated with CIG 0001 and CIG 0002 are shown Table 3.3.

Table 3.3: Companions of the CIG galaxies.[2]

CIG	Comp.	RA	Dec.	LogAREA	Mag.	Dist.	Diameter
0001	0	0.34147	-2.361358	1.77	15.626	2237.1	22.6
0001	1	0.393433	-2.356566	1.568	17.378	2098.6	16.4
0001	2	1.034508	-2.35613	1.518	17.38	1849.5	16.1
0001	3	1.024575	-2.346702	1.602	17.123	1802.2	17.5
0001	4	0.781704	-2.312119	1.698	17.03	1434.1	19.3
⋮	⋮	⋮	⋮	⋮	⋮	⋮	⋮
0002	0	1.112587	29.343813	1.826	16.384	1850.9	17.4
0002	1	0.62712	29.414143	1.77	16.42	1525.4	16.1
0002	2	0.467379	29.498917	1.662	16.904	1573.5	15.0
0002	3	0.467854	29.50506	1.505	16.957	1557.4	15.3
0002	4	1.149291	29.516792	1.826	16.435	1410.9	18.4
⋮	⋮	⋮	⋮	⋮	⋮	⋮	⋮

The parameters used during the SExtraction make the diameters of the detected objects being about two times smaller than the expected estimation of the D_{25}. In each field, we calculated the scale factor between the known D_{25} (from NED) and the SExtracted value of the CIG diameter. We reported this scale factor on the diameters of the companions in order to have an estimated value of their D_{25}. When the scale factor was outside 2 σ from the mean factor (equal to 2) calculated with the CIGs, we decided to replace it by the mean value. Hence, in these fields, the SExtracted factors of the companions were multiplied by 2 to infer the values of the D_{25}. An independent check of these values with the D_{25} listed in the LEDA database validate our method.

3.4 Quantification of the isolation

As we have a total of more than 54,000 companions over the 950 fields, we can use a statistical approach to quantify the environment of the CIG galaxies.

[2]The full table will be available in electronic form at the AMIGA web site.

3.4.1 Statistical criteria

We defined, compared and discussed various criteria to quantify the degree of isolation for these galaxies. They were calculated with the information available over the entire fields (except where specifically indicated a physical distance of 0.5 Mpc):

1. Karachentseva criterion
2. Pairs
3. k-density estimator *(similar size companions)* (Log)
4. Projected density within 0.5 Mpc
5. Projected density within 0.5 Mpc *(similar size companions)*
6. Tidal forces (Log)
7. Tidal forces *(similar size companions)* (Log)
8. Tidal forces within 0.5 Mpc (Log)
9. Tidal forces within 0.5 Mpc *(similar size companions)* (Log)

In the coming paragraphs, we detail these criteria.

3.4.2 Revision of the Karachentseva's criterion

Although the criteria used in our study are not equivalent to the Karachentseva's selection, they have allowed us to find some of the CIGs that failed her criterion. According to Karachentseva, a perturbative companion can be 4 times bigger and $20D_i$ away from the CIG galaxy (this is a huge distance: $20D_i = 20 \times 4D_p = 80D_p$!). We could only cover this area for 67 fields: among them, we can attest that 54 CIGs are isolated following Karachentseva's criterion.

For the remaining fields, we have found 284 CIG galaxies violating Karachentseva's isolation definition (although we were not able to check on the whole $80 \times D_p$). Hence, still 666 CIG galaxies remain isolated accordingly to Karachentseva, taking into account that we cannot assert that some of these latter galaxies will not move from the "isolated" to the "not isolated" sample, with a more exhaustive study. Figure 3.6 shows these two populations; the axes are defined with two criteria defined hereafter (local density vs. tidal forces estimations).

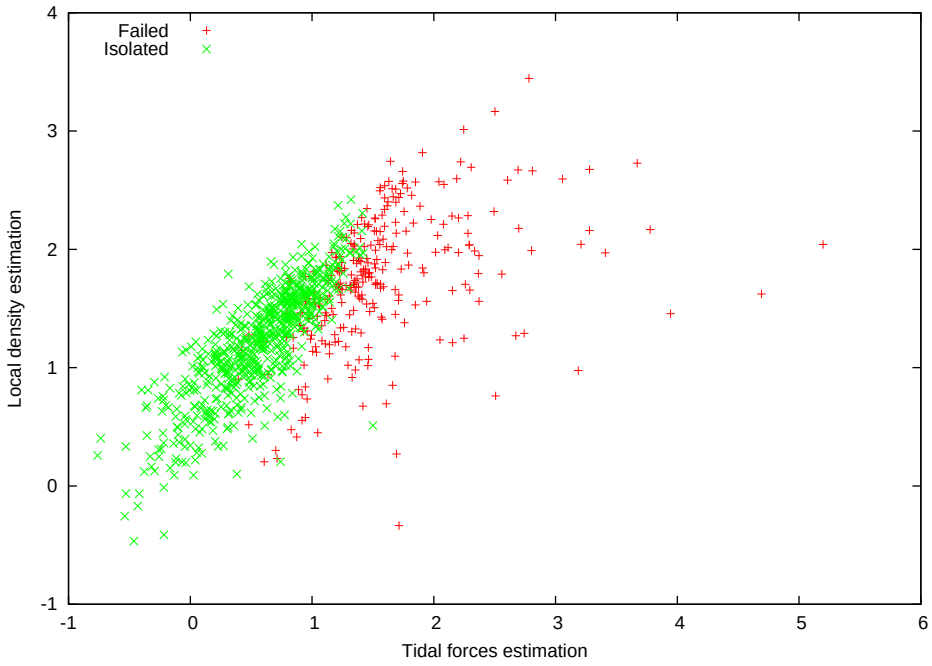

Figure 3.6: Green: still isolated galaxies; Red: galaxies that are violating Karachentseva's criterion *(Logarithmic scales on both axes)*.

3.4.3 Pair candidates

Table 3.4 lists all the pair candidates defined as a CIG galaxy with at least one companion (factor 2 in size with respect to D_p) within $5 \times D_p$. The fields of the 10 pair candidates detected (over the whole CIG sample of 950 primary galaxies) are shown in page 50. CIG 0019 has 2 companions nearby, one without known velocity and one with a recession velocity very similar to the one of the CIG: this constitutes a physical pair. Among the 4 other pair candidates having velocity information, 3 CIGs are physically associated with their companions (CIGs 0074, 0488, 0533) while this is not the case for CIG 0683 (velocity difference of $\sim$ 10,000 km s^{-1}).

Unfortunately, no velocities are available for the companions of the 5 remaining pairs (CIGs 0036, 0178, 0233, 0315, 0934). But, as 4 over 5 pair candidates appeared to be real pairs when the velocity is known, we can expect that, again, about 80% of the 5 pair candidates would be physically bounded.

Table 3.4: Pair candidates.

Galaxy	RA (degrees)	Dec. (degrees)	Distance (arcsec.)	Diameter (arcsec.)	Velocity (km s^{-1})
CIG 0019	6.067841	14.237	2.0	54.0	5390
Comp. 20	6.074004	14.272449	129.3	32.7	5396
Comp. 22	6.130088	14.260384	234.6	39.1	No data
CIG 0036	12.861758	40.725868	1.4	60.0	5855
Comp. 8	12.952467	40.762981	282.3	36.5	No data
CIG 0074	29.330297	28.590328	1.2	36.0	10188
Comp. 62	29.314213	28.614264	100.0	29.1	10300
CIG 0178	107.163582	61.305061	1.8	18.0	7610
Comp. 17	107.11628	61.299938	82.8	10.9	No data
CIG 0233	122.907974	27.538559	1.7	24.0	11225
Comp. 21	122.879021	27.524349	104.2	12.1	No data
CIG 0315	137.892471	-3.536764	2.3	54.0	5088
Comp. 26	137.853882	-3.599669	265.2	33.3	No data
CIG 0488	173.924164	73.452034	1.8	84.0	12501
Comp. 35	174.137344	73.470009	229.6	56.9	12425
CIG 0533	187.935638	-1.010247	1.6	24.0	21663
Comp. 93	187.933319	-1.005513	18.8	13.5	21585
CIG 0683	232.688354	-0.369905	1.1	36.0	11362
Comp. 53	232.679489	-0.383188	57.1	20.0	21285
CIG 0934	328.329865	-2.225402	2.2	42.0	5378
Comp. 33	328.308563	-2.192905	138.8	25.0	No data

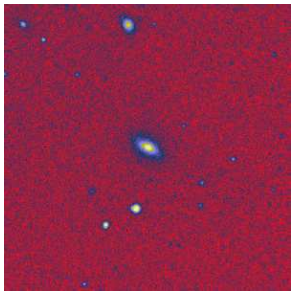

Figure 3.7: CIG 0019.

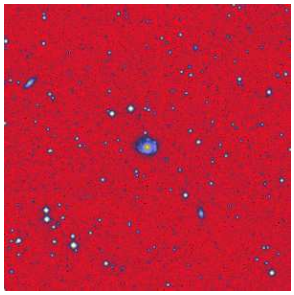

Figure 3.8: CIG 0036.

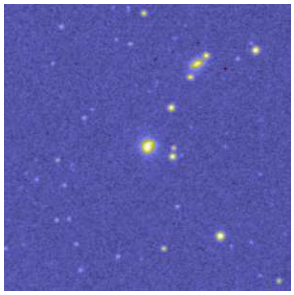

Figure 3.9: CIG 0074.

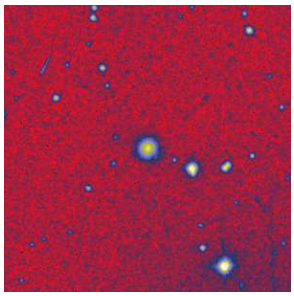

Figure 3.10: CIG 0178.

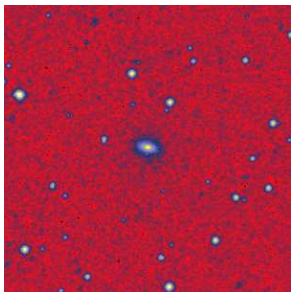

Figure 3.11: CIG 0233.

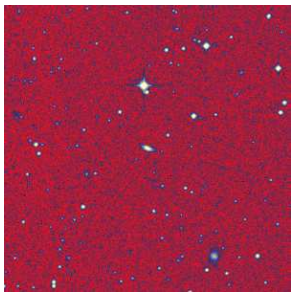

Figure 3.12: CIG 0315.

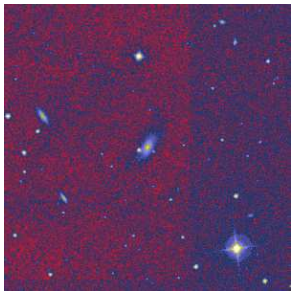

Figure 3.13: CIG 0488.

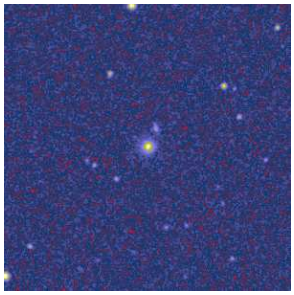

Figure 3.14: CIG 0533.

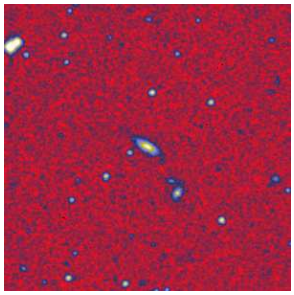

Figure 3.15: CIG 0683.

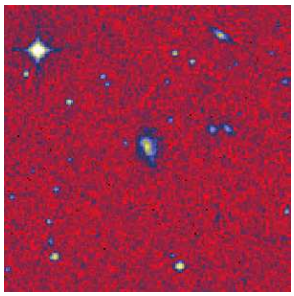

Figure 3.16: CIG 0934.

3.4.4 Local density estimation

An estimation of the local density can be found by considering the distance to the k^{th} nearest neighbour. An unbiased estimator can be obtained if neither the central galaxy nor the k^{th} neighbour are counted, see Casertano & Hut (1985). For this parameter, only the companions with similar size (0.25 to 4 D_p) were taken into account. k is equal to 5, or less if there were not enough companions in the field:

$$\rho_k \propto \frac{k-1}{V(r_k)}$$

with $V(r_k) = 4\pi r_k^3/3$, where r_k is the distance to the k^{th} nearest neighbour. We saved these values using a Logarithmic (Log_{10}) scale, after applying an arbitrary scaling constant to shift the range of values near the unity.

Forty CIG galaxies do not have at least two companions in the field considered: we did not estimate the local density in these cases.

3.4.5 Projected surface density estimation

A variation of the previous k-density estimation can be calculated by counting directly all the companions over a fixed surface. We have the redshift for 888 CIGs (over 950), so we can derive isolation parameters associated with physical radius. Hence, we chose to count all the companions within a physical projected distance of 0.5 Mpc around each CIG.

A refinement was to remove the background and foreground companions: we used the Karachentseva's argument and only consider the companions having a size similar to the CIGs (a factor of 4).

These two criteria were not calculated for the 62 CIG galaxies which do not possess redshift information, as we could not derive the physical 0.5 Mpc associated.

3.4.6 Tidal forces estimation

To estimate the tidal forces (T. F.) affecting the primary galaxies, we used a formalism developed by Dahari (1984): the tidal force per unit mass produced by a companion is proportional to $M_i R_{ip}^{-3}$, where M_i is the mass of the companion, and R_{ip} is its distance from the centre of the primary. However, no information on either M_i or on the absolute R_{ip} is available in most cases. The dependence of M_i on size is uncertain, we adopted $\gamma = 1.5$ (Dahari 1984). Since we are not using redshift information, the diameters of the primary galaxies are used as scaling factors, i.e., $r_i \propto D_i/D_p$, and

$R_{ip} \propto S_{ip}/D_p$. Accordingly,

$$\frac{M_i}{R_{ip}^3} \propto \frac{(D_i D_p)^{1.5}}{S_{ip}^3} \equiv Q$$

where S_{ip} is the *projected* R_{ip} distance. Q, defined by this equation, is a dimensionless estimation of the gravitational interaction strength. Again, these values were saved using a Logarithmic scale, after applying an arbitrary scaling constant to shift the range of values near the unity.

In spite of the lack of the redshift information, Q is expected to give a reasonable estimate of the tidal interaction strength in a statistical sense as can be seen from the following argument. If the candidate companion galaxy is in reality a background object we have underestimated the true distance but also underestimated the true size and mass. Both effects partly cancel out. Only in the case of the candidate companion being a foreground object Q is overestimated. Foreground objects are however rarer than background objects because of the smaller volume spanned.

Like for the previous criteria, we used two kind of criteria: one including all the companions, another including only the similar size ones.

For the 888 CIGs with redshifts, we also derived the same tidal forces criteria including the companions within 0.5 Mpc, to palliate biases that could rise from the different surfaces of our POSS-I digitised plates (see Fig 3.3).

3.4.7 Table of the isolation criteria

Table 3.5 gathers all the isolation values obtained for each CIG. There is a good concordance between the different criteria as shown in Fig. 3.6 (Karachentseva revision, k^{th} local density, tidal forces). Of course each criterion has its own specificities and is complementary with respect to the others. For instance, a companion very close to a CIG would be counted as one regular object by the k^{th} local density estimation but will drastically increase the value of the tidal forces affecting the CIG (see for instance the CIG in the very right part Fig. 3.6).

Table 3.5: The first lines showing the values of the isolation criteria defined in the previous sections. The k^{th} local density and the tidal forces estimations are in Logarithmic scale (Log_{10}).
[4] This note indicates that the criterion only included the similar size companions (factor of 4 with respect to the CIG diameter).

CIG	Kara.[4]	Pairs	k^{th}-density[4]	Proj. dens. (0.5 Mpc)	Proj. dens.[4] (0.5 Mpc)	T. F.	T. F.[4]	T. F. (0.5 Mpc)	T. F.[4] (0.5 Mpc)
0001	1.000	0.000	1.814	12.000	3.000	2.296	1.213	2.267	1.089
0002	0.000	0.000	0.971	2.000	2.000	0.435	0.435	0.064	0.064
0003	0.000	0.000	1.018	-98.000	-98.000	0.786	0.786	-98.000	-98.000
0004	0.000	0.000	0.987	99.000	2.000	1.950	0.264	1.941	0.203
0005	1.000	0.000	1.588	12.000	12.000	1.067	1.067	1.038	1.038
0006	0.000	0.000	1.373	7.000	7.000	0.769	0.751	0.467	0.467
0007	0.000	0.000	0.843	2.000	2.000	0.575	0.573	0.471	0.471
0008	...	...	...	...	...	...	...	...	...
⋮	⋮	⋮	⋮	⋮	⋮	⋮	⋮	⋮	⋮

Chapter 4

Comparison samples

Contents

4.1 Introduction

The CIG is complemented by catalogues of galaxy pairs (Karachentsev 1972), triplets (Karachentseva et al. 1979) and compact groups (Hickson 1982). All of these interacting comparison samples were visually compiled using also an isolation criterion. All avoid the pitfalls associated with computer compilation from a magnitude-limited catalogue (i.e. selecting the brightest galaxy or galaxies in a cluster).

To estimate the isolation degree of the CIG galaxies and to place it in a more general context of space galaxy distribution, we apply some of the isolation criteria defined in the previous Chapter on triplets, compact groups and clusters of galaxies. We followed the method described in the previous Chapter (POSS-I digitised fields, first and second visual checks, ...) to avoid to be biased by technical differences during the discussion and interpretation of this comparative study.

4.2 Karachentseva Triplets of Galaxies

Karachentseva et al. (1979) listed 84 northern isolated galaxy triplets (KTG) compiled in a manner similar as the one used to compile the CIG. The apparent magnitudes are brighter than 15.7 and the Catalogue was built up on the basis of a complete examination of Palomar Sky Survey prints (POSS-I). Karachentseva et al. (1979) showed that triple systems constitute 0.8% of northern galaxies brighter than 15.7 mag, 64% of the triplets are "completely isolated", and 24% of the triplet members are elliptical and lenticular galaxies, while 76% are spirals and irregulars.

From the 84 triplets, we selected all of them with the 3 galaxies having V $>$ 4,687 km s^{-1} (to use one single 55 $\times$ 55 square arcminutes field, see previous Chapter). We applied the isolation parameters on the "A" galaxy (primary galaxy which will play the role of the CIG galaxy). The result is that **41 triplets** were selected (see Table 4.1). The coordinates, major axis and velocity are those of the galaxy on which the isolation parameters are applied.

Figure 4.1 shows the triplet of galaxies 04 as an example.

The results of this study are summarised Figure 4.4.

Table 4.1: Karachentseva Triplets of Galaxies sample.

KTG number	RA (degrees)	Dec (degrees)	Major axis (arcmin.)	Velocities (km s^{-1})
02	14.412716	43.800764	1.4	5539
04	19.018667	46.730500	0.8	5602
06	20.627667	39.199278	0.6	8084
07	21.090833	32.224167	1.0	5214
10	48.980138	37.154116	0.6	6168
11	105.614000	86.579556	0.9	5000
12	101.516492	43.845451	0.4	6379
13	106.753208	44.849694	1.0	15339
19	116.618958	58.962556	1.4	6684
29	156.854215	1.241640	0.3	9148
31	160.434293	21.185364	0.8	7461
32	161.774101	7.237705	0.4	6395
34	164.880292	75.191278	1.2	7392
35	167.232042	26.610278	1.3	6559
36	170.194057	0.470549	0.5	7151
37	171.946667	7.987778	1.5	6251
41	181.180579	31.177281	0.9	7454
43	185.258643	39.899982	0.55	6914
44	188.779417	63.960000	0.6	10890
46	199.494339	4.403461	1.7	6192
47	204.618779	0.510336	0.8	6612
48	205.917250	3.896389	1.4	6810
49	206.555250	-3.384694	0.7	6728
51	209.305000	12.021250	0.8	6309
52	210.519975	-1.357981	1.2	7400
56	215.667333	6.166833	1.1	6650
57	216.825963	4.802831	2.2	8353
58	220.878375	11.202694	1.0	8438
59	228.899750	69.315806	0.85	6959
60	230.075884	3.518260	0.6	11216
61	230.732387	-1.356472	0.2	8427
65	235.874542	4.794444	1.3	8217
66	254.361458	40.735628	0.85	8770
72	315.020105	9.582957	1.4	9495
74	328.931614	5.807938	0.7	8952
75	341.040706	9.989141	0.6	7632
76	342.169400	27.611700	1.3	9918
77	347.662250	9.188778	0.5	11850
78	348.764185	18.973441	1.1	5093
79	350.389583	27.118056	0.9	6134
83	0.158083	28.384556	1.1	9084

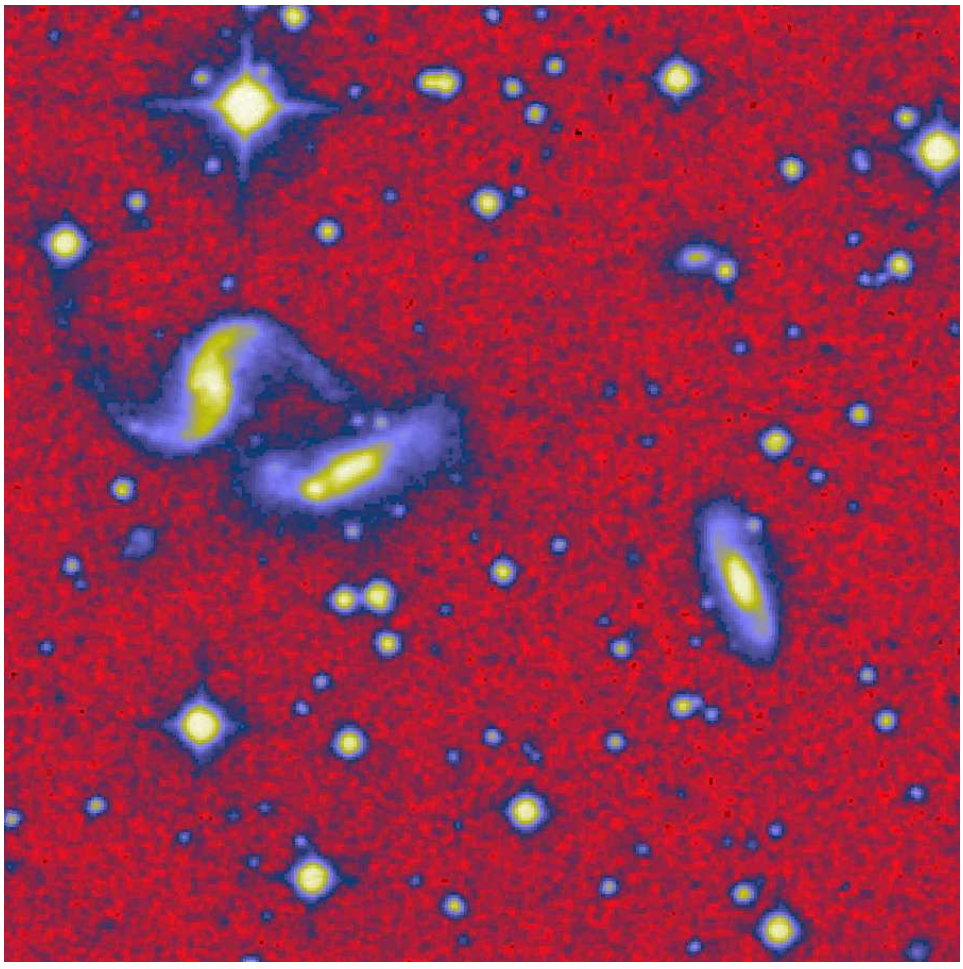

Figure 4.1: Karachentseva triplet of galaxies 04.

4.3 Hickson Compact Groups

The Hickson Compact Groups catalogue (HCG, Hickson 1982) compiled 100 groups (largely quartets). Our selection process is fully consistent with the KTG one: we selected the groups in the northern hemisphere (because the POSS-I digitised plates are only available in the northern hemisphere and we wanted to mimic the study done for the CIG). We kept only the true physical groups following the work by Sulentic (1997). To fit in our 55 × 55 square arcminutes fields, the recession velocities had to be greater than 4,687 km s^{-1}. It remained **34 Hickson Compact Groups**. The coordinates, major axis and velocity are those of the galaxy on which the isolation criteria are applied are shown Table 4.2.

Figure 4.2 shows the compact group 33 as an example.

The value of all the isolation parameters are higher than the ones of the CIG galaxies (see Figure 4.4).

4.4 Abell clusters

Only in the northern hemisphere, the Abell Clusters of Galaxies catalogue (ACO, Abell 1958; Abell et al. 1989) lists more than 2,700 clusters in six richness classes (with only one cluster in the richest class!). We selected all the clusters with available recession velocities between 4,687 and 15,000 km s^{-1}. The ACO is a deeper sample than the CIG, KTG and HCG: the higher cut (15,000 km s^{-1}) is used in order to sample a volume of space roughly equivalent to the one spanned by the CIG and avoid possible biases. Among these, **15 clusters** have a known diameter less than 55 arcminutes. Table 4.3 summarises the main properties of the clusters selected (*left*) along with information on the primary galaxies (*right*) on which the isolation criteria have been applied (central cD galaxy, or central brightest galaxy).

Figure 4.3 shows the Abell cluster 2666 as an example.

The comparison between the ACO and the other samples is discussed in the next section.

Table 4.2: Hickson Compact Groups sample.

HCG number	RA (degrees)	Dec (degrees)	Major axis (arcmin.)	Velocity (km s^{-1})
1	6.529708	25.725194	1.25	10237
8	12.392292	23.578250	0.9	16077
10	21.590750	34.703028	3.0	5189
15	31.971167	2.167611	1.1	6967
17	33.52135	13.31104	0.36	18228
20	41.050292	26.099389	0.48	14477
25	50.178917	-1.108583	1.3	6285
33	77.698375	18.019667	0.37	7464
35	131.338480	44.520873	0.3	15919
39	142.365458	-1.345722	0.35	21119
47	156.442792	13.716861	1.0	9692
49	164.173375	67.184750	0.48	9937
50	169.276667	54.917139	0.20	> 30000
51	170.609792	24.299139	1.33	7626
55	173.029000	70.815472	0.44	16070
56	173.194333	52.940861	1.23	8245
58	175.546208	10.277750	1.4	6138
66	204.659500	57.312361	0.45	20688
69	208.874000	25.073667	1.58	8856
70	211.041851	33.337530	1.2	8238
72	221.972459	19.076982	0.5	12506
74	229.853042	20.896278	0.82	12255
75	230.376625	21.190639	0.73	12538
76	232.948250	7.308222	0.7	10088
80	239.829500	65.232722	0.85	8975
82	247.093217	32.849311	0.9	11177
83	248.901286	6.265361	0.26	15560
84	251.095095	77.838748	0.59	16654
85	282.576860	73.351452	0.53	11155
93	348.816699	18.961797	1.4	5072
94	349.306500	18.708167	1.0	12045
95	349.875208	9.508222	0.88	11879
99	0.158083	28.384556	1.1	8705
100	0.333208	13.111250	1.0	5366

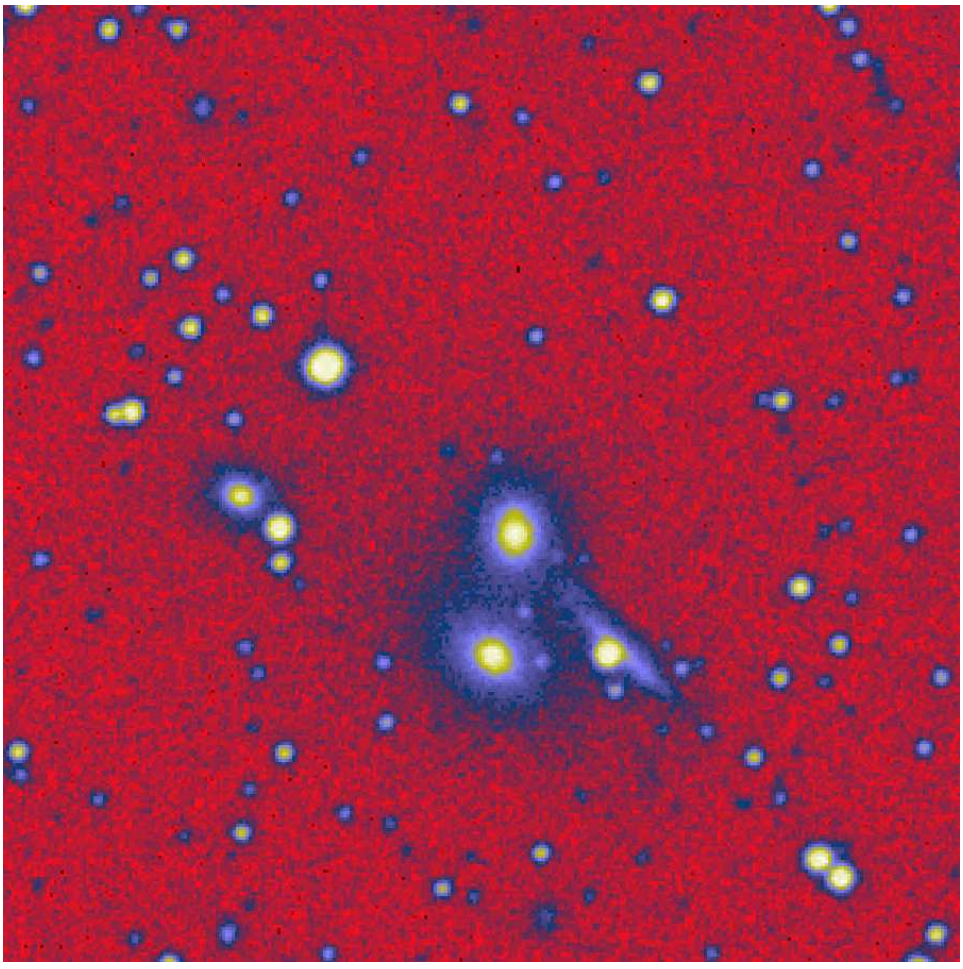

Figure 4.2: Hickson compact group 33.

Table 4.3: ACO clusters (*left*) and primary galaxies selected (*right*).

ACO number	RA (J2000)	Dec (J2000)	Velocity (km s^{-1})	Richness class	Diameter (arcmin.)	RA (J2000)	Dec (J2000)	Velocity (km s^{-1})	Diameter (arcmin.)	Hubble type
0160	01 12.9	+15 31	13410	0	40	18.248726	15.491506	13137	0.78	cD
0260	01 51.9	+33 10	10440	1	50	28.024008	33.190811	...	0.72	...
0671	08 28.5	+30 25	14820	0	50	127.132118	30.432072	15087	...	...
0957	10 14.0	-00 55	13200	1	50	153.409729	-0.925455	13293	1.5	E+ pec
0999	10 23.4	+12 51	9540	0	50	155.849396	12.835186	9764	1.2	BCG
1100	10 48.9	+22 14	13650	0	40	162.190262	22.217989	13990	0.45	BCG
1177	11 09.5	+21 42	9480	0	50	167.435104	21.759527	9589	1.8	BCG
1213	11 16.5	+29 16	14040	1	50	169.095093	29.252588	13581	1.0	SB0
2040	15 12.8	+07 26	13680	1	32	228.197601	7.435083	13683	1.0	BCG
2152	16 05.4	+16 27	11220	1	50	241.371292	16.435858	13211	1.3	E
2506	22 56.6	+13 20	9930	1	20	344.288147	13.188705	6860	0.5	...
2572	23 18.4	+18 44	11850	0	50	349.626160	18.689167	11263	0.9	cD
2593	23 24.5	+14 38	12990	0	50	351.084259	14.646864	12489	1.3	cD
2657	23 44.9	+09 09	12420	1	46	356.239227	9.193000	12063	0.8	cD
2666	23 50.9	+27 09	7950	0	50	357.744812	27.147602	8191	1.6	cD

4.5 Discussion

Figure 4.4 gathers the results obtained in this Chapter. We can compare the isolation level of the CIG with the k^{th} local density and tidal forces estimations on galaxies from the KTG, HCG and ACO. The scale is logarithmic (Log_{10}) on both axes.

The first striking feature is that, along the x axis (tidal forces estimation), the CIG, KTG and HCG samples are classified following the expected order. The CIG is normally only constituted by isolated galaxies, the KTG by 3 galaxies and the HCG mainly by 4 galaxies. The tidal forces estimation is sensitive enough to disentangle these samples.

Along the y axis, reflecting the k^{th} local density estimation, these three samples are more confounded. This reflects the fact that the KTG and the HCG are samples constructed also with the help of isolation requirements: these are isolated triplets and isolated groups. Nevertheless, by definition, two of the triplet galaxies and at least three of the group galaxies are very close to the primary galaxy. This is why the 5^{th} neighbour is, in average, closer to the triplet or the group than the 5^{th} neighbour of an isolated galaxy. The value of the k^{th} local density estimation is the result of a compromise between the two effects cited above. The CIG, KTG and HCG samples are also in a logical order along the y axis, but less separated than along the x axis. The tidal forces and the k^{th} local density estimations are complementary criteria and it is important to use both in order to have an accurate picture of the repartition of galaxies surrounding a primary galaxy.

The ACO entities are physically very different from the CIG, KTG or HCG as they can involve several thousand of galaxies. The average value of tidal forces applied on the primary ACO galaxies is in between the KTG and HCG ones. This is mainly because our ACO sample is biased towards the poorest clusters. The 15 clusters selected are not representative of the mean characteristics of the ACO sample for various reasons: among the nearest ones, belonging to the 2 poorest richness classes, having a diameter minor than 55 arcminutes. The effects in ACO are mostly the cumulation of smaller interactions. Nevertheless one may expect that result as the HCGs are the densest concentration of galaxies in the Universe. The ACO sample possess the highest k^{th} local density estimation, as expected because all the 5 neighbours are included in the cluster: there is no effect due to an isolation requirement. A relevant value to characterise the ACO sample is the ratio k^{th} local density over tidal forces estimation: they have the lowest value compared to the other samples. This is due to the combination in a single parameter, of the two effects just cited.

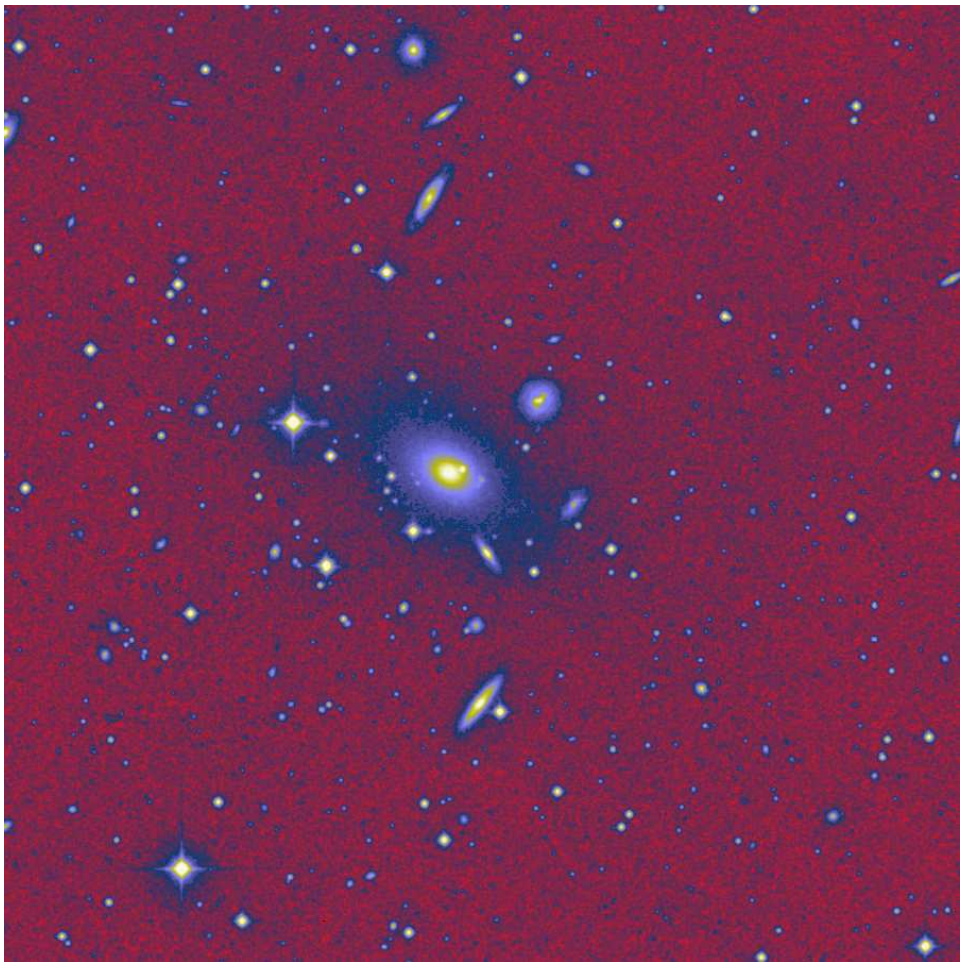

Figure 4.3: Abell cluster 2666.

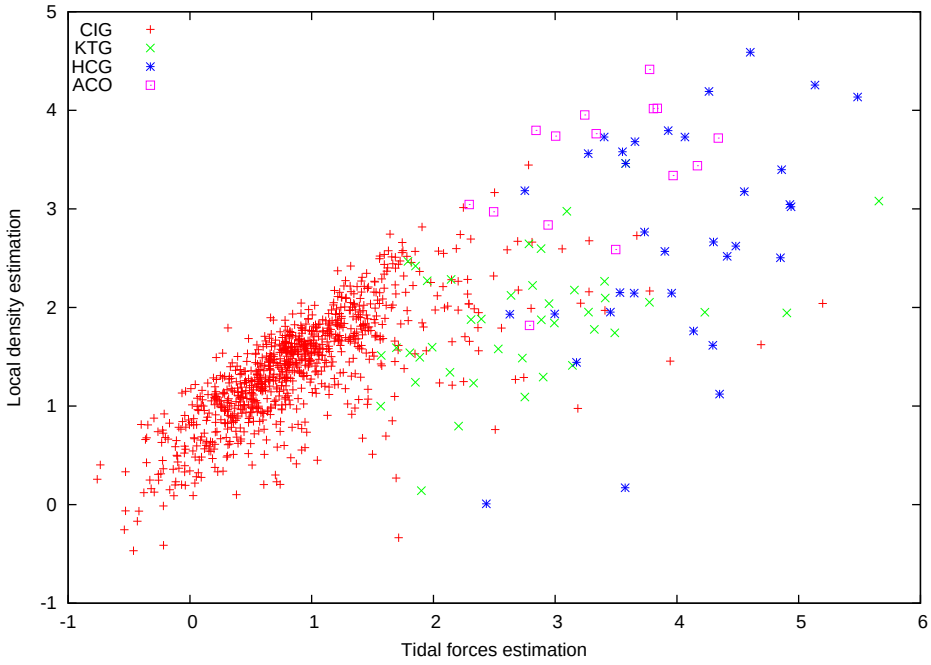

Figure 4.4: Isolation criteria for the comparison samples *(Logarithmic scales on both axes)*.

Chapter 5

Redshifts

Contents

5.1 Introduction

We used more than a dozen databases and surveys for two reasons: 1) confirm the types of our objects when they were matched, 2) make use of the redshifts when they were available to try to identify a background population among the CIG companions. We sent batch for all the 54,000 companions to each database, matching the coordinates within a tolerance of 6 arcseconds.

5.2 Redshift catalogues and surveys

5.2.1 NED

The NED database gathers 8.1 million objects over the whole sky. The redshifts are available for 972 thousand objects[1]. Over the 54,000 companions, we obtained 35,811 matching including 8,024 with redshift.

5.2.2 HyperLEDA

At present the HyperLEDA database contains about 3 million objects, out of them 1.5 million are certainly galaxies (with a high level of confidence)[2]. This database covers the whole sky. We obtained 28564 detections including 11608 with redshift.

5.2.3 SDSS - DR3

The SDSS - DR3 is a major, recent survey. We used the spectrophotometric catalogue. The DR3 spectroscopic data include data from 826 plates of 640 spectra each, and cover 4188 square degrees[3]. We obtained 12166 detections

[1]This research has made use of the NASA/IPAC Extragalactic Database (NED) which is operated by the Jet Propulsion Laboratory, California Institute of Technology, under contract with the National Aeronautics and Space Administration.

[2]We have made use of the LEDA database (http://leda.univ-lyon1.fr).

[3]Funding for the Sloan Digital Sky Survey (SDSS) has been provided by the Alfred P. Sloan Foundation, the Participating Institutions, the National Aeronautics and Space Administration, the National Science Foundation, the U.S. Department of Energy, the Japanese Monbukagakusho, and the Max Planck Society. The SDSS Web site is http://www.sdss.org/.
The SDSS is managed by the Astrophysical Research Consortium (ARC) for the Participating Institutions. The Participating Institutions are The University of Chicago, Fermilab, the Institute for Advanced Study, the Japan Participation Group, The Johns Hopkins University, the Korean Scientist Group, Los Alamos National Laboratory, the Max-Planck-Institute for Astronomy (MPIA), the Max-Planck-Institute for Astrophysics (MPA), New Mexico State University, University of Pittsburgh, University of Portsmouth, Princeton University, the United States Naval Observatory, and the University of Wash-

with redshift.

5.2.4 2dF

The 2dF Galaxy Redshift Survey (2dFGRS) is also a major spectroscopic survey. The 2dFGRS obtained spectra for 245591 objects, mainly galaxies, brighter than a nominal extinction-corrected magnitude limit of bJ=19.45. Reliable (quality>=3) redshifts were obtained for 221414 galaxies. The galaxies cover an area of approximately 1500 square degrees, mainly in the southern hemisphere. We obtained 3018 detections with redshift.

5.2.5 CfA

The CfA Redshift Survey gathers various surveys in one. We obtained 9103 detections including 8864 with redshift (velocity.dat catalogue). 106 and 866 objects with redshift were matched in two smaller catalogues (CfA1 and CfA2, respectively).

5.2.6 UZC

In the UZC catalogues (Falco et al. 1999), respectively 1461 and 1445 detections with redshift were obtained in the catalogues UZC and UZC2000, respectively.

5.2.7 Nearby Optical Galaxies

The Nearby Optical Galaxy sample (NOG, Giuricin et al. 2000) is a complete, distance-limited (cz $\leq$ 6000 km s-1) and magnitude-limited (B $<$ 14) sample of $\sim$ 7000 optical galaxies. We obtained 67 identifications with redshift.

5.2.8 SSRS2

The Southern Sky Redshift Survey (SSRS, da Costa et al. 1998) reports redshifts, magnitudes and morphological classifications for 5369 galaxies with $m_B \leq 15.5$ and 57 galaxies fainter than this limit, in two regions covering a total of 1.70 steradians in the southern celestial hemisphere. The galaxy catalogue is drawn primarily from the list of non-stellar objects identified in the Guide Star Catalogue. We matched 50 objects with redshift.

---

ington.

Table 5.1: The vast majority of the companions are GALAXY.

Database or survey	Number of redshifts	Number of matched objects	Percentage of GALAXY
NED	8024	35317	99.97%
hyperLEDA	11608	25614	99.99%
SDSS	12166	12166	99.79%
CfA (velocity)	8864	9103	99.86%
2dF	3018	3018	-
UZC	1461	1488	-
UZC J2000	1445	1485	-
CfA2	866	866	100%
CfA1	106	106	100%
NOG2	67	67	-
NOG4	66	66	-
SSRS2	50	50	-

5.3 Type of the companions

First, we used the databases to confirm the star/galaxy separation done in section 3.3. NED, HyperLEDA, SDSS, CfA give types for the objects in their databases (Table 5.1). **The CIG companions are classified as GALAXY in more than 99.90% of the cases.**

5.4 Redshift analysis

We gathered all the data coming from the various databases above cited. We treat the widely different formats in order to end with one single, homogeneous (J2000 coordinates, heliocentric velocities, ...) final catalogue. **A total of 16126 (29.9%) objects have redshift listed in at least one database.**

The typical error on the velocities is about $\sim$ 40 km s^{-1}. For some galaxies, the redshifts were listed several times. The agreement is generally very good between the different databases. Only one redshift per companion was kept for the following study. To have the most homogeneous final database, we chose to keep preferentially the data in provenance from the larger surveys. The SDSS gave 12166 objects (75% of the redshift sample) and besides this it gave the smallest error and confident data. Next, in order, we used: the 2dF, the CfA (velocity), NED, LEDA, UZC. Because of the redundancy, the UZCJ2000, CfA1, NOG4 and SSRS2 were not used.

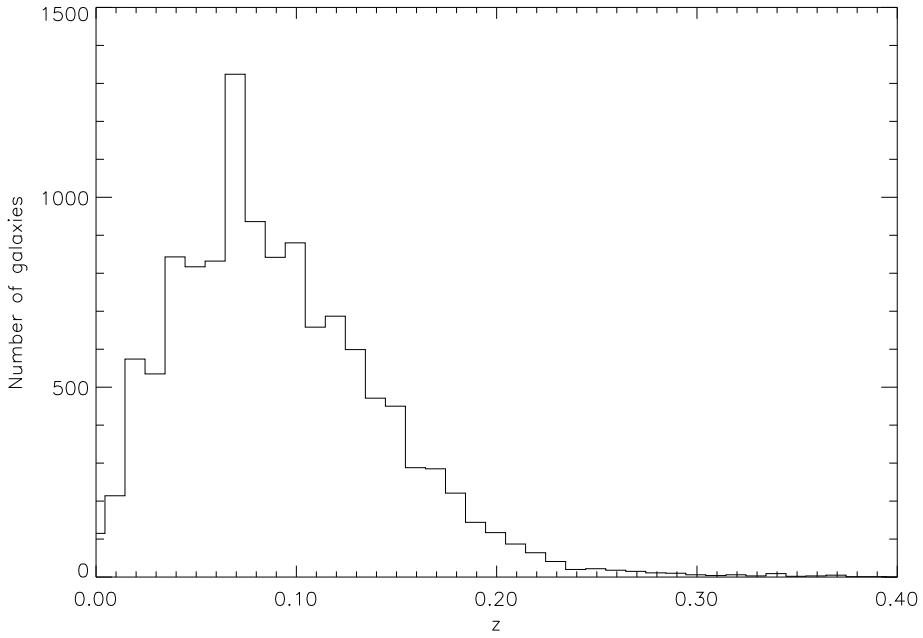

Figure 5.1: SDSS redshifts of the companions.

Figure 5.1 presents the distribution of the velocities available in the Sloan. The mean is z = 0.097 (about 30,000 km s^{-1}). Compared with the histogram of the CIG recession velocities Figure 2.3 with a mean z = 0.022 ($\sim$ 6624 km s^{-1}), we saw that the redshifts available concerned a deeper sample of galaxies. Hence, most of the companion galaxies are background galaxies.

We are missing the redshifts for 70% of the companions in our sample. 520 fields are strictly less than 10% complete, 641 fields less than $<$ 20% complete. Nevertheless, some of our fields are rather complete (see Figure 5.2). Even five of them are 100% complete: CIG 0213 (25 objects), CIG 0359 (18), CIG 0492 (27), CIG 0655 (8), CIG 0892 (23).

A total of 89 fields are at least 80% complete (see Figure 5.2). We have made use of these data in order to perform a reliability test of our method. We have used these 89 fields in order to estimate the isolation criteria defined in Chapter 3 including only the companions that can be considered physically associated to the CIGs, based on their redshift difference with respect to CIG galaxy. Two different values of the difference in velocity (ΔV) between the companions and the main galaxy have been considered: ΔV = 500 km s^{-1} and ΔV = 1000 km s^{-1}.

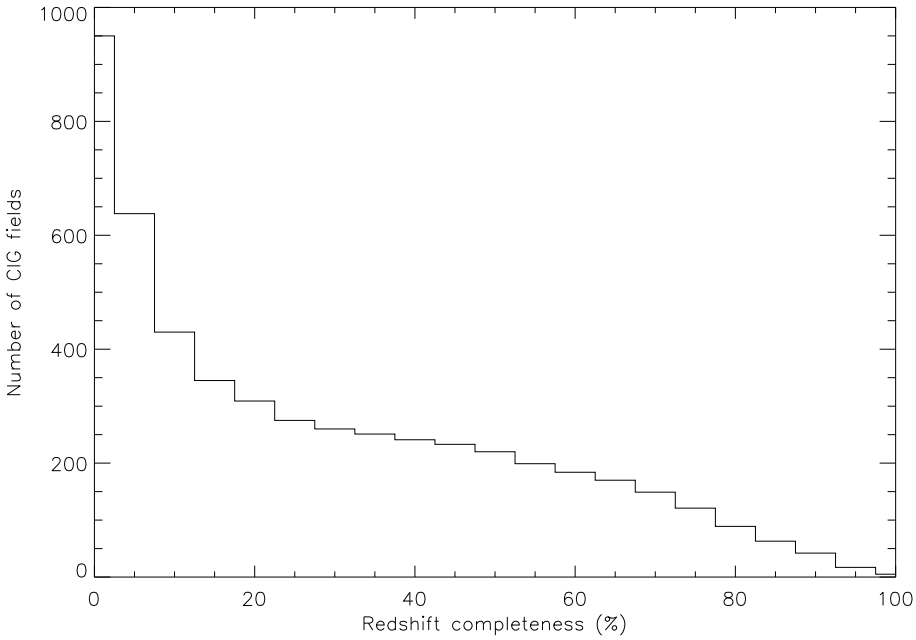

Figure 5.2: Redshift completeness.

The high general level of isolation of the CIG sample is confirmed by the low number of companions identified in these fields at the CIG redshift (typically, about 4 companions!). Furthermore, respectively 35/27 fields could not be used in our test since only 1 or even zero companions were found within 500/1000 km s^{-1} from the CIG.
Hence our tests have been performed using respectively the 54/62 galaxies of this list for which at least 2 companions have been found. First we have checked Karachentseva criterion (see section 3.4.2) and we find that 44/51 galaxies were fond isolated by Karachentseva and are still isolated when redshift data are available. On the other hand 10/11 were not considered isolated while now 7/7 of them are reclassified as isolated. This supports that Karachentseva's selection was very restrictive.

In Figure 5.3, we compare the tidal force estimations within 0.5 Mpc (see section 3.4.6), for all companions (X axis) and for those with a velocity within 500 and 1000 km s^{-1}, respectively, from the CIG (each point in the figure represents a CIG galaxy). The dotted line represents the Y = X correlation as a reference. The solid line represents a fit to the data, with a slope very similar, within the errors, to 1. Hence, the tidal force estimation obtained from the whole set of companions behaves in the same way as the

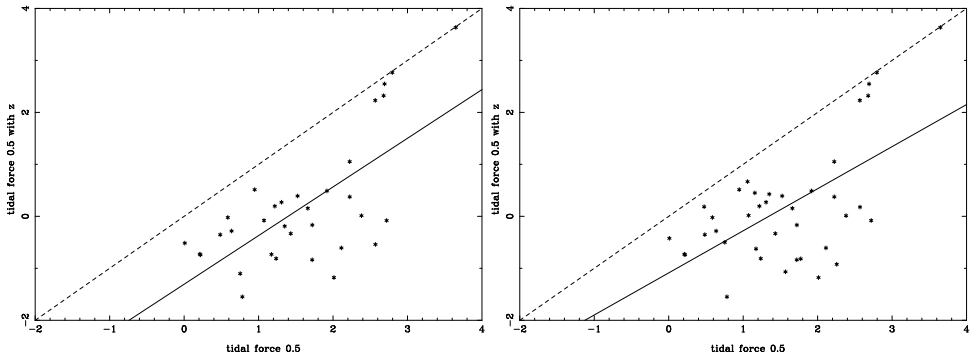

Figure 5.3: *Left*: $\Delta V < 500$ km s^{-1}; *Right*: $\Delta V < 1000$ km s^{-1} *(Logarithmic scales on both axes).*

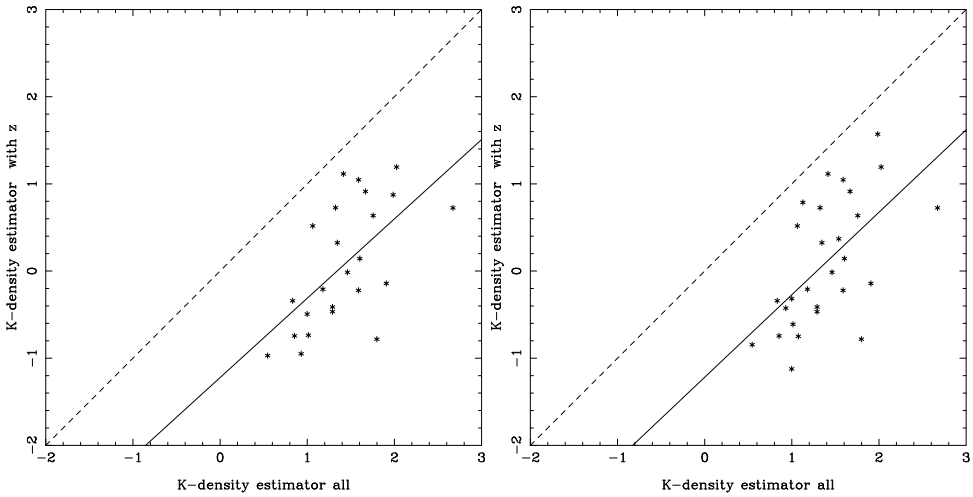

Figure 5.4: *Left*: $\Delta V < 500$ km s^{-1}; *Right*: $\Delta V < 1000$ km s^{-1} *(Logarithmic scales on both axes).*

estimation from the physical companions, shifted (as can be expected) towards lower values. The obtained fits are shown in the Figure (slope of 0.82 $\pm$ 0.16 and an offset of -1.39 $\pm$ 0.27 for $\Delta V = 500$ km s^{-1} and a slope of 0.80 $\pm$ 0.14 and an offset of -1.34 $\pm$ 0.23 for $\Delta V = 1000$ km s^{-1}.).
Similar conclusions can be reached with the other isolation parameters defined in Chapter 3. In Figure 5.4, we show similar plots for the k^{th} local density estimation, as well as the corresponding fits.

The similarity of the results obtained with $\Delta V < 500$ km s^{-1} with those increasing the considered velocity difference to $\Delta V < 1000$ km s^{-1} supports the robustness of our statistical study of the isolation.

The dispersion of the fits reflects on one hand the low ($< 20\%$) but

still existing incompleteness in the redshift coverage of the fields, and the errors in the isolation parameters produced by the inclusion of background or foreground companions. The projected physical density shows that once redshifts are taken into account the number of physical companions decreases dramatically, more frequently due to the presence of background companions than to foreground ones, indicating that our method is very sensible to fainter and/or farther galaxies.

5.5 Conclusions

The 30% of the companions having redshift information does not represent any particular subsample among the whole sample of companions. The redshifts are not available only for the nearest galaxies and missing for the faintest galaxies or the ones which would have recession velocities of several tens of km s^{-1}. Indeed, Figure 5.1 shows that the companions do have recession velocities of about 30,000 km s^{-1}. Principally, the redshifts are missing for zones in the sky where no surveys were ever undertaken, and for which the only available data come from particular projects.

The similarity of the samples with and without known recession velocities can be seen, for instance, by looking at the distributions of their magnitudes: Figure 5.5 shows that the missing velocities are randomly distributed (in magnitude) among the companions. Hence, we can infer that the study done above for the fields with a redshift completeness smaller than 80%, would provide similar results if the redshifts were known for most of the companions. With this argument, we can confirm the validity of the statistical study done in Chapter 3.

All these results support the use of the data derived in Chapter 3 for the CIG companions, without taking into account redshift information. This will allow us to study a sample of 950 CIG galaxies, instead of the order of 60. Therefore, we give the final results of the isolation study using the data without using the redshift information. This has the advantage of giving **homogeneous** estimation of the isolation parameters for the **950 CIG galaxies**. Table 5.2 sums up the main results of this study.

We have revised the isolation of 950 CIG galaxies, discussed Karachentseva's criterion, but also refined this complete sample in a homogeneous way, by giving continuous parameters of isolation, based on local density and tidal forces estimations. From now, the AMIGA project is using a revised sample based on the CIG, from which the galaxies not really isolated were removed (pairs, galaxies highly affected by tidal forces).

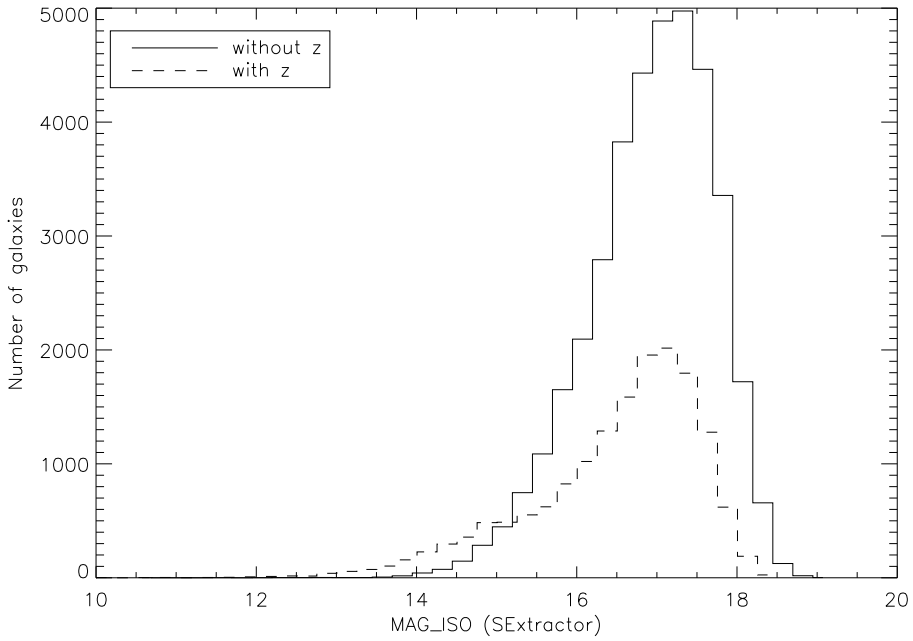

Figure 5.5: Magnitude distributions.

Table 5.2: Classification of the isolation.

	Very isol.	Isol.	Quite isol.	Poorly isol.	Interacting
Tidal forces	0	1	2	3	
Num. of CIGs	**28**	**333**	**446**	**117**	**26**

Part II

Star formation in isolated spiral galaxies

Chapter 6

The Hα study

Contents

6.1 Introduction

The triggering of star formation at large scale in a galaxy can come from several dynamical phenomenons, interactions between galaxies and density waves such as bars are among the main. Already, Larson & Tinsley (1978) interpreted the big dispersion in colours U-B/B-V of galaxies in interaction due to bursts in star formation, intense but brief.

The interactions between galaxies can also produce enhancements in far infrared (Joseph & Wright 1985; Surace et al. 1993), in radio-continuum (Stocke 1978), in Hα emission (Kennicutt et al. 1987), and also in CO emission (Braine & Combes 1993; Combes et al. 1994).

There are, nevertheless, lots of uncertainty concerning the efficacy of interactions in the triggering of star formation and, still, no law is really well established, which could linked the local density of gas, or its velocity dispersion, to the star formation rate (SFR). Globally in a given galaxy, one of the best relation seems to be the Schmidt law (Kennicutt 1998), linking the available quantity of gas (essentially the HI reserve) to the rate of stars newly formed, but lots of exceptions are observed to this relation, showing that others parameters have to be taken into account.

One purpose of studying an Hα sample of galaxies is to disentangle the interconnections between interactions, starbursts, nuclear activity, by analysing isolated galaxies. This would also provide information about the following issue: do high star formation rates indicate a better efficiency in the mechanisms that form stars or that there is a larger quantity of fuel (molecular gas, HI+H_2)?

6.1.1 Influence of environment on star formation

The star formation rate derived from Hα, in the absence of nuclear activity, dominated by young ($t < 20Myr$), massive ($M > 10M_\odot$) stars is about 2.5 times higher in interacting than in isolated galaxies (Bushouse 1987). Kennicutt (1989) showed that this rate, averaged over the disk, has a better correlation with the superficial density of HI than H_2 in normal galaxies, which is a surprising result because of the differences in the distributions of HI and Hα. Similar conclusions were derived from studies based on global averages (Boselli 1994; Casoli et al. 1996). This was attributed to variations in the conversion factor CO/H_2, suggested by a better correlation between H_2 and the star formation rate for luminous galaxies (Kennicutt 1998) although arguing that the global superficial HI + H_2 gas density shows a better correlation (Kennicutt 1989, 1998).

6.1.2 The Hα emission line as a tracer of star formation

If a young star is hot enough (T > 10,000 K), its UV photons can ionise the surrounding medium (circumstellar medium), forming an HII region. The free electrons and nuclei created this way can recombinate and emit new photons, or warm up the gas by collisions with other atoms. This way, the radiation emitted by the star is transmitted to the surrounding medium and making this latter also to emitt radiation. The radiation field diminishes as we are farther from the central star. Due to geometric dilution, the farther from the star, the less the number of ionising photons by volume unit. Besides, during the recombination of the electrons and ions, the new emitted photons can be cast in any direction, scattering and diluting the original radiation field from the star. Also, the energy radiated during the recombination process can be emitted by photons with energies minor than the original ionising photon. All these processes diminish the ionising capacity of the radiation field and put limits to the extension of the ionised region. The shape of the HII region depends on the initial distribution of the gas around the central star and its size depends on the total quantity of energy radiated by the star. If the radiation field is intense enough, when reaching the limits of the cloud, the radiation escapes: the HII region is defined as limited by density.

6.2 The Hα sample of isolated spiral galaxies

For the AMIGA CO and the Hα studies, the observations of the whole catalogue would have been too time-consuming. So we decided to focus on a smaller sample. To avoid well known biases due to flux- or magnitude-limited samples and to end with a complete and homogeneous sample, we kept all the galaxies in a volume-limited sample, i.e. with observed recession velocities V:

$$1500 kms^{-1} \leq V \leq 5000 kms^{-1}.$$

It represents about one fourth (251 galaxies) of the whole CIG. Among them, 27 were early-type galaxies according to our new morphological classification (Sulentic et al. 2005), hence left apart. We finally ended up with 224 late-type galaxies or lenticulars (S0a included). It is still a rather big sample allowing statistical studies of the properties of isolated spiral galaxies in the local Universe.

The observations are not complete since we only recently slightly change our initial strategy: we incorporate the CIGs with Karachentseva's isolation codes 1 & 2. The list of the 24 galaxies which are still to be observed are given in the Appendix A, Table A.2.

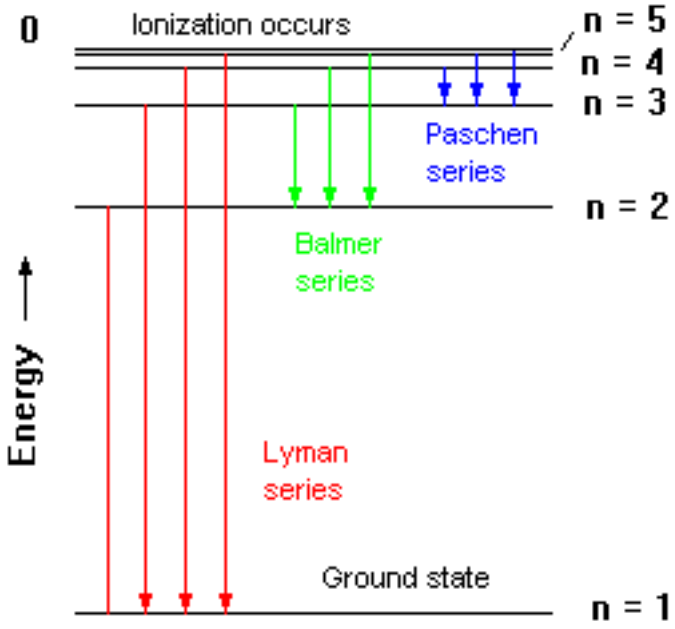

Figure 6.1: Hydrogen series.

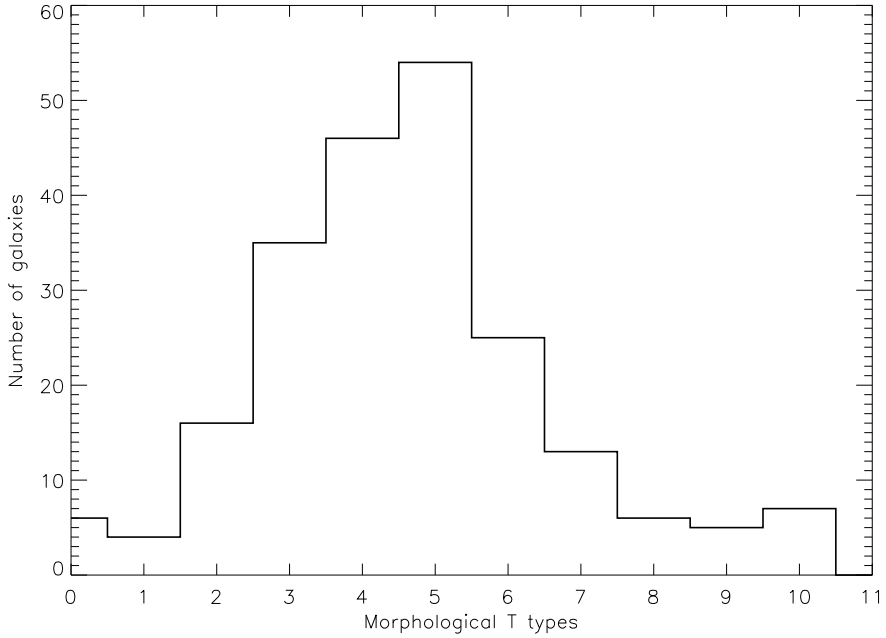

Figure 6.2: Morphologies.

The sample consists of 224 galaxies across all Hubble types from S0a to Im (see Figure 6.2).
The major axes of the galaxies are shown in Figure 6.3 (bin = 0.33 arcmin., only CIG 0080 with D = 7.2 arcmin. is not shown).
Figure 6.4 shows an histogram of the recession velocities of the galaxies in the sample (bin = 150 km s^{-1}).
Finally, Figure 6.5 shows the distribution of the blue luminosities (bin = 0.1 mag.).

6.3 The observations

6.3.1 Report on the obtained data

Next, we indicate the so far obtained data:

Observed galaxies Appendix A Table A.1

Among the 224 galaxies from the Hα sample presented in subsection 6.2, 200 have been observed. The Hα Galaxy Survey (James et al. 2004, 2005), kindly gave us 19 reduced galaxies that were in common in our two programs.

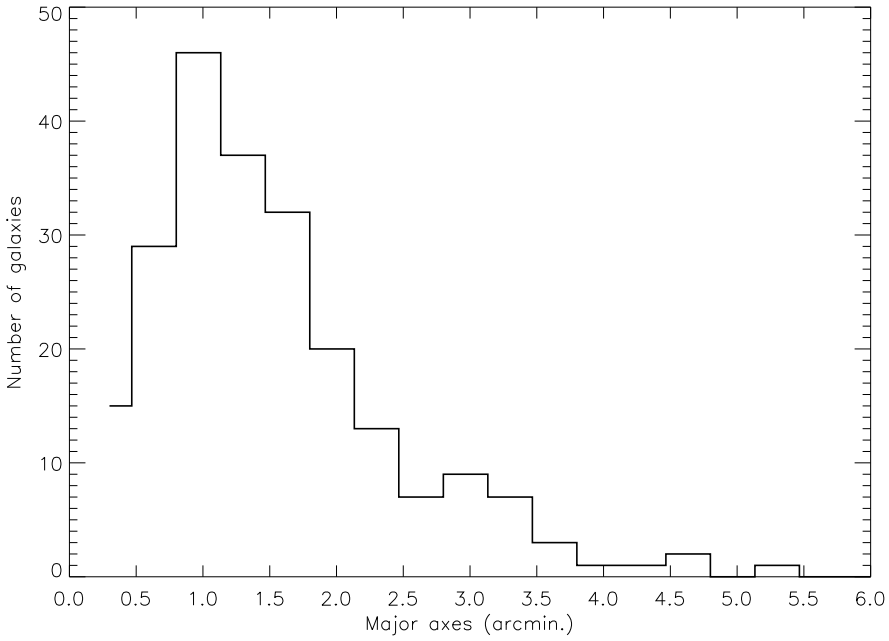

Figure 6.3: Major axes.

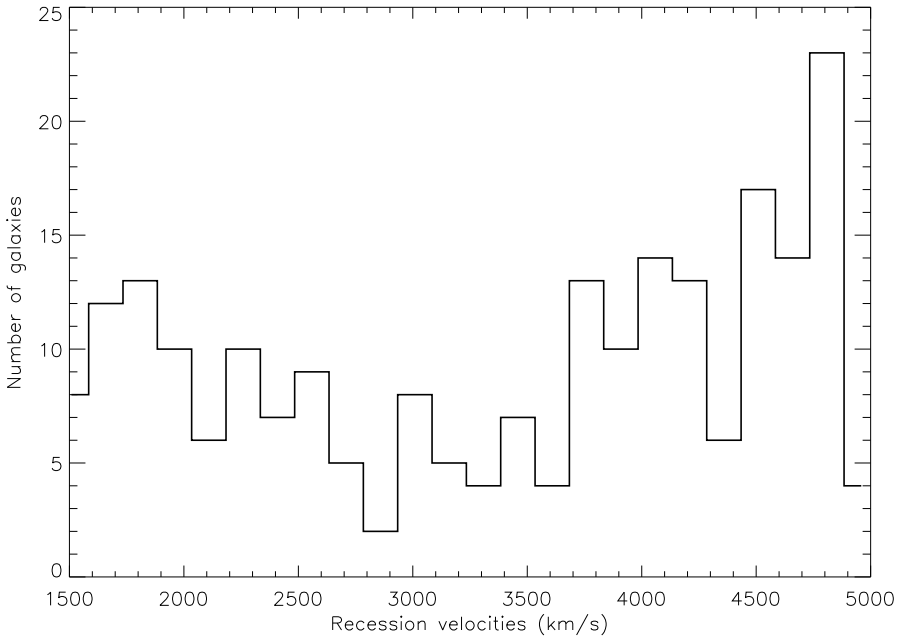

Figure 6.4: Recession velocities.

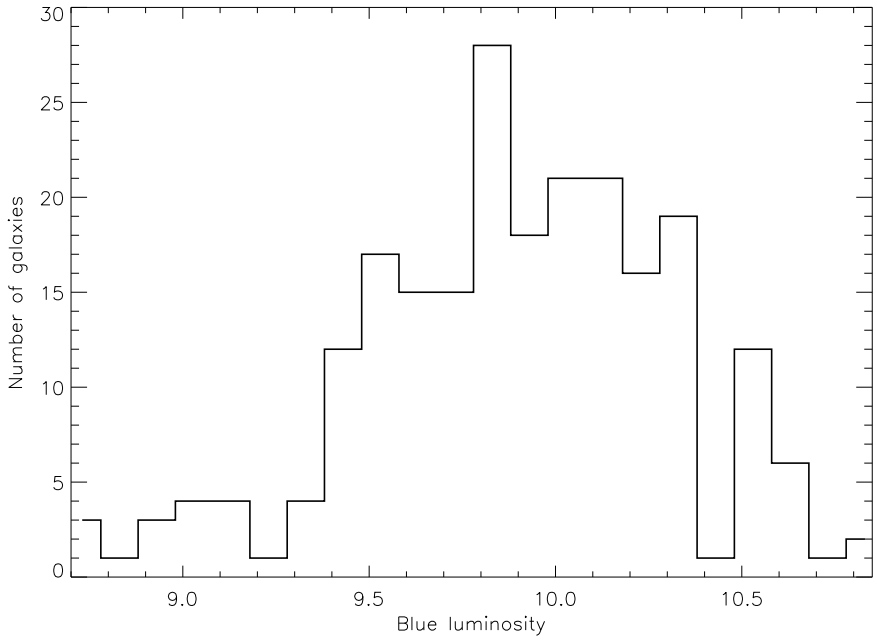

Figure 6.5: Blue luminosities.

Galaxies still to be observed Table A.2

24 galaxies of our sample remain to be observed because we include recently the galaxies with Karachentseva's 1986 isolation code 0 and 1 that we first discarded.

Galaxies with V $<$ 1500 km s^{-1} Table A.3

Data in the literature for CIGs with V $<$ 1500 km s^{-1}:

- Hα Galaxy Survey: 22 galaxies (James et al. 2004, 2005)
- GHASP: 16 galaxies (Garrido et al. 2002, 2003, 2004, 2005)
- BhaBAR: 7 galaxies (Hernandez et al. 2005)

6.3.2 The telescopes

The galaxies of our sample sweep all the northern sky, and we used 5 different (1-2 metre class) telescopes to collect our data: four in Spain, one in Mexico (see Table 6.1, hereafter).

Telescope	Diameter	Instrument	Resolution	Field of view	Altitude	Country
OSN[(1)]	1.5 m	Wright	0.338 arcsec./pixel	5.7×5.7 arcmin.^{2}	2896 m	Spain
	1.5 m	Roper scientific	0.232 arcsec./pixel	7.92×7.92 arcmin.^{2}	2896 m	Spain
CAHA[(2)]	2.2 m	CAFOS SITe-1d	0.53 arcsec./pixel	16×16 arcmin.^{2}	2200 m	Spain
EOCA[(3)]	1.52 m	Tektronics	0.4 arcsec./pixel	6.9×6.9 arcmin.^{2}	2200 m	Spain
JKT[(4)]	1.0 m	SITe2 CCD	0.33 arcsec./pixel	10×10 arcmin.^{2}	2400 m	Spain
SPM[(5)]	1.5 m	CCD SITe3	0.274 arcsec./pixel	4.7×4.7 arcmin.^{2}	2830 m	Mexico

Table 6.1: Telescopes
(1) Observatorio de Sierra Nevada - IAA
(2) Calar Alto Hispano-Alemán - MPI, IAA
(3) Estación de Observación de Calar Alto - OAN
(4) Jakobus Kapteyn Telescope - ING
(5) San Pedro Mártir - UNAM

6.3.3 The campaigns

Table 6.2 summarises the campaigns we obtained observing time for. We also reduced data from a couple of other campaigns done before October 2002, at Sierra Nevada Observatory.

Telescope	Date	Number of nights
OSN[(1)] 1.5 m	03/31/2003 - 04/06/2003	7
	04/30/2003 - 05/03/2003	3
	08/25/2003 - 08/31/2003	7
	11/24/2003 - 11/30/2003	7
	06/18/2004 - 06/27/2004	10
	08/16/2004 - 08/20/2004	5
	09/13/2004 - 09/18/2004	6
	12/05/2004 - 12/12/2004	8
	01/10/2005 - 01/16/2005	7
	03/10/2005 - 03/16/2005	7
	04/11/2005 - 04/15/2005	5
	05/23/2005 - 05/23/2005	1
	06/06/2005 - 06/07/2005	2
	10/01/2005 - 10/01/2005	1
	11/13/2005 - 11/13/2005	1
CAHA[(2)] 2.2 m	01/01/2003 - 01/06/2003	6
	08/01/2003 - 08/06/2003	6
	09/01/2003 - 09/01/2003	1
	09/16/2003 - 09/16/2003	1
	02/21/2004 - 02/26/2004	6
	04/20/2004 - 04/25/2004	6
EOCA[(3)] 1.52 m	10/20/2003 - 10/25/2003	6
	02/22/2004 - 02/24/2004	3
	05/19/2004 - 05/21/2004	3
JKT[(4)] 1.0 m	07/22/2003 - 07/31/2003	10
SPM[(5)] 1.5 m	05/01/2003 - 05/04/2003	4

Table 6.2: Schedule of observation runs
[(1)] Observatorio de Sierra Nevada - IAA
[(2)] Calar Alto Hispano-Alemán - MPI, IAA
[(3)] Estación de Observación de Calar Alto - OAN
[(4)] Jakobus Kapteyn Telescope - ING
[(5)] San Pedro Mártir - UNAM

Chapter 7

Data reduction

Contents

7.1 Introduction

The galaxies composing the sample described in section 6.2 were observed in 1-2 metre class telescopes as a compromise between our large number of objects (more than two hundreds) and the needed resolution and quality of the data. A significant amount of time was spent writing applications in order to obtain observing time as well as preparing the observations (specificities of the telescope, selection of the more adequate targets for each telescope, observing strategy, etc.), which have been mostly carried out in situ. We observed all over the year as our objects range the entire right ascension domain.

We specifically asked for dark nights because of the magnitudes of our objects and the use of narrow-band filters. In order to derive the Hα luminosity function, we needed also photometric data for our galaxies: we observed spectrophotometric standard stars (about 3 different stars per night, 3 times each star). When a night occurred not to be fully photometric, we still took data for the galaxies without observing the stars. In order to be able to calibrate these images we repeated one Hα exposure during the next photometric night, together with exposures of standard stars. This method allowed us to calibrate the whole set of images previously obtained. The spectrophotometric standard stars were chosen from the ING catalogue.

Hereafter, we detail the filters used in the observations:

1. **Hα** (narrow-band filter, typically 50 Å) - The Hα filter traces the regions ionised by newly born stars. For every galaxy, we selected the more appropriate redshifted Hα filter based on its observed recession velocity.

2. **r Gunn** (broad-band filter, typically 870 Å) - The r Gunn filter gives the bulk of the optical emission in a galaxy. As it includes wavelengths containing the Hα line, it is also used to subtract the continuum contribution affecting the narrow-band filter.

The telescopes we used are equipped with recent Charge-Coupled Device (CCD) instruments. The CCD is constituted by a solid surface sensitive to the light, and contains an integrated circuit to read and store electronically the images projected on it.

7.2 Instrumental signature

The technical aspects and scripts that automated the reduction are given in Appendix B so as to render these sections more legible. We automated

and adapted scripts to reduce our data in an homogeneous way and get high quality final images[1].

The CCD raw images suffer various limitations but the final quality of the images can be significantly improved following a basic treatment. In the most frequent cases, the raw images contain at least three artifacts: the *dark current*, the *variations in sensitivity* on the detector surface and the *noise* from different origins (mainly the read out noise).
To remove the instrumental signature from our data, we employed one of the most extensively used software in Astrophysics: the Image Reduction and Analysis Facility (IRAF). As an example of the typical reduction process we have followed, we show all the steps for the April 2005 campaign done at the OSN (see Table 6.2). The galaxy that we consider is CIG 0744.

7.2.1 Bias

For details, please see ▶ *B.1.1.*

The bias frames result from a current injected in the chip which defines the level zero of the electronics, so its contribution has to be removed from each of the images, including the flat fields. During the observation nights, we took a long sequence of bias at the beginning and end of the night, and also controlled the bias level various times (typically 5 times) distributed all along the night to check for systematic changes. For example, in this particular campaign (one single night), we took 25 biases:
cl> imstat @bias.lis[2]

After checking the stability of the bias frames during the night, we decided to keep the 25 of them to produce the super-bias. We used the median for the combination, less sensitive to discrepant values than the average:
cl> imcombine @bias.lis superBias.fit combine=median reject=avsigclip

7.2.2 Flat fields

For details, please see ▶ *B.1.2.*

We always used sky flat fields to remove the differences in sensitivity (quantum efficiency, dust, ...) to the light from pixel to pixel in the CCDs, because they give more accurate results (evenly illuminated) in the estimation than dome flats, more dependent on the illumination conditions under which they are taken (illumination differences, ...). We used both sunset and sunrise exposures to improve the statistics and have a reduced noise in

[1] This reduction process greatly benefited from the help of **Jorge Iglesias-Páramo**.
[2] All the command lines will be typed in this manner: showing the IRAF Command Language prompt "cl>", followed by the command line in red.

our final super-flat fields.

We first subtracted the super-bias to each flat field:
cl> cl < flat-b.cl

Then, we compared the flat fields among themselves, dividing one by another, to check if there were peculiar ones:
cl> cl < flat-comp.cl

We created a super-flat field for each filter (r Gunn and Hα). We did not compute the statistics over the whole chip but on slightly smaller regions to avoid edge effects (due to the placement of the filters in the wheel for instance):
cl> imcombine @superFlatH.lis superFlatH.fit combine=median reject=avsigclip scale=mean statsec=[300:1750,300:1750]
cl> imcombine @superFlatR.lis superFlatR.fit combine=median reject=avsigclip scale=mean statsec=[300:1750,300:1750]

We had to normalise to 1 the level of these flat fields in order to further keep the real counts from the galaxies:
cl> cl < superFlatN.cl

7.3 Science images

For details, please see ▶ B.2.

At this point we can proceed to remove the additive and multiplicative errors estimated in the previous section from the images of the galaxies.

For our images of galaxies, we needed to build up signal to noise using long exposures, especially using narrow-band filters. Unfortunately there are some obstacles to make extremely long exposures, including imperfect tracking, accumulation of cosmic rays, ...
The way to get around this is to take several exposures and combine them. We systematically took 3 to 5 images in each filter (but up to 72 when the presence of nearby bright star prevented long time exposures!). We used auto-guiding pointing on relatively bright stars near the galaxy observed.

It took more than a couple of hours to complete the observations of a galaxy. The typical exposure times were 300 seconds for the r Gunn filter and 1200 seconds in Hα. We applied small shifts between two successive exposures to be able to treat bad pixels or bad lines on the chip and punctual events (cosmic rays, passage of space satellites, ...).

7.3.1 Cosmic rays

For details, please see ▶ B.2.1.

Cosmic rays are high energy particles which pass through the CCD detector and deposit large amounts of energy. They show up in the images as pixels significantly brighter than their surroundings.

Because of the long integration time of the Hα exposures, the number of cosmic rays reaching the chip meanwhile became very significant. On the other hand, the r Gunn images are only slightly affected by the presence of cosmic rays which will be well removed during the final combination of the exposures. Hence, we first removed the cosmic rays from the Hα images:
cl> cl < cig0744-cr.cl

7.3.2 Bias

For details, please see ▶ B.2.2.

In this step, the pedestal level of the super-bias obtained as explained in subsection 7.2.1 was subtracted from all the images (including the flat fields):
cl> cl < cig0744-b.cl

7.3.3 Flat fields

For details, please see ▶ B.2.3.

We divided our images of galaxies by the normalised super-flat fields (obtained subsection 7.2.2) corresponding to each filter:
cl> cl < cig0744-bf.cl

7.3.4 Sky background

For details, please see ▶ B.2.4.

The background contribution was estimated from a region surrounding the galaxy (again to avoid edge effects where the level of the sky is generally smaller due to small vignetting by the filter stiles) and then, subtracted from the images:
cl> cl < cig0744-bfs.cl

7.3.5 Exposure Time

For details, please see ▶ *B.2.5.*

We divided each image by its exposure time to have the flux of the galaxy per second:
cl> cl < cig0744-bfst.cl

7.3.6 Centring

For details, please see ▶ *B.2.6.*

We needed to align the multiple images before the stacking. We centred all the images (both filters), taking as a reference the first image in Hα. The coordinates (precise to the tenth of a pixel, after applying a Gaussian fit) of at least five stars shared in common by all the images were used:
cl> cl < cig0744-bfstc.cl

7.3.7 Point Spread Function

For details, please see ▶ *B.2.7.*

In order to combine the images they need to have the same Point Spread Function (PSF). We degraded the seeing of the best images to reach the PSF of the image possessing the worst seeing:
cl> display TMP/c0744_002H6607-bfstc.fit 1 fi+
cl> rimcursor > starsPsf0744.lis
cl> cl < cig0744-bfstcp.cl

Sometimes, when the seeings of the images were very close and the matched images degraded too much or added parasite features to our science images, we did not use this option. We simply used the original centred images for the remaining steps. This is not critical because in these cases, all the images of a given galaxy were taken on the same instrument, the same night, within a couple of hours.

7.3.8 Combining

For details, please see ▶ *B.2.8.*

In each filter, the final image was obtained, using an algorithm to keep the median value of each pixel. The rejection algorithm removed quite effectively the few cosmic rays in the r Gunn images:
cl> imcombine @c0744rG.lis Im/cig0744rG.fit combine=median reject=avsigclip
cl> imcombine @c0744Ha.lis Im/cig0744Ha.fit combine=median reject=avsigclip

7.3.9 Continuum subtraction

For details, please see ▶ B.2.9.

The removal of the continuum contribution to the flux in the images taken through the narrow-band Hα filter is the most delicate task. James et al. (2004) tested various methods: numerical integration to find the ratio of the filter profile integrals, photometry of standard spectrophotometric stars through the pair of filters to find the scaling factor, use of foreground stars in the narrow-band and continuum images of each galaxy. The two last methods gave the most consistent and accurate results. The latter method has two advantages: it takes into account any changes in the sky transparency between the two images and the possibility to use several stars improves the statistics and lead to the most accurate removal. Hence, we used this last method to find the scaling factor to be applied to the images used for continuum subtraction. To estimate the fluxes, we use the task qphot with the following parameters (Massey et al. 1989; Stetson 1990):

photometric aperture: 1.5-2 $\times$ the seeing

inner radius: 4-5 $\times$ the aperture

width annulus: 2 $\times$ the aperture

centering box: 10 pixels

To have good precision, we estimated the flux of at least 10 stars in the two filters (see Figs. 7.1 & 7.2), they should not be saturated, not to distort a real estimation of the counts. When we traced the flux in r Gunn vs. the flux in Hα for each stars, the slope of a linear fit provided the scale factor between the two images (Fig. 7.3):
ap> qphot Im/cig0744Ha.fit
ap> qphot Im/cig0744rG.fit

The Hα image after the continuum subtraction is shown Fig. 7.4. The positions of the stars used to find the scale factor are marked with green circles. All the stars in the image have disappeared, only residuals can be seen for the most brilliant ones, for which the matching is the most difficult.

7.3.10 Final images

For details, please see ▶ B.2.10.

Stamps of 512 $\times$ 512 pixels

To have the very final images, we need to cut the images around the galaxy. We defined the centre as the maximum of the luminosity of the bulge. We cut 512 pixels per edge because these images will be involved in

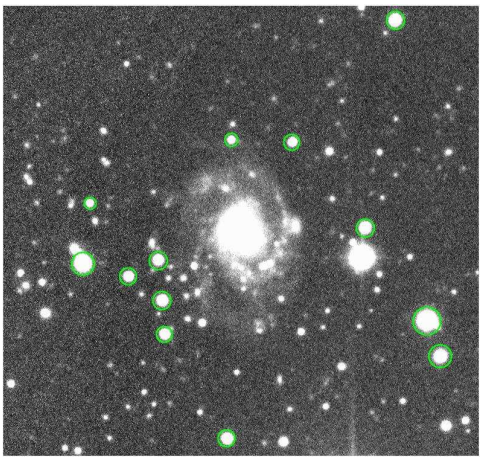

Figure 7.1: Raw r Gunn image.

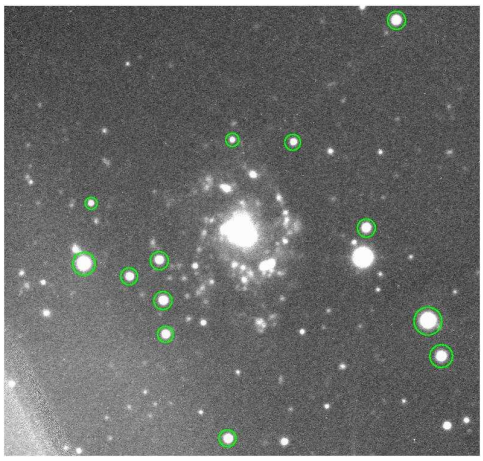

Figure 7.2: Raw Hα image.

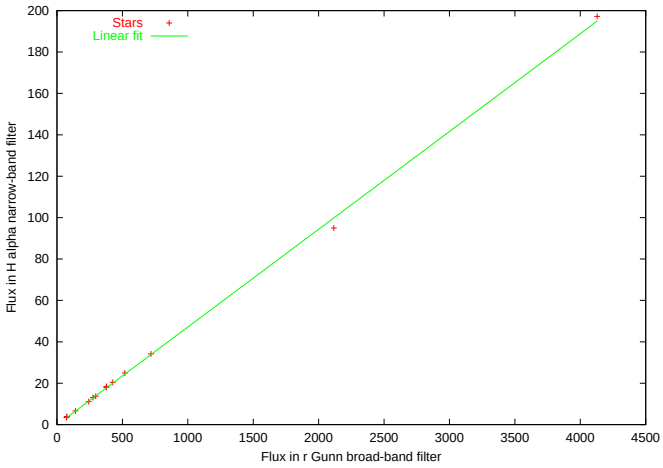

Figure 7.3: Scale factor.

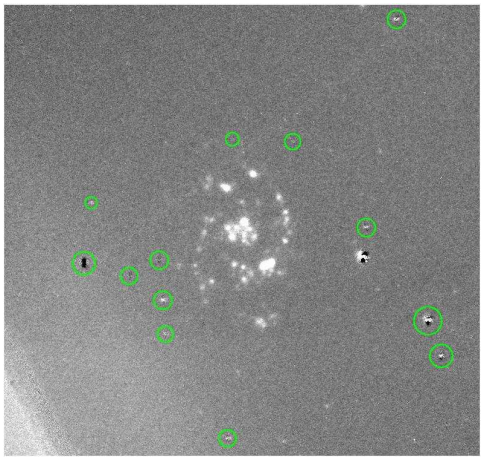

Figure 7.4: Hα - continuum.

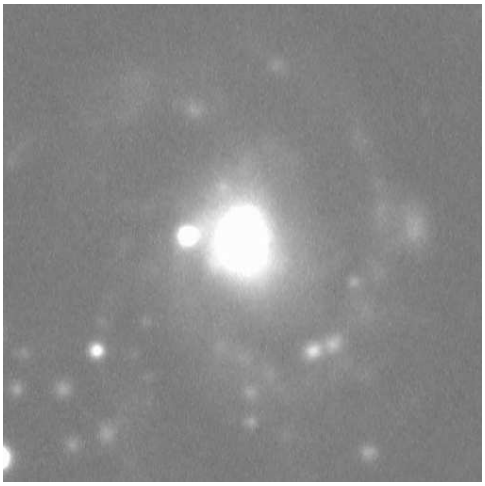

Figure 7.5: r Gunn with stars.

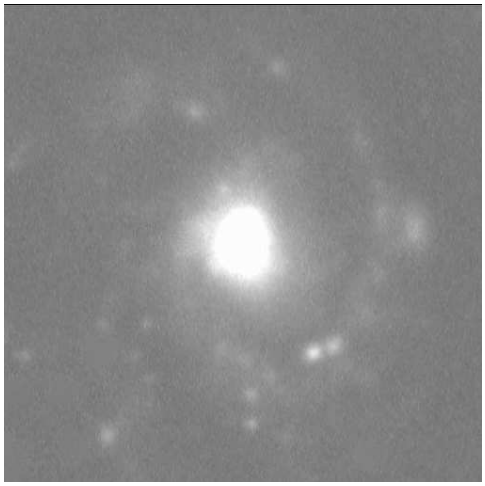

Figure 7.6: r Gunn without stars.

an Fast Fourier Transform treatment more effective with power of 2 sized images (see section 8.3). The centres in r and Hα continuum subtracted generally agreed perfectly. When there was no central emission in Hα, we used the centre defined in the r Gunn image. This is important because as we will derive the torques between the two components (see section 8.3.3), we do not want to add any artificial torque resulting from artifacts. But as the images were previously aligned to the tenth of a pixel, we are very confident, and this could be checked on the positions of more external Hα bursts.
For CIG 0744, the centre was: 1081.34 876.00.
cl> imcopy Im/cig0744rG.fit[826:1337,621:1132] Im/cig0744rG512.fit
cl> imcopy Im/cig0744Ha-rG.fit[826:1337,621:1132] Im/cig0744Ha-rG512.fit

Cleaning

As we will derive the potential from the luminosity, we need to erase all the foreground stars in the r Gunn image because we do not want spurious potential wells that would be created by the conversion of the luminosity of those stars. The Hα images were also revised to clean some noise which can arise from the residuals of saturated stars for example. Both in r and Hα, the areas occupied by the stars were replaced by rectangular (spikes of saturated stars for instance) or circular aperture regions of background values (see Figs. 7.5 & 7.6):
cl> imedit Im/cig0744rG512.fit Im/cig0744rG512cl.fit
cl> imedit Im/cig0744Ha-rG512.fit Im/cig0744Ha-rG512cl.fit

Final Images

Each telescope has its own proper configuration to store and save the

images: a final flip, rotation or mirror operation was generally needed to have the conventional orientation (North at the top, East in the left direction):
cl> imcopy Im/cig0744rG512cl.fit[*,-*] Im/c0744R.fit(flip around the X-axis)
cl> imcopy Im/cig0744Ha-rG512cl.fit[*,-*] Im/c0744H.fit

The final images for this galaxy are presented page 138.

Chapter 8

Analysis of the HII regions

Contents

8.1 Introduction

The presence of a bar in a spiral galaxy is a striking feature and, as such, is one of the fundamental elements of the first morphological classification done by Hubble, which gives the aspect of a "tuning fork". The bar frequency that can be determined in galaxies depends on the wavelength of the images but is always higher than 65%. Some estimations based on NIR images, not affected by extinction and tracing mainly the old population, reveal that as high as 90% have bars.

Numerical simulations have established that bars in gas-rich spiral galaxies are short-lived structures. There are at least two mechanisms able to weaken the bars. The first one is the building of a large central mass concentration, due to the gas inflow to the centre through the negative torques exerted on the gas by the bar. The torques are proportional to the phase shift between the gas and the stellar bar. It is well known that the gas is concentrated on the leading side of the bar (e.g., de Vaucouleurs & de Vaucouleurs 1963). The gravitational torque of the bar makes the gas lose angular momentum, driving it towards the centre and creating a central mass concentration. The latter is able to perturb the elongated orbits supporting the stellar bar, deflecting the stars passing close to the centre. This weakens the bar (Pfenniger & Norman 1990).

However, Bournaud et al. (2005) have just shown, using fully self-consistent simulations, that with gas parameters typical for normal spirals, the mass concentration is not sufficient to fully dissolve the bar, as was also claimed by Shen & Sellwood (2004).

The second mechanism is due to the bar torques themselves. From the equality between action and reaction, the gas exerts a positive torque on the bar, which then gains angular momentum. Since the bar is a negative angular momentum wave, this gain will weaken and destroy it. The angular momentum lost by the gas is gained by the bar, which dissolves progressively. For typical Sb-Sc galaxies, the bar is destroyed in about 2 Gyr (Bournaud & Combes 2002). The observation of a high bar frequency from $z \sim 0$ to $z \sim 0.7$ (Eskridge et al. 2002) cannot thus be interpreted to support the existence of robust, long-lived bars. Instead, this supports the frequent renewal of bars. Berentzen et al. (2004) have shown that interactions can only form bars in gas-poor galaxies, which is not the case for most spiral galaxies.

Bar renewal can occur when the disk of spiral galaxies are replenished in cold gas through external accretion, able to increase significantly the disk to bulge ratio. Block et al. (2002) suggests that external accretion of gas in the disk of spirals plays a fundamental role in explaining the high fraction of barred spirals and the observed torque distribution. Models of isolated, non accreting galaxies are very unlikely.

To better understand the frequency of bars and their origin, measurements of the gravitational torques and bar forces in field galaxies have been done (Block et al. 2002; Laurikainen et al. 2004a,b; Buta et al. 2004), but this is not the case for isolated galaxies.

We therefore present such a study in the following chapter: we analyse through Fourier analysis of gravitational potential and density, the intensity of $m = 1$, $m = 2$, .. perturbations in an isolated sample of 45 galaxies. From the Hα maps, we derive the gravitational torques exerted by the stellar bar on the gas component (phase shift measured). We can thus deduce the life time of the bar, when there is one, and check whether the time spent in various bar strength categories correspond to the frequency observed.

We also classify the different spatial distributions of star forming regions (Hα) in barred galaxies. The most frequent distribution does not coincide with that of the gas. This implies that the classical Schmidt law for star formation, only function of density, is too simple, and that a dependency as a function of velocity should be taken into account.

8.2 The Hα subsample

We studied the morphology of some isolated spiral galaxies in more details. We focused on a subsample drawn from the Hα sample defined in Chapter 6 (subsection 6.2).

From the sample of 200 spiral galaxies, with recession velocities 1500 $\leq V \leq$ 5000 km s^{-1}, we selected the galaxies with available data, respecting the following requirements:

Sufficient spatial resolution In the case of our observations, this translates into galaxies having major axis greater or equal to **1 arcmin**;

Low-inclination In order to obtain a sufficiently accurate deprojection, the inclination has to be minor or equal to **50**°.

With these criteria, we get 45 galaxies (almost one quarter of the whole Hα sample). The required data have been reduced following the method described in Chapter 7. The r Gunn broad-band images trace the stellar component of the galaxy, and the Hα images show the young stars born from the gas (HII regions).

Table 8.1 reports information about the main characteristics of the selected galaxies, along with some technical indications. The PA, inclination and rotation direction listed are those used to run the programs (24 counter-clockwise, 19 clockwise).

Special notes on individual galaxies:

CIG 0050 *Very irregular galaxy: the rotation sign was arbitrarily put to "+".*

CIG 0080 *We resample the initial image 2048 × 2048 of 0.23 arcsec/pix., gathering the pixels 2.5 by 2.5 (new pixels represent 0.58 arcsec.). We conserved the flux in order to derive real potential and density.*

CIG 0085 *Very irregular galaxy: the PA was put to 0 arbitrarily for the deprojection and the rotation sign to "+".*

CIG 1004 *Unfortunately, it seems that a guiding problem during the Hα exposure occurred. We had to resample the pixels 1.5 by 1.5 (new pixels represent 0.50 arcsec.) those images in order to have the full design of the galaxy into account in our work.*

CIG	Diam. (arcmin.)	PA (°)	Incl. (°)	Rotation (trigo.)	T (revised)	Velocity (km s^{-1})	Dist. (Mpc)	Seeing (arcsec.)	Size (pix.)	Pixel (arcsec.)	Telesc.	Date
0030	1.0	32	33.9	+	5	4586	57	1.6	256	0.23	OSN	Aug 04
0050	1.2	170	40.8	?	10	2132	24	1.7	256	0.33	JKT	Jul 03
0053	1.7	83	23.8	+	4	3128	38	1.4	256	0.33	JKT	Jul 03
0059	2.7	120	38.8	+	5	4303	53	2.3	256	0.23	OSN	Aug 03
0066	1.3	170	42.1	-	4	4655	51	2.1	256	0.53	CAHA	Apr 04
0068	2.3	45	26.6	+	1	1733	19	1.5	256	0.33	JKT	Oct 01
0080	7.2	130	48.5	+	998	2458	29	1.5	512	0.58	OSN	Aug 04
0084	1.7	164	38.2	-	5	4649	58	1.7	256	0.23	OSN	Aug 03
0085	2.2	0	20.8	?	998	2640	32	1.3	256	0.33	JKT	Jan 02
0096	4.7	20	47.9	+	5	1559	17	1.0	512	0.33	JKT	Oct 01
0116	1.4	110	44.7	-	2	3901	49	2.4	256	0.23	OSN	Aug 03
0176	1.3	100	40.4	+	5	4955	66	2.2	256	0.53	CAHA	Apr 04
0188	3.5	85	29.3	+	6	1733	24	1.6	512	0.33	JKT	Jan 01
0217	1.4	111	20.4	-	5	3504	48	2.6	256	0.34	OSN	Oct 02
0250	2.2	45	47.0	-	5	2125	31	1.6	512	0.33	JKT	Oct 01
0267	1.5	45	42.8	+	6	4256	57	1.8	512	0.23	OSN	Jan 05
0281	1.6	0	18.9	+	5	4244	60	2.4	256	0.53	CAHA	Jan 03
0291	1.4	175	41.7	+	5	2521	38	2.2	256	0.46	OSN	Nov 03
0359	1.8	40	44.5	-	1	4932	70	1.8	512	0.46	OSN	Jan 05
0376	1.5	106	26.0	+	5	3365	46	2.1	256	0.46	OSN	Jan 05
0382	1.7	7	35.6	-	4	2457	33	2.1	512	0.23	OSN	Apr 03
0512	2.6	150	29.0	-	5	1892	30	3.8	512	0.46	OSN	May 03
0575	1.7	50	44.1	+	3	2612	39	3.6	256	0.46	OSN	Apr 03

Continued on next page

CIG	Diam. (arcmin.)	PA (°)	Incl. (°)	Rotation (trigo.)	T (revised)	Velocity (km s^{-1})	Dist. (Mpc)	Seeing (arcsec.)	Size (pix.)	Pixel (arcsec.)	Telesc.	Date
0645	1.8	20	43.1	+	5	4027	55	3.0	512	0.27	SPM	May 03
0652	1.9	60	40.2	+	5	1962	29	1.9	256	0.23	OSN	Apr 03
0660	1.3	36	37.0	+	6	2137	29	2.2	256	0.23	OSN	May 03
0661	1.3	60	48.4	+	8	3341	45	1.4	256	0.33	JKT	Jul 03
0700	1.3	95	34.0	-	6	3838	53	2.1	256	0.33	JKT	Jul 03
0712	2.1	168	46.6	+	4	1854	26	1.6	512	0.46	OSN	Jul 05
0744	2.1	0	29.2	+	5	2596	35	2.9	512	0.23	OSN	Apr 05
0750	1.1	0	16.4	-	5	4020	54	1.7	256	0.53	CAHA	Aug 03
0754	1.0	140	39.5	-	5	4594	62	2.0	256	0.53	CAHA	Aug 03
0808	2.8	6	42.6	+	5	1691	22	1.2	256	0.33	JKT	Jul 03
0812	2.8	130	46.0	-	4	3119	41	2.6	512	0.46	OSN	Apr 03
0840	1.5	45	45.1	+	4	4757	62	1.6	256	0.53	CAHA	Aug 03
0854	1.5	15	39.0	-	5	4856	63	1.7	256	0.53	CAHA	Aug 03
0862	1.3	106	25.8	-	4	4671	61	1.8	256	0.23	OSN	Jun 04
0875	1.0	158	45.8	-	3	4880	64	1.7	256	0.53	CAHA	Aug 03
0924	1.5	160	43.6	+	5	4540	56	1.6	256	0.23	OSN	Aug 03
0931	1.5	85	18.9	-	4	4750	59	2.6	256	0.53	CAHA	Sep 03
0935	1.6	105	40.0	+	5	3985	49	2.4	256	0.34	OSN	Oct 02
0992	2.1	38	26.5	+	5	3506	42	2.1	512	0.23	OSN	Aug 03
1001	2.4	168	48.7	-	2	3078	36	1.3	512	0.33	JKT	Jul 03
1004	4.1	25	36.4	-	4	2376	27	1.1	512	0.50	JKT	Oct 01
1039	1.0	10	47.6	-	5	4859	60	1.1	256	0.23	OSN	Aug 03

Table 8.1: The 45 CIG galaxies selected.

8.3 Image analysis

I made use of programs coded by
Francoise Combes
to calculate the potential, density and torques.

- We used the raw r band image (not scaled to Hα) and the Hα continuum subtracted image. We defined the centre as the maximum in luminosity near the geometrical centre. The centre is the same on the r and Hα image to avoid artificial torques between the two components. We cut 512 $\times$ 512 pixels^2 stamps.
- We removed the stars to avoid a contamination in the density and potential derived from the luminosity of the pixels.
- We deprojected the galaxy to have the gravitational potential in the disk plane.
- We determined the bar/arm force at each radius.
- We made use of the method developed a dozen years ago by F. C.'s team to compute the gravitational potential, applying it to our red images, supposing a constant M/L ratio. A Fourier-component analysis of the potential was performed, with a special interest on the m = 2 component to identify the bar(s) (Block et al. 2002), and m = 0 to get the axisymmetric tangential and radial forces, depending on the radius. Their quotient provided us a measurement of the bar/arm force.
- We estimated the average torque depending on the radius: using the gravitational forces and the young stars born from the gas (Hα), we obtained the phase shift between gaseous arms and the potential well which creates the torques.
- We estimated the angular momentum transfer and therefore the evolution time for bars in isolated galaxies.
- Gas depletion time and possible requirement for an external source of gas.
- Comparison to galaxies in higher density environments, and with numerical models of evolution (Block et al. 2002; Bournaud et al. 2005).

8.3.1 Potential

To get the stellar disk potential, we have to know how the mass is distributed in a typical spiral galaxy: we use a model to infer the third dimension. Spiral

galaxies are composed by a bulge (spheroidal component in the centre) and a disk, very flat, extending far from the centre. The luminosity profile of 36 spiral galaxies (including S0) was studied by Freeman (1970) and can be represented by an exponential:

$$I(r) = I_0 \exp^{-r/r_0}$$

where I_0 is the brightness extrapolated in the centre and r_0 the characteristic radius.

The potential is decomposed as:

$$\Phi(r,\theta) = \Phi_0(r) + \sum_m \Phi_m(r)\cos(m\theta - \phi_m)$$

where the strength of the m-Fourier component is $Q_m(r) = m\Phi_m/r|F_0(r)|$, and its global strength over the disk: $\max_r(Q_m(r))$ (e.g., Combes & Sanders 1981).

8.3.2 Surface density

The (disk) surface density is decomposed as:

$$\mu(r,\phi) = \mu_0(r) + \sum_m a_m(r)\cos(m\phi - \phi_m(r))$$

where the normalised strength of the Fourier component m is $A_m(r) = a_m/\mu_0(r)$.

The density is more local and raw, more noisy also. It's complementary to the potential which is more model dependent (spherical dark matter) the information is diluted.

8.3.3 Torques

The maximal torque at a given radius is defined by:

$$Q_T(R) = \frac{F_T^{max}(R)}{F_0(R)} = \frac{\frac{1}{R}(\frac{\partial\Phi(R,\theta)}{\partial\theta})_{max}}{\frac{d\Phi_0(R)}{dR}}$$

where $F_T^{max}(R)$ represents the maximum amplitude of the tangential force at radius R, and $F_0(R)$ is the mean axisymmetric radial force inferred from the m=0 component of the gravitational potential.

Generally, the gas inflows towards the centre (negative torque) from the corotation radius to the inner Linblad resonance (ILR) and flows outwards

(positive torque) when outside the corotation radius, until the outer Lindblad resonance (OLR).

The next page shows a template summarising the information we present for each of the 45 galaxies. For the graphics of the potential and the density, the legend is the following:
- dashed line represents m = 1[0:2π];
- full line represents the m = 2 component (and the sum also for the amplitude of the potential as it is always above and cannot be confused with the others);
- dot-dash-dot-dash represents m = 3;
- dotted line represents m = 4.

8.4 Details of the 45 galaxies

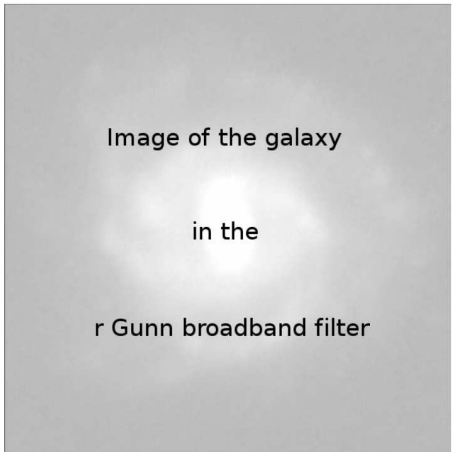

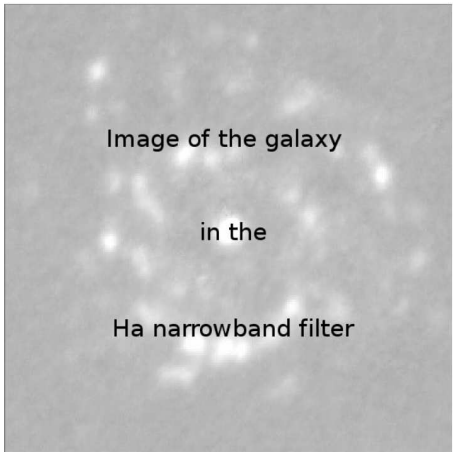

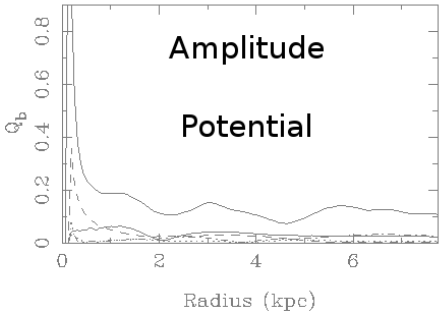

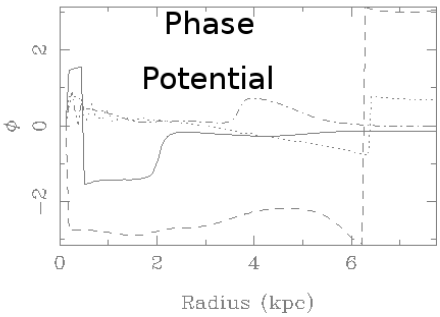

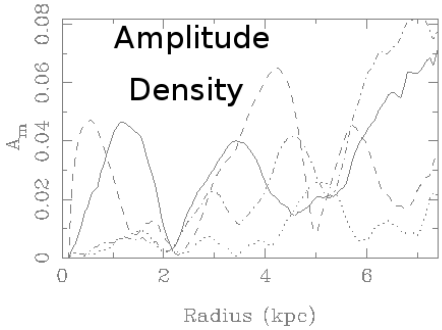

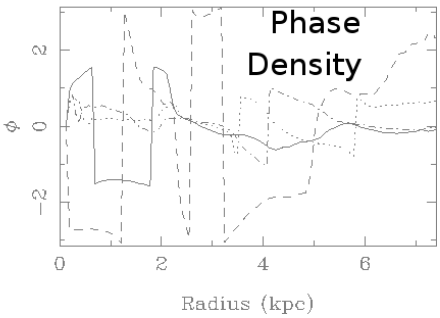

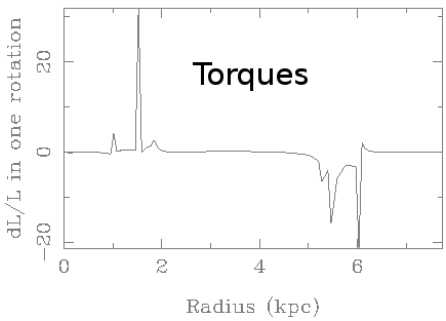

Figure 8.XX: **CIG number.**
Observed velocity: in km s^{-1}
Optical diameter: D_{25} in arcmin.
Blue luminosity: in $L_\odot$
Morphology: from NED
Group: see section 8.6.3

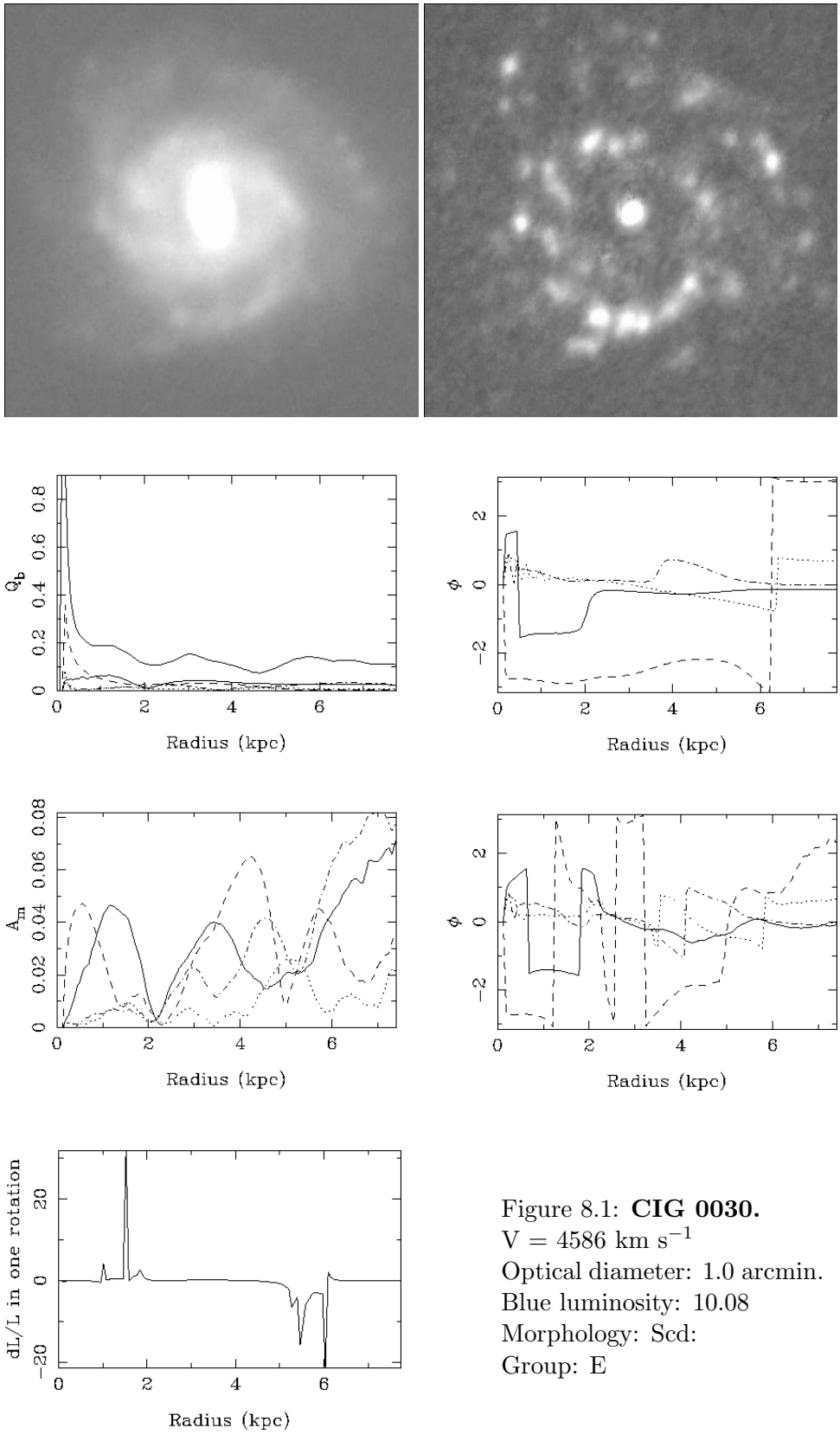

Figure 8.1: **CIG 0030.**
V = 4586 km s^{-1}
Optical diameter: 1.0 arcmin.
Blue luminosity: 10.08
Morphology: Scd:
Group: E

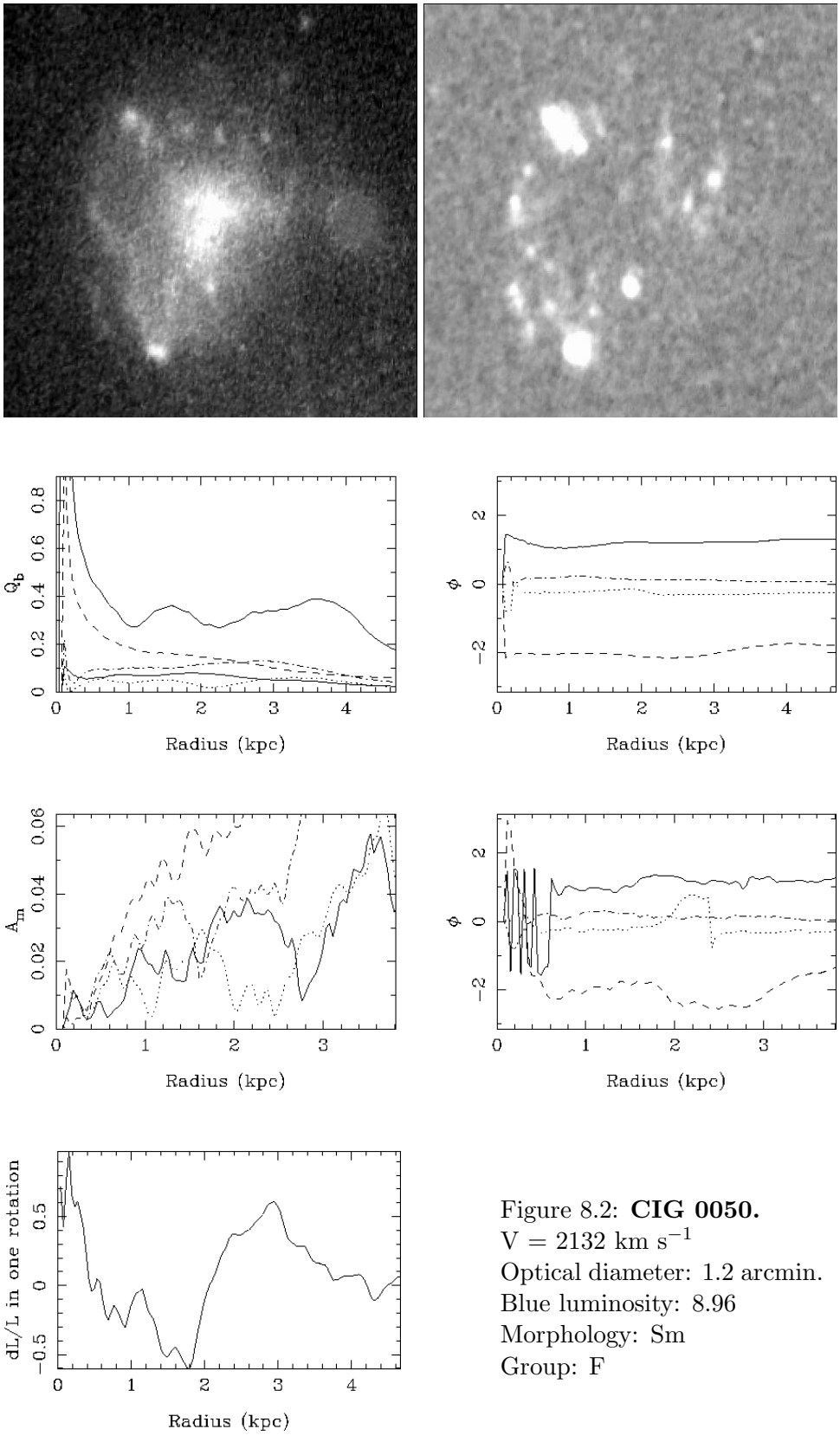

Figure 8.2: **CIG 0050.**
V = 2132 km s^{-1}
Optical diameter: 1.2 arcmin.
Blue luminosity: 8.96
Morphology: Sm
Group: F

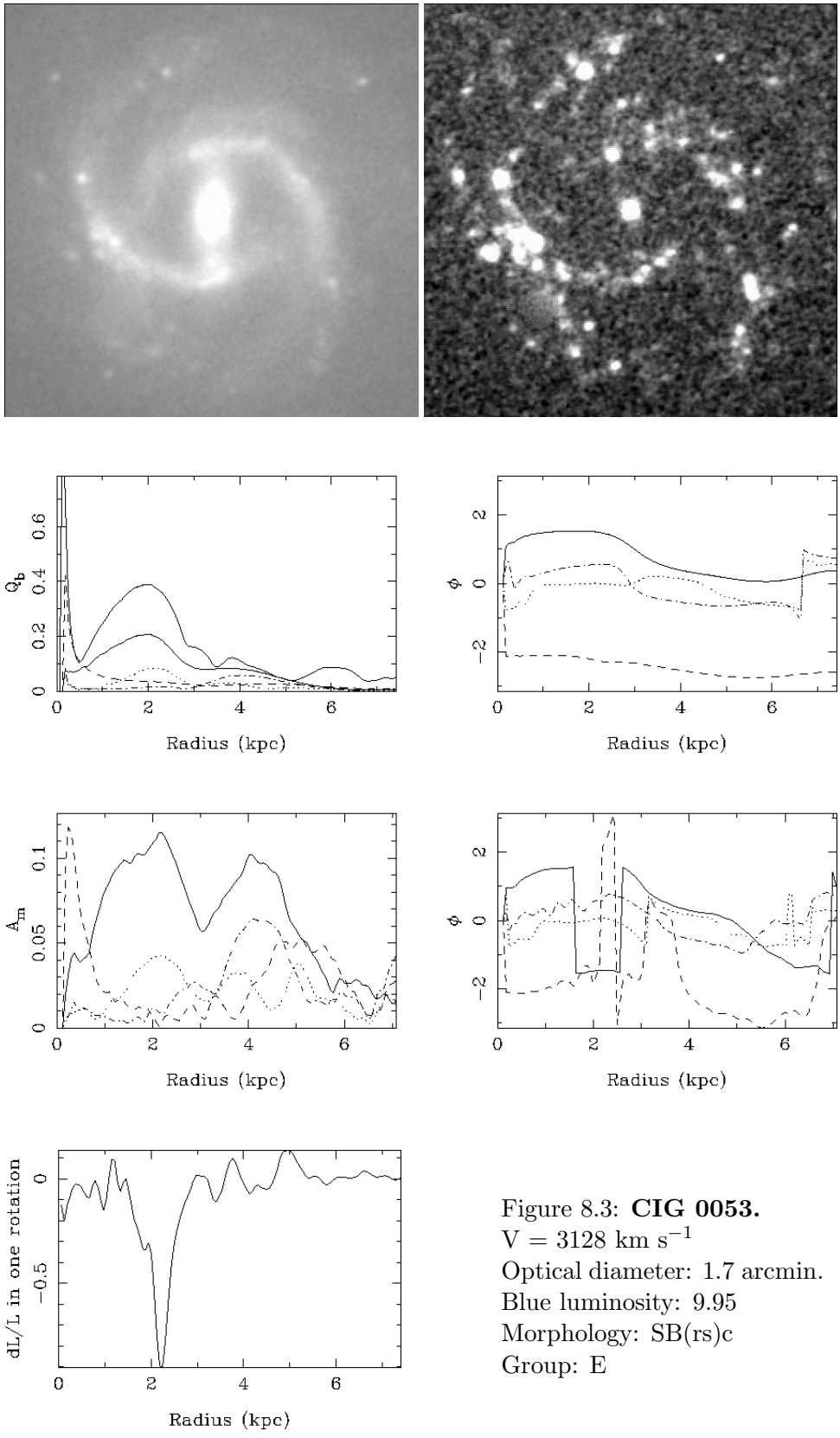

Figure 8.3: **CIG 0053.**
V = 3128 km s^{-1}
Optical diameter: 1.7 arcmin.
Blue luminosity: 9.95
Morphology: SB(rs)c
Group: E

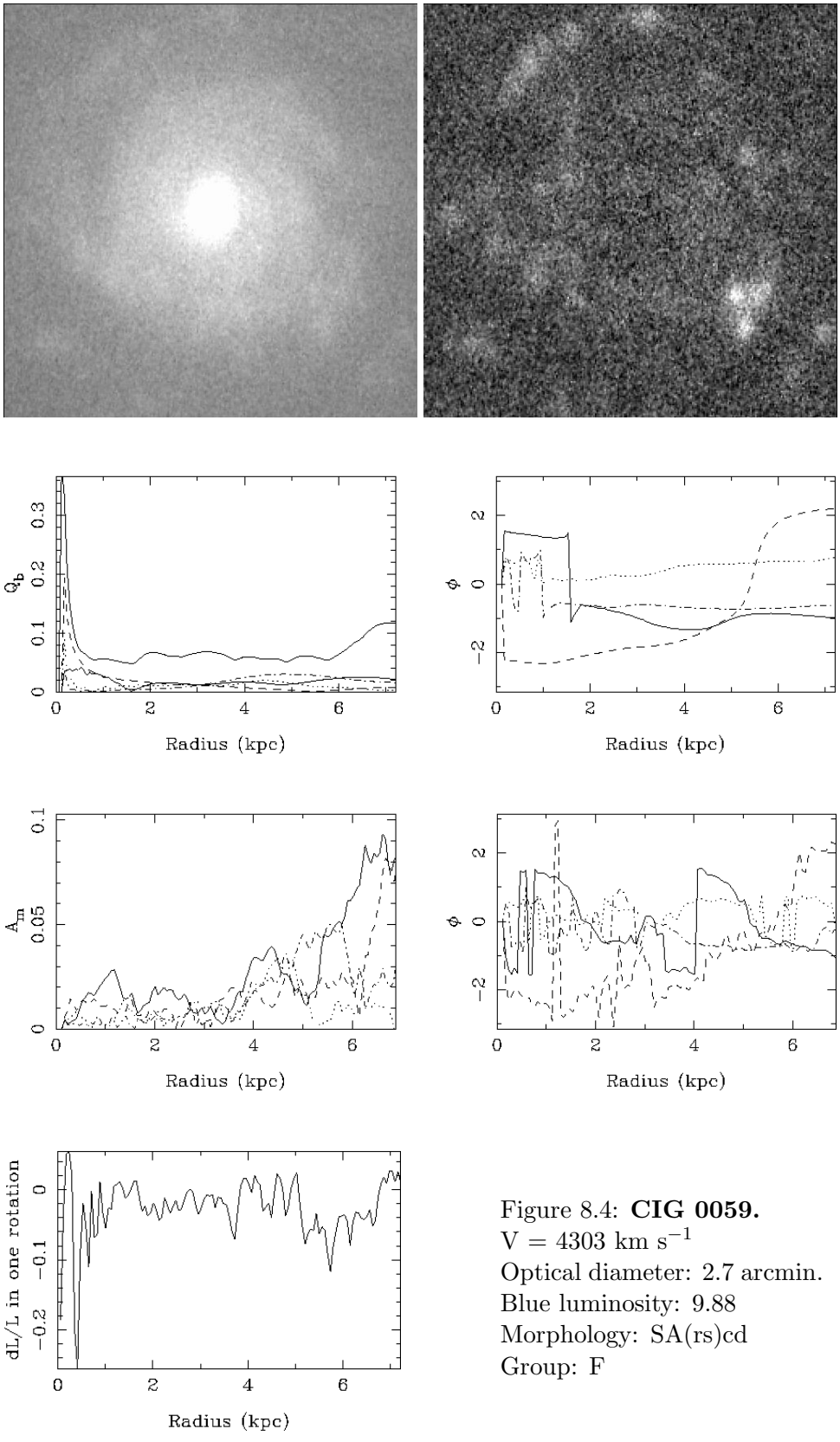

Figure 8.4: **CIG 0059.**
V = 4303 km s^{-1}
Optical diameter: 2.7 arcmin.
Blue luminosity: 9.88
Morphology: SA(rs)cd
Group: F

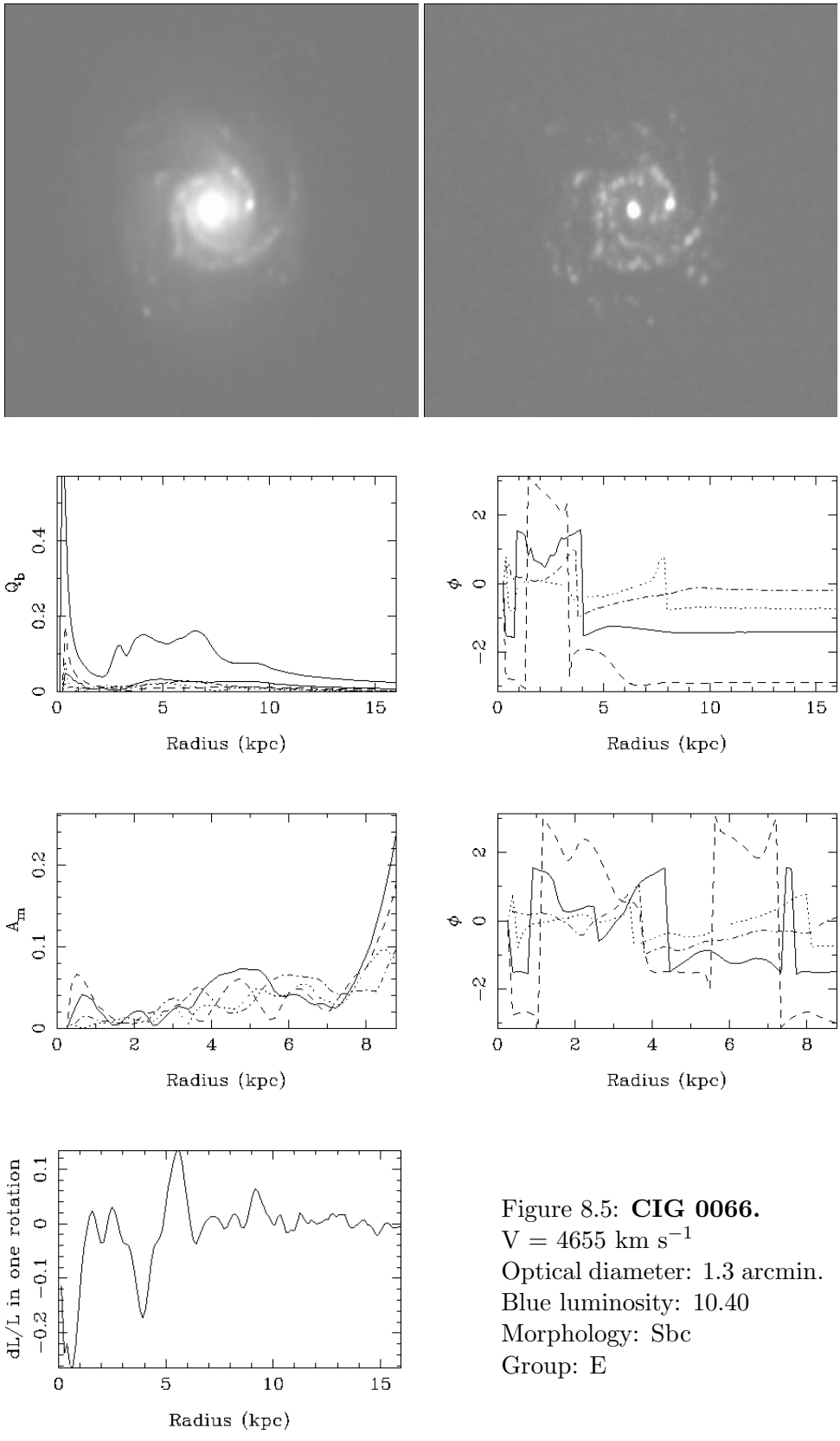

Figure 8.5: **CIG 0066.**
V = 4655 km s^{-1}
Optical diameter: 1.3 arcmin.
Blue luminosity: 10.40
Morphology: Sbc
Group: E

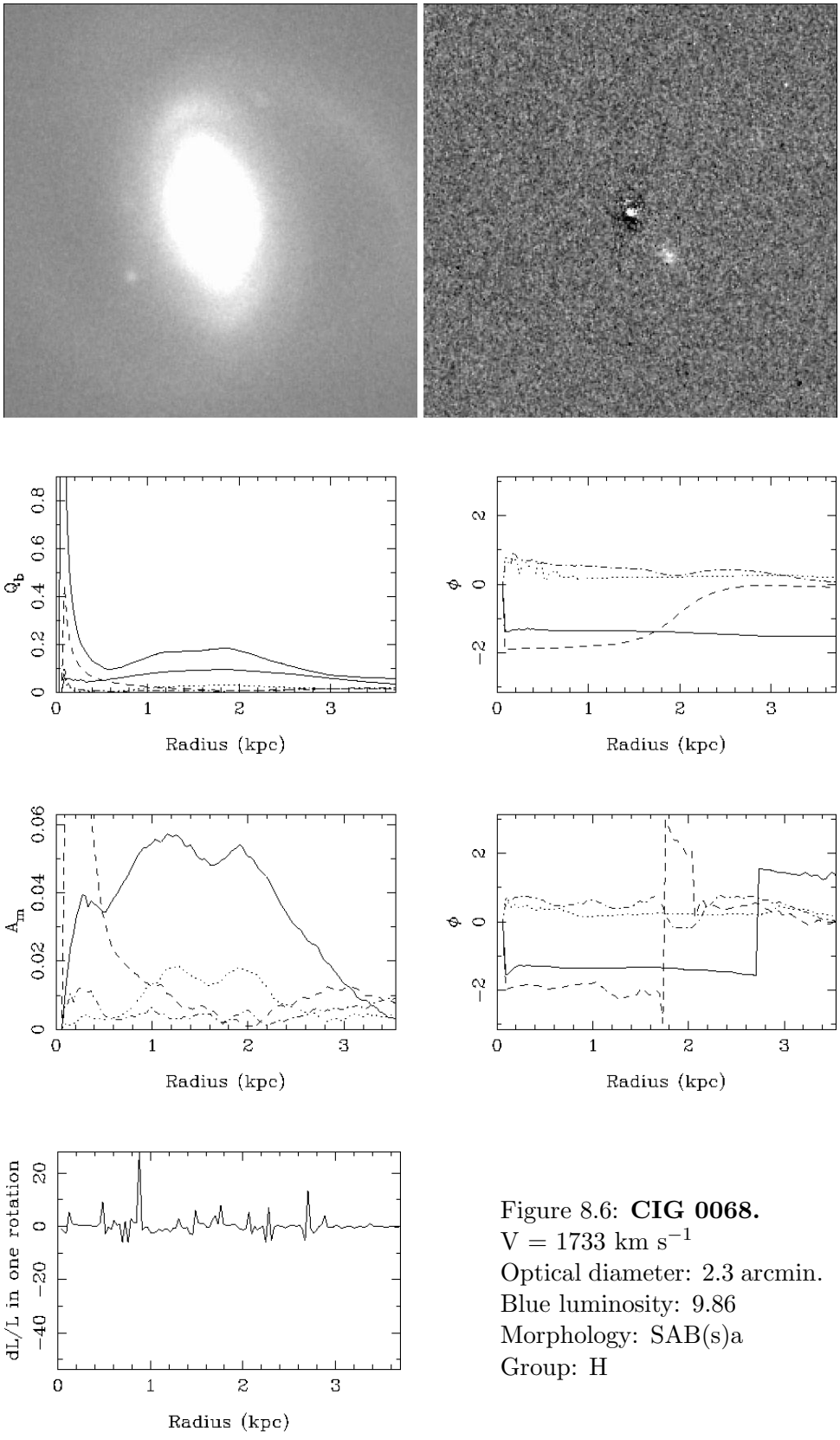

Figure 8.6: **CIG 0068.**
V = 1733 km s^{-1}
Optical diameter: 2.3 arcmin.
Blue luminosity: 9.86
Morphology: SAB(s)a
Group: H

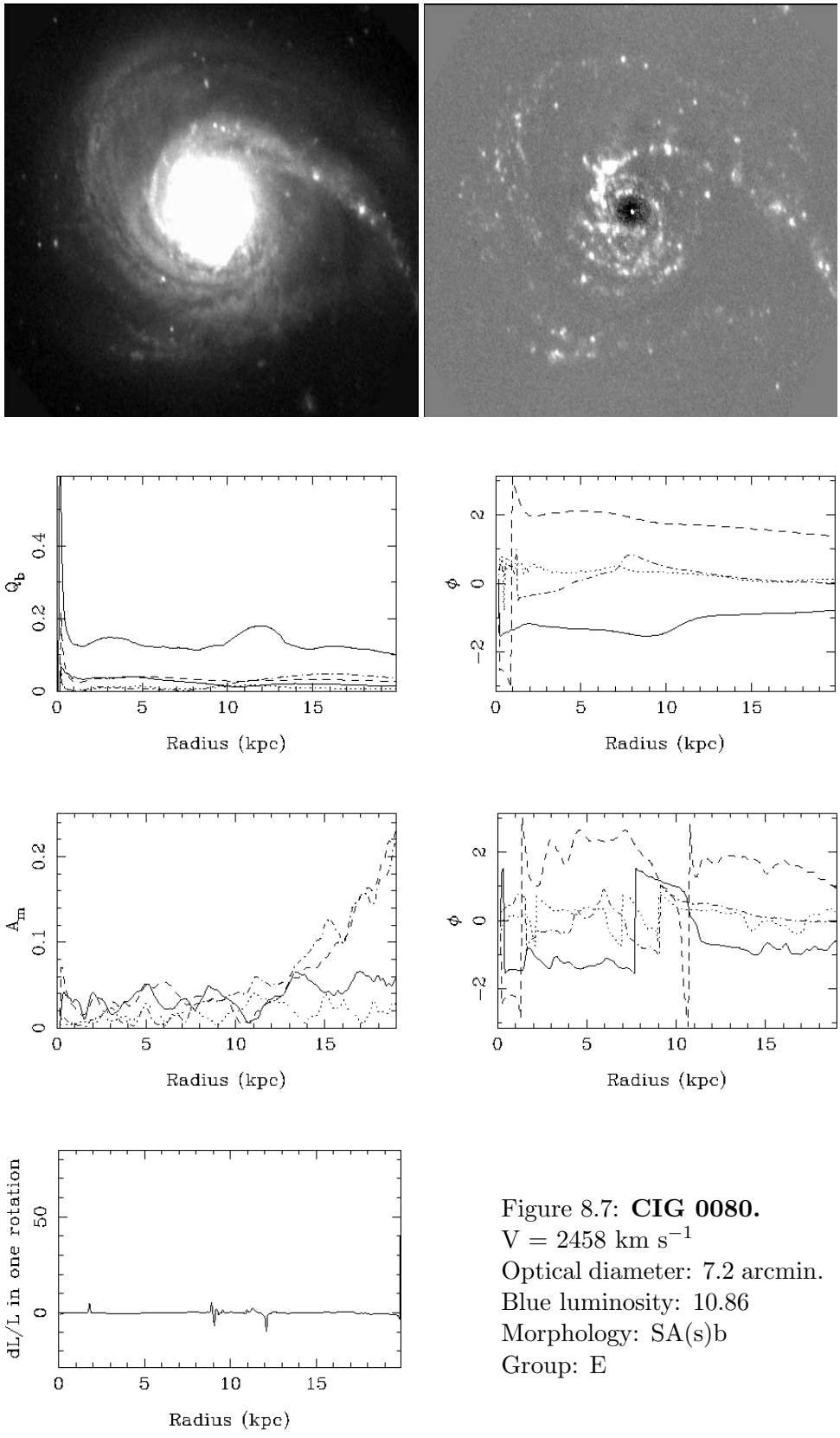

Figure 8.7: **CIG 0080.**
V = 2458 km s^{-1}
Optical diameter: 7.2 arcmin.
Blue luminosity: 10.86
Morphology: SA(s)b
Group: E

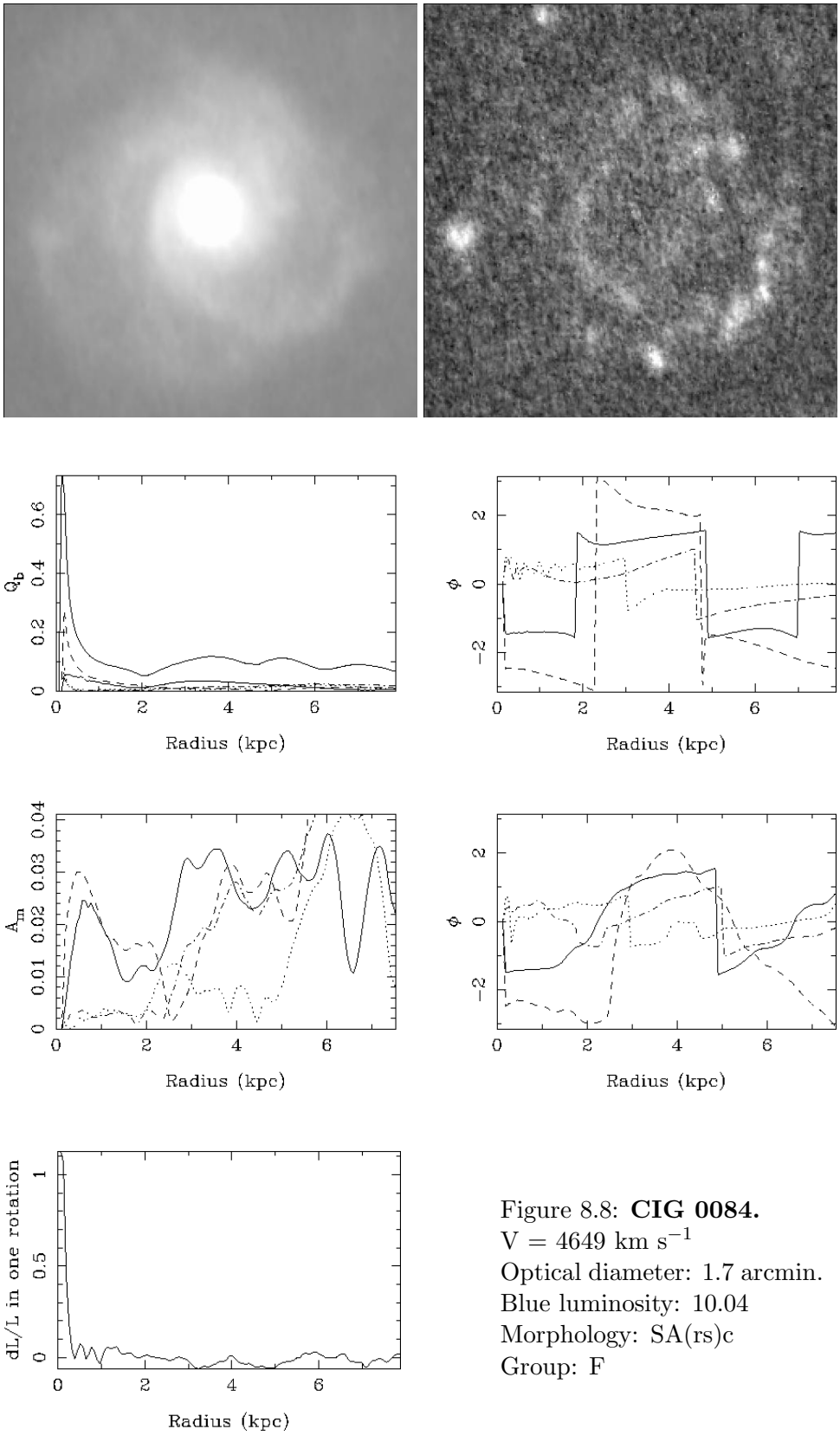

Figure 8.8: **CIG 0084.**
V = 4649 km s^{-1}
Optical diameter: 1.7 arcmin.
Blue luminosity: 10.04
Morphology: SA(rs)c
Group: F

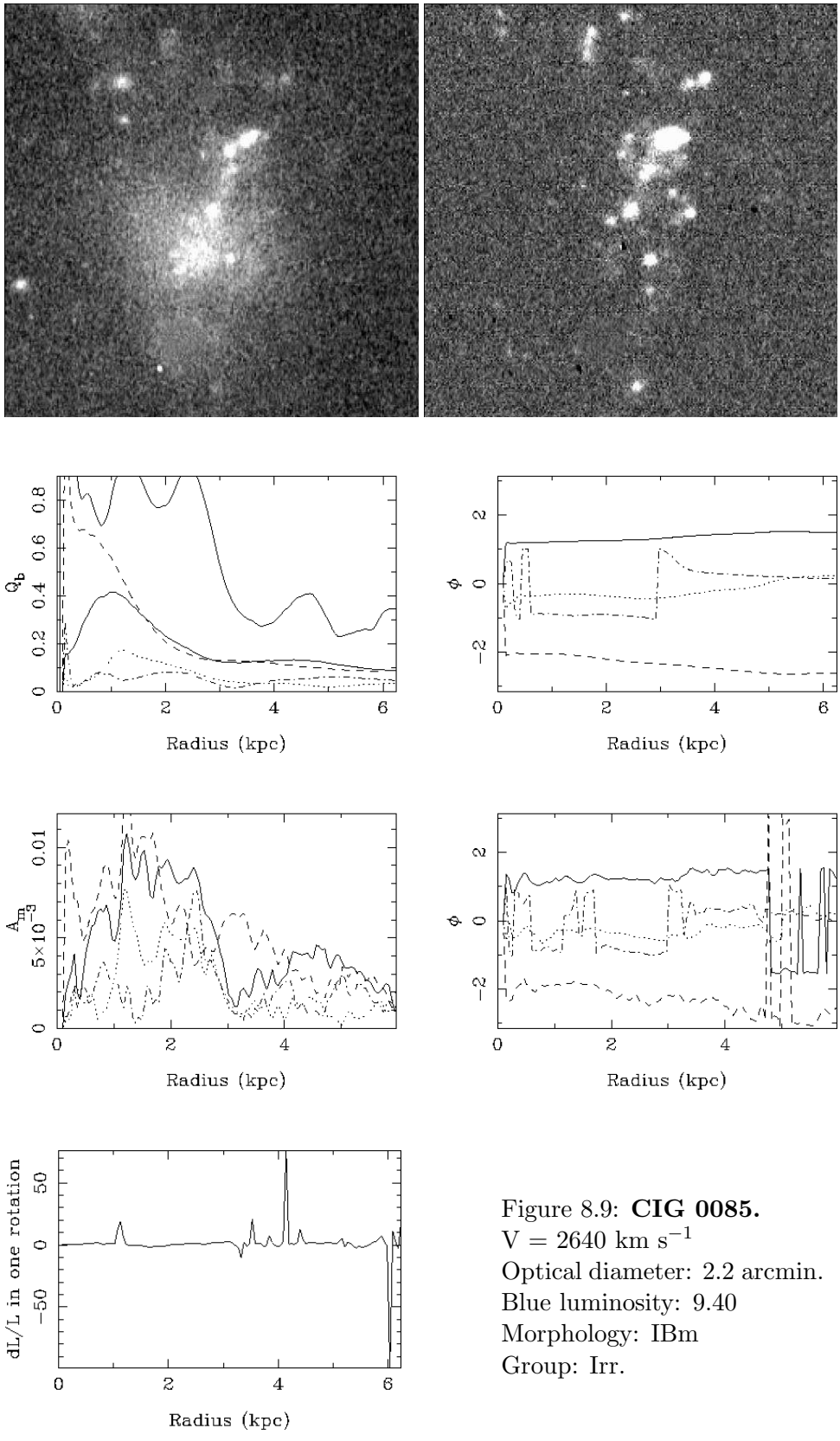

Figure 8.9: **CIG 0085.**
V = 2640 km s^{-1}
Optical diameter: 2.2 arcmin.
Blue luminosity: 9.40
Morphology: IBm
Group: Irr.

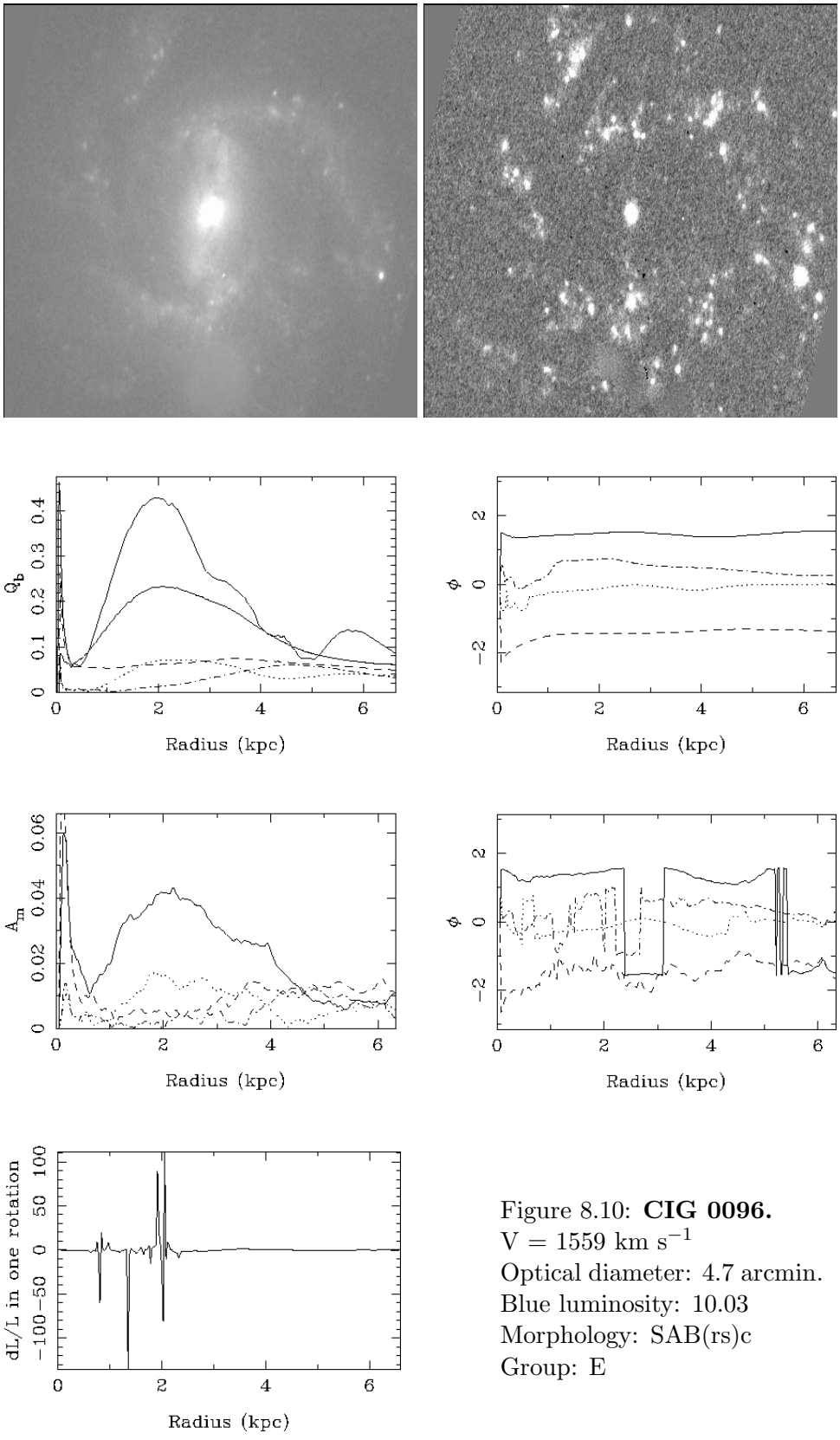

Figure 8.10: **CIG 0096.**
V = 1559 km s^{-1}
Optical diameter: 4.7 arcmin.
Blue luminosity: 10.03
Morphology: SAB(rs)c
Group: E

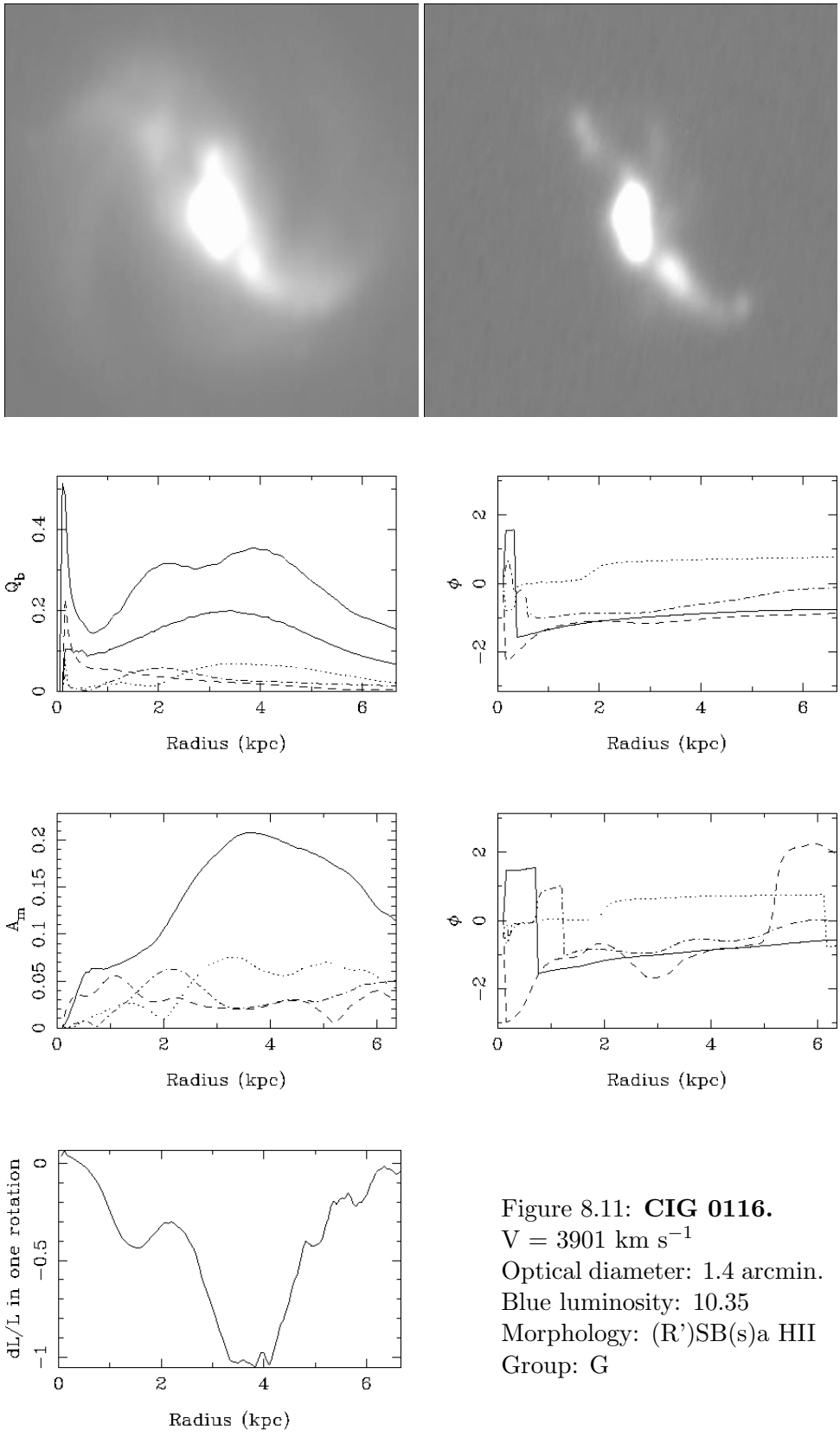

Figure 8.11: **CIG 0116.**
V = 3901 km s^{-1}
Optical diameter: 1.4 arcmin.
Blue luminosity: 10.35
Morphology: (R')SB(s)a HII
Group: G

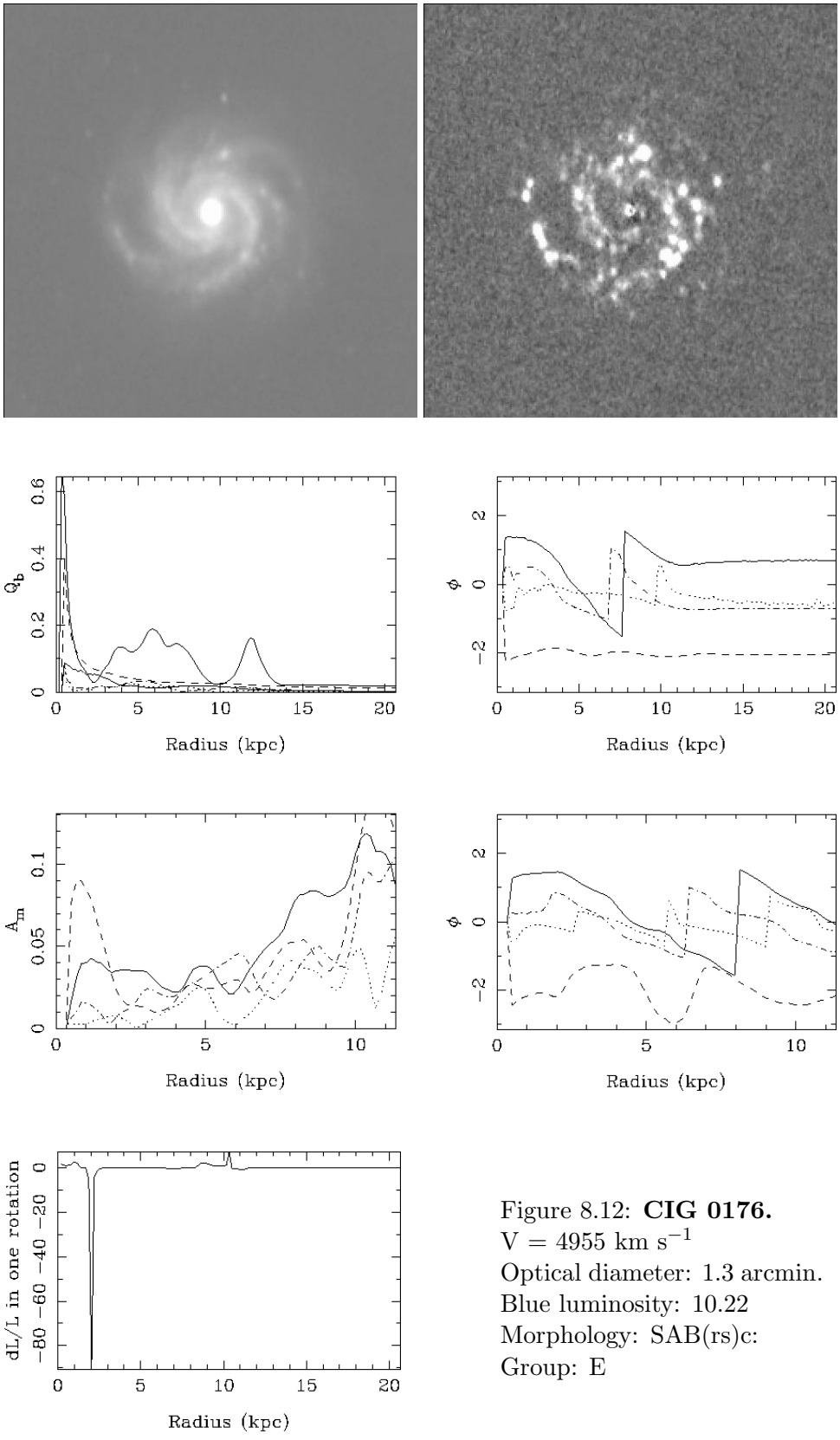

Figure 8.12: **CIG 0176.**
V = 4955 km s^{-1}
Optical diameter: 1.3 arcmin.
Blue luminosity: 10.22
Morphology: SAB(rs)c:
Group: E

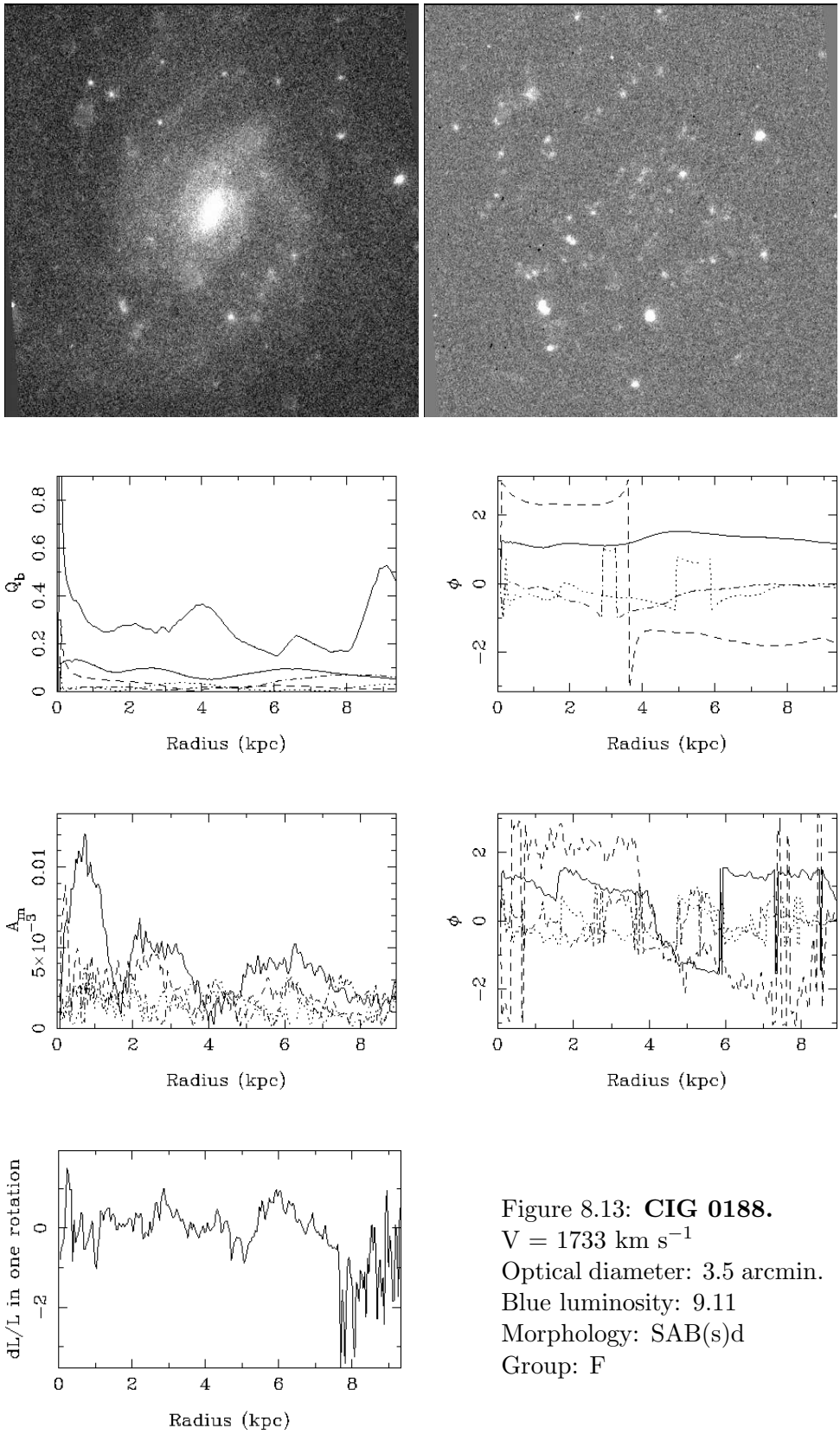

Figure 8.13: **CIG 0188.**
V = 1733 km s^{-1}
Optical diameter: 3.5 arcmin.
Blue luminosity: 9.11
Morphology: SAB(s)d
Group: F

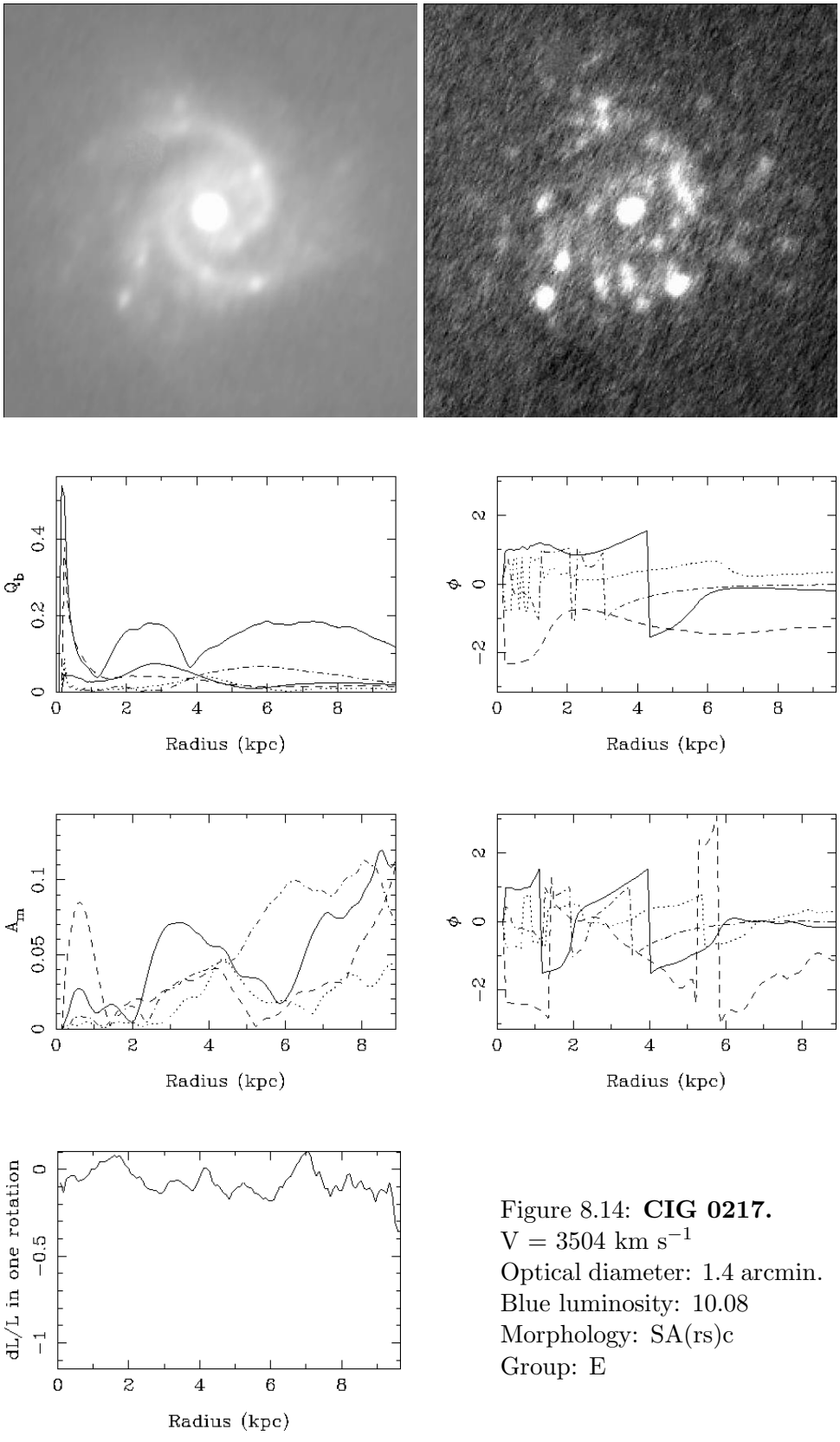

Figure 8.14: **CIG 0217.**
V = 3504 km s^{-1}
Optical diameter: 1.4 arcmin.
Blue luminosity: 10.08
Morphology: SA(rs)c
Group: E

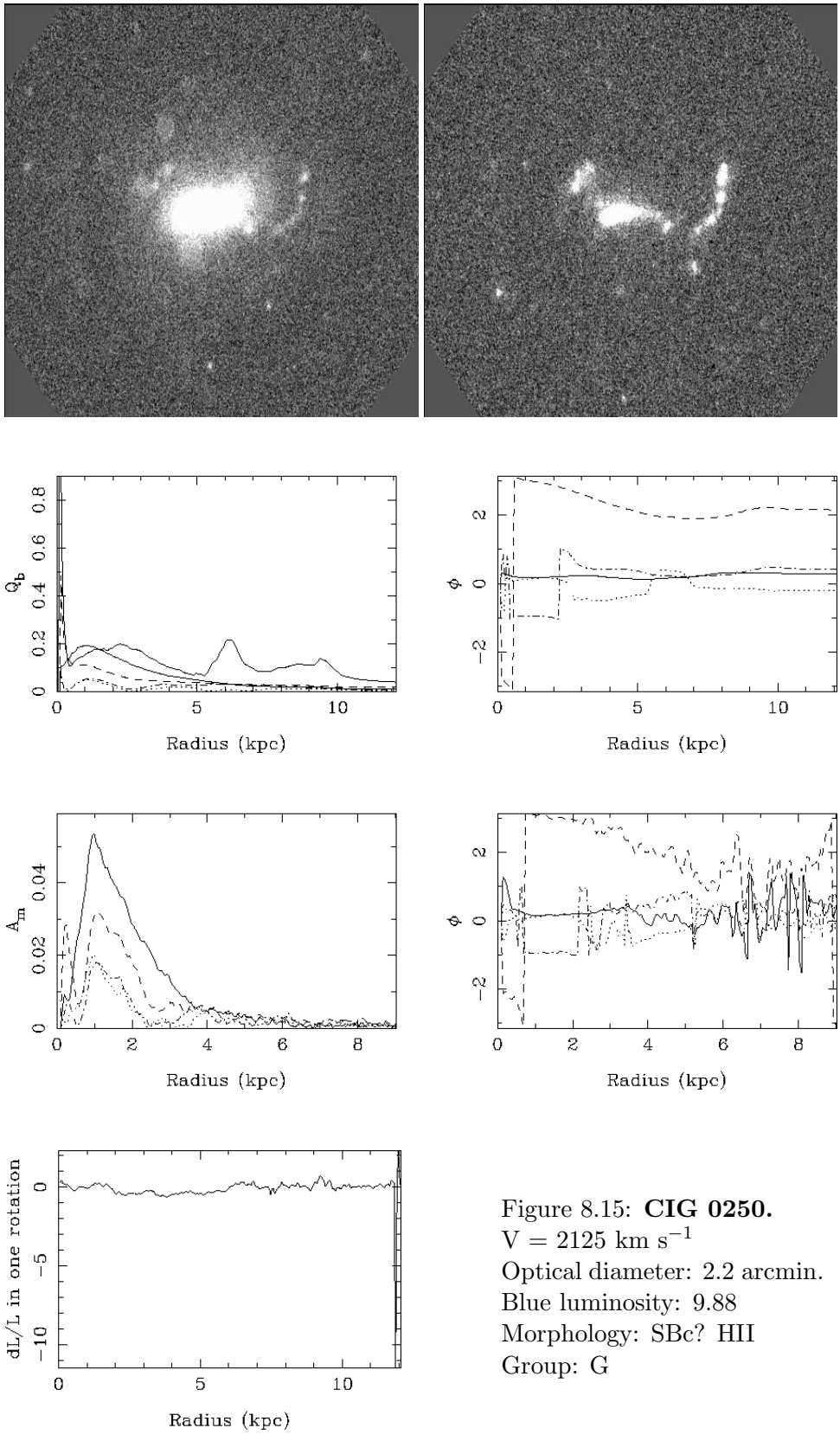

Figure 8.15: **CIG 0250.**
V = 2125 km s^{-1}
Optical diameter: 2.2 arcmin.
Blue luminosity: 9.88
Morphology: SBc? HII
Group: G

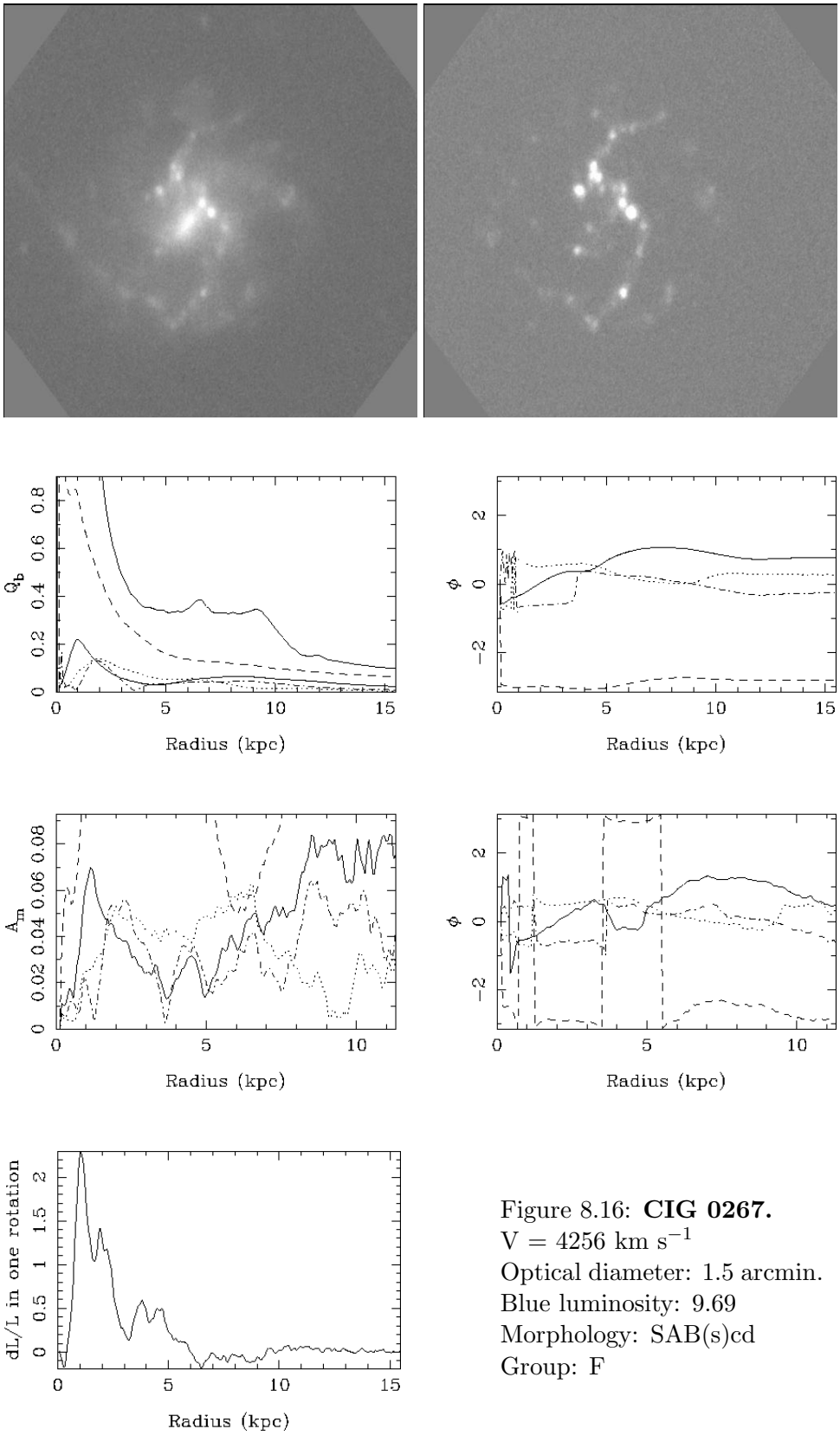

Figure 8.16: **CIG 0267.**
V = 4256 km s^{-1}
Optical diameter: 1.5 arcmin.
Blue luminosity: 9.69
Morphology: SAB(s)cd
Group: F

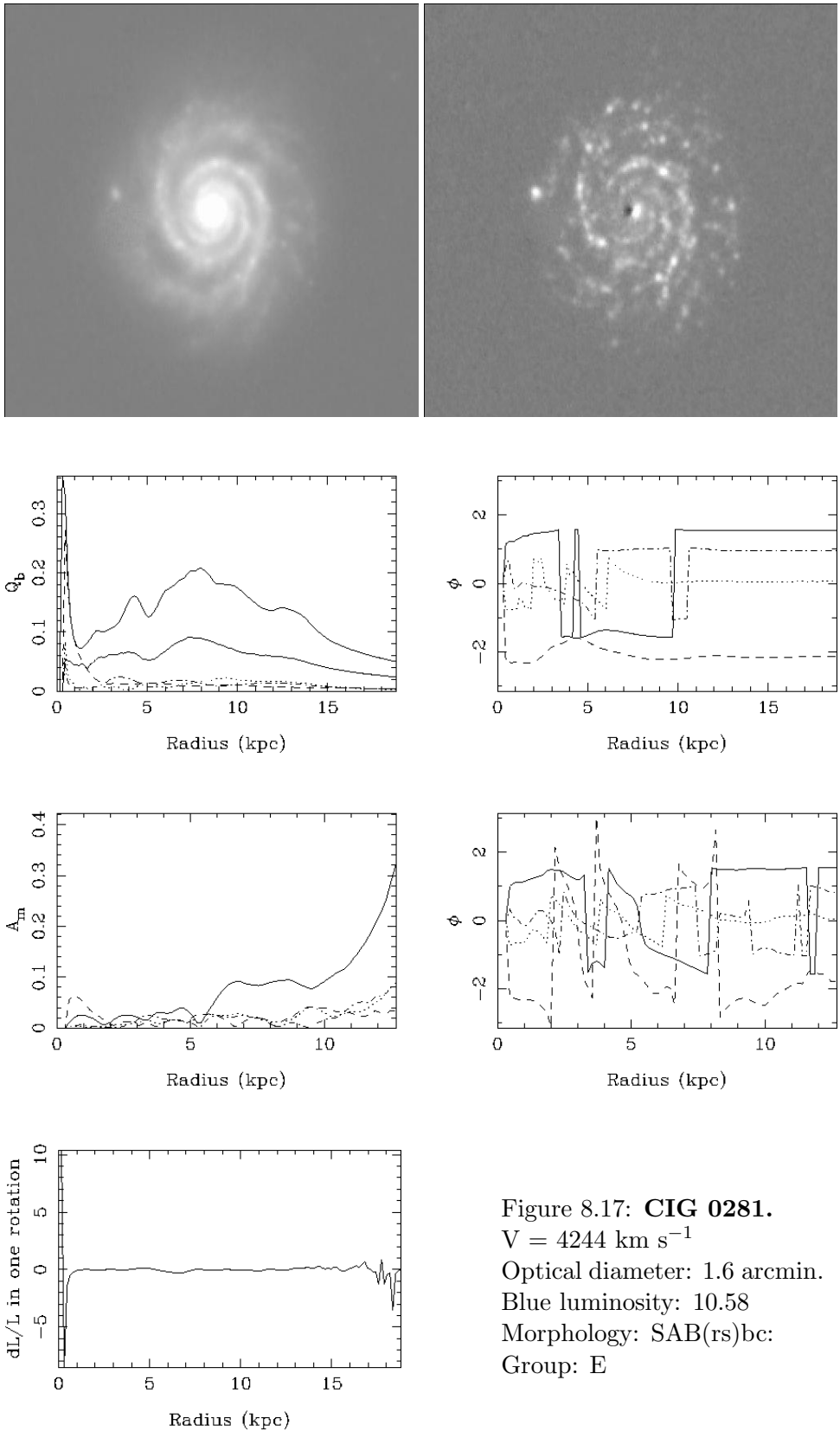

Figure 8.17: **CIG 0281.**
V = 4244 km s^{-1}
Optical diameter: 1.6 arcmin.
Blue luminosity: 10.58
Morphology: SAB(rs)bc:
Group: E

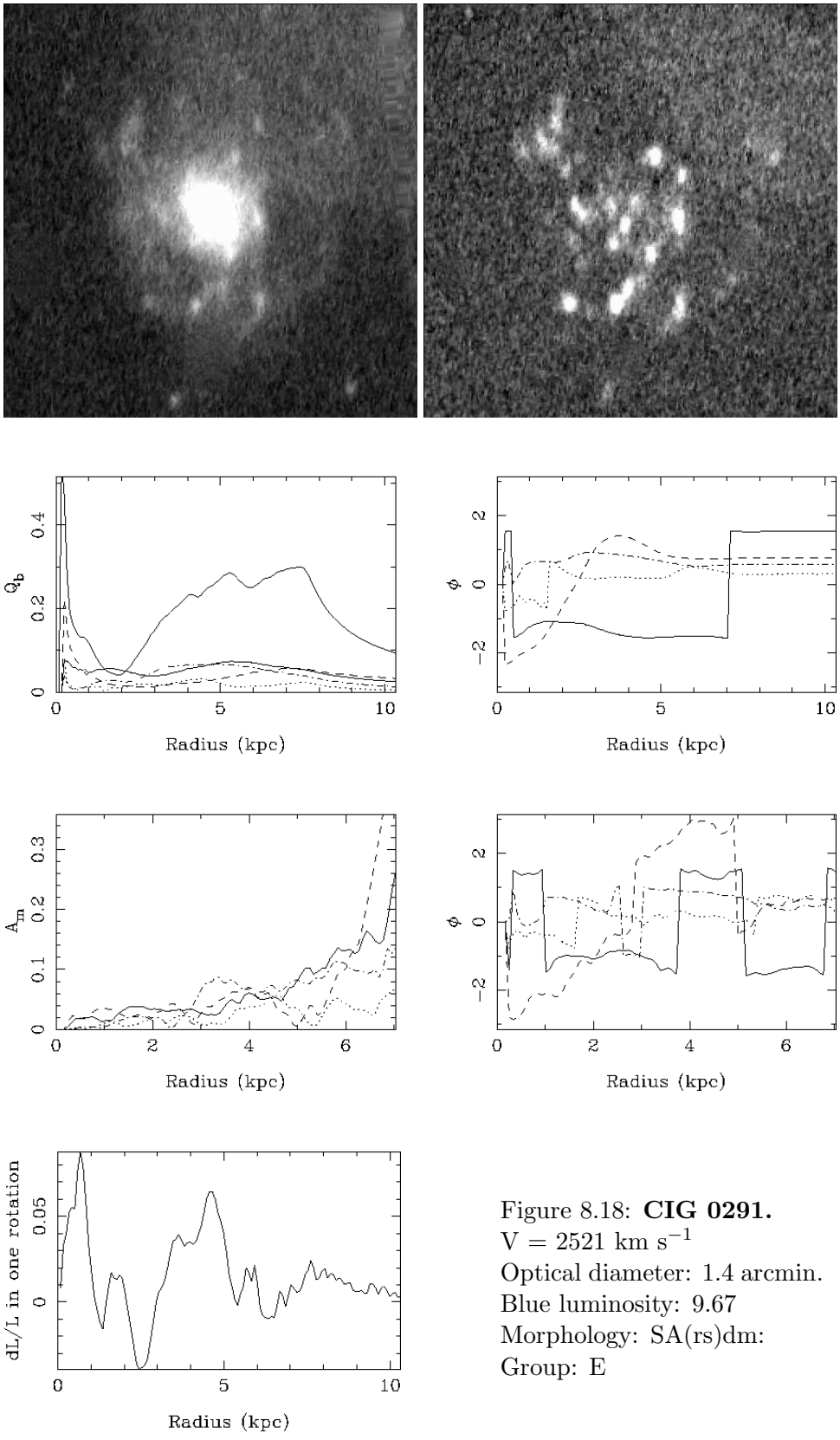

Figure 8.18: **CIG 0291.**
V = 2521 km s^{-1}
Optical diameter: 1.4 arcmin.
Blue luminosity: 9.67
Morphology: SA(rs)dm:
Group: E

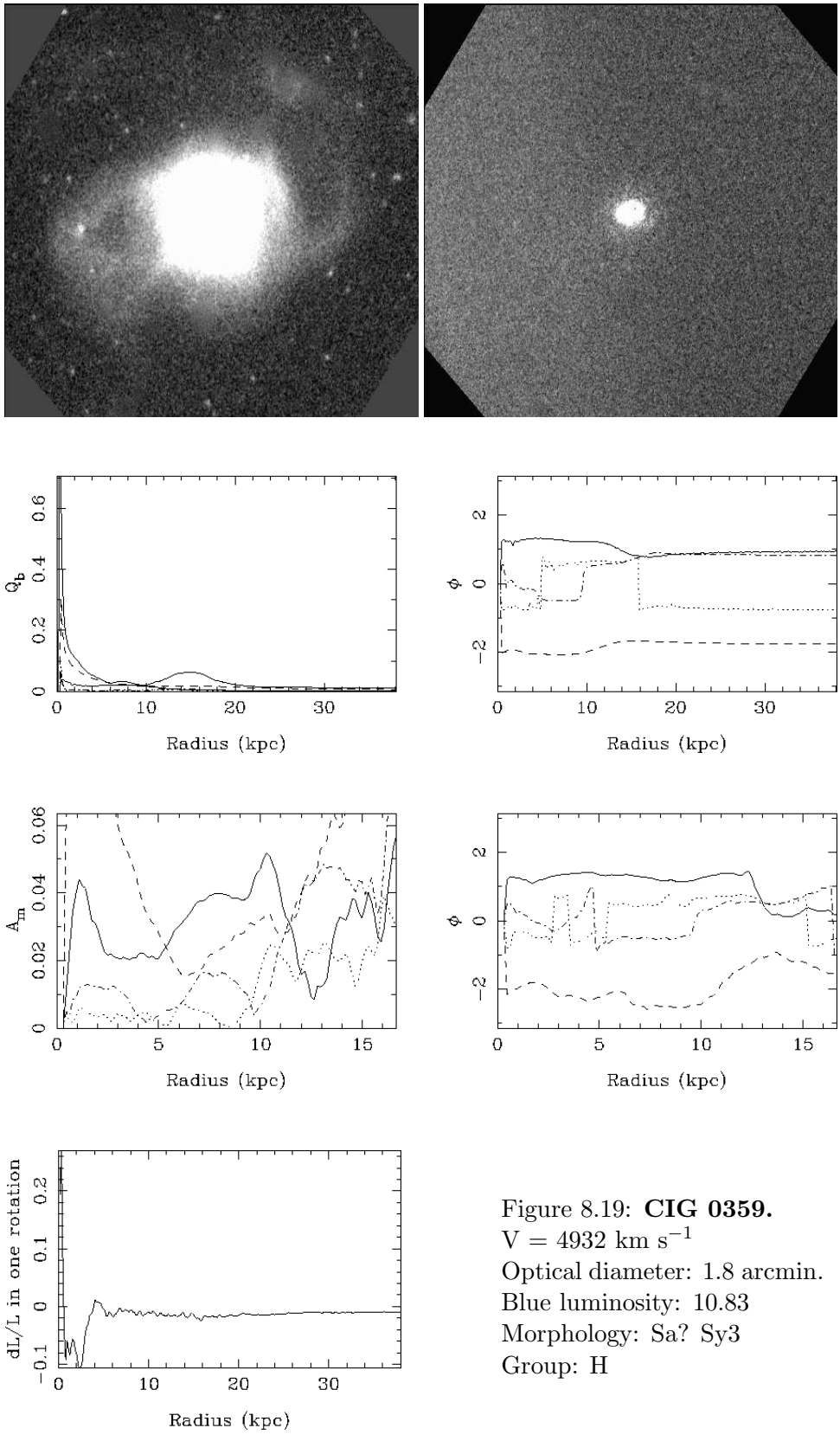

Figure 8.19: **CIG 0359.**
V = 4932 km s^{-1}
Optical diameter: 1.8 arcmin.
Blue luminosity: 10.83
Morphology: Sa? Sy3
Group: H

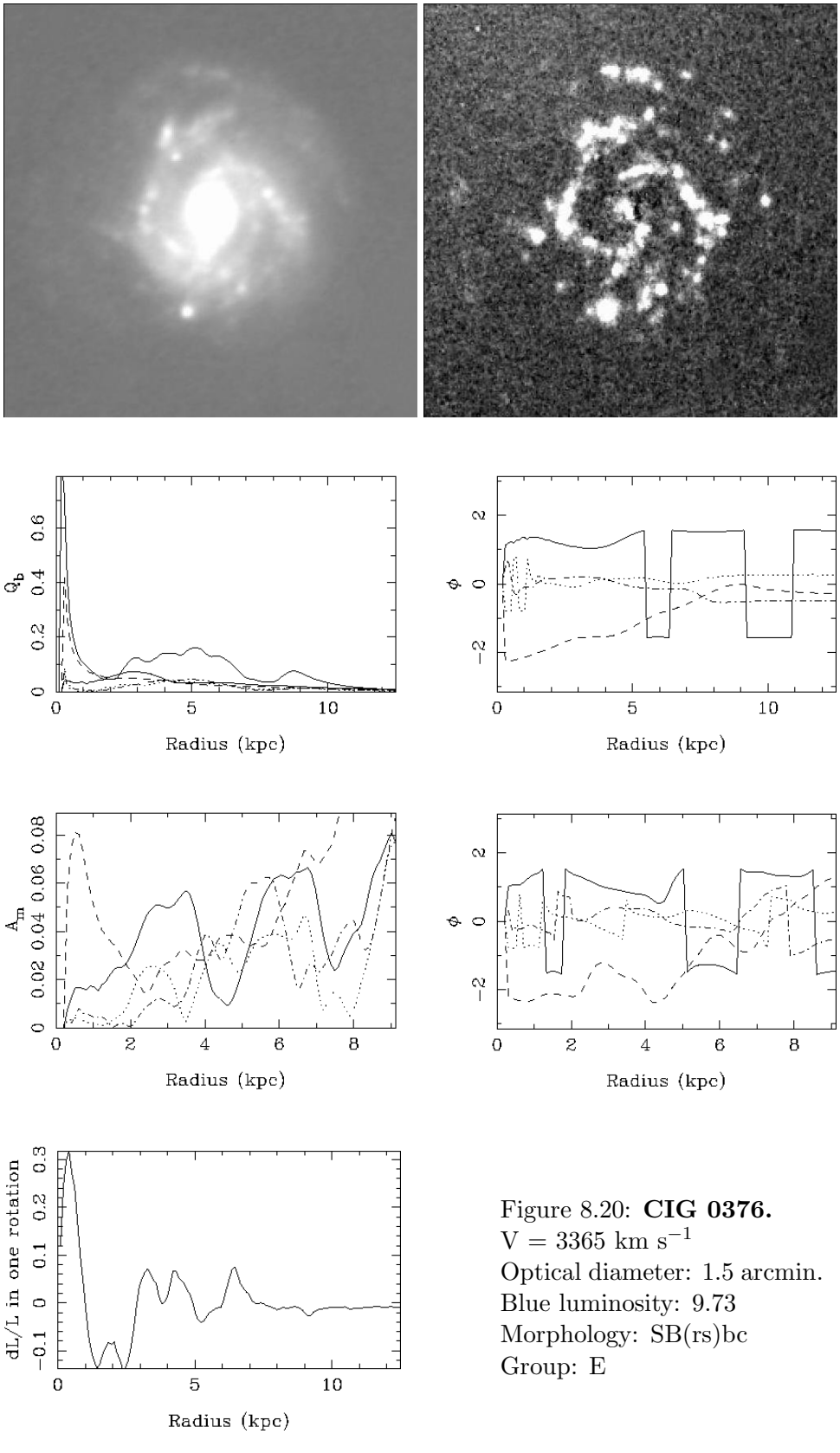

Figure 8.20: **CIG 0376.**
V = 3365 km s^{-1}
Optical diameter: 1.5 arcmin.
Blue luminosity: 9.73
Morphology: SB(rs)bc
Group: E

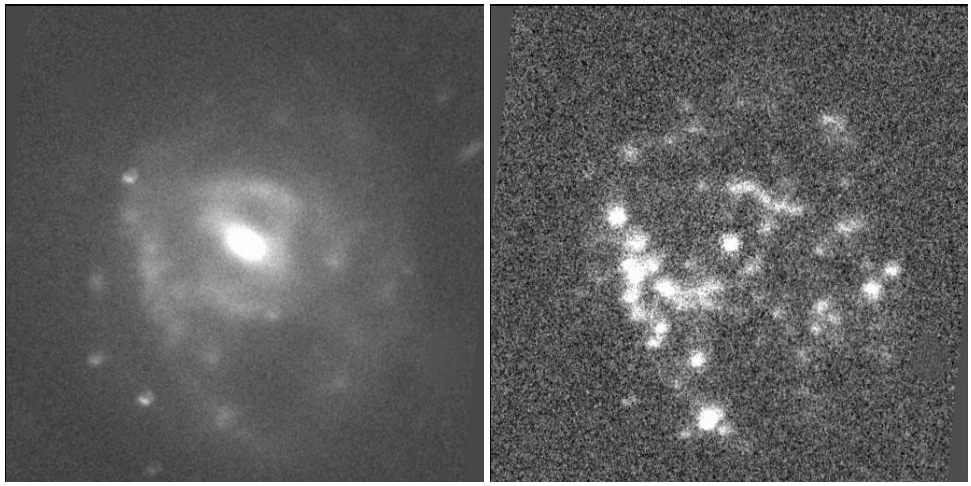

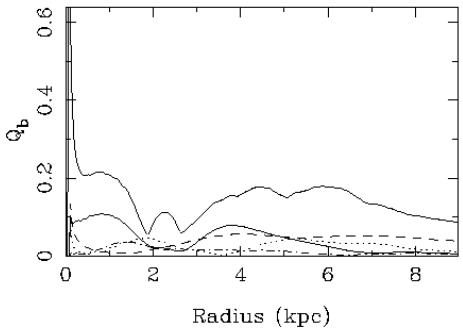

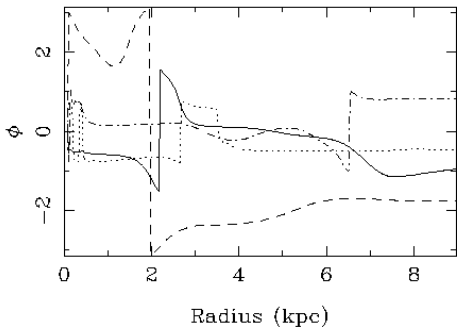

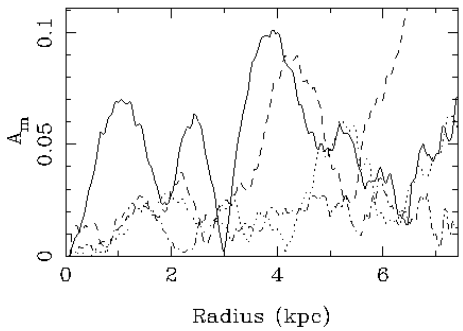

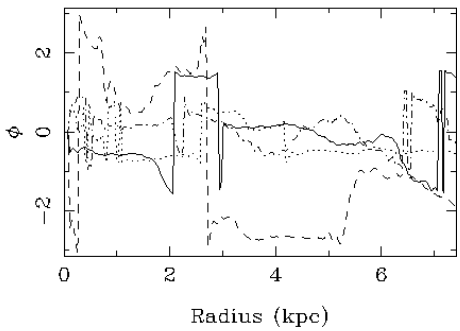

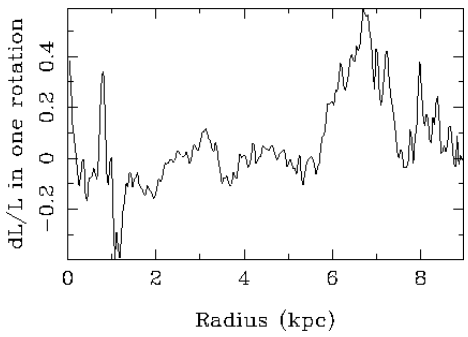

Figure 8.21: **CIG 0382.**
V = 2457 km s^{-1}
Optical diameter: 1.7 arcmin.
Blue luminosity: 9.78
Morphology: (R')SB(rs)c
Group: E

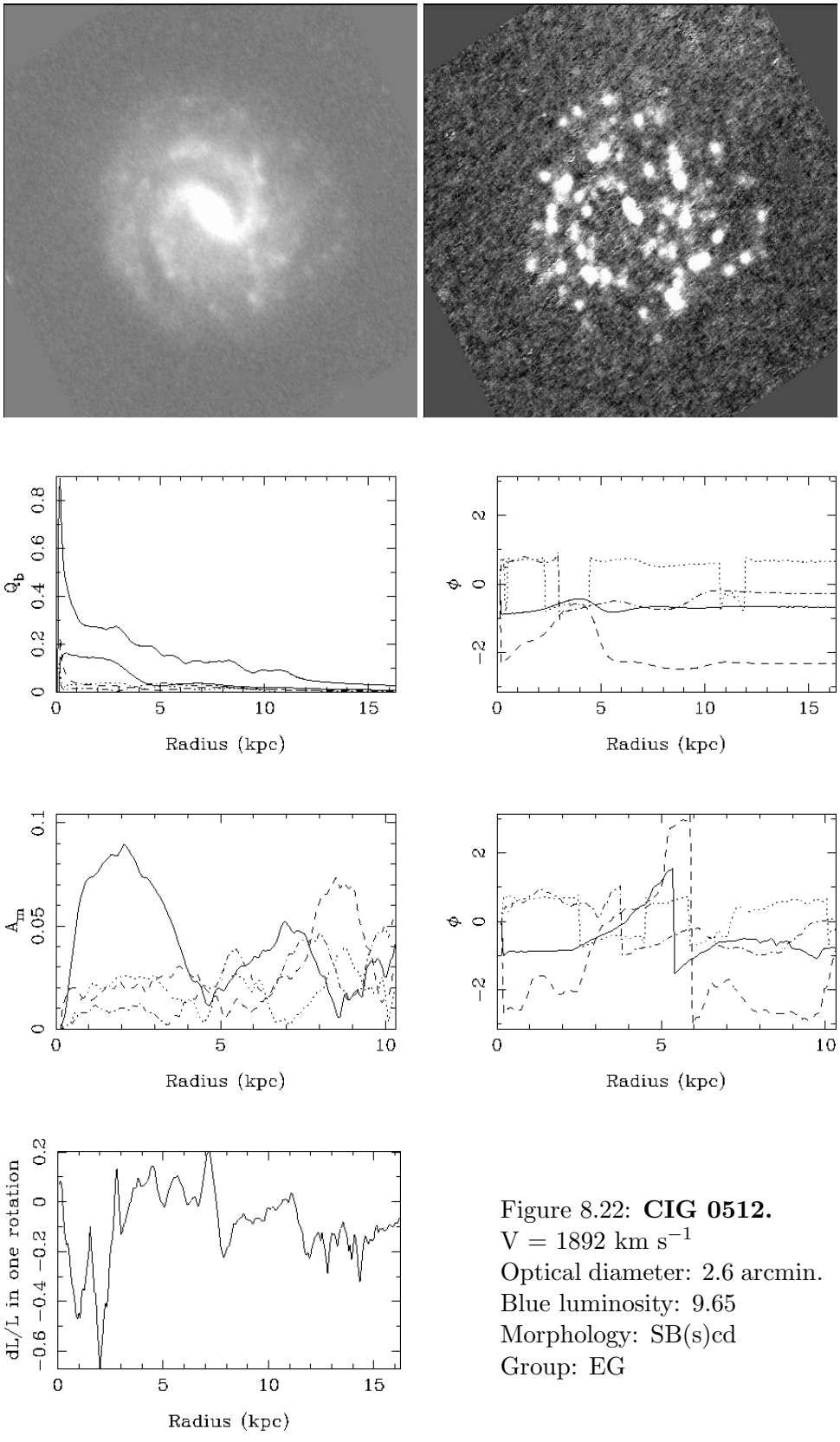

Figure 8.22: **CIG 0512.**
V = 1892 km s^{-1}
Optical diameter: 2.6 arcmin.
Blue luminosity: 9.65
Morphology: SB(s)cd
Group: EG

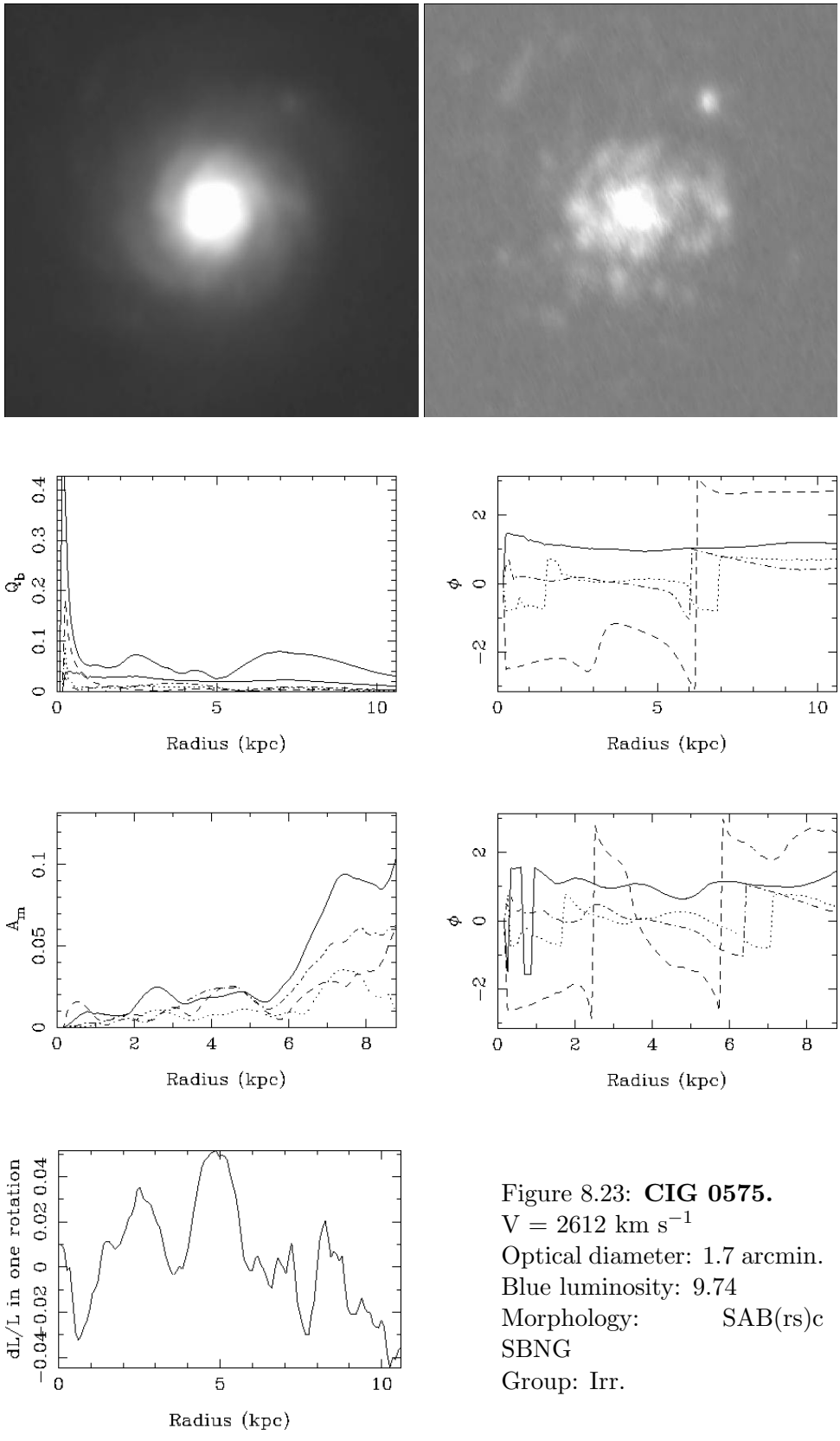

Figure 8.23: **CIG 0575.**
V = 2612 km s^{-1}
Optical diameter: 1.7 arcmin.
Blue luminosity: 9.74
Morphology: SAB(rs)c
SBNG
Group: Irr.

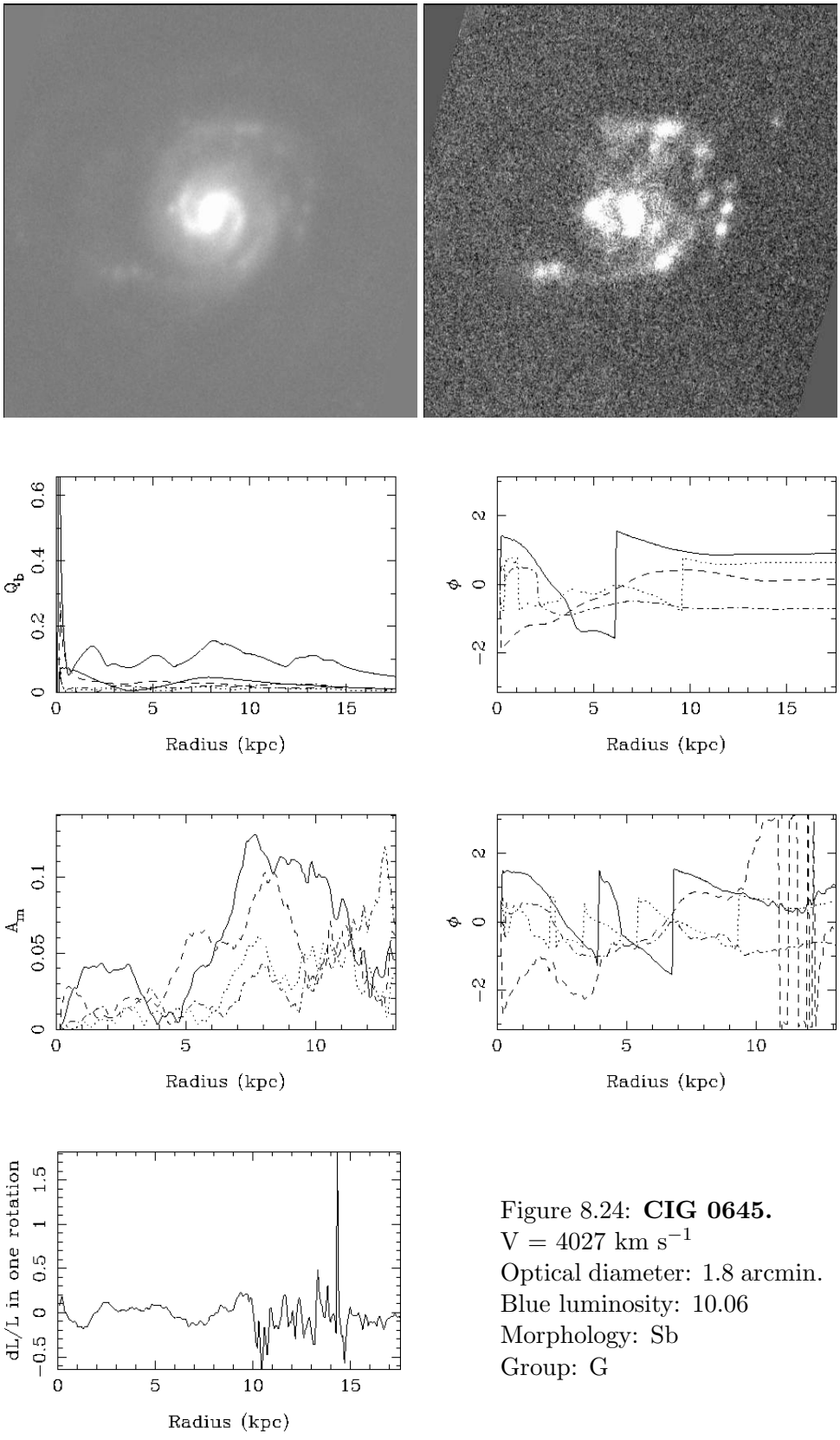

Figure 8.24: **CIG 0645.**
V = 4027 km s^{-1}
Optical diameter: 1.8 arcmin.
Blue luminosity: 10.06
Morphology: Sb
Group: G

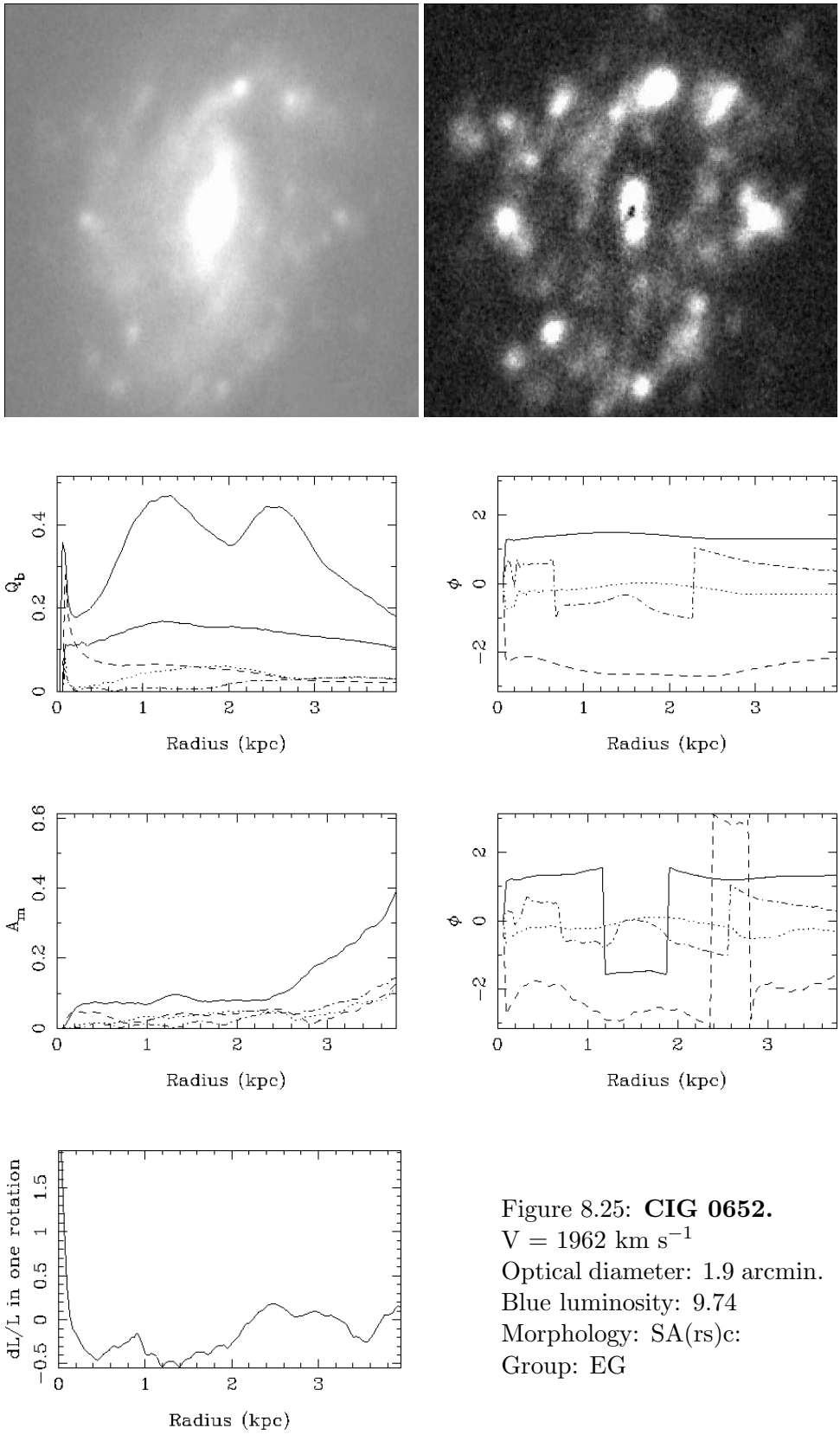

Figure 8.25: **CIG 0652.**
V = 1962 km s^{-1}
Optical diameter: 1.9 arcmin.
Blue luminosity: 9.74
Morphology: SA(rs)c:
Group: EG

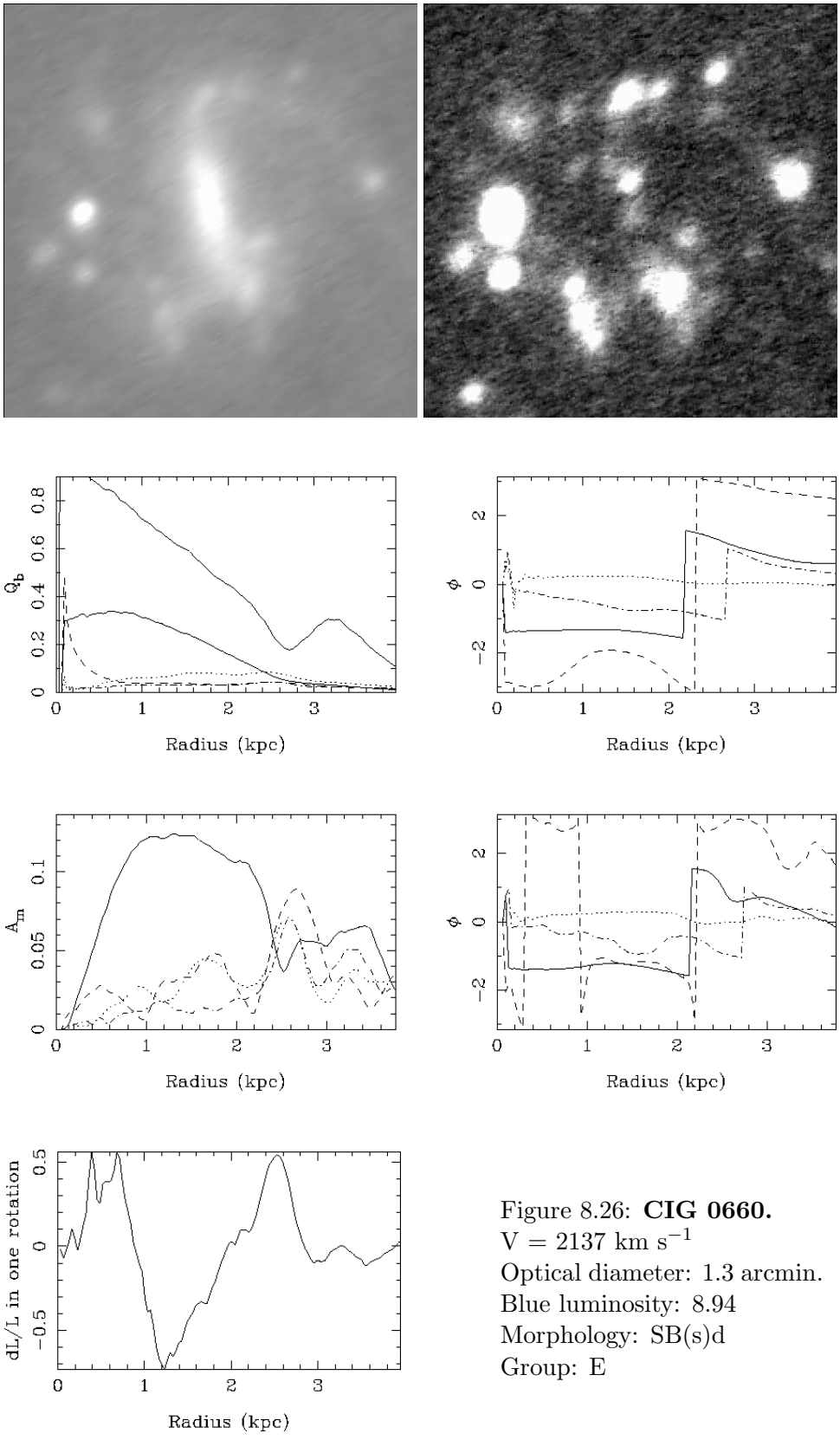

Figure 8.26: **CIG 0660.**
V = 2137 km s^{-1}
Optical diameter: 1.3 arcmin.
Blue luminosity: 8.94
Morphology: SB(s)d
Group: E

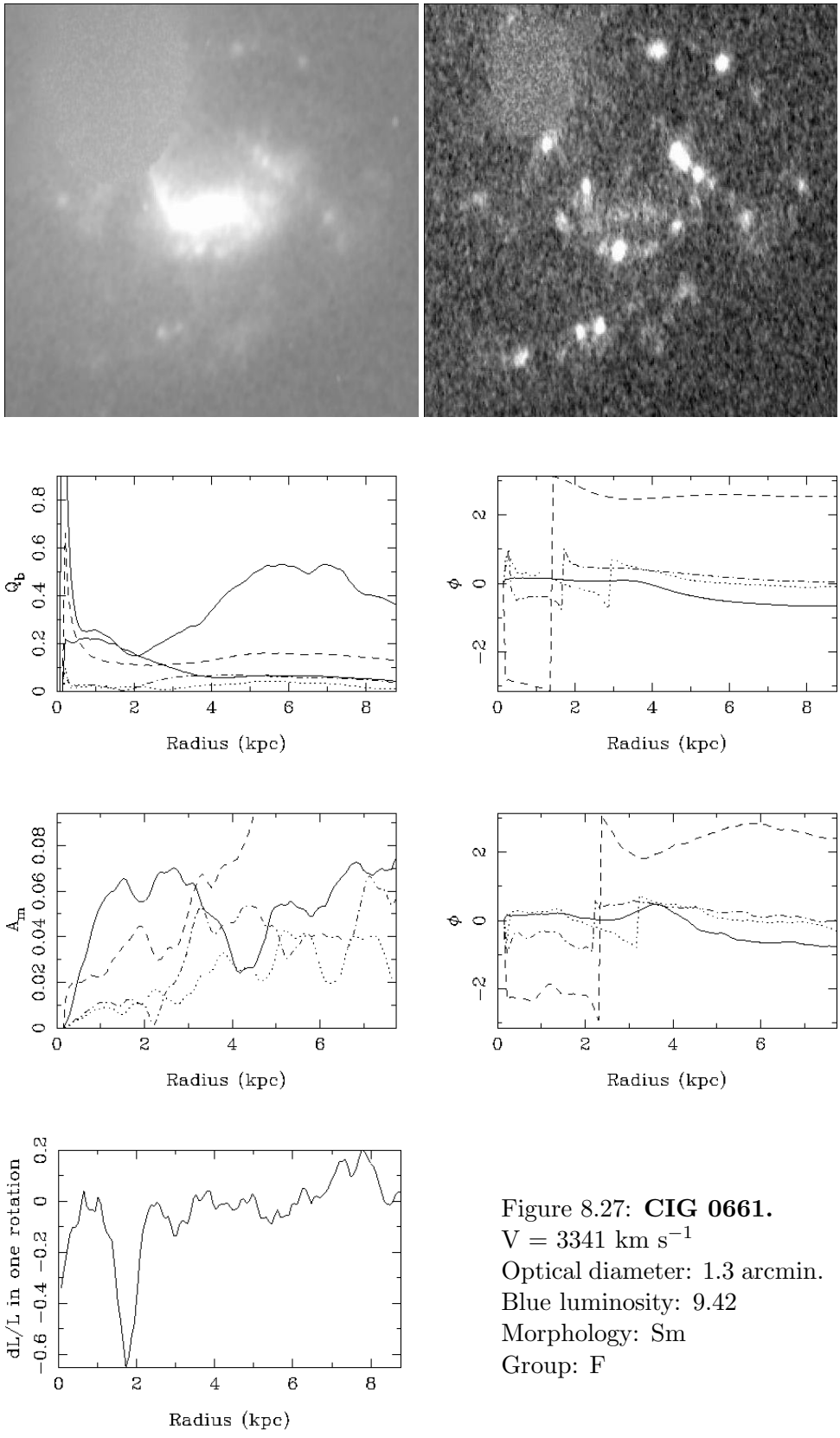

Figure 8.27: **CIG 0661.**
V = 3341 km s^{-1}
Optical diameter: 1.3 arcmin.
Blue luminosity: 9.42
Morphology: Sm
Group: F

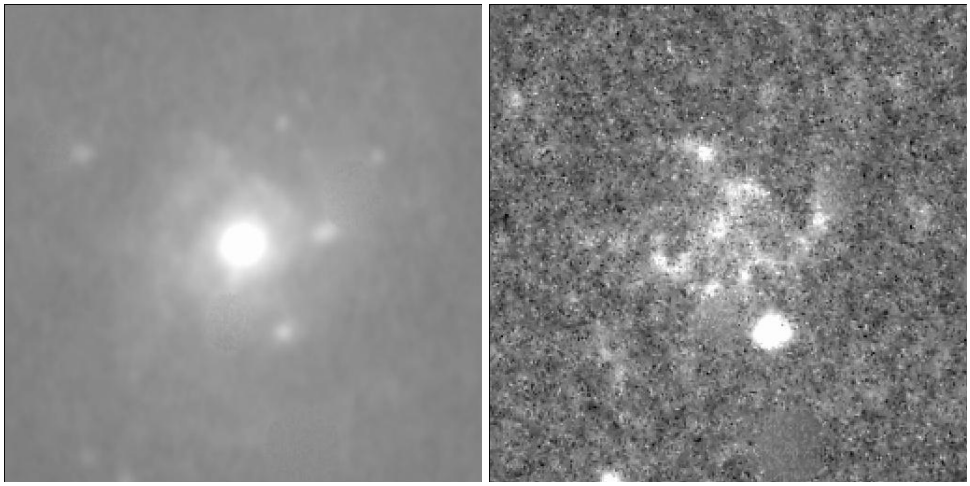

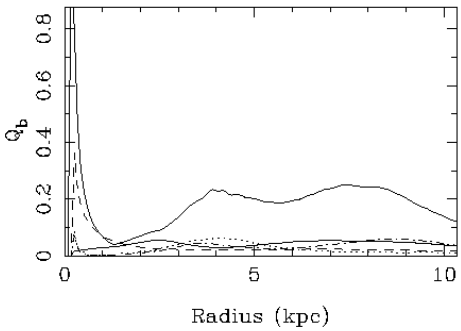

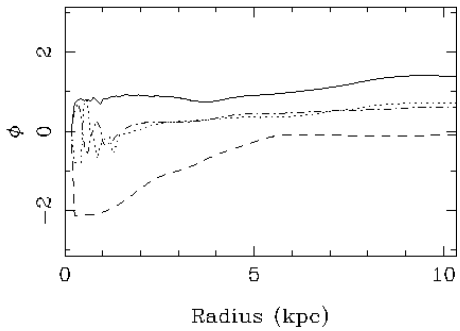

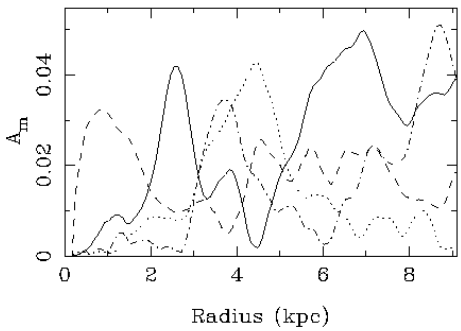

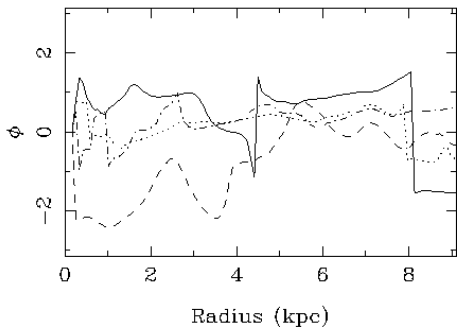

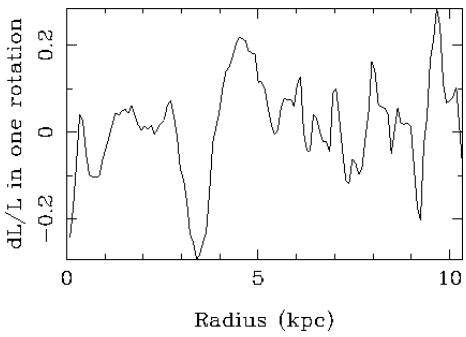

Figure 8.28: **CIG 0700.**
V = 3838 km s^{-1}
Optical diameter: 1.3 arcmin.
Blue luminosity: 9.55
Morphology: SA(s)d?
Group: G

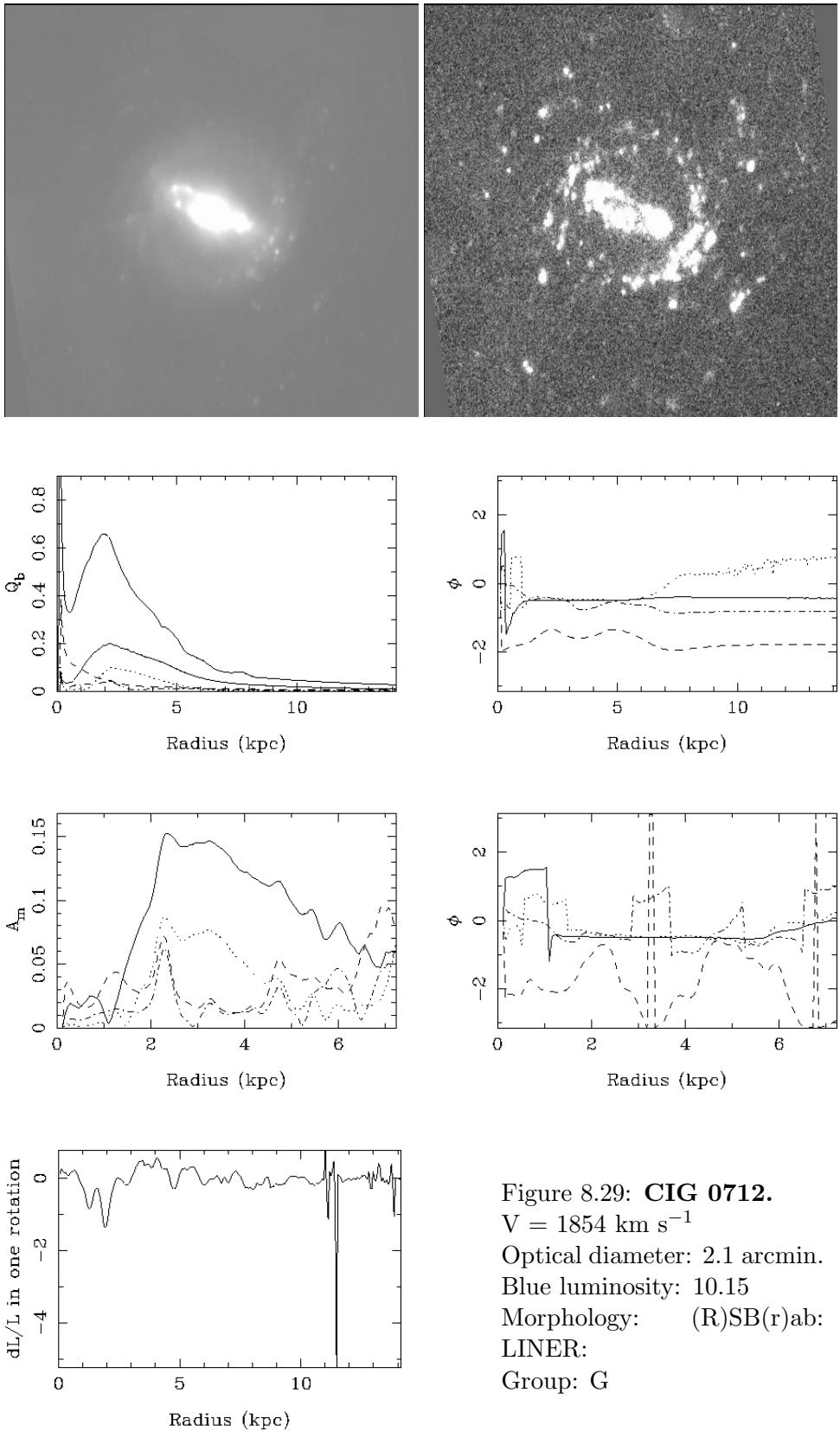

Figure 8.29: **CIG 0712.**
V = 1854 km s^{-1}
Optical diameter: 2.1 arcmin.
Blue luminosity: 10.15
Morphology: (R)SB(r)ab:
LINER:
Group: G

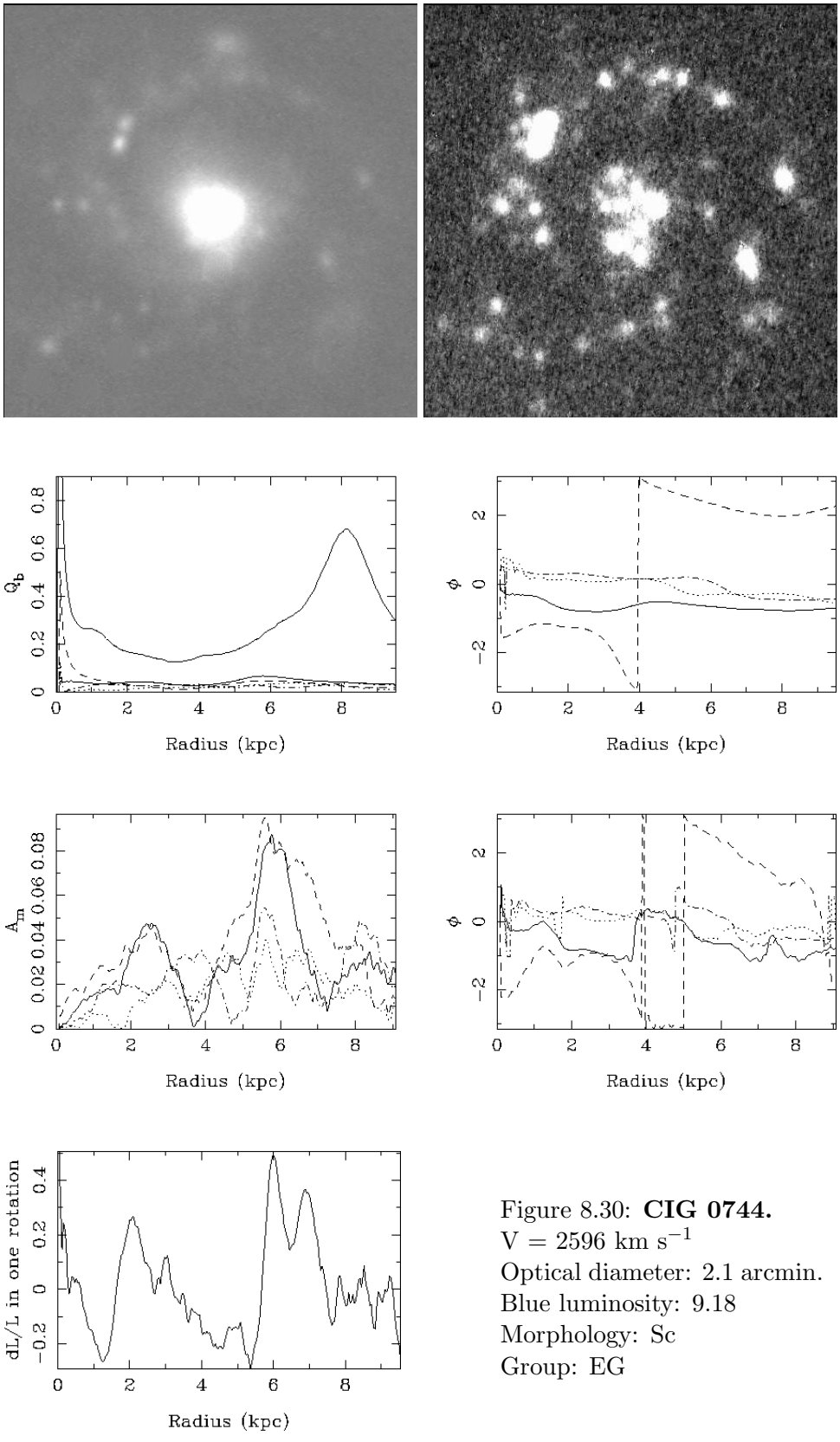

Figure 8.30: **CIG 0744.**
V = 2596 km s^{-1}
Optical diameter: 2.1 arcmin.
Blue luminosity: 9.18
Morphology: Sc
Group: EG

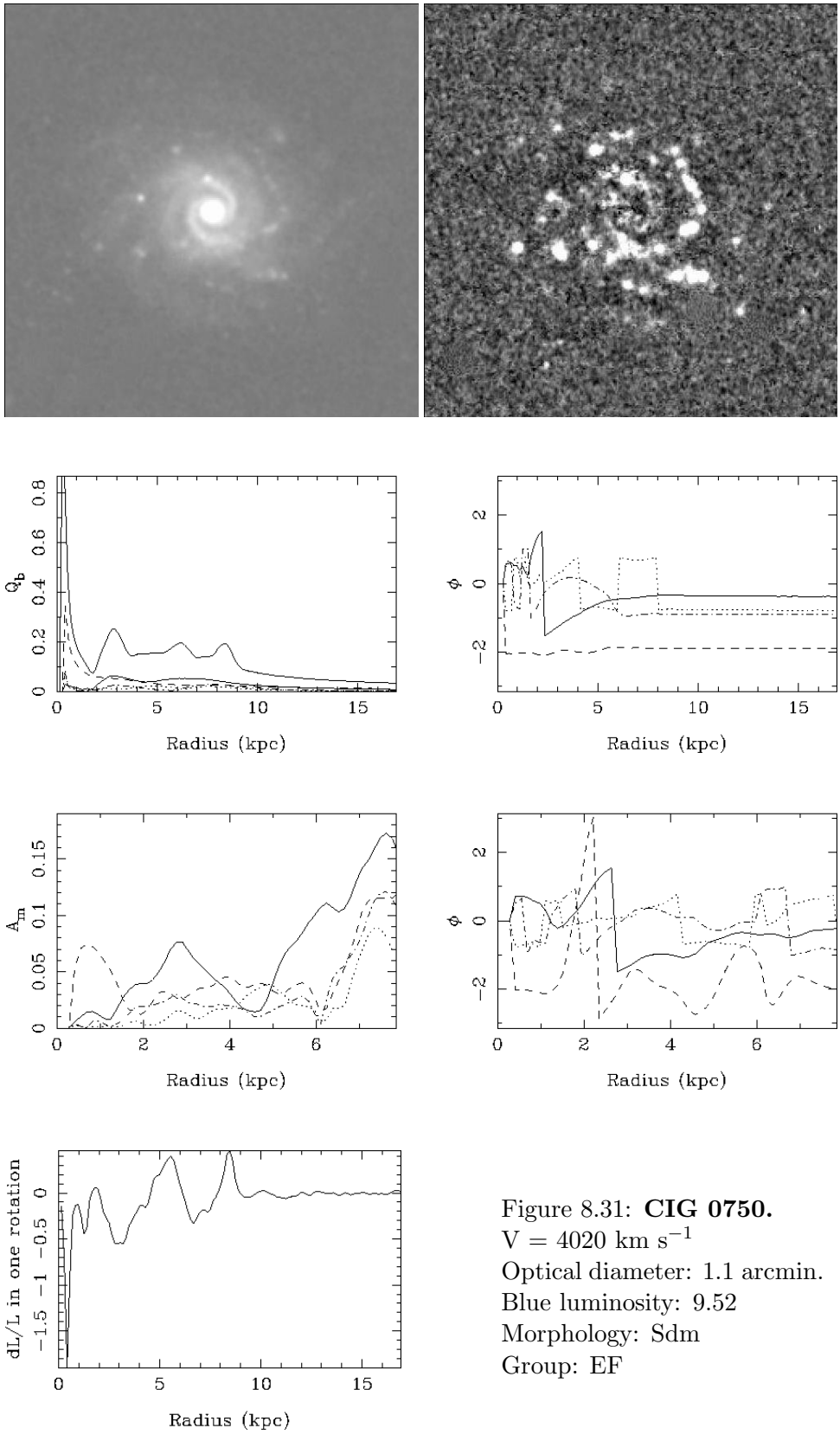

Figure 8.31: **CIG 0750.**
V = 4020 km s^{-1}
Optical diameter: 1.1 arcmin.
Blue luminosity: 9.52
Morphology: Sdm
Group: EF

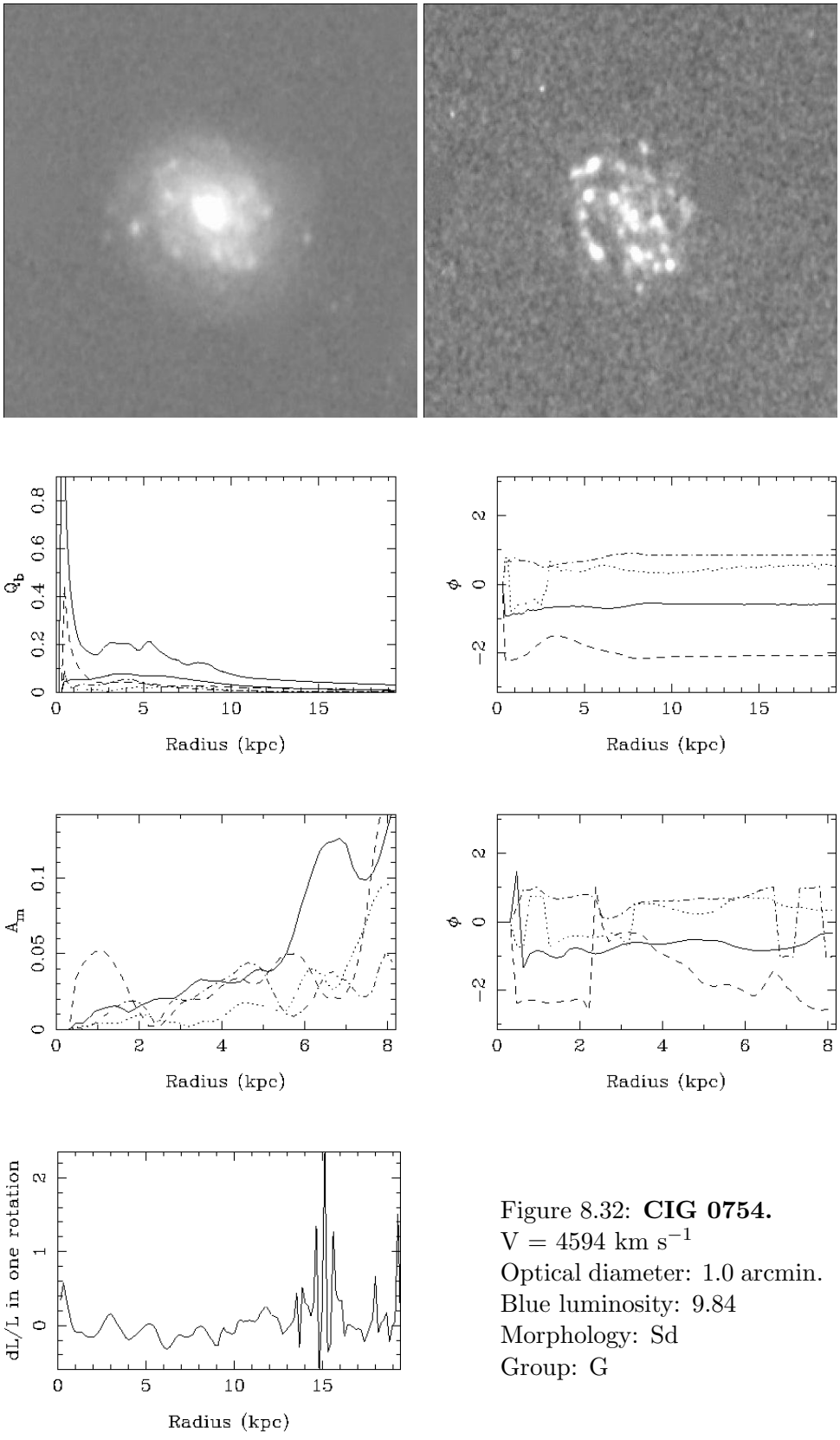

Figure 8.32: **CIG 0754.**
V = 4594 km s^{-1}
Optical diameter: 1.0 arcmin.
Blue luminosity: 9.84
Morphology: Sd
Group: G

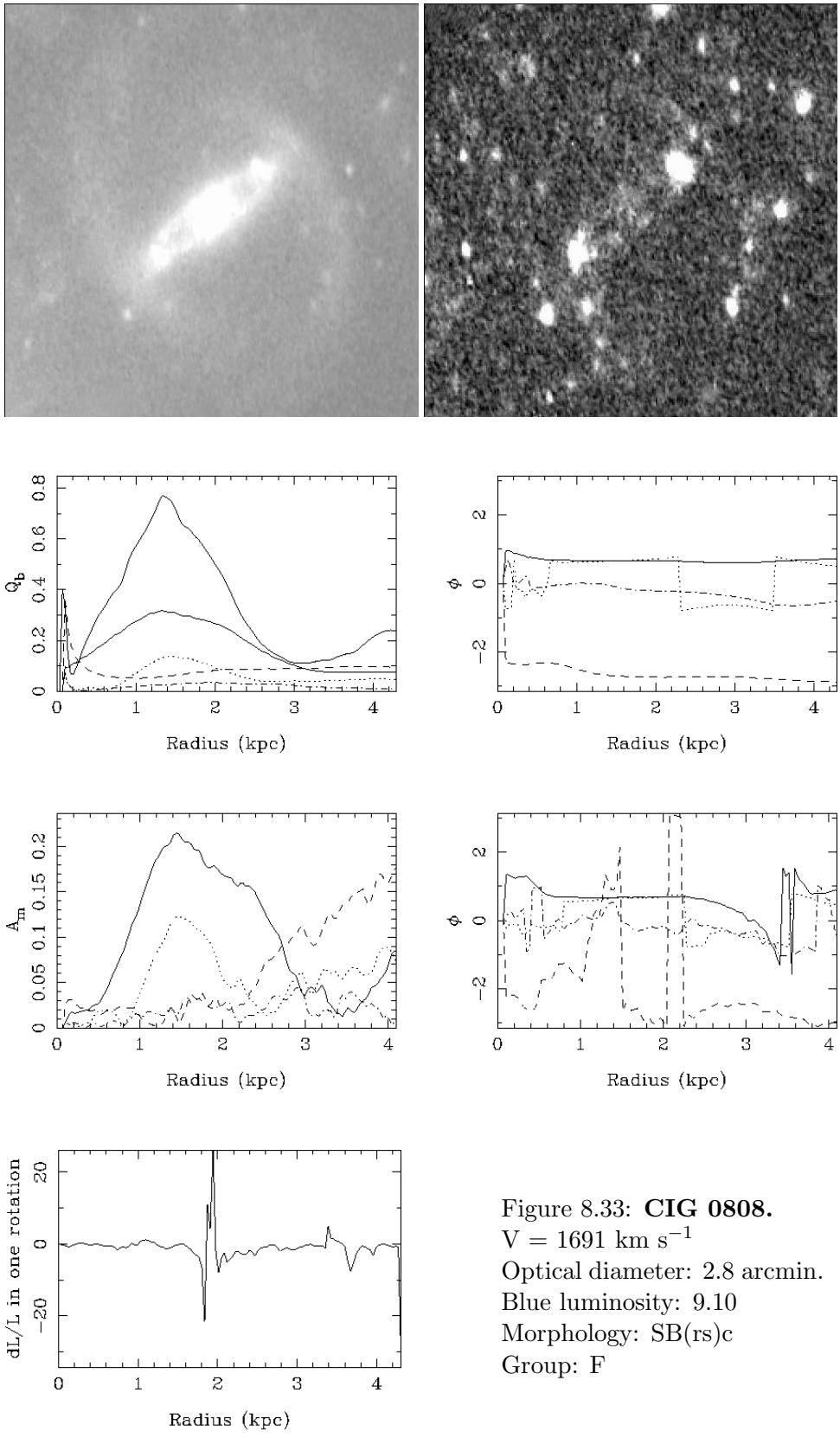

Figure 8.33: **CIG 0808.**
V = 1691 km s^{-1}
Optical diameter: 2.8 arcmin.
Blue luminosity: 9.10
Morphology: SB(rs)c
Group: F

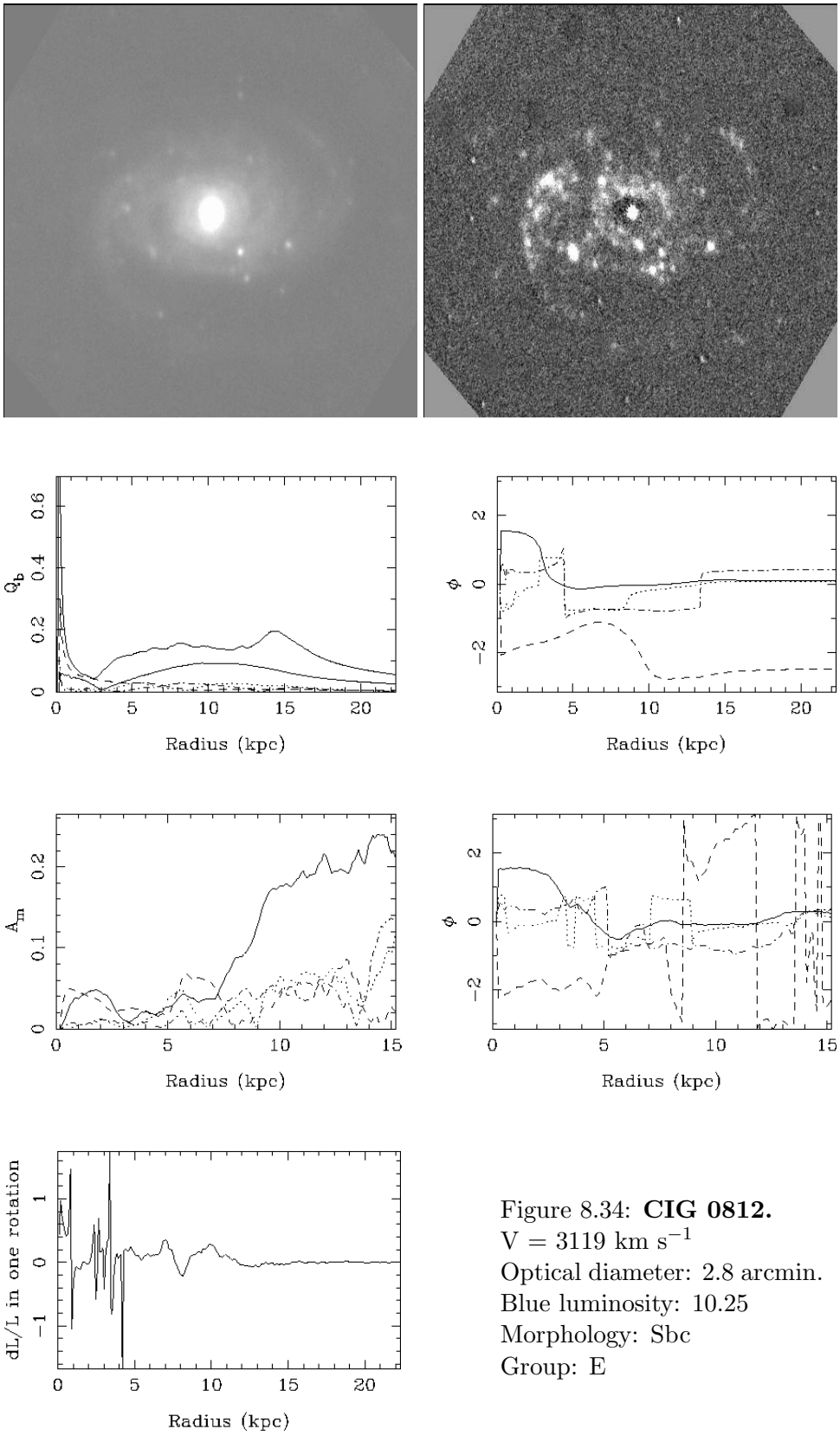

Figure 8.34: **CIG 0812.**
V = 3119 km s^{-1}
Optical diameter: 2.8 arcmin.
Blue luminosity: 10.25
Morphology: Sbc
Group: E

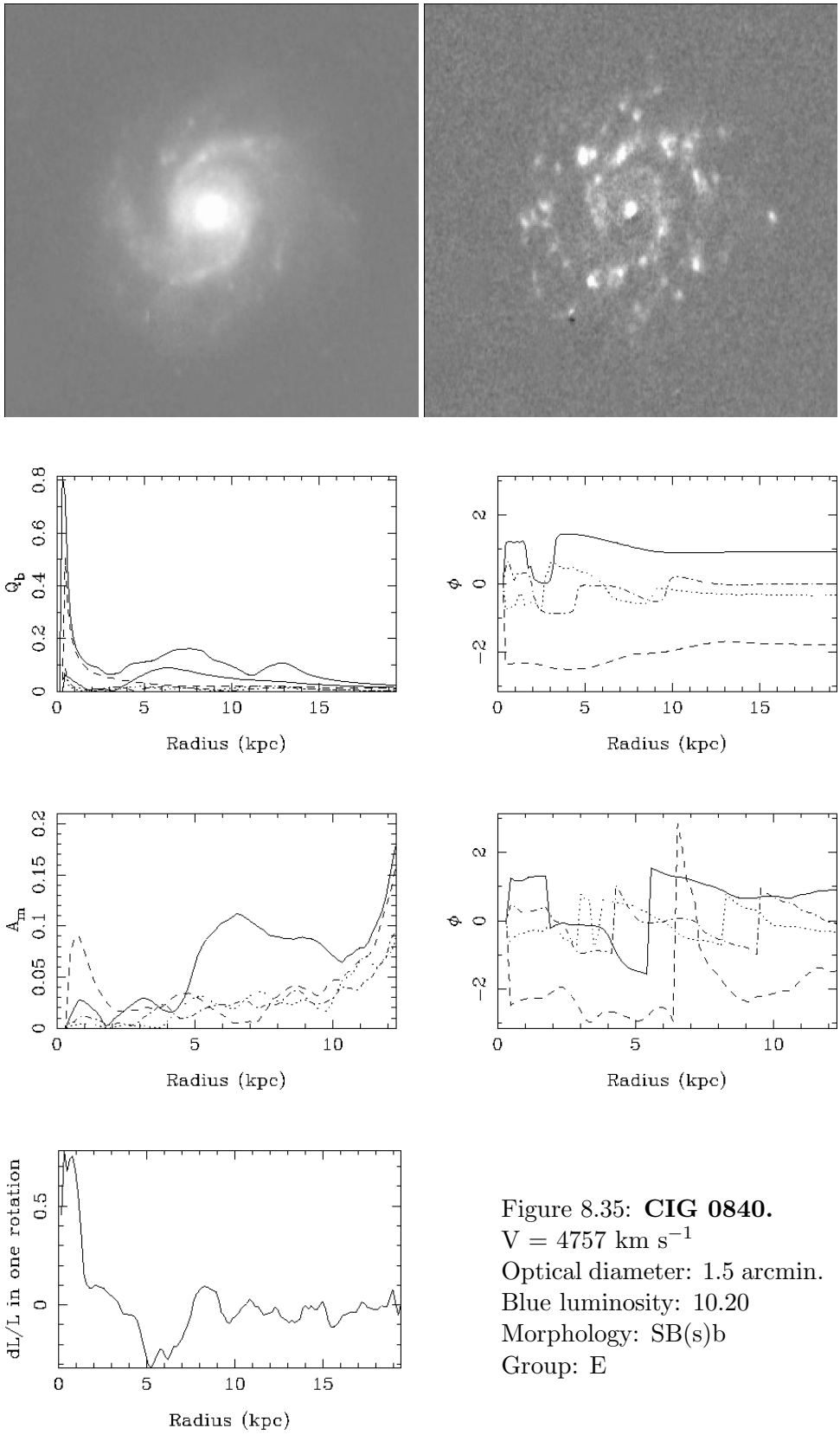

Figure 8.35: **CIG 0840.**
V = 4757 km s^{-1}
Optical diameter: 1.5 arcmin.
Blue luminosity: 10.20
Morphology: SB(s)b
Group: E

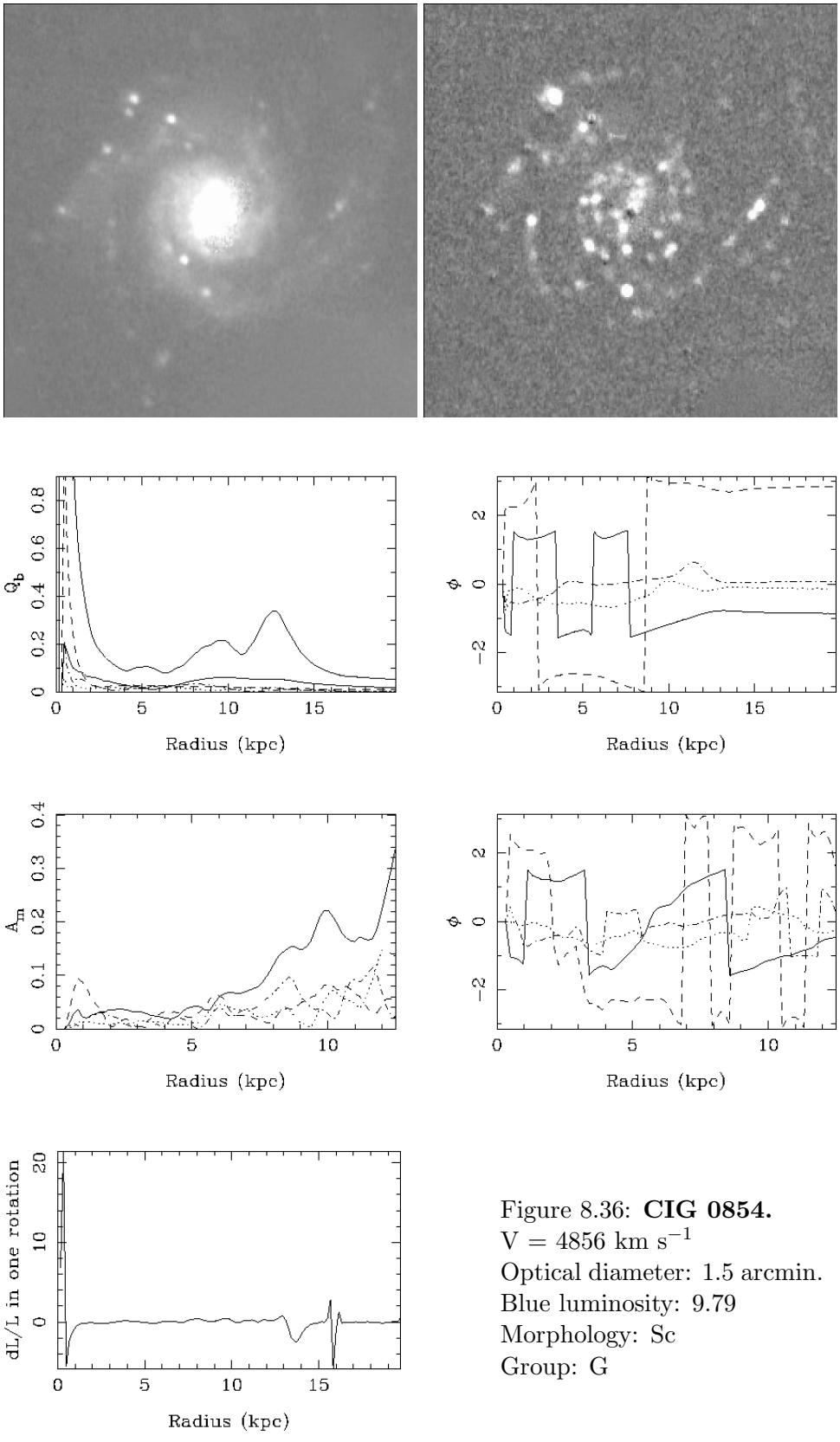

Figure 8.36: **CIG 0854.**
V = 4856 km s^{-1}
Optical diameter: 1.5 arcmin.
Blue luminosity: 9.79
Morphology: Sc
Group: G

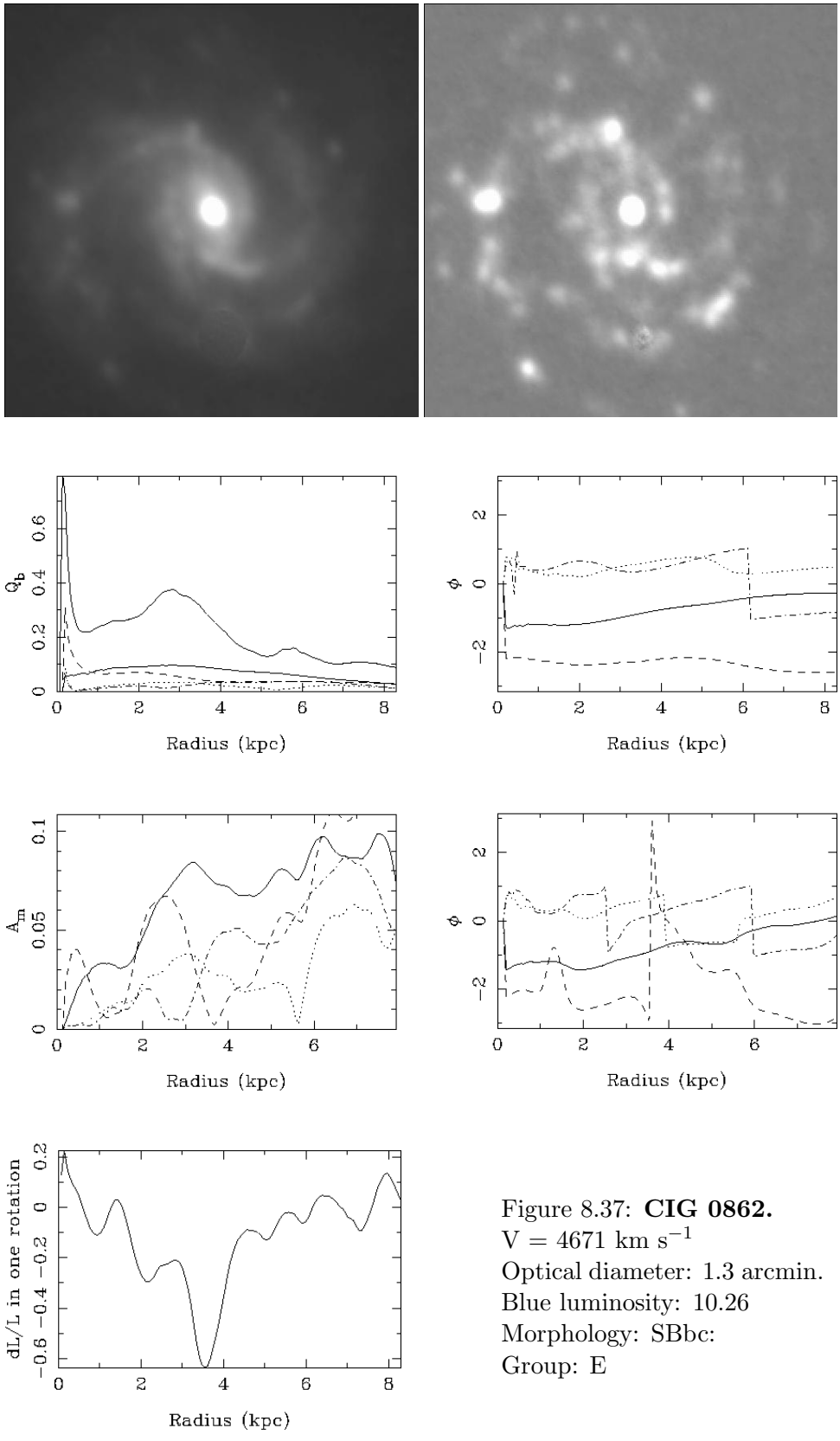

Figure 8.37: **CIG 0862.**
V = 4671 km s^{-1}
Optical diameter: 1.3 arcmin.
Blue luminosity: 10.26
Morphology: SBbc:
Group: E

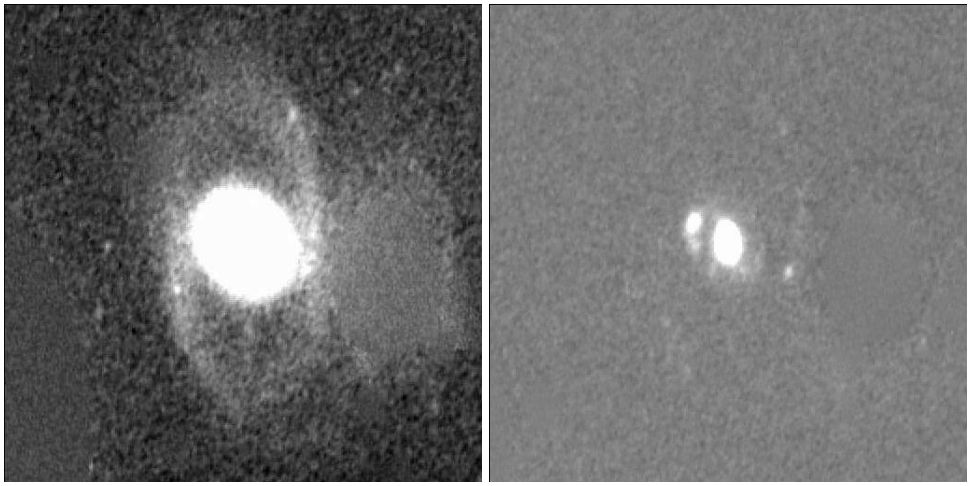

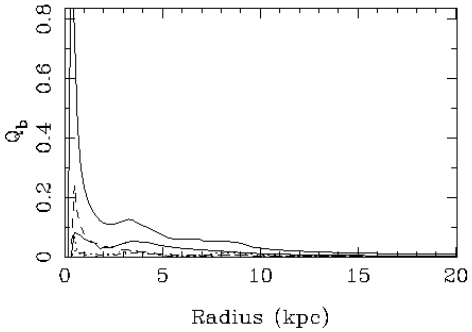

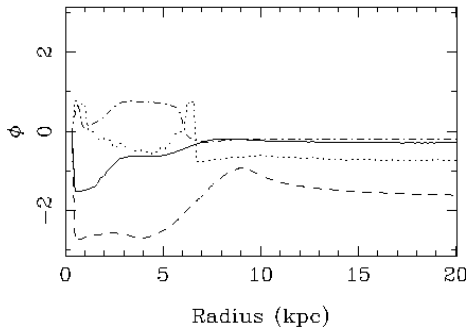

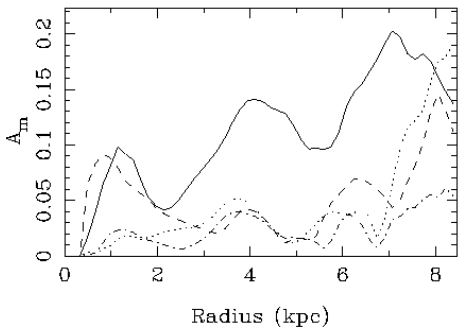

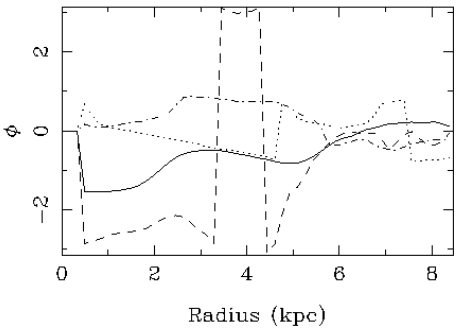

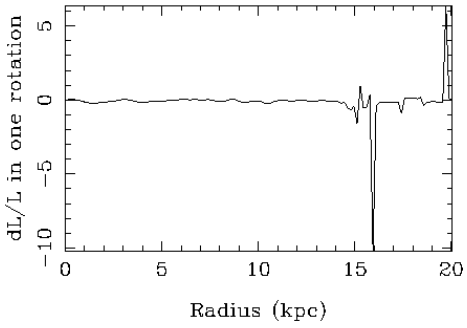

Figure 8.38: **CIG 0875.**
V = 4880 km s^{-1}
Optical diameter: 1.0 arcmin.
Blue luminosity: 9.89
Morphology: (R')SB(s)a
Group: H

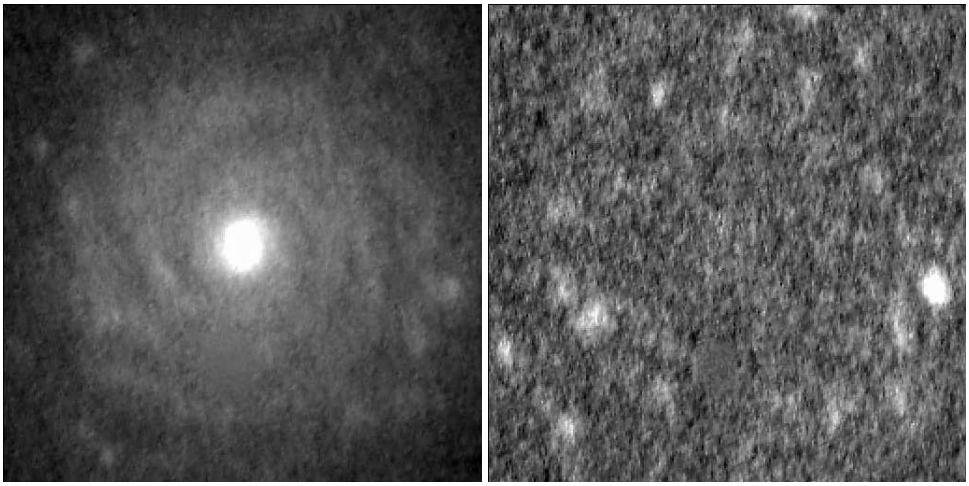

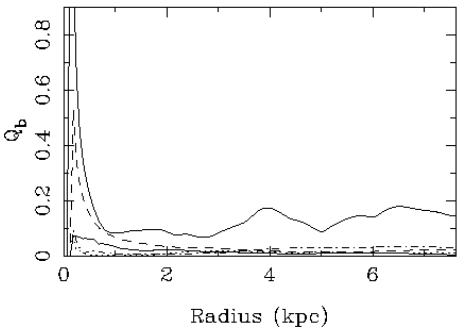

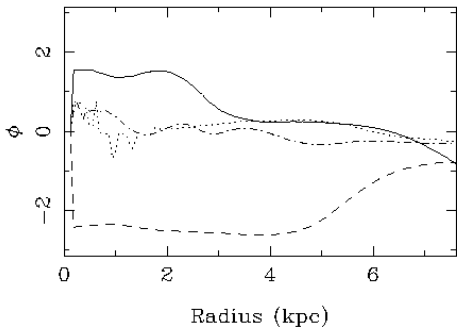

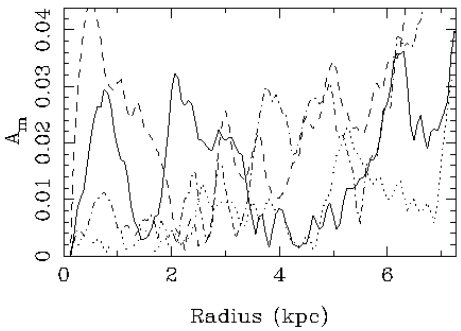

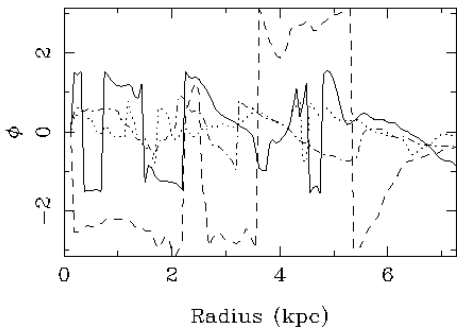

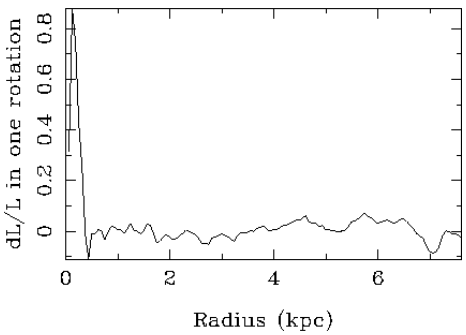

Figure 8.39: **CIG 0924.**
V = 4540 km s^{-1}
Optical diameter: 1.5 arcmin.
Blue luminosity: 9.78
Morphology: SA(rs)d:
Group: F

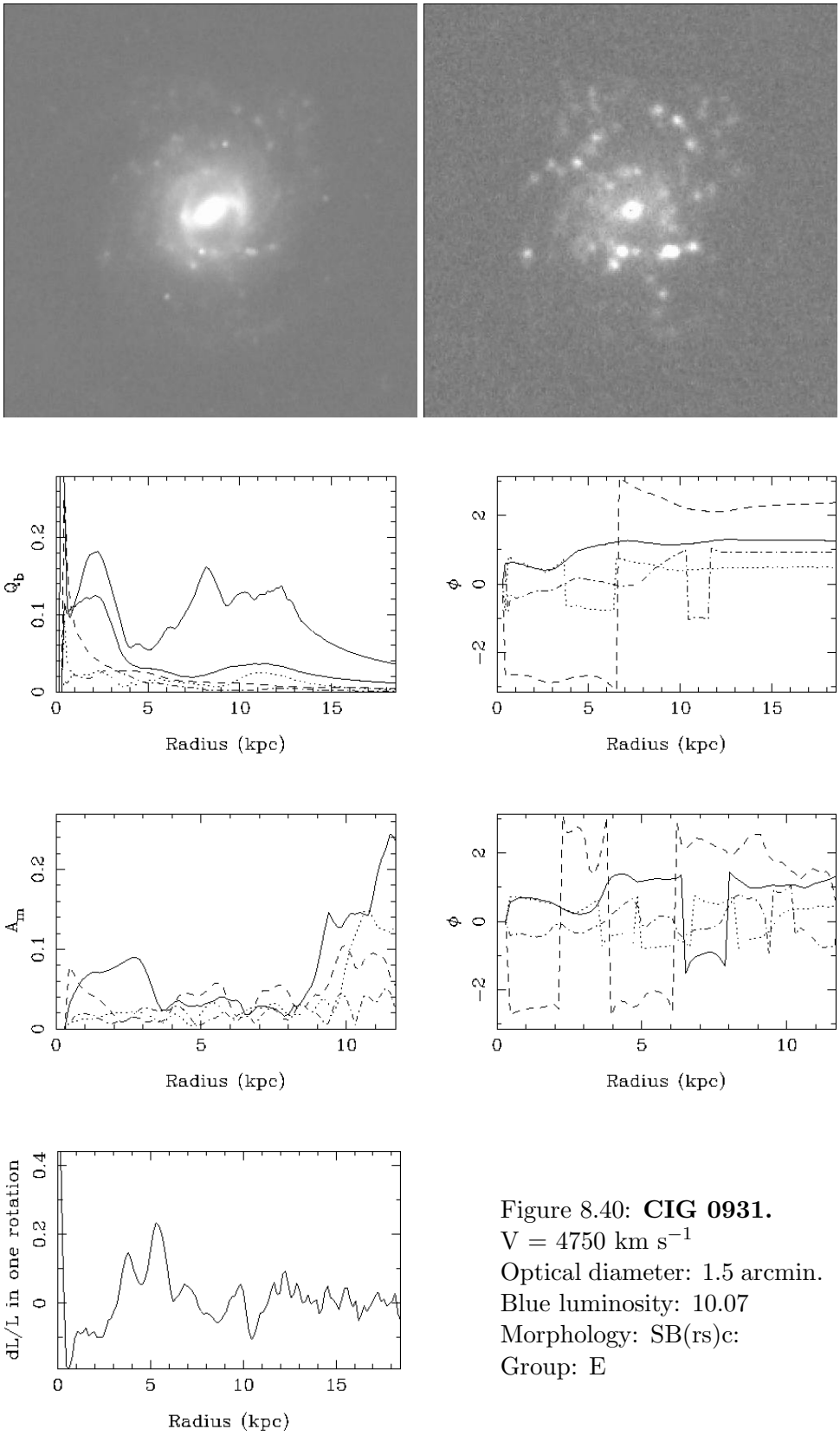

Figure 8.40: **CIG 0931.**
V = 4750 km s^{-1}
Optical diameter: 1.5 arcmin.
Blue luminosity: 10.07
Morphology: SB(rs)c:
Group: E

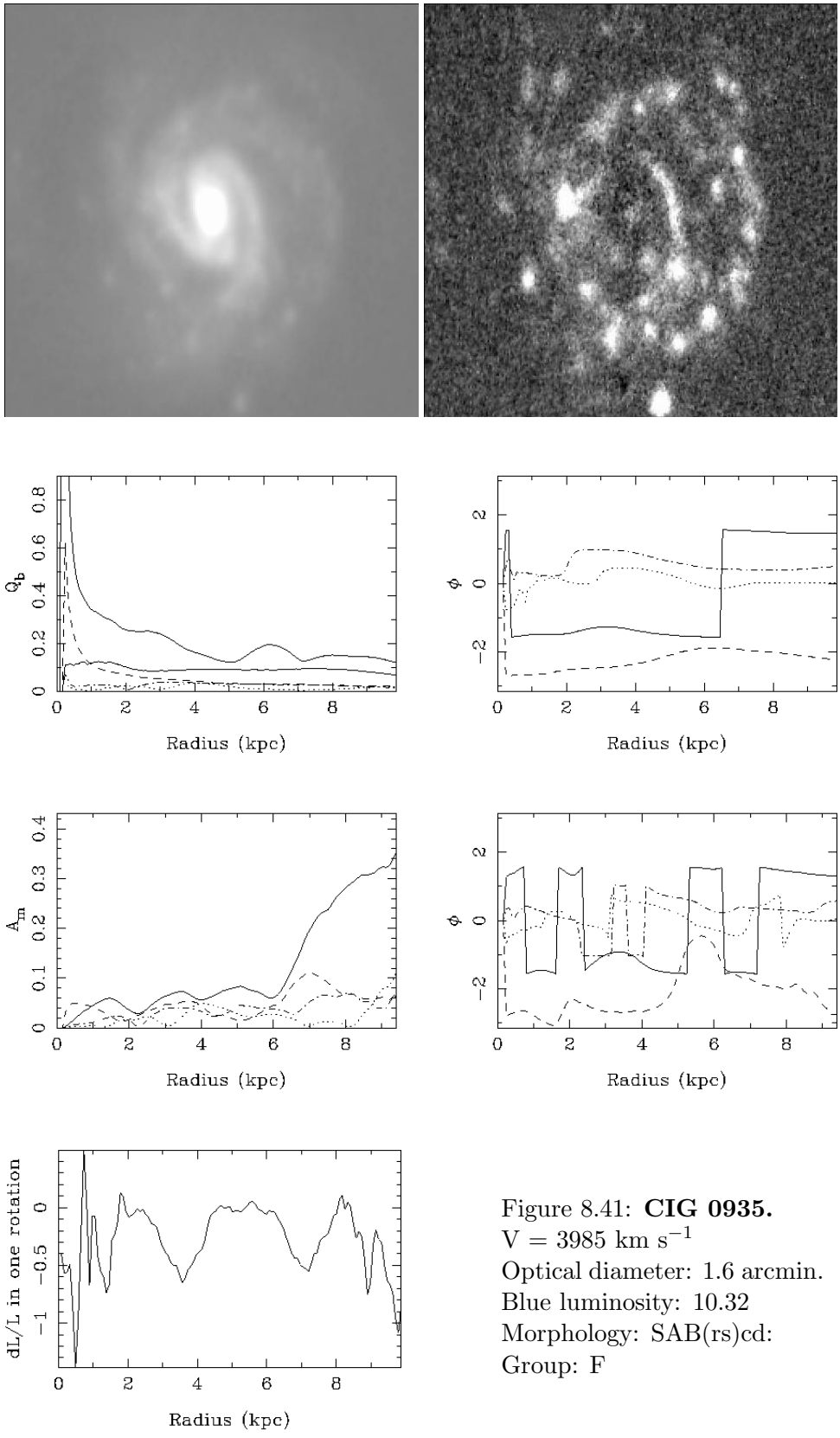

Figure 8.41: **CIG 0935.**
V = 3985 km s^{-1}
Optical diameter: 1.6 arcmin.
Blue luminosity: 10.32
Morphology: SAB(rs)cd:
Group: F

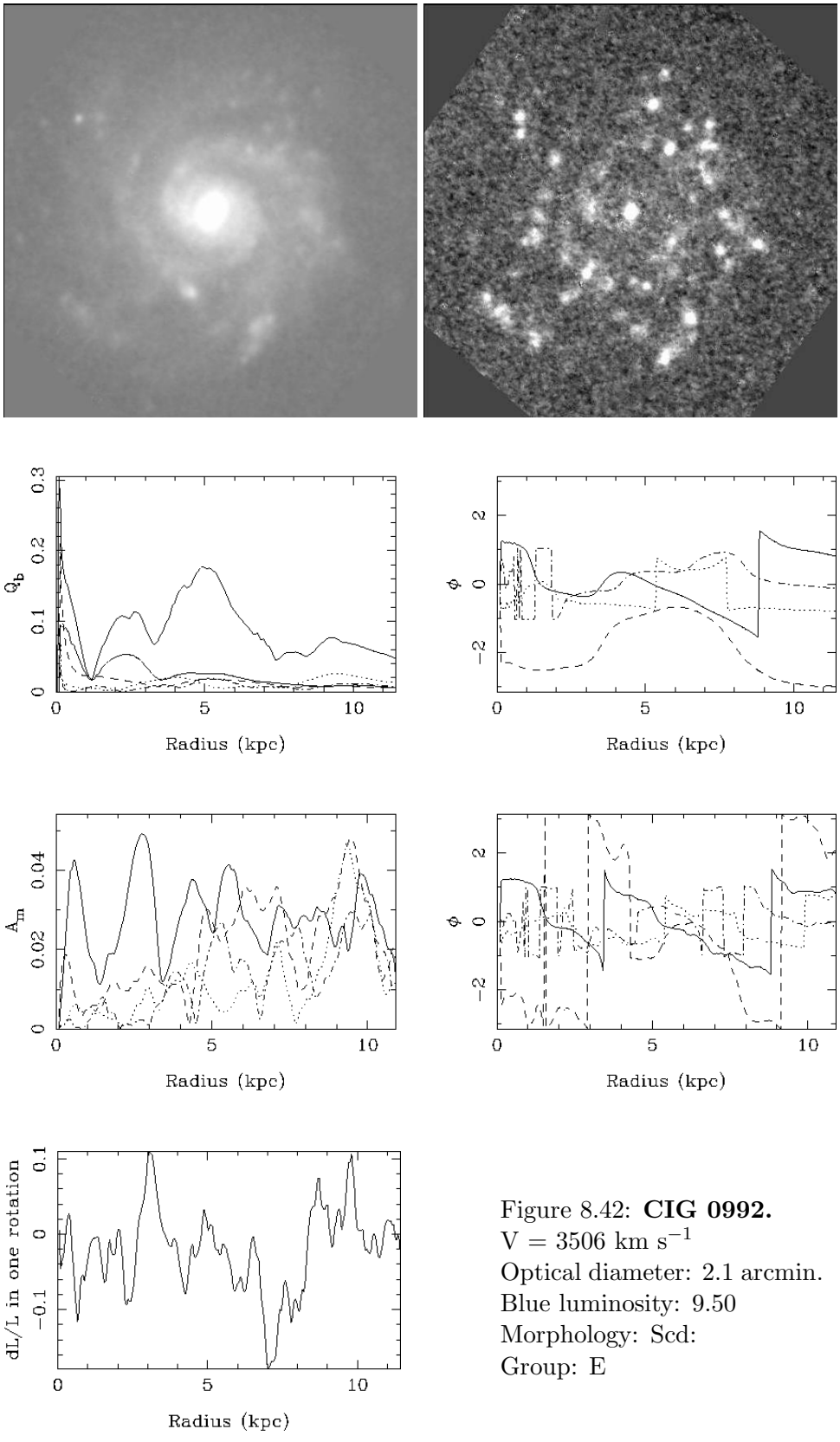

Figure 8.42: **CIG 0992.**
V = 3506 km s^{-1}
Optical diameter: 2.1 arcmin.
Blue luminosity: 9.50
Morphology: Scd:
Group: E

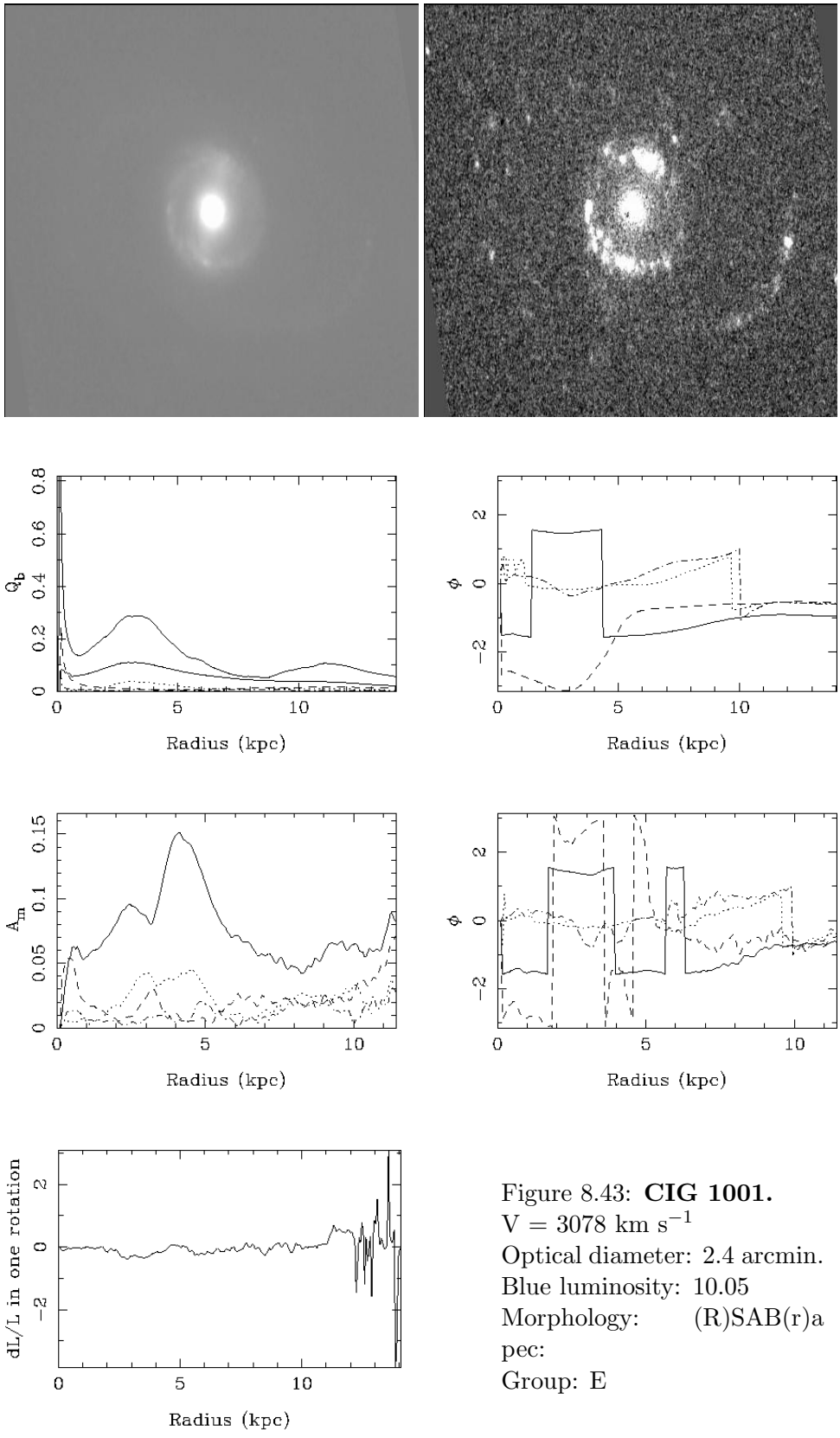

Figure 8.43: **CIG 1001.**
V = 3078 km s^{-1}
Optical diameter: 2.4 arcmin.
Blue luminosity: 10.05
Morphology: (R)SAB(r)a pec:
Group: E

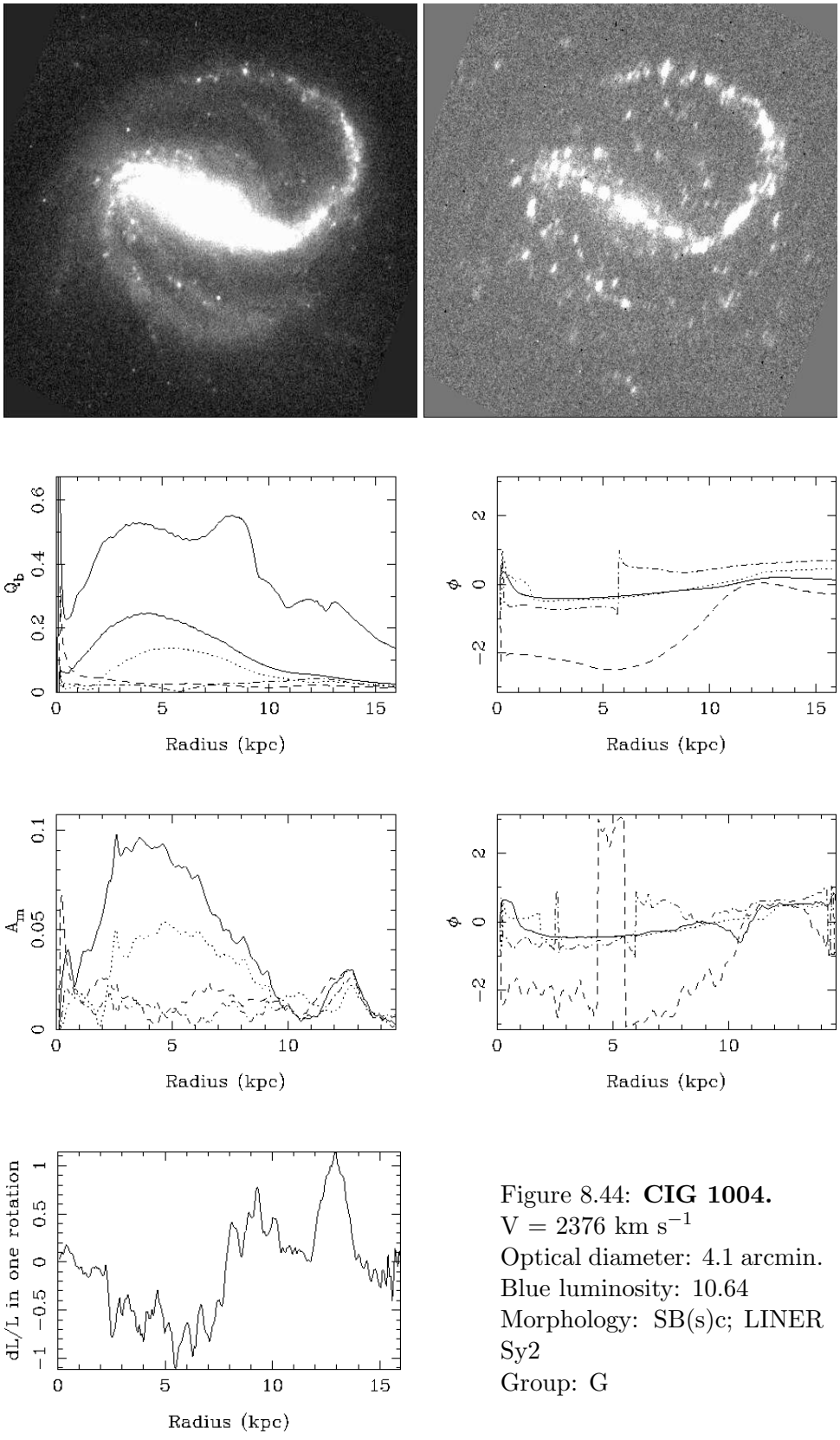

Figure 8.44: **CIG 1004.**
V = 2376 km s^{-1}
Optical diameter: 4.1 arcmin.
Blue luminosity: 10.64
Morphology: SB(s)c; LINER Sy2
Group: G

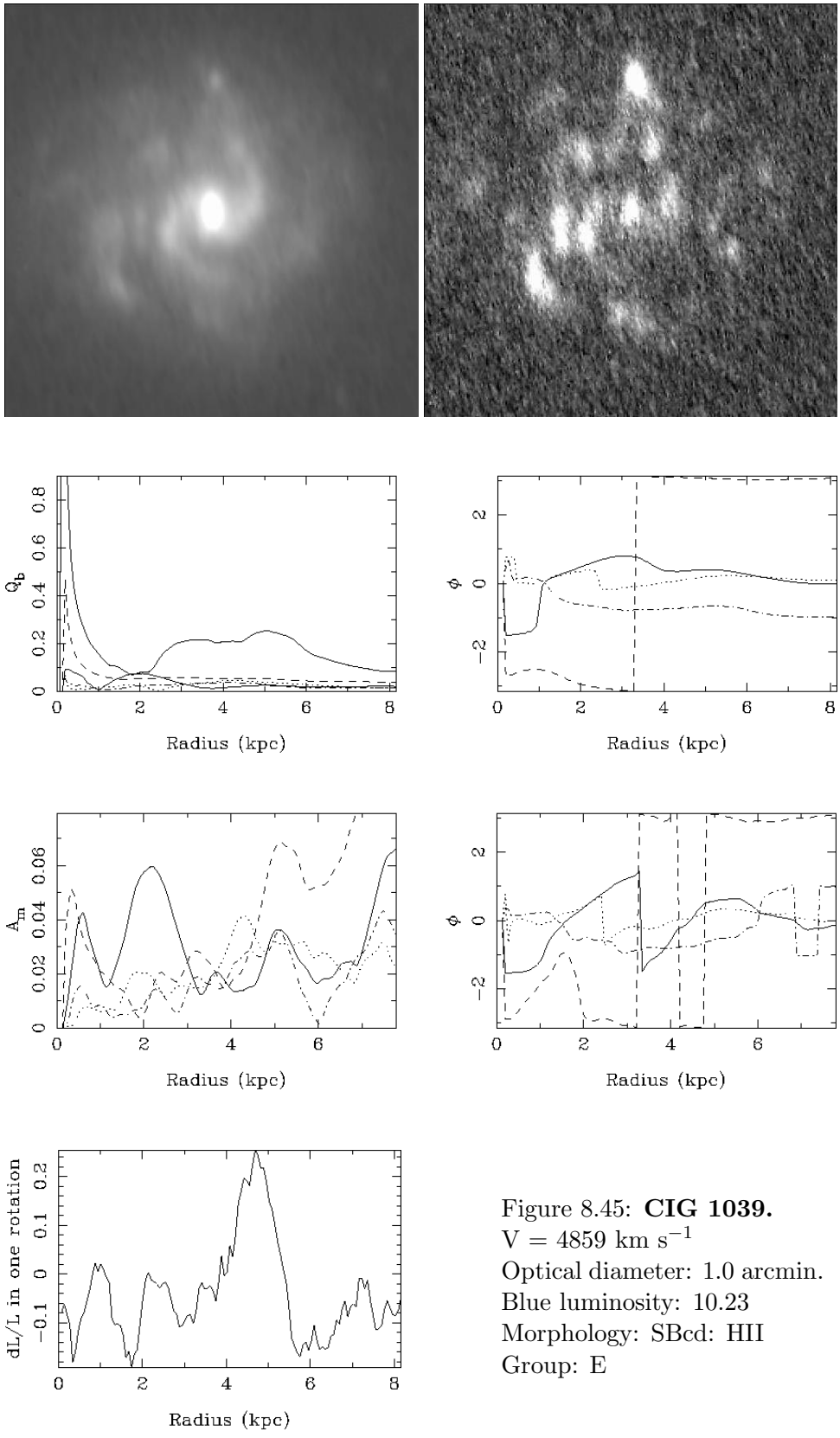

Figure 8.45: **CIG 1039.**
V = 4859 km s^{-1}
Optical diameter: 1.0 arcmin.
Blue luminosity: 10.23
Morphology: SBcd: HII
Group: E

8.5 Notes on individual galaxies

CIG 0030 T. F.[1] = 0.497

r Gunn Bar and spiral arms. m = 1 and m = 2 have roughly the same amplitude.

Hα A central peak and the spirals arms are well marked. A pseudo-ring and an external spiral are visible. No emission along the bar.

CIG 0050 T. F. = 1.089

r Gunn Very irregular galaxy. The m = 1 dominates both in the potential and in the density. No bar.

Hα No central Hα emission but external features: bright clumps.

CIG 0053 T. F. = 1.684

r Gunn Bar and two spiral arms. m = 2 strongly dominates, the galaxy is very symmetric.

Hα A central peak and the spirals arms are well designed but it seems that there is a shift between the Hα and the r Gunn. No emission along the bar.

CIG 0059 T. F. = 2.043

r Gunn The galaxy is quite regular. No bar.

Hα No central Hα emission. Only very few emission can be seen in the external part of the galaxy: it is maybe an early-type, without high amounts of gas, and no clumps.

CIG 0066 T. F. = 0.732

r Gunn Bulged and spiral galaxy. Faint bar.

Hα Central peak, starburst at the beginning of the brightest spiral arm, and emission along the spiral arms. No emission along the bar.

CIG 0068 T. F. = 1.804

r Gunn Dwarf galaxy. Lens and ansae, intermediate bar. The lenticular arms will dilute, this is the end of the evolution.

Hα Almost no emission in Hα.

CIG 0080 T. F. = 3.974

r Gunn Bulge and spiral arms. No bar. In the potential, m = 1 and

[1]The T. F. number is the estimation of the tidal forces of all the companions within 0.5 Mpc, obtained in the first part.

m = 2 have the same amplitude in the centre then m = 1 dominates in the outer parts of the galaxy, maybe due to the presence of a companion nearby. In the density, m = 1 dominates.
Hα Emission in the very centre and along the spiral arms.

CIG 0084 T. F. = 2.228

r Gunn Smooth and regular galaxy. No bar.
Hα No central emission, smooth and no clumps: the galaxy is evoluted.

CIG 0085 T. F. = 3.891

r Gunn Very irregular galaxy. No bar.
Hα The emission is also very irregular and very clumpy.

CIG 0096 T. F. = 2.019

r Gunn Bar and two spiral arms: the m = 2 component dominates all over the galaxy.
Hα There is a quite well defined ring which was not seen in the r Gunn. There is also a strong central emission, but no emission at all along the bar. The torques are noisy because of the very clumpy aspect of the galaxy.

CIG 0116 T. F. = 1.178

r Gunn Strong bar and two spiral arms. The m = 2 component dominates both in the potential and in the density.
Hα The emission follows the red image: star formation is present along the bar.

CIG 0176 T. F. = 2.691

r Gunn Bar and spiral arms.
Hα Central emission, star formation in the arms, not in the bar.

CIG 0188 T. F. = 1.182

r Gunn Smooth and faint emission. Bar.
Hα Very few emission, clumpy while this is smooth in r.

CIG 0217 T. F. = 1.906

r Gunn Bulge and three spiral arms. The m = 3 component dominates both in the potential and in the density. No bar.
Hα Central emission, and star formation in the arms.

CIG 0250 T. F. = 1.845

r Gunn Asymmetric galaxy: strong bar and one faint, small arm.
Hα Irregular but with emission in the bar.

CIG 0267 T. F. = 1.294

r Gunn Irregular galaxy: the arms are not centred respecting to the bulge. Very strong m = 1 component. Bar.
Hα The emission follows the arms and hence is not centred either. The torques are always positive: the gas is going outwards which could explain why there is no emission in the centre.

CIG 0281 T. F. = 1.194

r Gunn No bar and no ring. Very small pitch angle. Very symmetric galaxy: m = 2 dominates.
Hα The emission follows the arms.

CIG 0291 T. F. = 1.568

r Gunn Bright centre, fainter external emission. No bar.
Hα Clumpy emission in the centre but the design is not clear, the morphology corresponds to Magellanic dwarf type.

CIG 0359 T. F. = 1.478

r Gunn The ansae seem strange. Early type galaxy. Emission only in the centre. No bar.
Hα Strictly nothing apart from the very centre.

CIG 0376 T. F. = 2.155

r Gunn Bright bulge, bar and spiral arms.
Hα Central emission, pseudo-ring then spiral. Shift between the Hα and the r Gunn emission.

CIG 0382 T. F. = 2.220

r Gunn Bar and spiral arms. m = 2 dominates in the central part, m = 1 in the outer region.
Hα Emission in the centre and in the spiral arms, not in the bar.

CIG 0512 T. F. = 2.569

r Gunn Strong bar and two spiral arms.
Hα The bar is not complete in Hα but is well designed in the inner

part: transition stage.

CIG 0575 T. F. = 1.143

r Gunn Bright bulge.
Hα Central emission, smooth outer emission.

CIG 0645 T. F. = 2.160

r Gunn Nuclear spiral and two outer spiral arms. Bar.
Hα Central starburst may be due to the nuclear spiral.

CIG 0652 T. F. = 1.881

r Gunn Strong bar. m = 2 component dominates both in the potential and in the density.
Hα Star formation in the bar but not till the end. The torques are negative which means that the gas is falling towards the centre.

CIG 0660 T. F. = 0.987

r Gunn Bar and two spiral arms, almost a pseudo-ring. m = 2 component is very strong in the potential and in the density.
Hα Central emission, but not along the bar. Outer punctual bursts very strong, along the spiral arms.

CIG 0661 T. F. = 1.479

r Gunn Strong bar. The m = 1 component is not inevitably true: a nearby bright star could limit our interpretation.
Hα No emission in the centre or along the bar, only the outer parts show some clumps.

CIG 0700 T. F. = 1.421

r Gunn Bulge, no bar. Smooth outer emission.
Hα No central emission, one punctual burst very strong.

CIG 0712 T. F. = 0.811

r Gunn Very clear ring and a bar that is in a destructive state and will become a lens (loop).
Hα Emission along the bar: late state of the evolution.

CIG 0744 T. F. = 1.873

r Gunn Strong bulge, one spiral arm. m = 1 dominates.
Hα A second spiral arm is visible. Clumpy emission in the centre.

CIG 0750 T. F. = 0.948

r Gunn Bulge, spiral arms. No bar.
Hα No central emission. Clumps along the spiral arms.

CIG 0754 T. F. = 0.669

r Gunn Bulge and smooth outer emission.
Hα Emission in the bar. Clumps in the spiral arms.

CIG 0808 T. F. = 2.272

r Gunn Strong bar, ansae, two spiral arms. m = 2 component dominates both in the potential and in the density.
Hα No central emission but bursts at the end of the bar. Bar in destruction. In the torques, the signal shows the Hα structure.

CIG 0812 T. F. = 2.853

r Gunn Bulge, spiral arms extending far from the centre, pseudo-ring. m = 2 dominates both in the potential and in the density. No bar.
Hα Central emission, along the ring and in the spiral.

CIG 0840 T. F. = 0.533

r Gunn Bar and two regular spiral arms. m = 2 dominates both in the potential and in the density.
Hα Central emission, and in the spiral. No emission in the bar.

CIG 0854 T. F. = 0.924

r Gunn Bulge and two spiral arms.
Hα Emission in the bar and clumps along the spiral arms.

CIG 0862 T. F. = 1.236

r Gunn Bright centre, bar, ring and spiral arms. m = 2 component dominates.
Hα Central peak, ring and spiral. No emission along the bar.

CIG 0875 T. F. = 1.430

r Gunn Early type galaxy. Strong bulge. No Bar.
Hα Central emission. Very few external emission.

CIG 0924 T. F. = 1.006

r Gunn Bulge. No bar. Very faint, smooth emission.
Hα No central emission. Faint outer emission.

CIG 0931 T. F. = 1.055

r Gunn Bar and spiral arms.
Hα Central peak. No emission in the bar. Clumps in the arms.

CIG 0935 T. F. = 0.922

r Gunn Bar and spiral arms.
Hα Emission along the spiral arms but not in the centre.

CIG 0992 T. F. = 1.815

r Gunn Bright bulge. Spiral arms. No bar.
Hα Central peak. Emission along the spiral arms.

CIG 1001 T. F. = 3.213

r Gunn Bright bulge. Bar, ring and spiral arms.
Hα Central emission. Peaks at the end of the bar, in the ring and along the spiral arms.

CIG 1004 T. F. = 2.520

r Gunn Strong bar. Two spiral arms. m = 2 component dominates both in the potential and in the density.
Hα Clumps in the bar. Emission also along the spiral arms. Slight shift between the Hα and the r Gunn image.

CIG 1039 T. F. = 0.782

r Gunn Bulge. Spiral arms. m = 1 dominates the outer parts of the galaxy. Bar.
Hα Central peak. Peaks at the beginning of the arms. Clumpy emission.

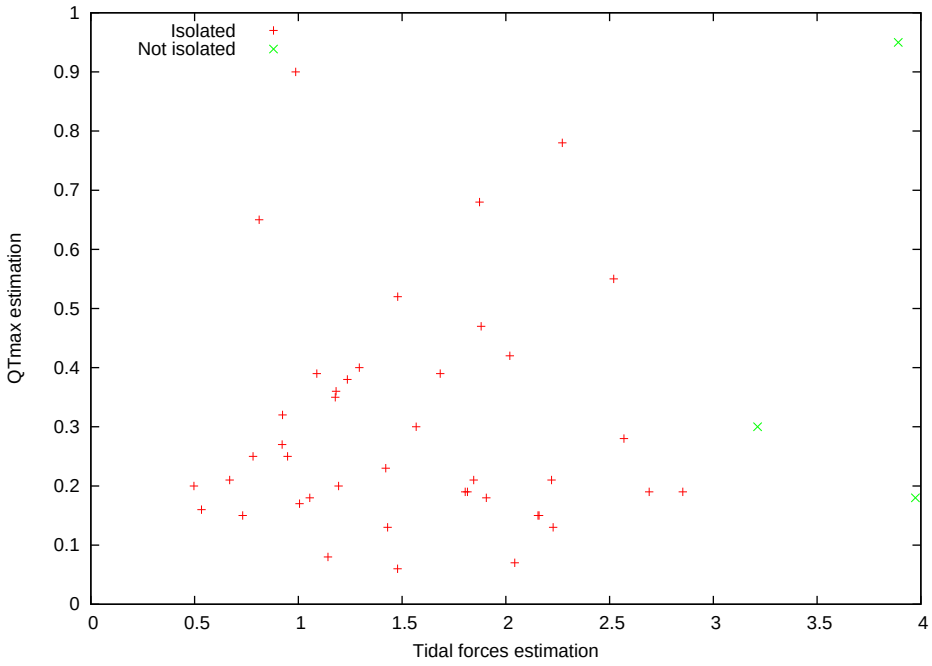

Figure 8.46: $Q_T$max.

8.6 Statistical study

Our sample is 94% complete (we are only missing data for 3 galaxies over 48). Hence, we can derive statistically significant characteristics for a sample of isolated galaxies.

8.6.1 Maxima of the amplitudes of the Fourier modes

Figures 8.46 to 8.50 present the tidal forces estimation in the x-axis and, along the y-axis, estimations of the maximal amplitudes of the m = 1 or m = 2 Fourier components. Three galaxies (CIGs 0080, 0085, 1001) possess an estimation of the tidal forces greater than 3. It is interesting to note that the m = 1 component dominates in the outer parts of CIG 0080, which possess a small companion nearby. CIG 0085 is a very irregular galaxy and seems to present features due to strong interactions. Last, CIG 1001 is classified as peculiar by NED. These remarks comfort the validity of the isolation study done in the first part of the thesis which affected strong values of the isolation parameters to these three galaxies.

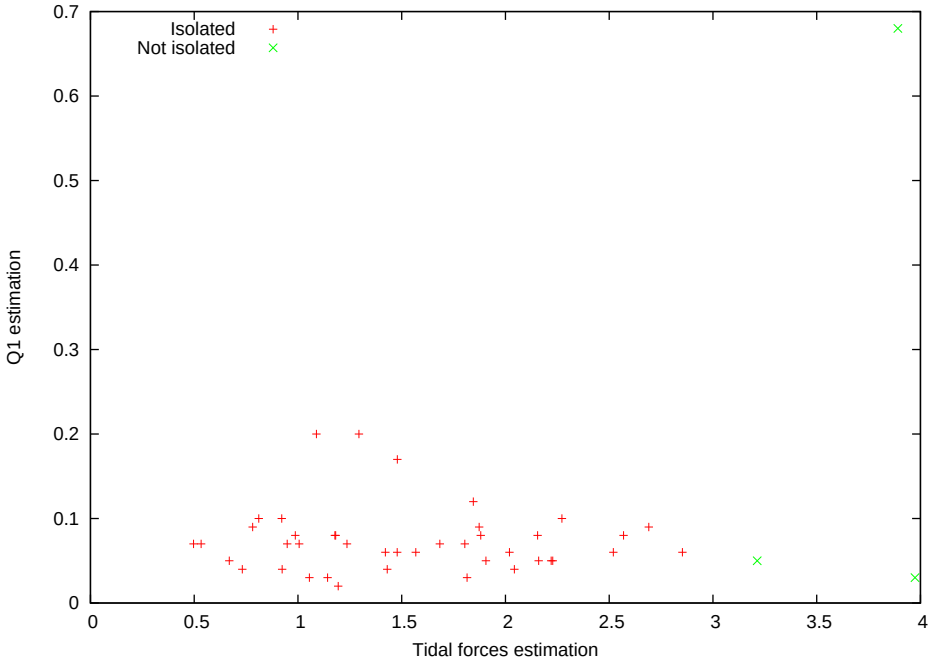

Figure 8.47: Q_1.

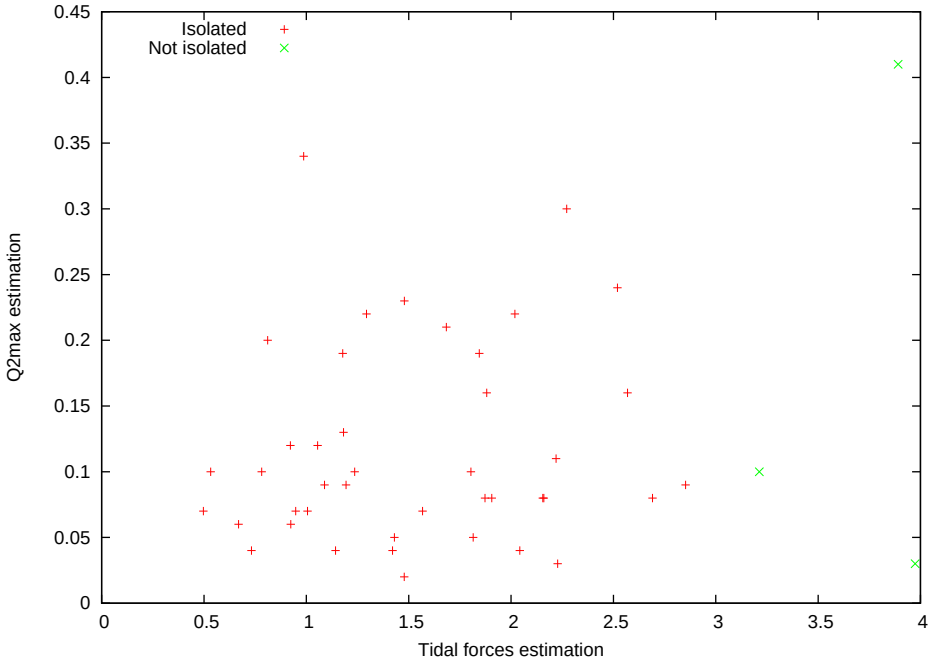

Figure 8.48: Q_2max.

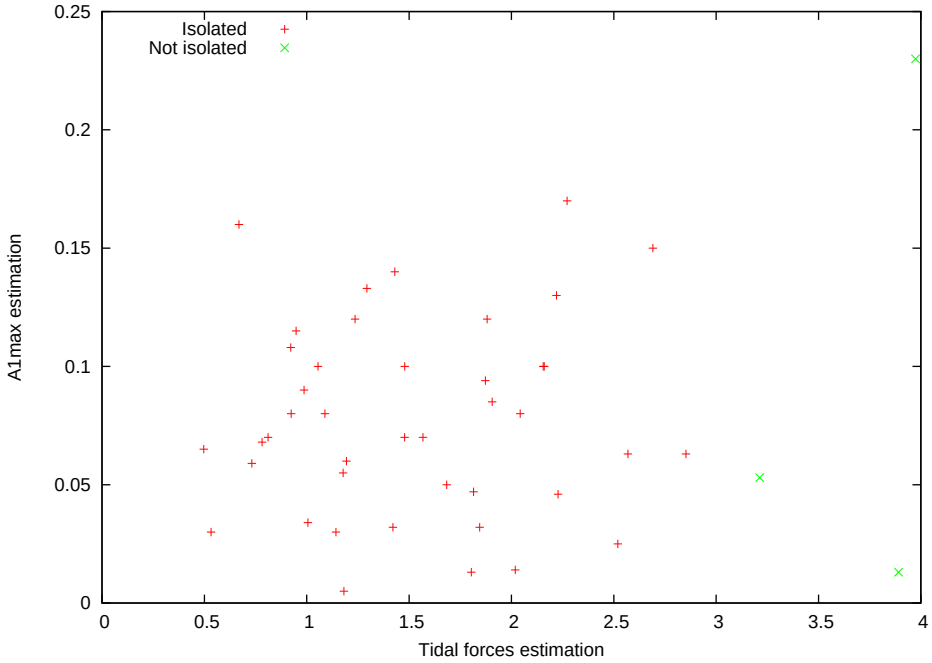

Figure 8.49: A_1max.

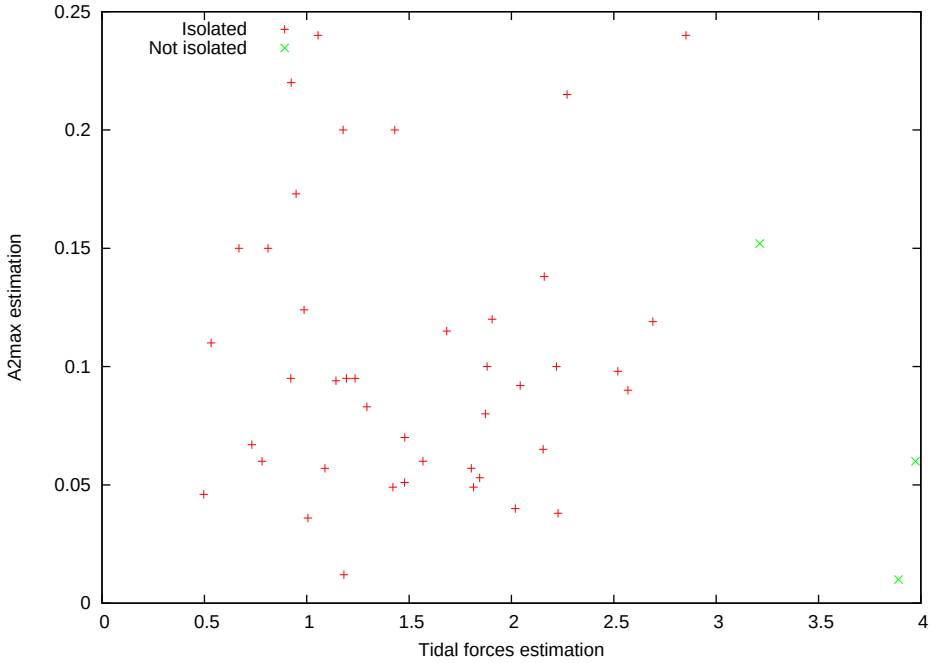

Figure 8.50: A_2max.

8.6.2 Bars

a) Percentage of bars

We class the 45 galaxies in three subsamples, as a function of the presence or absence of bar:

Bar 0030, 0053, 0066, 0096, 0116, 0176, 0188, 0250, 0267, 0376, 0382, 0512, 0645, 0652, 0660, 0661, 0712, 0754, 0808, 0840, 0854, 0862, 0931, 0935, 1001, 1004, 1039.

No bar 0050, 0059, 0080, 0084, 0085, 0217, 0281, 0291, 0359, 0700, 0750, 0812, 0875, 0924, 0992.

Intermediate 0068, 0575, 0744.

The barred galaxies represent 60% of our sample (the bar can be seen in r Gunn or Hα). As we are treating optical images, this result is consistent with the studies presented in the introduction. The unbarred galaxies represent 33% of the sample. Three galaxies have an intermediate stage bar, similar to the "SAB" kind, they represent 7% of the total. We can conclude that the isolated galaxies span the whole range of bar morphology, in quantities similar to the galaxies in denser environments. Isolated galaxies are not preferentially barred or unbarred galaxies. This result is marginally in contradiction with the recent study by Varela et al. (2004), who estimate that bars are twice more frequent in perturbed galaxies compared to isolated galaxies, especially for early-types. Also Elmegreen et al. (1990) find more bars in a sample of binary galaxies, and also more early-types.

b) Phase shift between gas and stellar components

Frequently, we see bright Hα knots at the end of the bars, even when there is no emission in the bar. It is sometimes difficult to define where exactly the arms begin because the Hα could be very clumpy, but we can use the star formation spots at the end of the bars, to define the starting point of the spiral arms. The Hα emission is always leading with respect to the bar in the r Gunn image. The most evident cases of bar shifts between the r Gunn and the Hα images are listed hereafter (in parentheses: an estimation of the shift angle in degrees): 0030 (20°); 0053 (10°); 0066 (5°); 0096 (10°); 0176 (10°); 0376 (30°); 0512 (10°); 0840 (15°); 1004 (5°).

8.6.3 Evolutive sequence

a) Classification

As some characteristics are frequently found among the galaxies of our sample, we chose to group the galaxies presenting the same features. In decreas-

ing frequency order, we defined the three main groups:

Group E *19 galaxies – CIGs 0030, 0053, 0066, 0080, 0096, 0176, 0217, 0281, 0291, 0376, 0382, 0660, 0812, 0840, 0862, 0931, 0992, 1001, 1039.*
The principal features of this group are the following: a strong central peak in the Hα emission; no Hα emission in the bar (for the barred galaxies in the r Gunn image); bright Hα knots at the end of the bar/beginning of the spiral arms; Hα emission along the spiral arms, generally clumpy.

Group F *9 galaxies – CIGs 0050, 0059, 0084, 0188, 0267, 0661, 0808, 0924, 0935.*
This group is constituted by galaxies with less gas, having a smoother morphology. The galaxies do not present any central emission spot in Hα.

Group G *8 galaxies – CIGs 0116, 0250, 0645, 0700, 0712, 0754, 0854, 1004.*
This group gathers galaxies presenting Hα emission in the bar. CIG 0700 presents a very faint emission, but a bar can be distinguished.

Some of the galaxies of our sample did not fit in any of the main groups above. Some others presented characteristics mixing features from two of the above groups. Nevertheless, we could class them as follow:

Group H *3 galaxies – CIGs 0068, 0359, 0875.*
This group is mostly constituted by early types galaxies, with very few emission in Hα and when it occurs, only in the centre.

Group EG *3 galaxies – CIGs 0512, 0652, 0744.*
This group is a transition between the **E** and **G** groups presented above: fragments of bars. The central emission of CIG 0744 is very clumpy but seems to follow the shape of a bar, this is why we included it in this group.

Group EF *1 galaxy – CIG 0750.*
CIG 0750 does not have a clear central peak in Hα but presents all the other features of the galaxies in the group **E**: clumpy Hα emission along the spiral arms. We call this group **EF** as a result of the mixed features presented by CIG 0750.

Group Irr. *2 galaxies – CIGs 0085, 0575.*
This last group gathers very irregular galaxies which do not fit particularly in any of the previous groups defined above.

b) Interpretation

We can try to estimate the lifetime of bars in galaxies if we consider the different features as different stages of an evolutive sequence. We see three main steps: by gravitational instability, a galaxy accretes gas from the intergalactic medium which makes it unstable for bar formation. The bar creates a torque which drives the gas inflow towards the centre. This phase corresponds to our identified (**G** phase).

The second step is a transition between the **G** and **E** phases: the gas inflows towards the center while a ring is slowly forming at the resonance (pseudo-ring due to the winding of the spiral arms).

In a third step, the gas is progressively depopulated from the bar, and accumulates first in the very center of the galaxy (or a very small nuclear ring, at ILR), and also at the UHR resonance, near the corotation. The gas there is quite stable, with almost zero velocity with respect to the bar pattern, and therefore the star formation is quite efficient. This corresponds to our identified more frequent phase, the **E** phase.

Since the gas infall destroys the bar, the latter becomes progressively weaker and weaker: the **F** phase is reached. The stars in the centre become an old population, contributing to increase the bulge mass. Without more gas fueling, the Hα spot in the centre is fading away in 10^8 years (OB stars). The frequency of the **F** phase means that a bar is typically destroyed in a few 10^8 years.

The efficiency of the star formation as a function of the gas density is still a challenging issue. We made simulations (see Appendix C) to confront our observations to the theory. Initially, the galaxy is launched axisymmetric and the bar forms spontaneously by gravitational instability. The gas subject to the bar torques inflows towards the centre. We used the Schmidt law (SFR $\propto \rho_g^{1.2}$, where ρ_g is the gas volumic density) to determine the star formation rate. In our simulations, the predicted frequency of the **G** Hα distribution is higher than the **E** phase. This is not in agreement with our observations where the **E** phase is about twice more frequent than the **G** phase. During the simulations, we can see the formation of rings at the Ultra Harmonic Resonance (UHR). But comparing with the galaxies from the group **E**, the ring gas density is relatively weaker than the gas density along the bar. To remove this discrepancy, it would be necessary to change the expression of the star formation rate: it should not only depend on ρ_g but should take into account the velocity of the gas too. In particular, the relative velocity of the gas with respect to the bar pattern is relevant. This work is in progress.

The question of star formation versus gas density means that the Hα emission is not a faithful tracer of gas density, but more of star formation (which should a good ersatz, in case of a simple Schmidt law). We can try to compare the quality of this tracer with that of CO emission.

We do not have galaxies in common with the BIMA Survey Of Nearby Galaxies (BIMA SONG, Helfer et al. 2002). But already, the BIMA SONG brings us some clues about the gas density. The **E** phase, although also present there, is less frequent, relative to the **G** phase, as we could expect. There is more CO emission in the bars of their galaxy sample (NGC 2903, 3627, 4535, 5457; see also Maffei2 by A. Weiss) compared to our Hα sample. Therefore the Hα emission is indeed a more efficient tracer of star formation than of the total amount of gas available.

Some isolated galaxies in our sample (16%) present signs of nuclear activity, from central HII regions: CIGs 0116, 0250, 1039 and Starburst Nucleus Galaxy (SBNG): CIG 0575 to LINER, Seyfert 2 or Seyfert 3: CIGs 0359, 0712, 1004. There is a very good correspondance between our observations and the HII activities listed in NED (which use the spectra of the AGN to confirm the types). Four galaxies (CIGs 0116, 0250, 0712, 1004) were listed in the group **G**, which is not really surprising because a bar is expected to enhance the gas flow towards the centre of galaxies and may provide a mechanism for triggering starbursts and fueling an AGN (e.g., Contini et al. 1998; Combes 2004).

Conclusion

One key problem in astrophysics is to understand the role played by the environment in the formation and evolution of galaxies. To address this issue, we characterised a sample of reference in which the influence from the environment is minimal and hence which evolution is totally determined by its intrinsic properties.

This thesis takes place in the AMIGA project "**A**nalysis of the Interstellar **M**edium of **I**solated **Ga**laxies" which is doing a multi-wavelength study of a large sample of isolated galaxies in order to examine their star formation activity and interstellar medium.

We begun with 950 galaxies from the Catalogue of Isolated Galaxies (Karachentseva 1973) and reevaluate isolation using an automated star-galaxy classification procedure (to $m_B = 17.5$) on large digitised POSS-I fields surrounding each isolated galaxy. We defined, compared and discussed various criteria to quantify the degree of isolation for these galaxies: Karachentseva's revised criterion, local surface density computations, estimation of the external tidal force affecting each isolated galaxy. We also applied our pipeline to triplets, compact groups and clusters which serve as control samples. The advantages of our isolation revision are:

(1) computer processing: We do not only use eye-search companions, we run computer programs in order to *detect* and *classify* sources;

(2) magnitude: We revised the CIG catalogue up to a magnitude $B = 17.5$ while the previous catalogue was limited to $B = 15.7$;

(3) isolation degree: We systematically defined general *isolation degrees* consistent for the whole sample;

(4) redshift: We used the largest spectroscopic galaxy databases to confirm the type of the companions identified: they do are galaxies. We used 3 dimensional information, when available, to better quantify the environment. With this material, we could confirm the validity of the statistical study done for the whole sample of 950 galaxies.

Also, we gathered and observed Hα and r Gunn data for 200 spiral galaxies from the CIG sample. Then, we focused on the 45 largest and less inclined galaxies to study their Hα morphologies. We interpreted the various bar and Hα morphologies observed in terms of the secular evolution experienced by galaxies in isolation. The observed frequency of particular patterns bring constraints on the lifetime of bars, and their fading timescales. Through numerical simulations, trying to fit the Hα distributions yields constraints on the star formation law, which is likely to differ from a simple Schmidt law.

Part III

Appendices

Appendix A

Tables

Contents

A.1 Hα galaxies

CIG	CGCG	UGC	NGC	IC	Vel.	Type
0004	456-028	00019	7817		2310	Sc
0006	477-059	00078	0009		4528	Sb
0010	518-018	00121			4613	Sc
0011	382-035	00139			3963	Sbc
0027	479-039				4599	Sb
0029	500-046	00345			4177	Sc
0030	434-026	00374		0035	4586	Sc
0033	383-079	00461	0237		4175	Sb
0034	479-072	00483			4949	Sd
0039	458-009	00550		1596	2674	Sb
0050	411-057	01014			2132	Im
0053	459-072	01081	0575	1710	3128	Sbc
0054	437-003	01115		1715	4176	Im
0059	412-010	01167			4303	Sc
0061	482-004	01194	0656		3916	Sab
0063	412-024				1606	Sm
0064	482-012	01244			3128	Sbc
0066	360-008	01285			4655	Sbc
0068	412-039	01356	0718		1733	Sa
0075	438-006				3470	Im
0080	461-018	01466	0772		2458	Sb
0084	438-017	01529		0193	4649	Sc
0085	482-059	01547			2640	Im
0088	483-003	01595			4962	Sc
0090	483-004	01638			4874	Sbc
0091	483-006	01648			4872	Sab
0094	483-009	01706			4794	Sc
0095	483-011	01733			4418	Scd
0096	413-066	01736	0864		1559	Sc
0098	504-061	01815			4762	Sm
0102	523-042	01886			4865	Sbc
0103	462-011	01888	0918		1509	Sc
0107	504-099	01975			3176	Sb
0116	523-092	02178	1050		3901	Sab
0138	392-001	02936			3812	Sd
0144	487-027	02988			3816	Sbc
0145	418-017	03003	1542		3714	Sab
0146	418-018	03010			3869	Scd
0147	327-017	03013	1530		2461	Sb

Continued on next page

CIG	CGCG	UGC	NGC	IC	Vel.	Type
0149	419-003				4972	Sb
0151	419-010	03059			4810	Scd
0152	393-031	03070			2515	Sbc
0154	394-013	03171			4553	Sc
0155	347-009	03190		0391	1556	Scd
0156	395-011	03258			2821	Sab
0159	347-018	03326			4085	Scd
0160	329-010				4016	Sab
0165	329-022	03416			4001	Scd
0168	284-014	03463		2166	2693	Sbc
0171	329-032	03474			3633	Scd
0176	348-027	03581			4955	Sc
0177	285-012				3275	Sb
0181	309-027	03764			4130	Sc
0188	286-016	03826			1733	Scd
0194	363-031	03890			2034	Sd
0196	177-031	03899			3884	Sc
0199	177-041	03944			3895	Sbc
0201	310-012	03979			4061	Sbc
0202	331-013	03984			3882	Sbc
0207	118-012				4908	Sbc
0208	118-015	04054			2121	Sb
0212	118-019				2106	Sd
0217	236-018	04107			3504	Sc
0240	331-035	04326			4727	Sc
0242	119-052			2288	4603	Sb
0243	088-060				4487	Sb
0247	089-015	04385			1969	Sm
0250	237-001	04393			2125	Sc
0267	331-053	04500			4256	Scd
0268	120-008	04504			4717	Scd
0276	032-050	04524			1939	Sdm
0277	120-021				4564	Sdm
0279	032-052	04533	2644		1939	Sb
0281	179-022	04555	2649		4244	Sc
0283	061-005	04568			4093	Im
0290	237-023	04659			1756	Sbc
0291	005-039	04684			2521	Sc
0292	238-001	04708	2712		1818	Sb
0293	120-056	04722			1794	Sd
0296	151-004	04747		2428	4310	Sc
0299	180-033	04777			2052	Sd

Continued on next page

CIG	CGCG	UGC	NGC	IC	Vel.	Type
0306	006-006				4919	Sc
0314	238-020	04838	2776		2626	Sc
0317	062-005	04845			2117	Sc
0319	062-010	04880		0530	4969	Sab
0322	238-038				1858	Sc
0329	151-076	05010	2862		4096	Sb
0330	238-052				4276	Sbc
0335	289-008	05034	2870		3214	Sbc
0340	091-098	05059		2487	4339	Sb
0342	091-099				4371	Sb
0354	007-007				3897	Sm
0355	181-066	05118	2922		4369	Sbc
0356	210-018				3600	Sb
0359	035-026	05159	2960		4932	Sa
0363	350-030	05175	2977		3072	Sbc
0376	312-028	05277			3365	Sc
0382	350-036	05319	3061		2457	Sbc
0385	289-023	05327	3043		2995	Sdm
0391	093-032				4922	Sc
0397	064-048	05425	3107		2791	Sb
0416	065-029	05642			2358	Sbc
0433	364-017	05820			3625	Sb
0444	010-035	05956		0651	4469	Sb
0463	267-041	06162			2203	Scd
0466	125-031	06194			2643	Sc
0476	213-042	06383			3156	Sd
0484	351-063	06515	3752		1913	Sbc
0496	351-068	06675	3901		1686	Scd
0498	314-040	06714			2717	S0a
0502	012-088	06780			1729	Sbc
0505	012-109	06838			3865	Sb
0507	127-087	06847			4941	Scd
0509	012-115	06879			2904	Scd
0512	013-004	06903			1892	Sc
0527	014-023		4348		2005	Sb
0528	244-010	07478	4357		4122	Sbc
0540	014-081	07798			2568	Im
0545	270-013	07847	4617		4655	Sb
0551	316-004	07941			2300	Sbc
0561	188-032	08079	4846		4534	Sab
0562	365-007	08101			1877	Sbc
0564	335-031	08120			1665	Sd

Continued on next page

CIG	CGCG	UGC	NGC	IC	Vel.	Type
0566	071-102	08166			2942	Sc
0571	294-011	08184	4964		2520	Sc
0575	130-019	08279	5016		2612	Sb
0593	102-022	08598			4909	Sbc
0604	246-027	08863	5377		1793	Sa
0605	162-035	08865	5375		2386	Sab
0609	247-003	08947	5439		1883	Sab
0615	018-074	09079	5496		1541	Sd
0622	163-023	09158		4403	4273	Sab
0625	133-034	09182			4655	Sd
0626	019-008	09201	5584		1640	Sc
0630	247-028	09248	5622		3861	Sb
0631	247-030	09271	5633		2334	Sab
0633	163-076			4452	4298	Sbc
0634	296-009	09358	5678		1922	Sab
0638	019-072	09416	5690		1753	Sc
0645	273-025	09516		1057	4027	Sc
0651	296-017	09556			2292	Sb
0652	020-026	09564	5768		1962	Sc
0653	220-060	09566	5772		4900	Sb
0660	354-016	09730			2137	Scd
0661	318-015	09734			3341	Sdm
0666	318-022	09773		1110	3373	Sbc
0669	021-079	09818	5913		2004	Sab
0678	077-132				4142	S0a
0689	107-013				4292	Sbc
0697	022-032	09980			3567	S0a
0698	107-028				3690	Sb
0700	022-034	10005			3838	Scd
0702	195-001				4466	Sc
0712	107-054	10083	6012		1854	Sbc
0728	023-024				2110	Sm
0733	137-071				4512	Sb
0734	298-028	10333	6123		3986	S0a
0736	024-008	10350	6118		1571	Sbc
0744	224-068	10437			2596	Sc
0750	298-045	10449			4020	Sc
0754	109-037	10490			4594	Sc
0769	138-067	10528			4272	Sab
0791	054-007	10743			2568	Sb
0793	111-011				4212	Sbc
0799	082-019	10805			1554	Scd

Continued on next page

CIG	CGCG	UGC	NGC	IC	Vel.	Type
0805	140-017	10829		1256	4730	Sbc
0808	054-029	10862			1691	Sc
0810	170-035	10890			4549	Scd
0812	112-005	10893	6389		3119	Sbc
0828	141-010	10972			4652	Sbc
0832	112-052				3300	Sc
0835	112-062				3833	Sb
0840	171-032	11058			4757	Sbc
0847	200-008	11132			2837	Sbc
0851	340-045	11238	6654		1821	Sab
0853	200-022	11251			2334	Sm
0854	255-007	11287			4856	Sc
0862	255-017	11361	6711		4671	Sbc
0875	357-010	11536			4880	Sb
0879	373-020	11575			3980	Sd
0886	374-004	11618	6954		4067	S0a
0889	400-002	11633	6969		4660	S0a
0890	357-011	11635			4804	Sb
0897	449-003	11681	7025		4968	Sa
0906	375-027	11723			4899	Sb
0910	449-018	11731		5104	4956	Sbc
0913	368-004	11738			4334	Sc
0916	375-038				4139	Sd
0922	376-020	11785			4074	Scd
0924	376-023	11790			4540	Sc
0930	376-031	11810		1401	4721	Sbc
0931	376-034	11816			4750	Sbc
0935	376-053	11843	7156		3985	Sc
0936	377-008	11859			3014	Sc
0937	377-009	11863			4881	Im
0938	428-006	11866			1708	Sdm
0941	494-001				4765	Sb
0949	428-037	11921			1678	Sdm
0950	451-016	11924			3803	Sc
0959	377-045	11982			4810	Scd
0969	359-001	12069			2367	Scd
0972	452-026	12090			1887	Im
0976	429-015	12118	7328		2827	Sc
0979	358-003	12141			2088	Sc
0983	514-103	12173			4774	Sc
0985	405-008	12178			1931	Scd
0990	430-014	12205			3400	Sd

Continued on next page

CIG	CGCG	UGC	NGC	IC	Vel.	Type
0991	369-002	12221			2057	Scd
0992	405-012	12224			3506	Sc
1001	379-016	12262	7428		3078	Sab
1003	405-023	12304			3470	Scd
1004	430-058	12343	7479		2376	Sbc
1005	430-063	12370			4891	Sc
1009	515-027	12415	7514		4843	Sbc
1019	476-038	12598	7664		3474	Sb
1028	476-073	12694	7712		3053	Sbc
1030	432-011	12705			3966	Scd
1035	455-045				4151	Sc
1036	432-028	12773		1508	4263	Scd
1038	498-008	12776			4936	Sbc
1039	498-011	12781		5355	4859	Sc
1047	382-007	12857			2459	Sbc
1048	498-045	12864			4682	Sbc
1050	477-034	12873			3251	Sc

Table A.1: Galaxies observed.

A.2 Hα galaxies still to be observed

CIG	J 2000	Filter	Type
0006	0 08 54.70 23 49 2.8	Ha6652	3
0144	4 13 38.89 25 28 58.7	Ha6652	4
0147	4 23 26.78 75 17 45.5	Ha6607	3
0165	6 13 40.03 69 43 45.5	Ha6601	6
0247	8 23 52.06 14 45 11.7	Ha6607	9
0277	8 41 9.87 20 53 47.6	Ha6652	8
0283	8 44 43.50 10 28 20.3	Ha6652	10
0293	9 00 23.53 25 36 40.5	Ha6607	998
0314	9 12 14.37 44 57 17.8	Ha6607	5
0354	9 36 26.27 -0 34 14.8	Ha6652	9
0391	10 02 51.86 20 12 6.0	Ha6652	5
0466	11 09 0.70 22 55 45.4	Ha6607	5
0505	11 51 56.10 -2 38 31.8	Ha6652	3
0634	14 32 5.80 57 55 17.1	Ha6607	998
0638	14 37 41.23 2 17 26.0	Ha6607	5
0832	17 49 30.17 18 33 55.3	Ha6652	5
0938	21 58 33.95 14 07 21.8	Ha6607	8
0972	22 34 47.25 15 56 56.5	Ha6607	10
1009	23 12 25.70 34 52 53.6	Ha6652	4
1028	23 35 51.58 23 37 7.6	Ha6607	4
1035	23 45 8.61 19 54 3.7	Ha6652	5
1038	23 46 12.27 33 22 11.7	Ha6652	998
1048	23 57 23.99 30 59 31.5	Ha6652	4
1050	23 58 32.13 26 12 53.3	Ha6607	5

Table A.2: Galaxies still to be observed.

A.3 Hα galaxies with V $<$ 1500 km s^{-1}

CIG	UGC or NGC name	Velocity
0105	UGC 01913	553
0112	UGC 02082	696
0121	UGC 02455	375
0180	UGC 03734	974
0235	UGC 04274	431
0239	UGC 04305	142
0265	UGC 04499	691
0428	UGC 05789	739
0434	UGC 05829	629
0656	UGC 09649	447
0699	UGC 09992	427
0748	UGC 10445	963
0813	UGC 10897	1313
0850	UGC 11218	1484
0855	UGC 11300	467
0947	UGC 11914	952
0105	NGC 0925	553
0197	NGC 2403	131
0347	NGC 2903	556
0442	NGC 3359	1014
0523	NGC 4236	
0610	NGC 5457	241
0691	NGC 5964	1447
0109	UGC 01983	611
0121	UGC 02455	381
0139	UGC 02947	856
0175	UGC 03580	1201
0180	UGC 03734	974
0224	UGC 04165	516
0235	UGC 04274	447
0265	UGC 04499	692
0300	UGC 04781	1442
0388	UGC 05373	301
0434	UGC 05829	629
0549	UGC 07901	805
0624	UGC 09179	305
0656	UGC 09649	447
0682	UGC 09866	435
0691	UGC 09935	1450

Continued on next page

CIG	UGC or NGC name	Velocity
0710	UGC 10075	833
0813	UGC 10897	1324
0850	UGC 11218	1489
0855	UGC 11300	488
0967	UGC 12048	987
0971	UGC 12082	804

Table A.3: Hα data for galaxies with V $<$ 1500 km s^{-1}.

Appendix B

IRAF reduction scripts

Contents

For the reduction, I made use of the IRAF software; you can find full details on the tasks at this web site.

I give here the details of the scripts to reduce a whole campaign quite automatically, and some tips that might be usefull.

B.1 Instrumental signature

B.1.1 Bias

cl> imstat @bias.lis

```
  image        npix      mean     stddev  min    max
bias-001.fit  4194304  125.4099  2.37175  115.  1097.
bias-002.fit  4194304  125.3325  3.308658  113.  3217.
bias-003.fit  4194304  125.2781  2.442328  113.  1090.
bias-004.fit  4194304  125.2989  3.579978  113.  3555.
bias-005.fit  4194304  125.2889  2.617491  114.  1598.
bias-006.fit  4194304  125.2848  2.75157  114.  1873.
bias-007.fit  4194304  125.2873  3.795262  114.  5479.
bias-008.fit  4194304  125.2489  2.949802  99.  2233.
bias-009.fit  4194304  125.3072  2.654542  113.  1762.
bias-010.fit  4194304  125.3155  3.343796  114.  2833.
bias-011.fit  4194304  125.2152  2.528024  114.  1714.
bias-012.fit  4194304  125.1778  2.449004  113.  847.
bias-013.fit  4194304  125.1352  3.364629  113.  5132.
bias-014.fit  4194304  125.1199  2.350584  113.  682.
bias-015.fit  4194304  125.0268  2.437266  114.  921.
bias-016.fit  4194304  125.3931  2.346065  114.  923.
bias-017.fit  4194304  125.3506  2.639712  113.  1600.
bias-018.fit  4194304  125.2769  2.45604  114.  1611.
bias-019.fit  4194304  125.2405  2.488502  115.  1274.
bias-020.fit  4194304  125.2782  3.996488  113.  5918.
bias-021.fit  4194304  125.5954  5.288763  113.  6848.
bias-022.fit  4194304  125.4974  2.747338  114.  2152.
bias-023.fit  4194304  125.4121  2.464162  114.  1122.
bias-024.fit  4194304  125.4368  3.469104  115.  2471.
bias-025.fit  4194304  125.3059  3.521842  113.  4850.
```

cl> imcombine @bias.lis superBias.fit combine=median reject=avsigclip

```
Sep 15 10:38: IMCOMBINE
  combine = median, scale = none, zero = none, weight = none
  reject = avsigclip, mclip = yes, nkeep = 1
  lsigma = 3., hsigma = 3.
  blank = 0.
                Images
          bias-001.fit
          bias-002.fit
```

```
            bias-003.fit
            bias-004.fit
            bias-005.fit
            bias-006.fit
            bias-007.fit
            bias-008.fit
            bias-009.fit
            bias-010.fit
            bias-011.fit
            bias-012.fit
            bias-013.fit
            bias-014.fit
            bias-015.fit
            bias-016.fit
            bias-017.fit
            bias-018.fit
            bias-019.fit
            bias-020.fit
            bias-021.fit
            bias-022.fit
            bias-023.fit
            bias-024.fit
            bias-025.fit

  Output image = superBias.fit, ncombine = 25
```

B.1.2 Flat fields

BIAS SUBSTRACTION

cl> cl < flat-b.cl

```
imarith flat-001H6607.fit - superBias.fit TMP/flat-001H6607-b.fit
imarith flat-002H6607.fit - superBias.fit TMP/flat-002H6607-b.fit
imarith flat-003H6607.fit - superBias.fit TMP/flat-003H6607-b.fit
imarith flat-004H6607.fit - superBias.fit TMP/flat-004H6607-b.fit
imarith flat-005H6607.fit - superBias.fit TMP/flat-005H6607-b.fit
imarith flat-006H6607.fit - superBias.fit TMP/flat-006H6607-b.fit
imarith flat-007H6607.fit - superBias.fit TMP/flat-007H6607-b.fit

imarith flat-001rGunn.fit - superBias.fit TMP/flat-001rGunn-b.fit
imarith flat-002rGunn.fit - superBias.fit TMP/flat-002rGunn-b.fit
imarith flat-003rGunn.fit - superBias.fit TMP/flat-003rGunn-b.fit
imarith flat-004rGunn.fit - superBias.fit TMP/flat-004rGunn-b.fit
imarith flat-005rGunn.fit - superBias.fit TMP/flat-005rGunn-b.fit
imarith flat-006rGunn.fit - superBias.fit TMP/flat-006rGunn-b.fit
imarith flat-007rGunn.fit - superBias.fit TMP/flat-007rGunn-b.fit
```

FLAT COMPARISONS

cl> cl < flat-comp.cl

```
imarith TMP/flat-001H6607-b.fit / TMP/flat-002H6607-b.fit TMP/compH1.fit
imarith TMP/flat-002H6607-b.fit / TMP/flat-003H6607-b.fit TMP/compH2.fit
imarith TMP/flat-003H6607-b.fit / TMP/flat-004H6607-b.fit TMP/compH3.fit
imarith TMP/flat-004H6607-b.fit / TMP/flat-005H6607-b.fit TMP/compH4.fit
imarith TMP/flat-005H6607-b.fit / TMP/flat-006H6607-b.fit TMP/compH5.fit
imarith TMP/flat-006H6607-b.fit / TMP/flat-007H6607-b.fit TMP/compH6.fit
imarith TMP/flat-007H6607-b.fit / TMP/flat-001H6607-b.fit TMP/compH7.fit

imarith TMP/flat-001rGunn-b.fit / TMP/flat-002rGunn-b.fit TMP/compR1.fit
imarith TMP/flat-002rGunn-b.fit / TMP/flat-003rGunn-b.fit TMP/compR2.fit
imarith TMP/flat-003rGunn-b.fit / TMP/flat-004rGunn-b.fit TMP/compR3.fit
imarith TMP/flat-004rGunn-b.fit / TMP/flat-005rGunn-b.fit TMP/compR4.fit
imarith TMP/flat-005rGunn-b.fit / TMP/flat-006rGunn-b.fit TMP/compR5.fit
imarith TMP/flat-006rGunn-b.fit / TMP/flat-007rGunn-b.fit TMP/compR6.fit
imarith TMP/flat-007rGunn-b.fit / TMP/flat-001rGunn-b.fit TMP/compR7.fit
```

SUPERFLATS

cl> imcombine @superFlatH.lis superFlatH.fit combine=median reject=avsigclip scale=mean statsec=[300:1750,300:1750]

```
Sep 15 11:12: IMCOMBINE
  combine = median, scale = mean, zero = none, weight = none
  reject = avsigclip, mclip = yes, nkeep = 1
  lsigma = 3., hsigma = 3.
  blank = 0.
  statsec = Sep 15 11:12
                Images     Mean  Scale
  TMP/flat-001H6607-b.fit  5249.5  1.000
  TMP/flat-002H6607-b.fit  4950.9  1.060
  TMP/flat-003H6607-b.fit  3926.3  1.337
  TMP/flat-004H6607-b.fit  2436.9  2.154
  TMP/flat-005H6607-b.fit  1361.3  3.856
  TMP/flat-006H6607-b.fit  1405.6  3.735
  TMP/flat-007H6607-b.fit  1974.7  2.658

  Output image = superFlatH.fit, ncombine = 7
```

cl> imcombine @superFlatR.lis superFlatR.fit combine=median reject=avsigclip scale=mean statsec=[300:1750,300:1750]

```
Sep 15 11:13: IMCOMBINE
  combine = median, scale = mean, zero = none, weight = none
  reject = avsigclip, mclip = yes, nkeep = 1
  lsigma = 3., hsigma = 3.
  blank = 0.
  statsec = Sep 15 11:13
```

```
                Images     Mean  Scale
  TMP/flat-001rGunn-b.fit  6976.4  1.000
  TMP/flat-002rGunn-b.fit   4623.  1.509
  TMP/flat-003rGunn-b.fit  3841.5  1.816
  TMP/flat-004rGunn-b.fit  4328.8  1.612
  TMP/flat-005rGunn-b.fit  3738.7  1.866
  TMP/flat-006rGunn-b.fit  5701.4  1.224
  TMP/flat-007rGunn-b.fit  4711.2  1.481

  Output image = superFlatR.fit, ncombine = 7
```

NORMALISITION OF THE SUPERFLATS

cl> cl < superFlatN.cl

```
list = " "
s3 = "temp.file"
imstat.format=no
imstat.fields = "mean"
imstat superFlatH.fit[300:1750,300:1750] > (s3)
list = (s3)
i = fscan(list,x)
imarith ("superFlatH.fit","/",x,"superFlatH-n.fit")
delete ("temp.file",verify=no)
imexa superFlatH-n.fit

list = " "
s3 = "temp.file"
imstat.format=no
imstat.fields = "mean"
imstat superFlatR.fit[300:1750,300:1750] > (s3)
list = (s3)
i = fscan(list,x)
imarith ("superFlatR.fit","/",x,"superFlatR-n.fit")
delete ("temp.file",verify=no)
imexa superFlatR-n.fit
```

B.2 Galaxies

B.2.1 Cosmic rays

REMOVING THE COSMICRAYS (Ha images only!)

cl> cl < cig0744-cr.cl

```
cosmicrays("c0744_001H6607.fit","TMP/c0744_001H6607-cr.fit",
           threshold=23,fluxratio=50,npasses=15,window=7)
cosmicrays("c0744_002H6607.fit","TMP/c0744_002H6607-cr.fit",
           threshold=23,fluxratio=50,npasses=15,window=7)
```

```
cosmicrays("c0744_003H6607.fit","TMP/c0744_003H6607-cr.fit",
            threshold=23,fluxratio=50,npasses=15,window=7)
```

B.2.2 Bias

subtraction
cl> cl < cig0744-b.cl

```
imarith TMP/c0744_001H6607-cr.fit - superBias.fit TMP/c0744_001H6607-b.fit
imarith TMP/c0744_002H6607-cr.fit - superBias.fit TMP/c0744_002H6607-b.fit
imarith TMP/c0744_003H6607-cr.fit - superBias.fit TMP/c0744_003H6607-b.fit

imarith c0744_001rGunn.fit - superBias.fit TMP/c0744_001rGunn-b.fit
imarith c0744_002rGunn.fit - superBias.fit TMP/c0744_002rGunn-b.fit
imarith c0744_003rGunn.fit - superBias.fit TMP/c0744_003rGunn-b.fit
```

B.2.3 Flat fields

division
cl> cl < cig0744-bf.cl

```
imarith TMP/c0744_001H6607-b.fit / superFlatH-n.fit TMP/c0744_001H6607-bf.fit
imarith TMP/c0744_002H6607-b.fit / superFlatH-n.fit TMP/c0744_002H6607-bf.fit
imarith TMP/c0744_003H6607-b.fit / superFlatH-n.fit TMP/c0744_003H6607-bf.fit

imarith TMP/c0744_001rGunn-b.fit / superFlatR-n.fit TMP/c0744_001rGunn-bf.fit
imarith TMP/c0744_002rGunn-b.fit / superFlatR-n.fit TMP/c0744_002rGunn-bf.fit
imarith TMP/c0744_003rGunn-b.fit / superFlatR-n.fit TMP/c0744_003rGunn-bf.fit
```

B.2.4 Sky background

SKY BACKGROUND SUBSTRACTION
(epar imstat: format = no)

cl> cl < cig0744-bfs.cl

```
list = " "
s3 = "temp.file"
imstat TMP/c0744_001H6607-bf.fit[300:1750,300:1750] fields="mode" > (s3)
list = (s3)
i = fscan(list,x)
imarith ("TMP/c0744_001H6607-bf.fit","-",x,"TMP/c0744_001H6607-bfs.fit")
delete ("temp.file",verify=no)

list = " "
s3 = "temp.file"
imstat TMP/c0744_002H6607-bf.fit[300:1750,300:1750] fields="mode" > (s3)
```

```
list = (s3)
i = fscan(list,x)
imarith ("TMP/c0744_002H6607-bf.fit","-",x,"TMP/c0744_002H6607-bfs.fit")
delete ("temp.file",verify=no)

list = " "
s3 = "temp.file"
imstat TMP/c0744_003H6607-bf.fit[300:1750,300:1750] fields="mode" > (s3)
list = (s3)
i = fscan(list,x)
imarith ("TMP/c0744_003H6607-bf.fit","-",x,"TMP/c0744_003H6607-bfs.fit")
delete ("temp.file",verify=no)

list = " "
s3 = "temp.file"
imstat TMP/c0744_001rGunn-bf.fit[300:1750,300:1750] fields="mode" > (s3)
list = (s3)
i = fscan(list,x)
imarith ("TMP/c0744_001rGunn-bf.fit","-",x,"TMP/c0744_001rGunn-bfs.fit")
delete ("temp.file",verify=no)

list = " "
s3 = "temp.file"
imstat TMP/c0744_002rGunn-bf.fit[300:1750,300:1750] fields="mode" > (s3)
list = (s3)
i = fscan(list,x)
imarith ("TMP/c0744_002rGunn-bf.fit","-",x,"TMP/c0744_002rGunn-bfs.fit")
delete ("temp.file",verify=no)

list = " "
s3 = "temp.file"
imstat TMP/c0744_003rGunn-bf.fit[300:1750,300:1750] fields="mode" > (s3)
list = (s3)
i = fscan(list,x)
imarith ("TMP/c0744_003rGunn-bf.fit","-",x,"TMP/c0744_003rGunn-bfs.fit")
delete ("temp.file",verify=no)
```

B.2.5 Exposure Time

EXPTIME DIVISION
cl> cl < cig0744-bfst.cl

```
list = " "
s3 = "temp.file"
hselect TMP/c0744_001H6607-bfs.fit exptime yes > (s3)
list = (s3)
i = fscan(list,x)
imarith ("TMP/c0744_001H6607-bfs.fit","/",x,"TMP/c0744_001H6607-bfst.fit")
delete ("temp.file",verify=no)
```

```
list = " "
s3 = "temp.file"
hselect TMP/c0744_002H6607-bfs.fit exptime yes > (s3)
list = (s3)
i = fscan(list,x)
imarith ("TMP/c0744_002H6607-bfs.fit","/",x,"TMP/c0744_002H6607-bfst.fit")
delete ("temp.file",verify=no)

list = " "
s3 = "temp.file"
hselect TMP/c0744_003H6607-bfs.fit exptime yes > (s3)
list = (s3)
i = fscan(list,x)
imarith ("TMP/c0744_003H6607-bfs.fit","/",x,"TMP/c0744_003H6607-bfst.fit")
delete ("temp.file",verify=no)

list = " "
s3 = "temp.file"
hselect TMP/c0744_001rGunn-bfs.fit exptime yes > (s3)
list = (s3)
i = fscan(list,x)
imarith ("TMP/c0744_001rGunn-bfs.fit","/",x,"TMP/c0744_001rGunn-bfst.fit")
delete ("temp.file",verify=no)

list = " "
s3 = "temp.file"
hselect TMP/c0744_002rGunn-bfs.fit exptime yes > (s3)
list = (s3)
i = fscan(list,x)
imarith ("TMP/c0744_002rGunn-bfs.fit","/",x,"TMP/c0744_002rGunn-bfst.fit")
delete ("temp.file",verify=no)

list = " "
s3 = "temp.file"
hselect TMP/c0744_003rGunn-bfs.fit exptime yes > (s3)
list = (s3)
i = fscan(list,x)
imarith ("TMP/c0744_003rGunn-bfs.fit","/",x,"TMP/c0744_003rGunn-bfst.fit")
delete ("temp.file",verify=no)
```

B.2.6 Centring

CENTRE THE IMAGES
(the first Ha image is taken as a reference; epar geomap: interactive = no)

it is important to write the coordinates to the tenth of arcsec. accuracy for a good centring

a typical file of coordinates "ali0744-2H.coo", the first two columns are the x and y coordinates of the reference stars always

```
 254.3  314.2  178.0  399.9
 557.4  770.9  481.0  857.0
1493.6  889.7 1417.4  975.5
1592.8 1577.7 1516.4 1663.5
1761.2  234.1 1684.6  320.1
```

cl> cl < cig0744-bfstc.cl

```
imcopy TMP/c0744_001H6607-bfst.fit TMP/c0744_001H6607-bfstc.fit

geomap ali0744-2H.coo ali0744-2H.data 1 2048 1 2048 > ali0744-2H.log
geomap ali0744-3H.coo ali0744-3H.data 1 2048 1 2048 > ali0744-3H.log

geomap ali0744-1R.coo ali0744-1R.data 1 2048 1 2048 > ali0744-1R.log
geomap ali0744-2R.coo ali0744-2R.data 1 2048 1 2048 > ali0744-2R.log
geomap ali0744-3R.coo ali0744-3R.data 1 2048 1 2048 > ali0744-3R.log


geotran TMP/c0744_002H6607-bfst.fit TMP/c0744_002H6607-bfstc.fit ali0744-2H.data ali0744-2H.coo
geotran TMP/c0744_003H6607-bfst.fit TMP/c0744_003H6607-bfstc.fit ali0744-3H.data ali0744-3H.coo

geotran TMP/c0744_001rGunn-bfst.fit TMP/c0744_001rGunn-bfstc.fit ali0744-1R.data ali0744-1R.coo
geotran TMP/c0744_002rGunn-bfst.fit TMP/c0744_002rGunn-bfstc.fit ali0744-2R.data ali0744-2R.coo
geotran TMP/c0744_003rGunn-bfst.fit TMP/c0744_003rGunn-bfstc.fit ali0744-3R.data ali0744-3R.coo
```

B.2.7 Point Spread Function

TMP/c0744_001H6607-bfstc.fit 11.05
TMP/c0744_002H6607-bfstc.fit 12.75 <- reference image
TMP/c0744_003H6607-bfstc.fit 11.60
TMP/c0744_001rGunn-bfstc.fit 9.80
TMP/c0744_002rGunn-bfstc.fit 11.35
TMP/c0744_003rGunn-bfstc.fit 11.35

cl> display TMP/c0744_002H6607-bfstc.fit 1 fi+
cl> rimcursor > starsPsf0744.lis
cl> cl < cig0744-bfstcp.cl

```
psfmatch.psfdata="starsPsf0744.lis"
psfmatch.reference="TMP/c0744_002H6607-bfstc.fit"

imcopy TMP/c0744_002H6607-bfstc.fit Im/c0744_002H6607-bfstcp.fit

psfmatch TMP/c0744_001H6607-bfstc.fit output="Im/c0744_001H6607-bfstcp.fit"
```

```
psfmatch TMP/c0744_003H6607-bfstc.fit output="Im/c0744_003H6607-bfstcp.fit"
psfmatch TMP/c0744_001rGunn-bfstc.fit output="Im/c0744_001rGunn-bfstcp.fit"
psfmatch TMP/c0744_002rGunn-bfstc.fit output="Im/c0744_002rGunn-bfstcp.fit"
psfmatch TMP/c0744_003rGunn-bfstc.fit output="Im/c0744_003rGunn-bfstcp.fit"
```

B.2.8 Combining

COMBINING
cl> imcombine @c0744rG.lis Im/cig0744rG.fit combine=median reject=avsigclip

```
Sep 16 11:15: IMCOMBINE
  combine = median, scale = none, zero = none, weight = none
  reject = avsigclip, mclip = yes, nkeep = 1
  lsigma = 3., hsigma = 3.
  blank = 0.
                Images
  Im/c0744_001rGunn-bfstcp.fit
  Im/c0744_002rGunn-bfstcp.fit
  Im/c0744_003rGunn-bfstcp.fit

  Output image = Im/cig0744rG.fit, ncombine = 3
```

cl> imcombine @c0744Ha.lis Im/cig0744Ha.fit combine=median reject=avsigclip

```
Sep 16 11:16: IMCOMBINE
  combine = median, scale = none, zero = none, weight = none
  reject = avsigclip, mclip = yes, nkeep = 1
  lsigma = 3., hsigma = 3.
  blank = 0.
                Images
  Im/c0744_001H6607-bfstcp.fit
  Im/c0744_002H6607-bfstcp.fit
  Im/c0744_003H6607-bfstcp.fit

  Output image = Im/cig0744Ha.fit, ncombine = 3
```

B.2.9 Continuum subtraction

ap> display Im/cig0744Ha.fit 1
ap> qphot Im/cig0744Ha.fit

```
# The centering box width in pixels (10.):
# The inner radius of sky annulus in pixels (0.:) (60.): 60
# The width of the sky annulus in pixels (1.:) (30.): 30
# The list of photometry apertures (15): 15
```

ap> display Im/cig0744rG.fit 1
ap> qphot Im/cig0744rG.fit
ap> txdump cig0744Ha.fit.mag.1 flux > c0744Ha.flu
ap> txdump cig0744rG.fit.mag.1 flux > c0744rG.flu
paste c0744rG.flu c0744Ha.flu > c0744flux.gnu
gnuplot> f(x) = a*x + b
gnuplot> fit f(x) "c0744flux.gnu" via a, b
gnuplot> plot "c0744flux.gnu", f(x)

```
# a               = 0.04724          +/- 0.0004183    (0.8855%)
# b               = -0.1075          +/- 0.5568       (517.9%)
```

ap> imarith Im/cig0744rG.fit * 0.047 Im/cig0744rG-scaled.fit
ap> imarith Im/cig0744Ha.fit - Im/cig0744rG-scaled.fit Im/cig0744Ha-rG.fit

B.2.10 Final images

Stamps of 512 × 512 pixels
centre: 1081.34 876.00
cl> imcopy Im/cig0744rG.fit[826:1337,621:1132] Im/cig0744rG512.fit
cl> imcopy Im/cig0744Ha-rG.fit[826:1337,621:1132] Im/cig0744Ha-rG512.fit

Cleaning
cl> imedit Im/cig0744rG512.fit Im/cig0744rG512cl.fit
cl> imcopy Im/cig0744Ha-rG512.fit Im/cig0744Ha-rG512cl.fit # already clean

Final Images
flip around the X-axis
cl> imcopy Im/cig0744rG512cl.fit[*,-*] Im/c0744R.fit
cl> imcopy Im/cig0744Ha-rG512cl.fit[*,-*] Im/c0744H.fit

Appendix C

Numerical simulations

Contents

The simulations were conducted by FRANCOISE COMBES.

In order to understand the observed Hα distributions, and the different phases identified, we performed N-body simulations with stars and gas, including star formation. Since we want to explore many physical parameters, we chose to carry out 2D simulations, which should capture the essential of the bar evolution, and location of star formation in these isolated galaxies. The 3D components, bulge and dark matter halo, are therefore considered as rigid and spherical potentials, in which the disk component evolves. Self-gravity is only included for the disk (gas + stars). 2D N-body simulations were carried out using the FFT algorithm to solve the Poisson equation, with a cartesian grid, varying from 256x256 to 512x512 (useful grid, free of periodic images). Two spatial resolutions were selected, to appreciate its influence on the star formation physics. The cell size is then from 62.5 to 125pc, and the total size of the grid is 32kpc. The softening length of the gravity has the characteristic scale of the cell (62 to 125pc). More details on the numerical techniques can be found in Combes et al. (1990).

The stellar component is represented by 100k or 400k particles, and the gas component by 40k and 160k for the low and high resolutions adopted respectively.

The bulge is modelled as rigid spherical potential with Plummer shape:

$$\Phi_b(r) = -\frac{GM_b}{\sqrt{r^2 + r_b^2}}$$

for M_b and r_b the mass and characteristic radius of the bulge.

The stellar disk is initially a Kuzmin-Toomre disk of surface density

$$\Sigma(r) = \Sigma_0 (1 + r^2/r_d^2)^{-3/2}$$

truncated at 15kpc, with a mass M_d. It is initially quite cold, with a Toomre Q parameter of 1. The halo is also a Plummer sphere, with mass M_h and characteristic radius r_h. The time step is 0.5 and 1 Myr. The initial conditions of the runs described here are given in Table C.1.

Table C.1: Initial conditions parameters.

Run	r_b kpc	M_b $M_\odot$	r_d kpc	M_d $M_\odot$	r_h kpc	M_h $M_\odot$	F_{gas} %	f_{el}
Run 0	1.1	2.5e10	4.4	8.0e10	16.	7.2e10	14	0.65
Run 1	1.1	6.8e10	4.4	8.0e10	16.	11.8e10	14	0.65
Run 2	1.1	6.8e10	4.4	8.0e10	16.	11.8e10	14	0.85

The gas is treated as a self-gravitating component in the N-body simulation, and its dissipation is treated by a sticky particle code, as in Combes & Gerin (1985). The initial gas-to-total mass ratio (F_{gas}) in the disk ranges between 6 and 14%, since the star formation in the simulation is capable of reducing $F_{\rm gas}$ to a final lower value. The mass of one gas particle therefore varied between 8 10^4 and 3 10^5 $M_\odot$.

The initial distribution of gas in the model is an exponential disk, truncated at 15 kpc, and with a characteristic radial scale of 6 kpc. Initially, its velocity dispersion corresponds to a Toomre Q-parameter of 1. The gas clouds are subject to inelastic collisions, with a collision cell size between 60 and 120pc (region where particles are selected to possibly collide). This corresponds to a lower limit for the average mean free path of clouds between two collisions. The collisions are considered every 5 to 10 Myr. In a collision, the sign of the relative cloud velocities is reversed and the absolute values are reduced: relative velocities after the collision are only f_{el} times their original value, the elasticity factor f_{el} being between 0.65 and 0.85, as indicated in Table C.1. The dissipation rate is controlled by this factor. All gas particles have the same mass.

Star formation is taken into account following a generalised Schmidt law: the star formation rate is proportional to the volume density to the power n=1.2, provided that the density is larger than 1 H-atom cm^{-3}, i.e. the rate of gas mass transformed into stars is $dm = dtC_*\rho^{1.2}$. To compute this rate, at regular intervals of dt= 5-10 Myr, the gas density is averaged in each cell, and the probability of the gas particles being transformed into stars is computed by

$$P = dm/M_{cell}$$

for all particles in this cell, of mass M_{cell}. Each new star formed has exactly the same mass as each gas particle, about 3 times smaller than any old stellar particle. This simple scheme corresponds to an instantaneous recycling of matter, since the continuous mass-loss from recently formed stars is not followed. The rate of star formation is normalised so that in unperturbed runs (without galaxy interaction, galaxies are quiescently and regularly forming stars), the timescale for consumption of half of the gas mass is of the order of 2 Gyr (SFR $\sim$ 1-2 $M_\odot$/yr). At each star formation event, the neighbouring gas particles are given a small extra velocity dispersion of order $\sim$ 10 km/s.

C.1 Gaseous component

The second run used a less dissipative gaseous component.

C.1.1 First run

Stars Gas 0.3Gyr

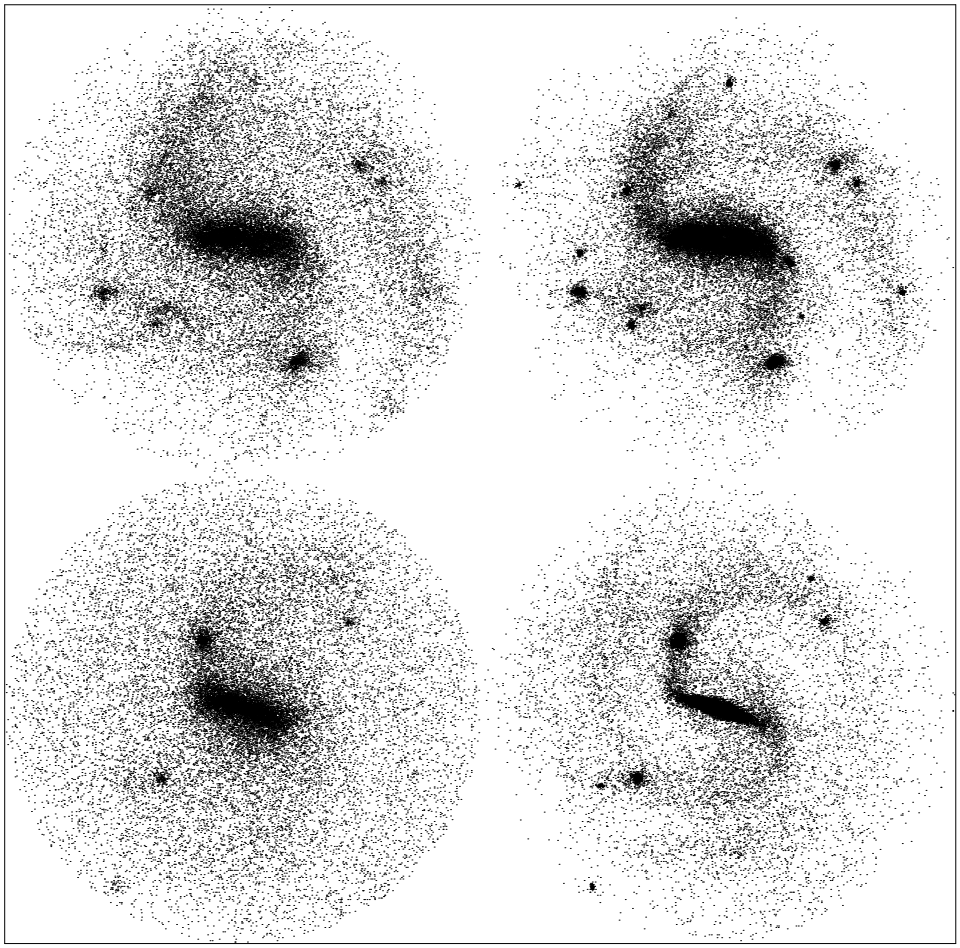

Stars Gas 0.7Gyr

Stars Gas 0.3Gyr

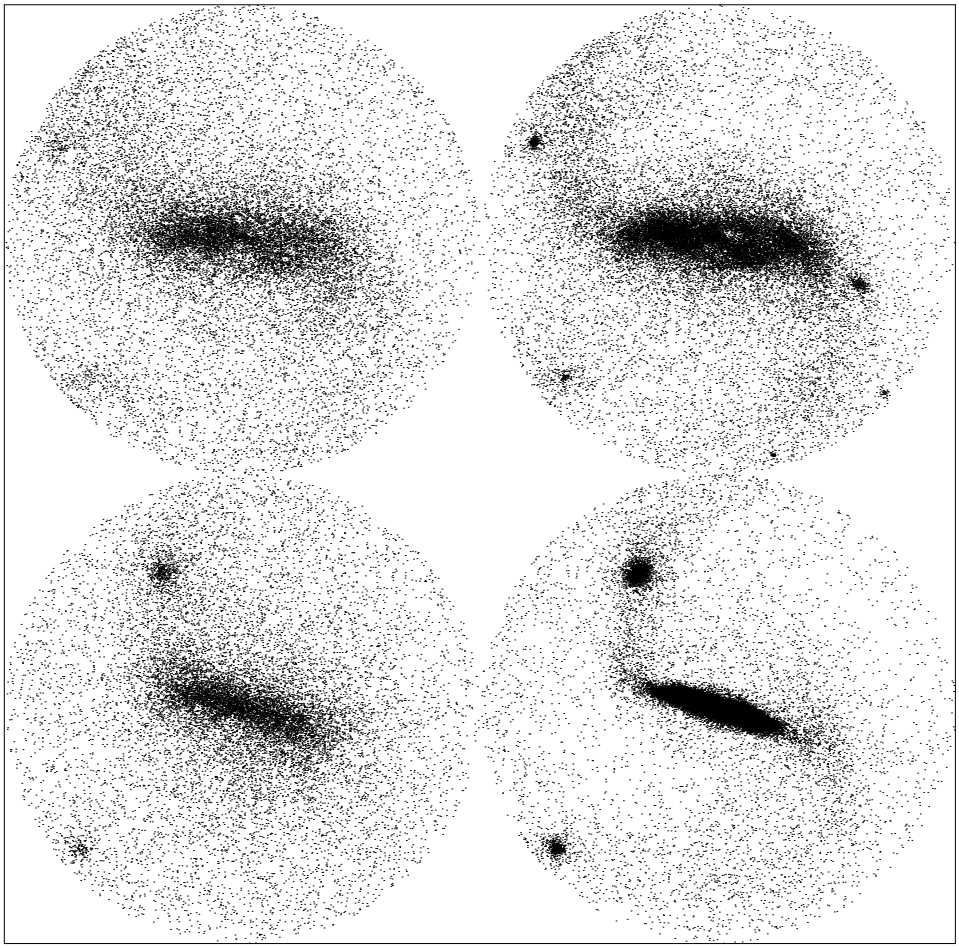

Stars Gas 0.7Gyr

Stars Gas 1.1Gyr

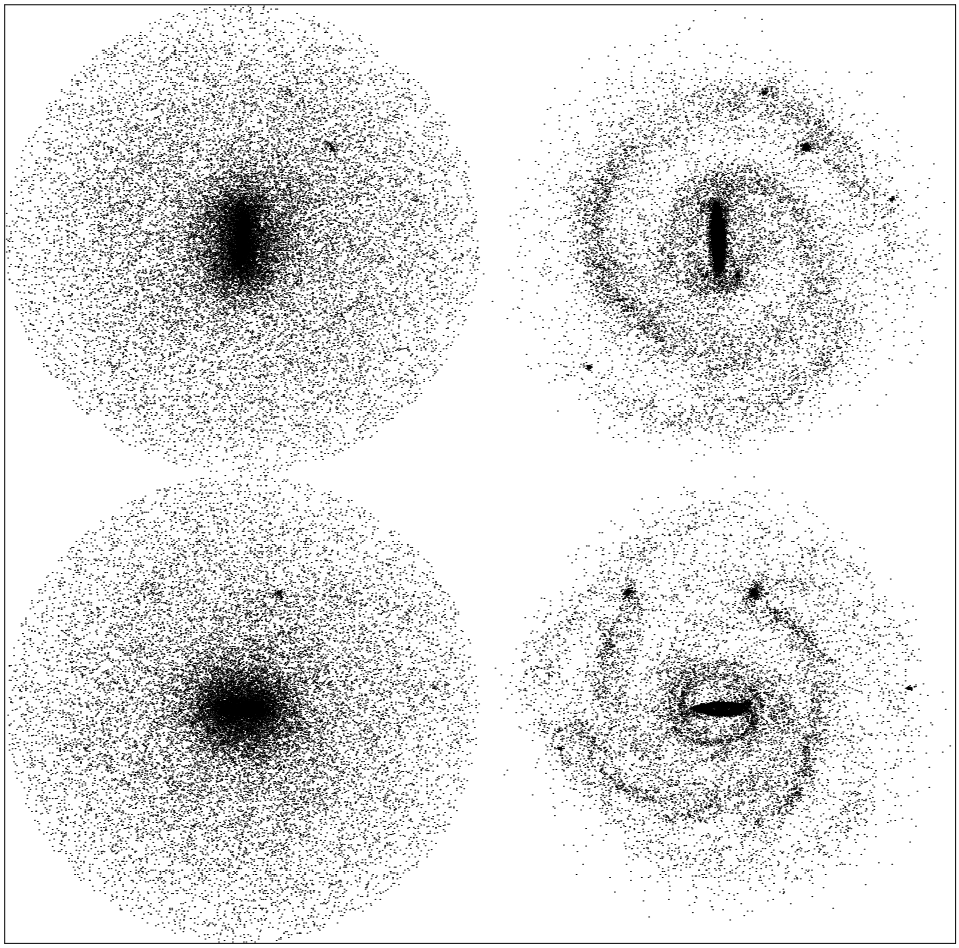

Stars Gas 1.5Gyr

Stars Gas 1.1Gyr

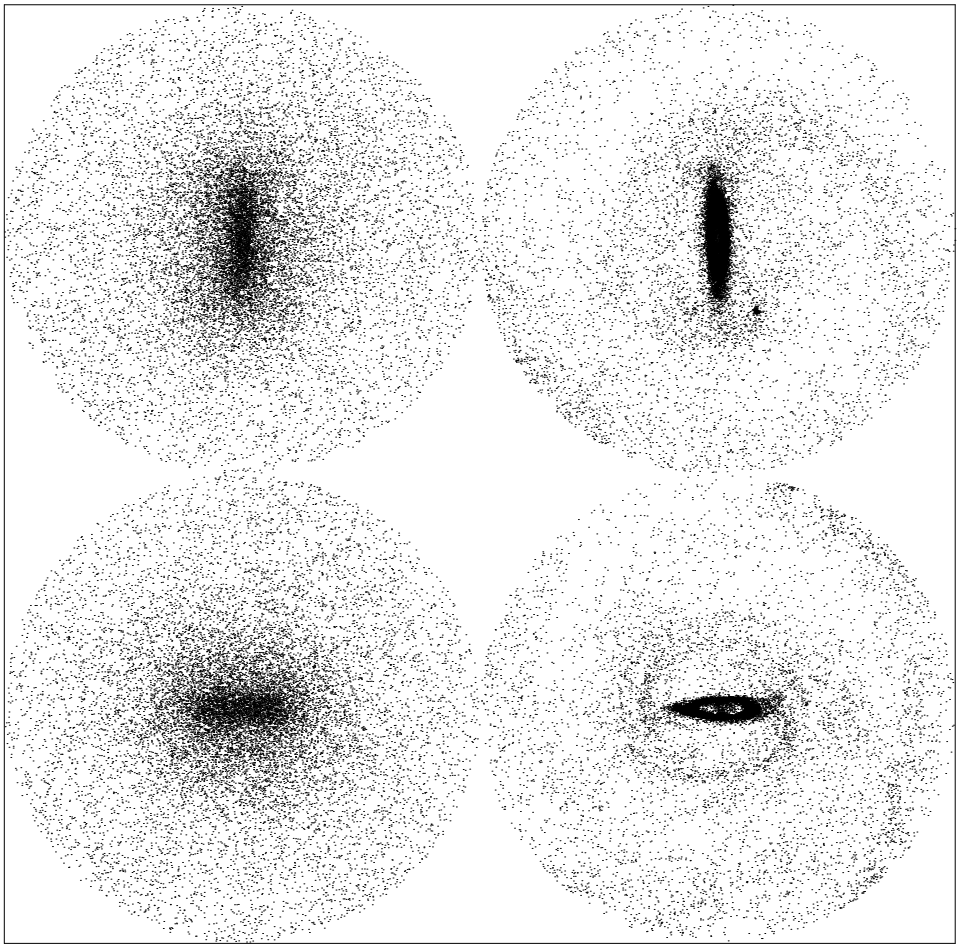

Stars Gas 1.5Gyr

Stars Gas 1.9Gyr

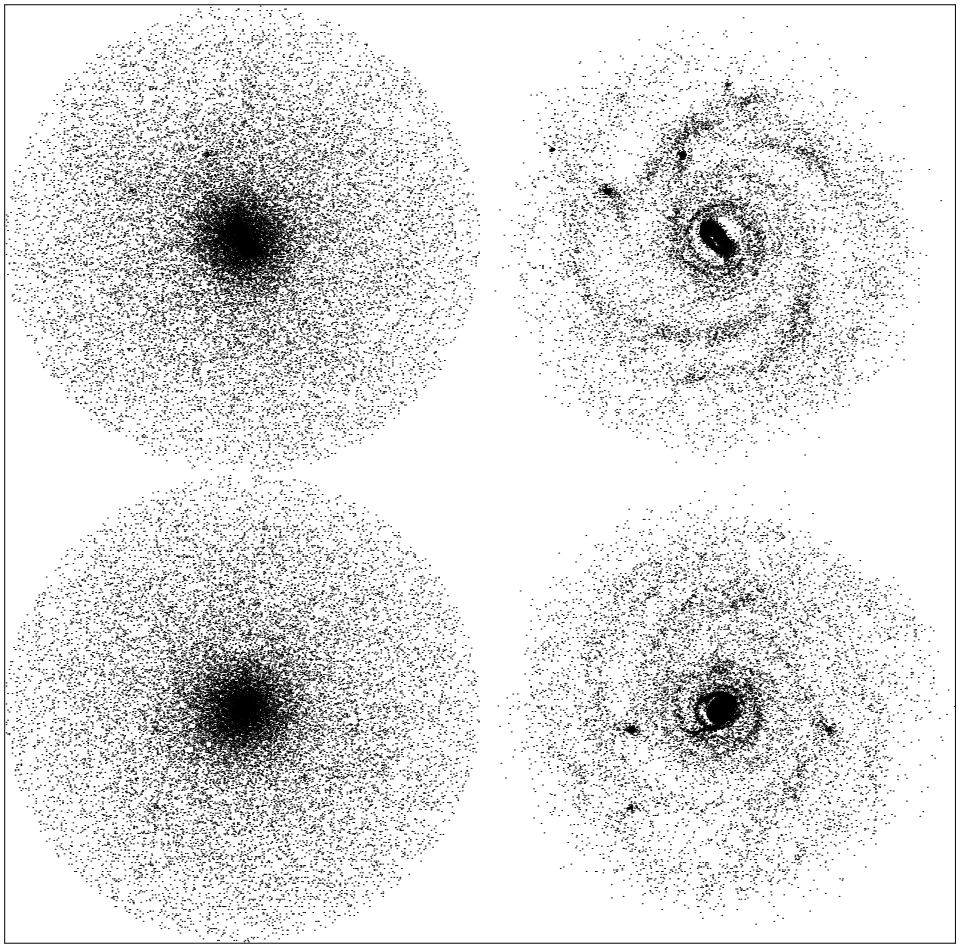

Stars Gas 2.4Gyr

Stars Gas 1.9Gyr

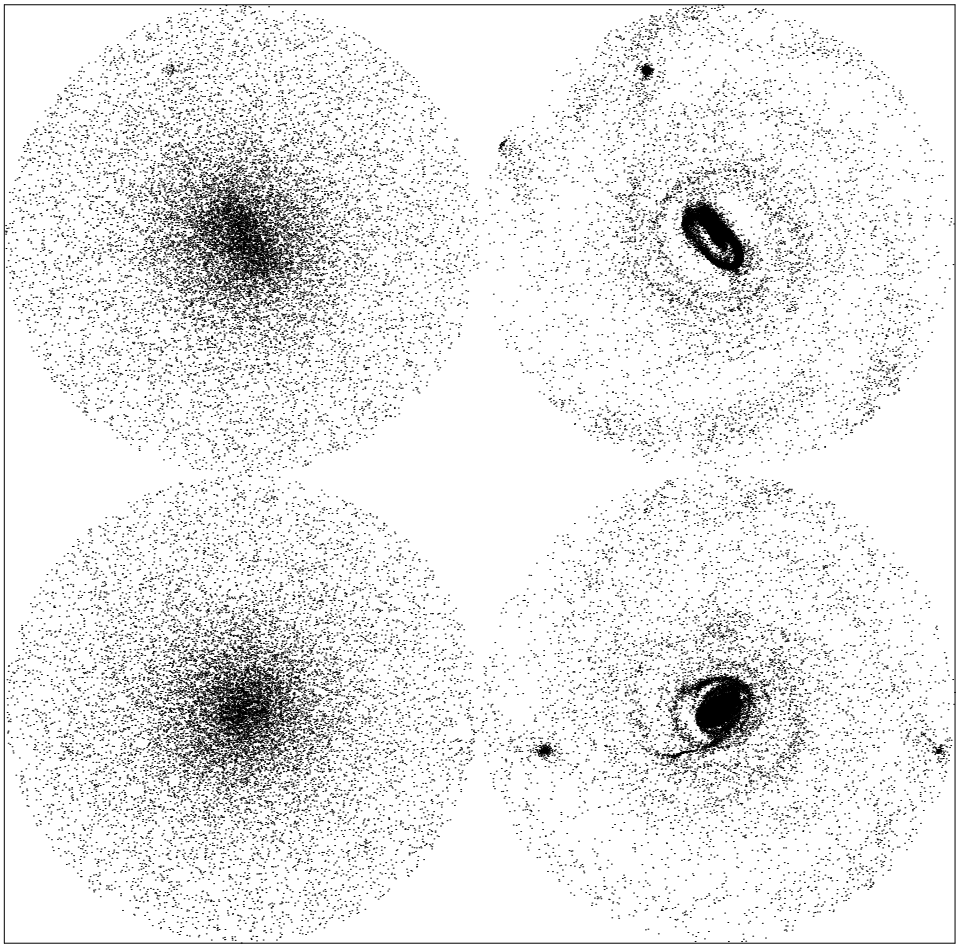

Stars Gas 2.4Gyr

C.1.2 Second run

Stars Gas 0.3Gyr

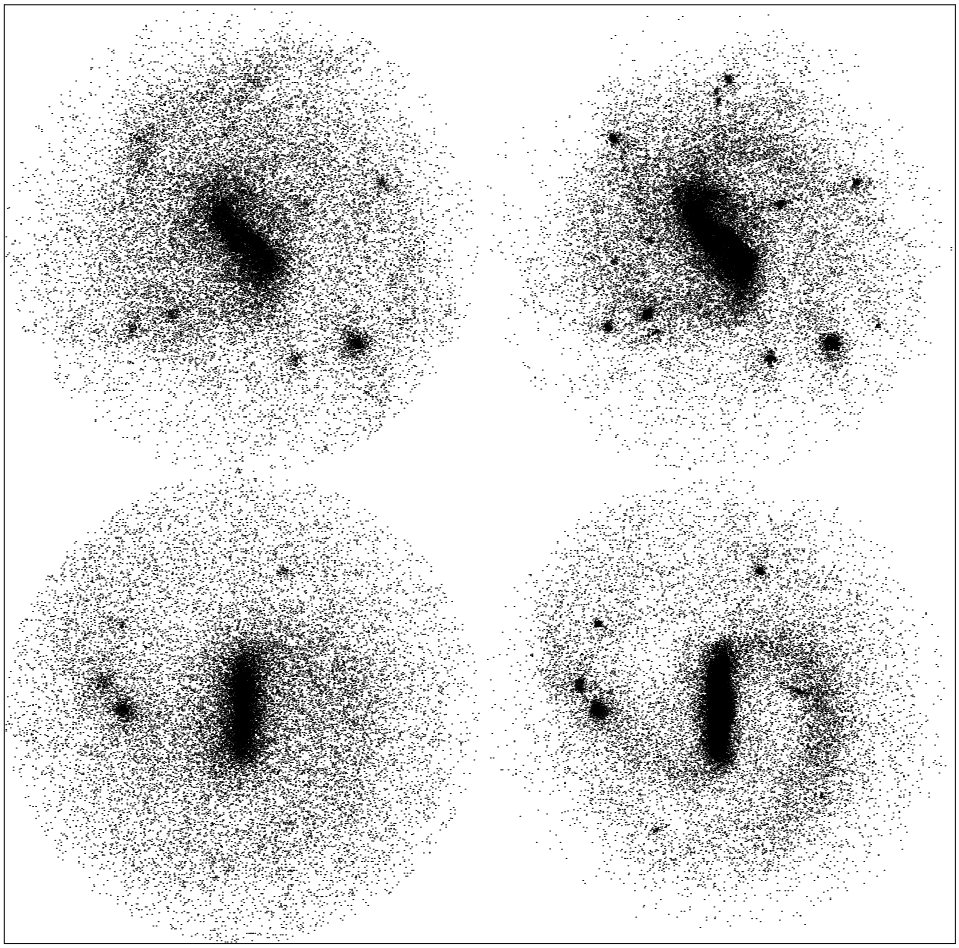

Stars Gas 0.6Gyr

Stars Gas 0.3Gyr

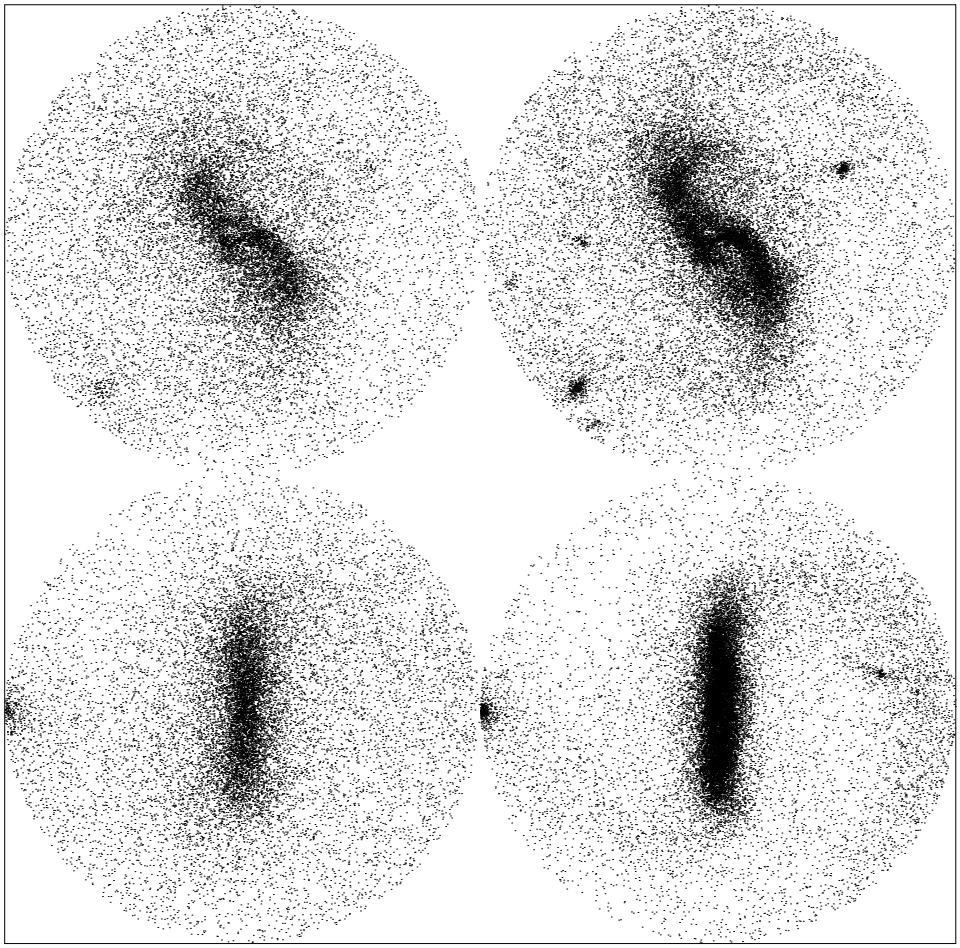

Stars Gas 0.6Gyr

Stars Gas 0.9Gyr

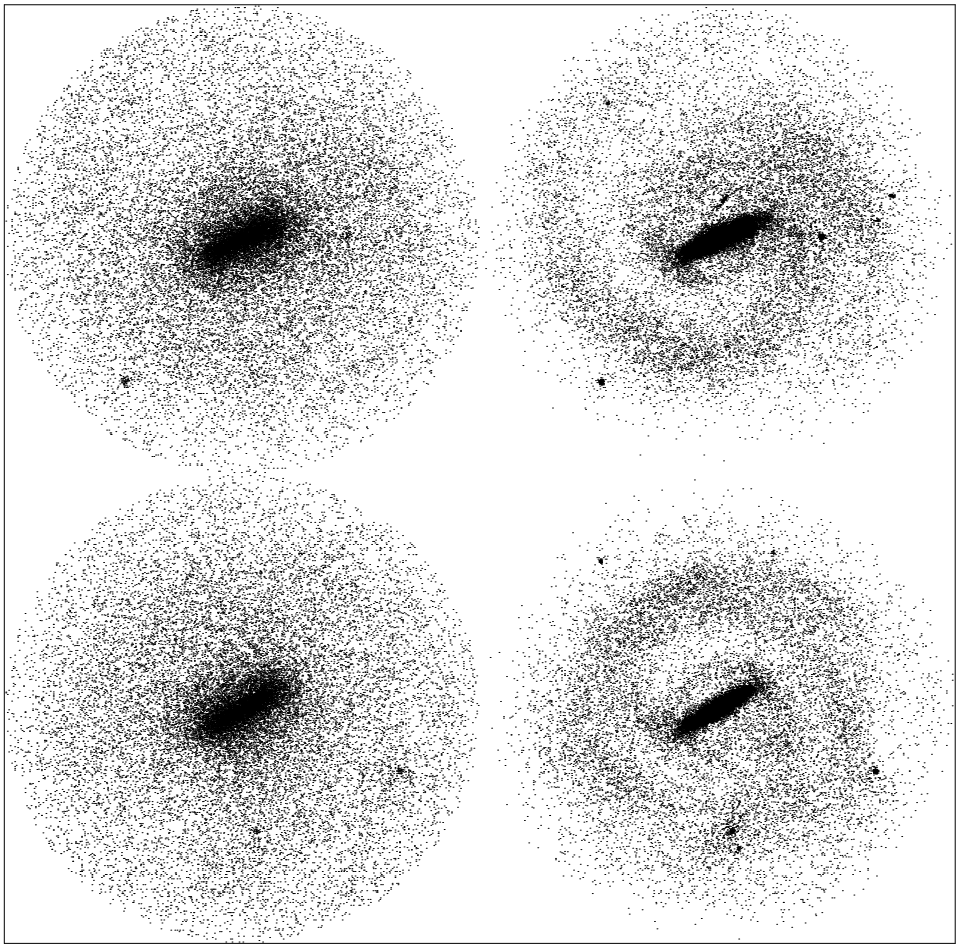

Stars Gas 1.2Gyr

Stars Gas 0.9Gyr

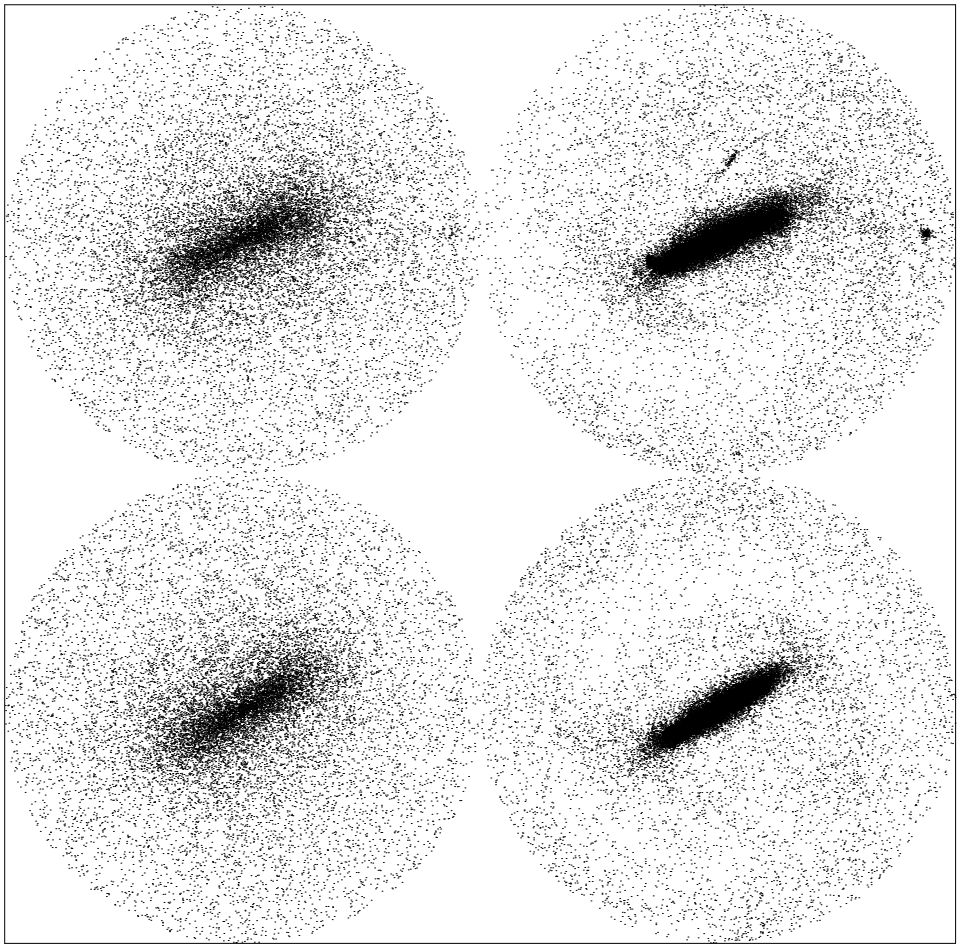

Stars Gas 1.2Gyr

Stars Gas 1.4Gyr

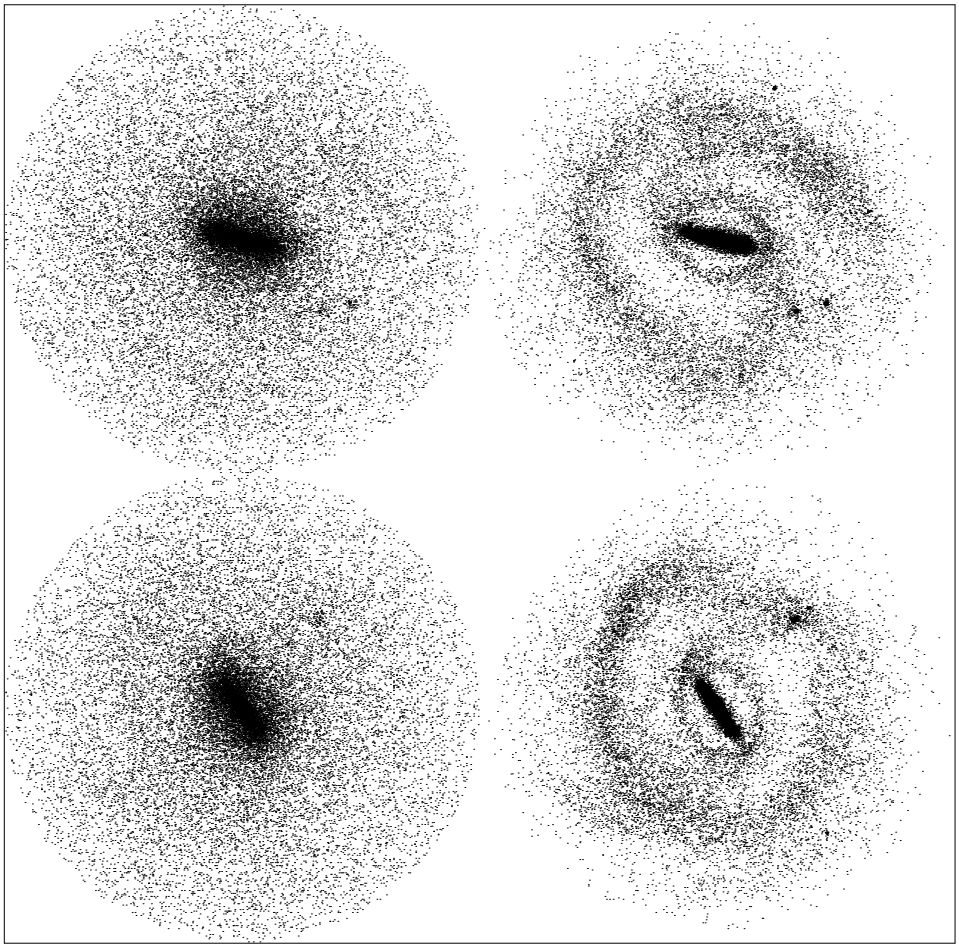

Stars Gas 1.6Gyr

Stars Gas 1.4Gyr

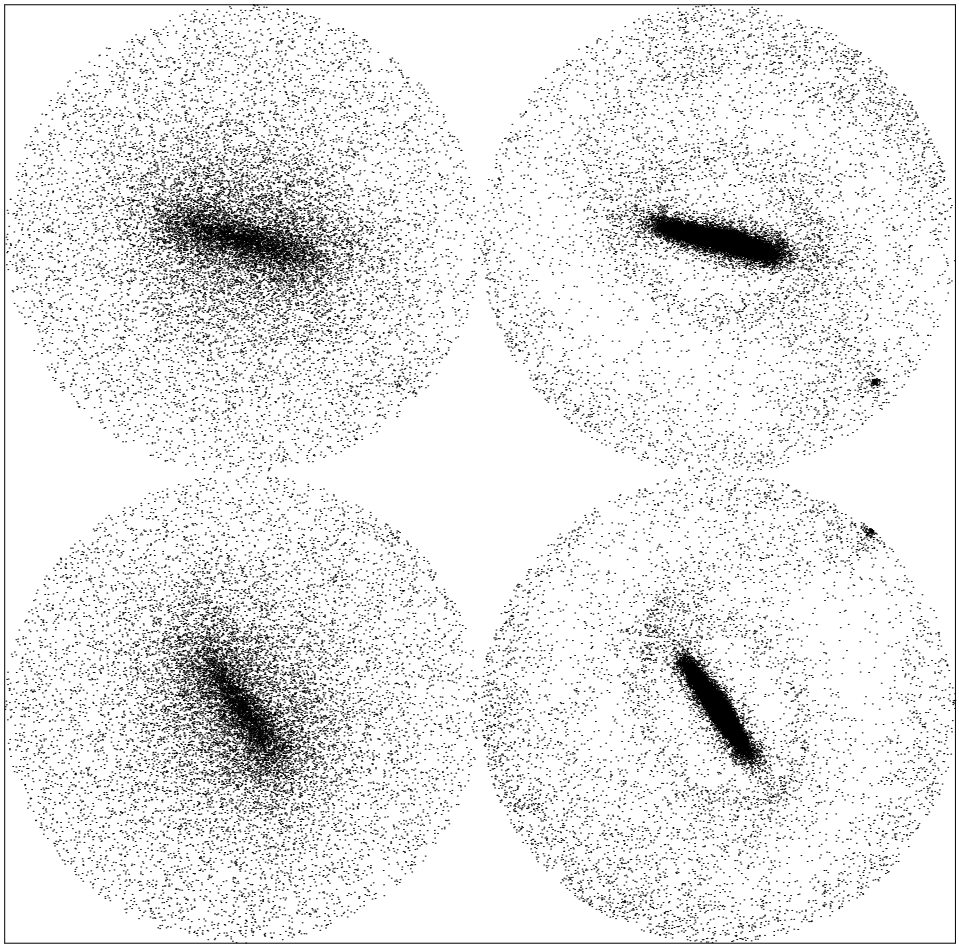

Stars Gas 1.6Gyr

Ha 0.3Gyr Ha 0.7Gyr

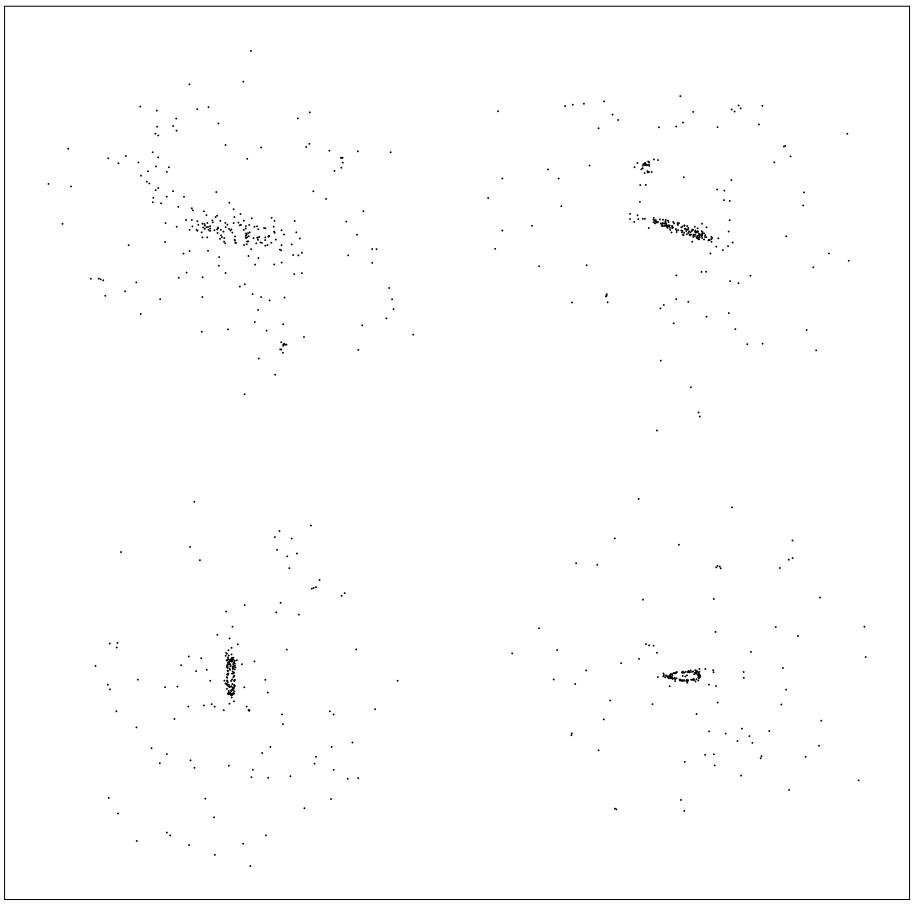

Ha 1.1Gyr Ha 1.5Gyr

C.2 Stellar component

C.2.1 First run

Ha 0.3Gyr Ha 0.7Gyr

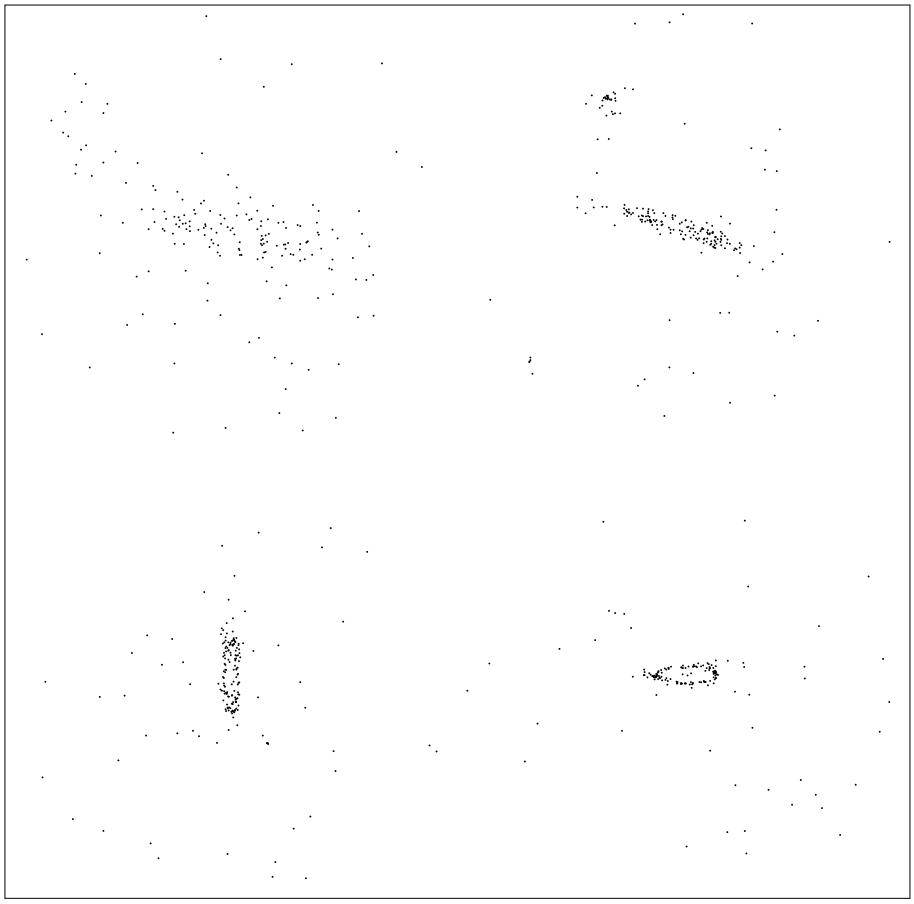

Ha 1.1Gyr Ha 1.5Gyr

Ha 1.9Gyr Ha 2.4Gyr

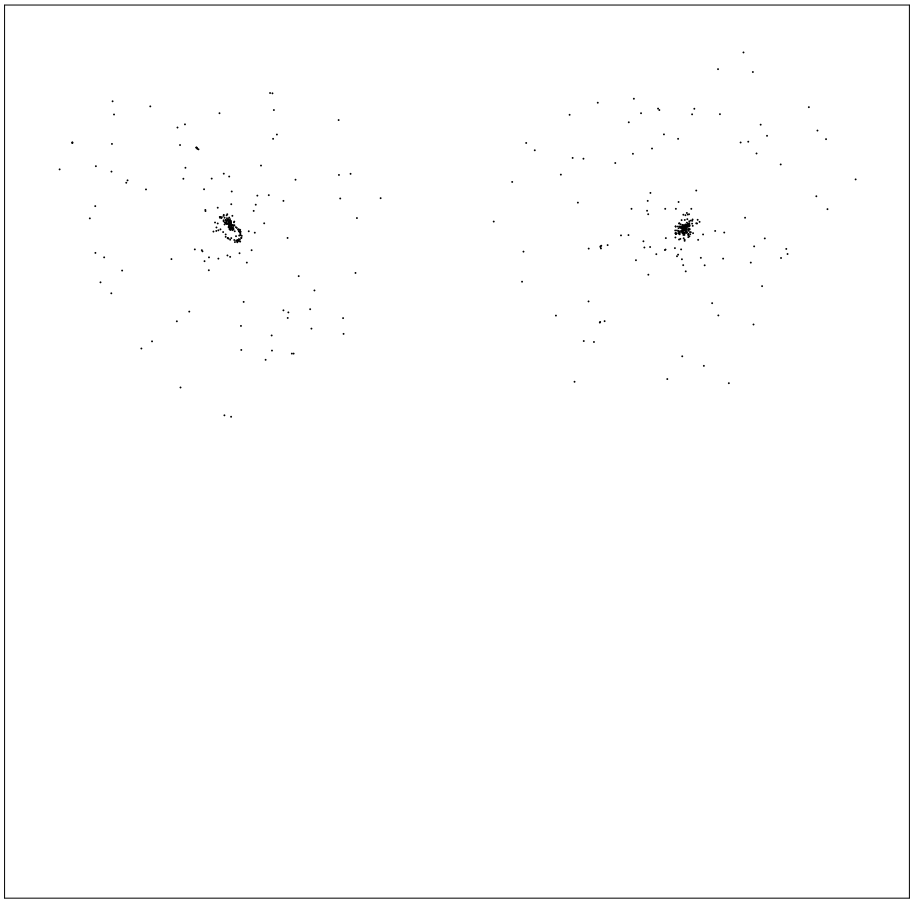

Ha 1.9Gyr Ha 2.4Gyr

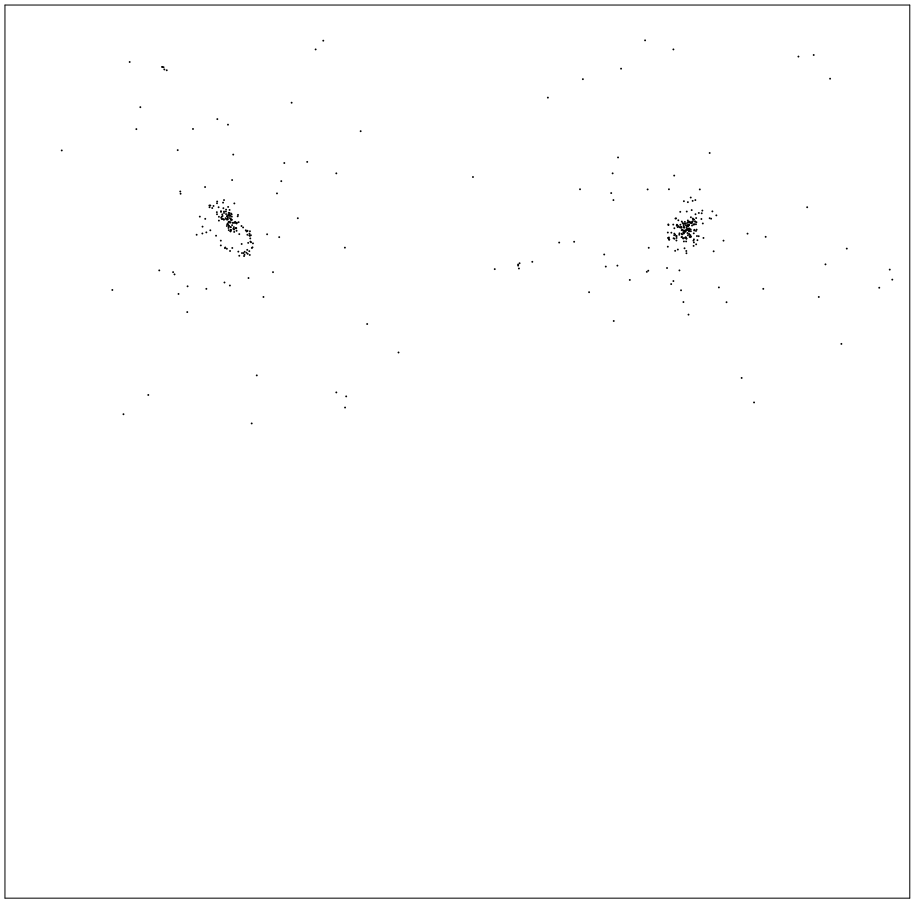

Ha 0.3Gyr Ha 0.6Gyr

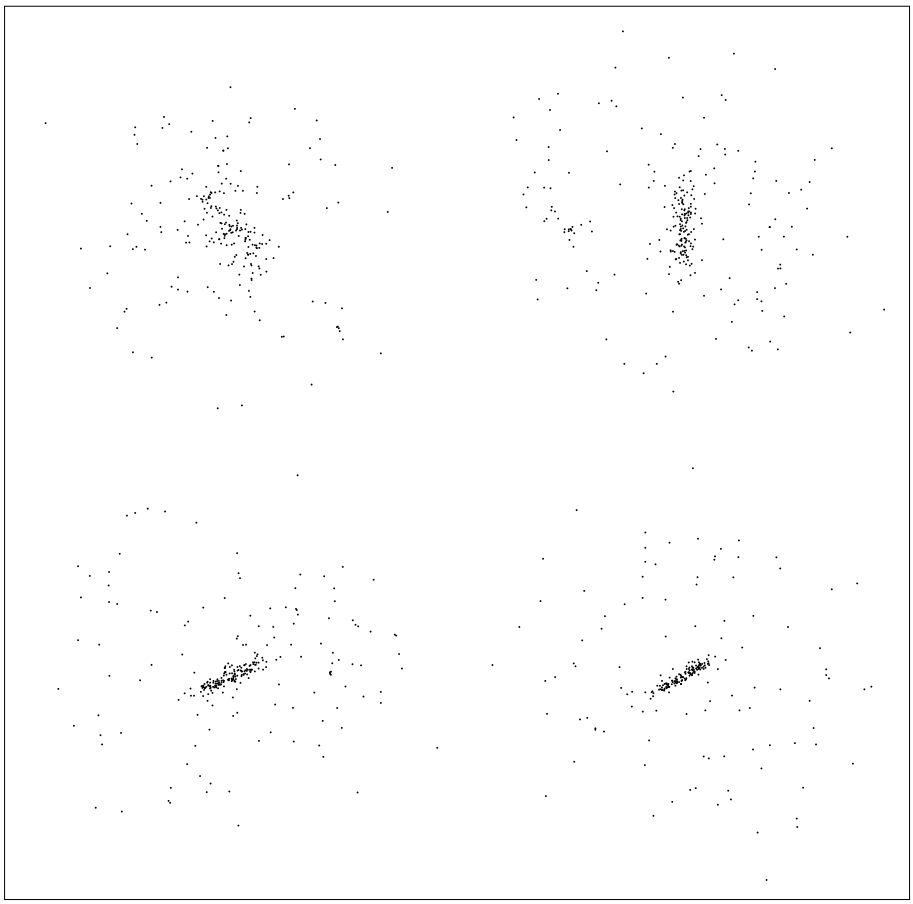

Ha 0.9Gyr Ha 1.2Gyr

C.2.2 Second run

Ha 0.3Gyr Ha 0.6Gyr

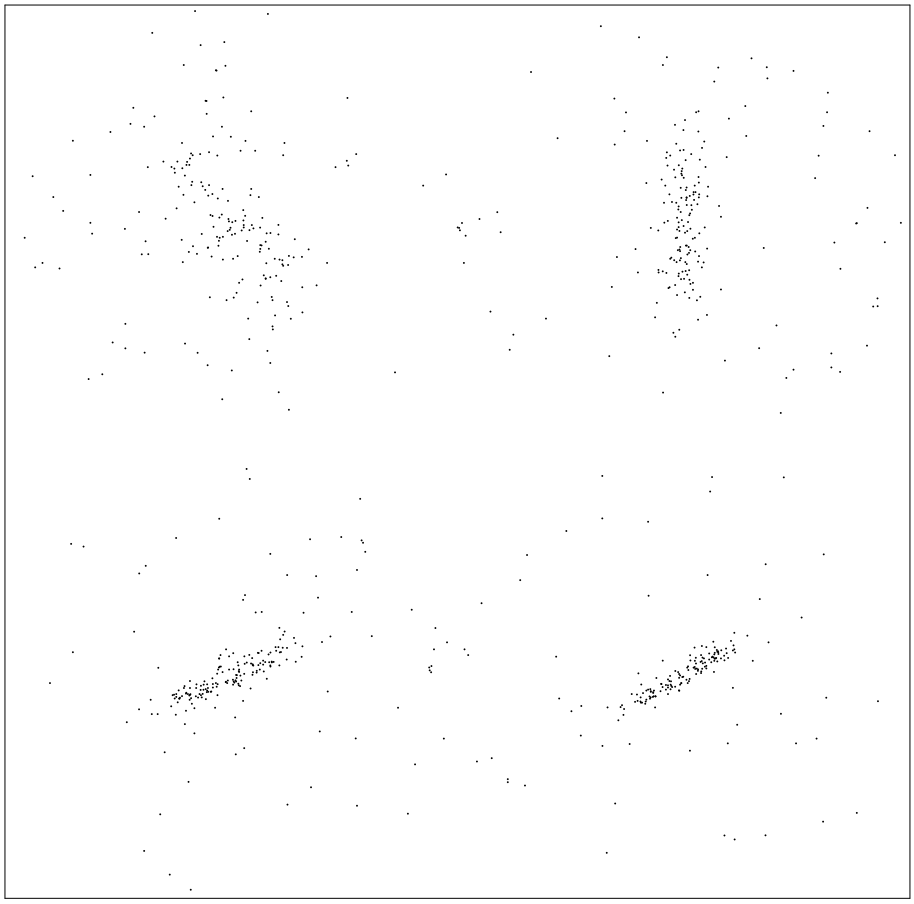

Ha 0.9Gyr Ha 1.2Gyr

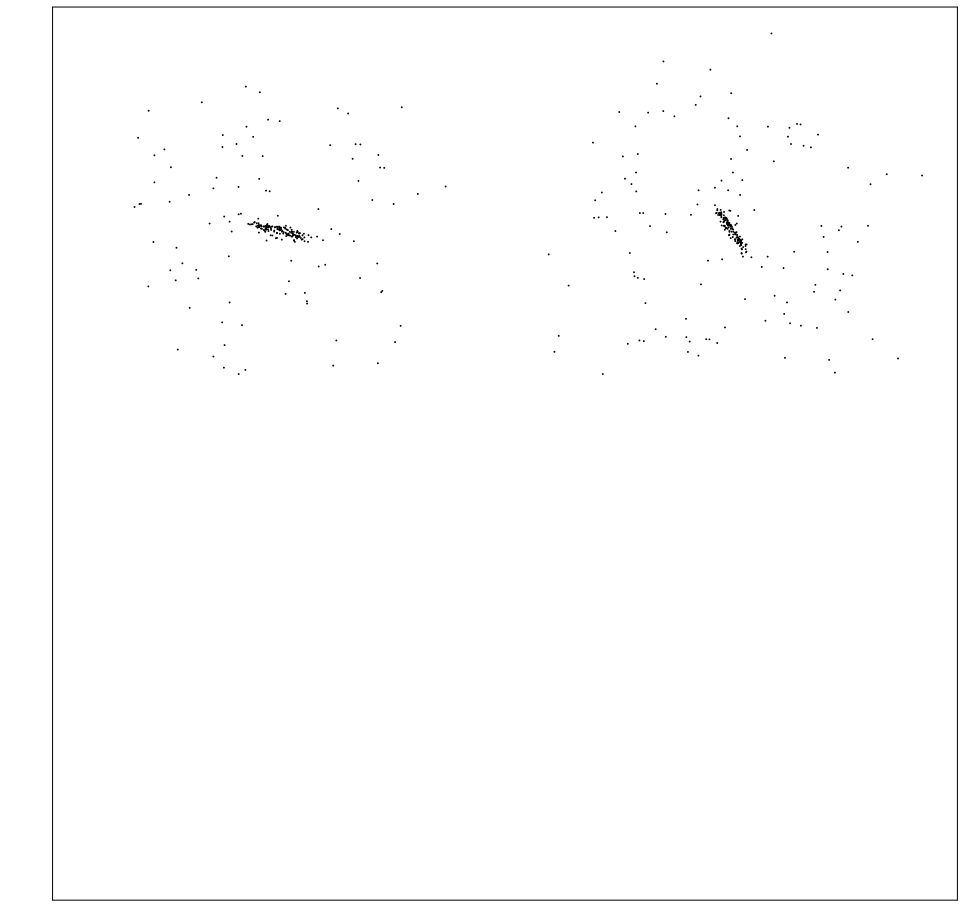
Ha 1.4Gyr
Ha 1.6Gyr

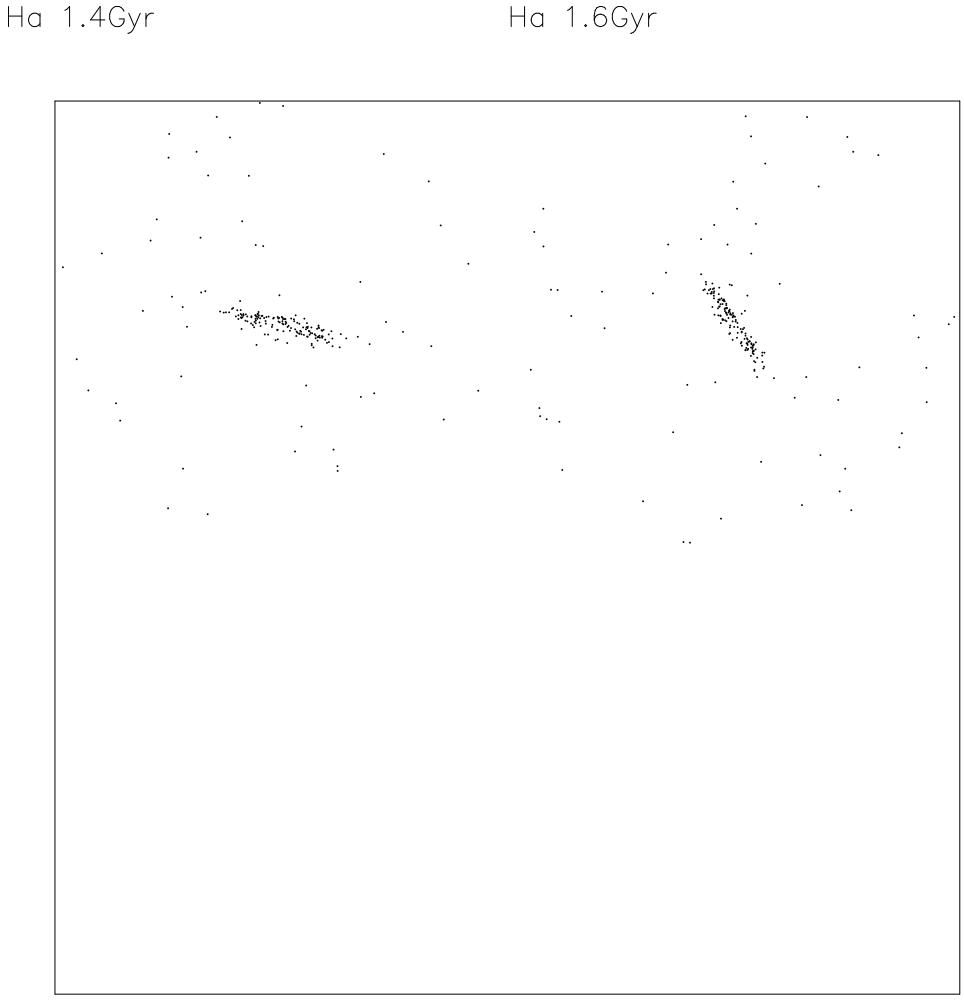
Ha 1.4Gyr
Ha 1.6Gyr

Bibliography

Aars, C. E., Marcum, P. M., & Fanelli, M. N. 2001, AJ, 122, 2923

Abell, G. O. 1958, ApJS, 3, 211

Abell, G. O., Corwin, H. G., & Olowin, R. P. 1989, ApJS, 70, 1

Adams, M. T., Jensen, E. B., & Stocke, J. T. 1980, AJ, 85, 1010

Balkowski, C. & Chamaraux, P. 1981, A&A, 97, 223

Berentzen, I., Athanassoula, E., Heller, C. H., & Fricke, K. J. 2004, MNRAS, 347, 220

Bertin, E. & Arnouts, S. 1996, A&AS, 117, 393

Binney, J. & Merrifield, M. 1998, Galactic astronomy (Galactic astronomy / James Binney and Michael Merrifield. Princeton, NJ : Princeton University Press, 1998. (Princeton series in astrophysics) QB857 .B522 1998 ($35.00))

Block, D. L., Bournaud, F., Combes, F., Puerari, I., & Buta, R. 2002, A&A, 394, L35

Boselli, A. 1994, A&A, 292, 1

Boselli, A., Gavazzi, G., Donas, J., & Scodeggio, M. 2001, AJ, 121, 753

Bournaud, F. & Combes, F. 2002, A&A, 392, 83

Bournaud, F., Combes, F., & Semelin, B. 2005, ArXiv Astrophysics e-prints

Braine, J. & Combes, F. 1993, A&A, 269, 7

Bushouse, H. A. 1987, ApJ, 320, 49

Buta, R., Laurikainen, E., & Salo, H. 2004, AJ, 127, 279

Casertano, S. & Hut, P. 1985, ApJ, 298, 80

Casoli, F., Dickey, J., Kazes, I., et al. 1996, A&A, 309, 43

Cayatte, V., Kotanyi, C., Balkowski, C., & van Gorkom, J. H. 1994, AJ, 107, 1003

Colbert, J. W., Mulchaey, J. S., & Zabludoff, A. I. 2001, AJ, 121, 808

Combes, F. 2004, in IAU Symposium, 383–388

Combes, F., Prugniel, P., Rampazzo, R., & Sulentic, J. W. 1994, A&A, 281, 725

Combes, F. & Sanders, R. H. 1981, A&A, 96, 164

Contini, T., Considere, S., & Davoust, E. 1998, A&AS, 130, 285

Courteau, S. & van den Bergh, S. 1999, AJ, 118, 337

da Costa, L. N., Willmer, C. N. A., Pellegrini, P. S., et al. 1998, AJ, 116, 1

Dahari, O. 1984, AJ, 89, 966

de Vaucouleurs, G. 1959, Handbuch der Physik, 53, 275

de Vaucouleurs, G. & de Vaucouleurs, A. 1963, AJ, 68, 278

Dressler, A. 1980, ApJ, 236, 351

Dressler, A., Oemler, A. J., Couch, W. J., et al. 1997, ApJ, 490, 577

Dultzin-Hacyan, D., Krongold, Y., Fuentes-Guridi, I., & Marziani, P. 1999, ApJ, 513, L111

Elmegreen, D. M., Elmegreen, B. G., & Bellin, A. D. 1990, ApJ, 364, 415

Eskridge, P. B., Frogel, J. A., Pogge, R. W., et al. 2002, ApJS, 143, 73

Espada, D., Bosma, A., Verdes-Montenegro, L., et al. 2005, A&A, 442, 455

Falco, E. E., Kurtz, M. J., Geller, M. J., et al. 1999, PASP, 111, 438

Fixsen, D. J., Cheng, E. S., Gales, J. M., et al. 1996, ApJ, 473, 576

Freeman, K. C. 1970, ApJ, 160, 811

Garrido, O., Marcelin, M., & Amram, P. 2004, MNRAS, 349, 225

Garrido, O., Marcelin, M., Amram, P., et al. 2005, MNRAS, 362, 127

Garrido, O., Marcelin, M., Amram, P., & Boissin, O. 2003, A&A, 399, 51

Garrido, O., Marcelin, M., Amram, P., & Boulesteix, J. 2002, A&A, 387, 821

Giuricin, G., Marinoni, C., Ceriani, L., & Pisani, A. 2000, ApJ, 543, 178

Haynes, M. P. & Giovanelli, R. 1980, ApJ, 240, L87

Haynes, M. P. & Giovanelli, R. 1983, ApJ, 275, 472

Haynes, M. P. & Giovanelli, R. 1984, AJ, 89, 758

Helfer, T. T., Thornley, M. D., Regan, M. W., et al. 2002, Astronomy Data Image Library, 1

Hernandez, O., Carignan, C., Amram, P., Chemin, L., & Daigle, O. 2005, MNRAS, 360, 1201

Hickson, P. 1982, ApJ, 255, 382

Hoyle, F. & Vogeley, M. S. 2004, ApJ, 607, 751

Hubble, E. 1929, Proceedings of the National Academy of Science, 15, 168

Hubble, E. P. 1936, Yale University Press

Huchra, J. & Thuan, T. X. 1977, ApJ, 216, 694

James, P. A., Shane, N. S., Beckman, J. E., et al. 2004, A&A, 414, 23

James, P. A., Shane, N. S., Knapen, J. H., Etherton, J., & Percival, S. M. 2005, A&A, 429, 851

Joseph, R. D. & Wright, G. S. 1985, MNRAS, 214, 87

Karachentsev, I. D. 1972, Soobshcheniya Spetsial'noj Astrofizicheskoj Observatorii, 7, 1

Karachentsev, I. D. 1980, ApJS, 44, 137

Karachentseva, V. E. 1973, Astrofizicheskie Issledovaniia Izvestiya Spetsial'noj Astrofizicheskoj Observatorii, 8, 3

Karachentseva, V. E. 1980, Soviet Astronomy, 24, 665

Karachentseva, V. E., Karachentsev, I. D., & Shcherbanovskii, A. L. 1979, Astrofizicheskie Issledovaniia Izvestiya Spetsial'noj Astrofizicheskoj Observatorii, 11, 3

Keeler, J. E. 1899, MNRAS, 59, 537

Kennicutt, R. C. 1989, ApJ, 344, 685

Kennicutt, R. C. 1998, ApJ, 498, 541

Kennicutt, R. C. & Kent, S. M. 1983, AJ, 88, 1094

Kennicutt, R. C., Roettiger, K. A., Keel, W. C., van der Hulst, J. M., & Hummel, E. 1987, AJ, 93, 1011

Kirshner, R. P., Oemler, A., Schechter, P. L., & Shectman, S. A. 1981, ApJ, 248, L57

Larson, R. B. & Tinsley, B. M. 1978, ApJ, 219, 46

Laurikainen, E., Salo, H., & Buta, R. 2004a, ApJ, 607, 103

Laurikainen, E., Salo, H., Buta, R., & Vasylyev, S. 2004b, MNRAS, 355, 1251

Leon, S., Combes, F., & Menon, T. K. 1998, A&A, 330, 37

Leon, S., Lim, J., Combes, F., & van-Trung, D. 2001, in QSO Hosts and Their Environments, 185–+

Leon, S. & Verdes-Montenegro, L. 2003, A&A, 411, 391

Lequeux, J. 1971, A&A, 15, 42

Lisenfeld, U., Verdes-Montenegro, L., Leon, S., & Sulentic, J. 2005, ArXiv Astrophysics e-prints

Lisenfeld, U., Voelk, H. J., & Xu, C. 1996a, A&A, 306, 677

Lisenfeld, U., Voelk, H. J., & Xu, C. 1996b, A&A, 314, 745

Márquez, I., Masegosa, J., Moles, M., et al. 2002, A&A, 393, 389

Márquez, I., Masegosa, J., Moles, M., et al. 2003, Ap&SS, 284, 711

Márquez, I. & Moles, M. 1996, A&AS, 120, 1

Márquez, I. & Moles, M. 1999, A&A, 344, 421

Márquez, I., Durret, F., Masegosa, J., et al. 2000, A&A, 360, 431

Massey, P., Silkey, M., Garmany, C. D., & Degioia-Eastwood, K. 1989, AJ, 97, 107

Menon, T. K. 1991, ApJ, 372, 419

Messier, C. 1781, Catalogue des nébuleuses et des amas d'étoiles

Moore, B., Katz, N., Lake, G., Dressler, A., & Oemler, A. 1996, Nature, 379, 613

Niklas, S. 1997, A&A, 322, 29

Niklas, S., Klein, U., & Wielebinski, R. 1995, A&A, 293, 56

Odewahn, S. C. 1995, PASP, 107, 770

Odewahn, S. C., Cohen, S. H., Windhorst, R. A., & Philip, N. S. 2002, ApJ, 568, 539

Odewahn, S. C., Windhorst, R. A., Driver, S. P., & Keel, W. C. 1996, ApJ, 472, L13+

Oemler, A. J. 1974, ApJ, 194, 1

Peebles, P. J. E. 1974a, ApJ, 189, L51+

Peebles, P. J. E. 1974b, A&A, 32, 197

Perea, J., del Olmo, A., Verdes-Montenegro, L., & Yun, M. S. 1997, ApJ, 490, 166

Pfenniger, D. & Norman, C. 1990, ApJ, 363, 391

Pisano, D. J., Wilcots, E. M., & Liu, C. T. 2002, ApJS, 142, 161

Postman, M. & Geller, M. J. 1984, ApJ, 281, 95

Prada, F., Vitvitska, M., Klypin, A., et al. 2003, ApJ, 598, 260

Richter, O.-G. & Sancisi, R. 1994, A&A, 290, L9

Roberts, M. S. & Haynes, M. P. 1994, ARA&A, 32, 115

Rojas, R. R., Vogeley, M. S., Hoyle, F., & Brinkmann, J. 2004, ApJ, 617, 50

Rojas, R. R., Vogeley, M. S., Hoyle, F., & Brinkmann, J. 2005, ApJ, 624, 571

Sauty, S., Casoli, F., Boselli, A., et al. 2003, A&A, 411, 381

Schmidt, M. 1968, ApJ, 151, 393

Schmitt, H. R. 2001, AJ, 122, 2243

Shen, J. & Sellwood, J. A. 2004, ApJ, 604, 614

Slipher, V. M. 1911a, Lowell Observatory Bulletin, 1, 66

Slipher, V. M. 1911b, Lowell Observatory Bulletin, 1, 56

Slipher, V. M. 1917, The Observatory, 40, 304

Solomon, P. M., Downes, D., Radford, S. J. E., & Barrett, J. W. 1997, ApJ, 478, 144

Soneira, R. M. & Peebles, P. J. E. 1977, ApJ, 211, 1

Stetson, P. B. 1990, PASP, 102, 932

Stocke, J. T. 1978, AJ, 83, 348

Sulentic, J. W. 1976, ApJS, 32, 171

Sulentic, J. W. 1989, AJ, 98, 2066

Sulentic, J. W. 1997, ApJ, 482, 640

Sulentic, J. W. & Arp, H. 1983, AJ, 88, 489

Sulentic, J. W., Verdes-Montenegro, L., Bergond, G., et al. 2005, ArXiv Astrophysics e-prints

Surace, J. A., Mazzarella, J., Soifer, B. T., & Wehrle, A. E. 1993, AJ, 105, 864

Toledo, H. M. H., Dultzin-Hacyan, D., Gonzalez, J. J., & Sulentic, J. W. 1999, AJ, 118, 108

Turner, E. L. & Gott, J. R. 1975, ApJ, 197, L89

van Gorkom, J. 1996, in ASP Conf. Ser. 106: The Minnesota Lectures on Extragalactic Neutral Hydrogen, 293–+

Varela, J., Moles, M., Márquez, I., et al. 2004, A&A, 420, 873

Verdes-Montenegro, L., Sauvage, M., Sempere, M. J., Sulentic, J., & Cernicharo, J. 2002, Ap&SS, 281, 427

Verdes-Montenegro, L., Sempere, M. J., Sulentic, J., & Cernicharo, J. 2001a, in ESA SP-460: The Promise of the Herschel Space Observatory, 515–+

Verdes-Montenegro, L., Sulentic, J., Espada, D., et al. 2004, in IAU Symposium, 220–+

Verdes-Montenegro, L., Sulentic, J., Lisenfeld, U., et al. 2005, A&A, 436, 443

Verdes-Montenegro, L., Yun, M. S., Perea, J., del Olmo, A., & Ho, P. T. P. 1998, ApJ, 497, 89

Verdes-Montenegro, L., Yun, M. S., Williams, B. A., et al. 2001b, A&A, 377, 812

Vettolani, G., de Souza, R., & Chincarini, G. 1986, A&A, 154, 343

Xu, C., Lisenfeld, U., & Voelk, H. J. 1994, A&A, 285, 19

Xu, C. & Sulentic, J. W. 1991, ApJ, 374, 407

Young, J. S., Allen, L., Kenney, J. D. P., Lesser, A., & Rownd, B. 1996, AJ, 112, 1903

Young, J. S., Kenney, J. D., Tacconi, L., et al. 1986, ApJ, 311, L17

Young, J. S. & Scoville, N. Z. 1991, ARA&A, 29, 581

Zaritsky, D., Smith, R., Frenk, C., & White, S. D. M. 1993, ApJ, 405, 464

Zasov, A. V. & Sulentic, J. W. 1994, ApJ, 430, 179

Zwicky, F., Herzog, E., & Wild, P. 1968, Catalogue of galaxies and of clusters of galaxies (Pasadena: California Institute of Technology (CIT), 1961-1968)